



**A novel approach to determine lipid inducing
conditions in microalgae with aggregation-
induced emission-based fluorophores**

By

A H M Mohsinul Reza

*Thesis
Submitted to Flinders University
for the degree of*

Doctor of Philosophy

College of Science & Engineering,
Flinders University

19 July 2022

TABLE OF CONTENTS

List of Tables	vi
List of Figures	vii
Abstract	xi
Declaration	xiii
Acknowledgement	xiv
Chapter 1: General Introduction	1
1.1 Importance of microalgae	2
1.2 Research of lipid drops in microalgae	5
1.2.1 Biosynthesis of lipid drops	5
1.2.2 Significance of lipid drops in different organisms	7
1.2.3 Lipid drops from microorganisms for human benefits	8
1.2.4 Factors affecting lipid biosynthesis and composition in microalgae	10
1.3 Potentials and challenges in the study of lipid droplets	12
1.3.1 Common methods applied in modern lipidomics analysis	13
1.3.2 Common probes in lipid droplets bioimaging, their utilization and disadvantages	14
1.4 Reactive oxygen species and their significance	17
1.5 Production of ROS in microalgae	18
1.5.1 ROS generation from mitochondria	19
1.5.2 ROS generation from chloroplasts	19
1.5.3 ROS Production in the endoplasmic reticulum	20
1.5.4 Peroxisomes, plasma membrane and cell wall as the sources of ROS	22
1.6 Putative roles of ROS in biomolecules synthesis	22
1.7 Current approaches for the detection of ROS molecules	26
1.7.1 ROS analysis with traditional technologies	26
1.7.2 Commercial fluorescent dyes for ROS detection	27
1.8 Fluorophores targeting H ₂ O ₂ in different organelles	32
1.9 Aggregation Induced Emission-based fluorescent bioprobes	34
1.10 Recent progress of lipid-specific probes with aggregation-induced emission	36
1.10.1 Photostable lipid-specific probes based on simple AIEgens	37

1.10.2	Two-photon lipid droplets specific AIE bio-probes	39
1.10.3	AIE-based fluorophore to visualize LD-lysosome interplay	43
1.10.4	Lipid-specific AIEgens system with wide emission tenability	44
1.10.5	Biocompatible AIEgen from natural resources	47
1.10.6	Lipid specific AIEgens in algae research	48
1.11	AIE-based molecules for H ₂ O ₂ detection	54
1.12	Study objectives	60
1.12.1	Study 1: Stress-induced lipid droplets conditions in a cell wall deficient alga, <i>Euglena gracilis</i> with aggregation induced emission (AIE) fluorophore	62
1.12.2	Study 2: Stress-induced lipid droplet conditions with aggregation induced emission fluorophores in a flagellate microalga <i>Chlamydomonas reinhardtii</i> with carbohydrate cell walls	62
1.13.3	Study 3: Supplementation of H ₂ O ₂ to the medium enhanced lipid accumulation in microalgae: visualizing lipid drops with a novel fluorescent probe	63
1.13	Thesis organization	63
1.14	References	66
Chapter 2: Stress-Induced Lipid Droplets Conditions in a Cell Wall Deficient Alga, <i>Euglena gracilis</i> with Aggregation Induced Emission (AIE) Fluorophore		100
2.1	Abstract	101
2.2	Introduction	102
2.3	Materials and Methods	107
2.3.1	Establishment of <i>Euglena gracilis</i> culture and lipid induction	107
2.3.2	Determination of autofluorescence properties of <i>Euglena gracilis</i>	110
2.3.3	Lipid extraction and analysis of fatty acids	110
2.3.4	Determination of fluorescent properties of DPAS in DMSO/water mixtures	111
2.3.5	Determination of algal growth in different concentration of DPAS	112
2.3.6	Preparation of <i>Euglena gracilis</i> samples for BODIPY and DPAS staining	112
2.3.7	Imaging of <i>Euglena gracilis</i> with confocal microscope	113
2.3.8	Flow cytometric analysis of lipid content	114
2.3.9	Data analysis	114

2.4	Results	115
2.4.1	Screening algal growth conditions in different treatments	115
2.4.2	Autofluorescence properties of <i>Euglena gracilis</i>	117
2.4.3	Effects of DPAS on <i>Euglena gracilis</i> growth	121
2.4.4	Fluorescent properties of DPAS	123
2.4.5	Optimization of DPAS concentration and incubation periods	124
2.4.6	Labeling of stress induced lipid droplets by DPAS in <i>Euglena gracilis</i>	124
2.4.7	Flow cytometric analysis of lipid content	132
2.4.8	Fatty acid analysis	135
2.5	Discussion	139
2.6	Conclusion	146
2.7	References	147
Chapter 3: Stress-Induced Lipid Droplet Conditions with Aggregation Induced Emission Fluorophores in a Flagellate Microalga <i>Chlamydomonas reinhardtii</i> with Carbohydrate Cell Walls		166
3.1	Abstract	167
3.2	Introduction	168
3.3	Materials and Methods	172
3.3.1	Microalga cultivation and lipid induction	172
3.3.2	The fluorescence properties of <i>Chlamydomonas reinhardtii</i> and AIEgens	173
3.3.3	Determination of algal growth in different concentrations of AIEgens	174
3.3.4	Determination of H ₂ O ₂ content	174
3.3.5	Sample preparation for fluorescent staining of lipid and H ₂ O ₂	174
3.3.6	Imaging of <i>Chlamydomonas reinhardtii</i> with confocal microscope	175
3.3.7	Flow cytometric analysis of lipid content	175
3.3.8	Lipid extraction and analysis of fatty acids	176
3.3.9	Data analysis	177
3.4	Results	178
3.4.1	Effects of nutrient and light manipulation on algal growth	178
3.4.2	Autofluorescence properties of <i>Chlamydomonas reinhardtii</i>	179
3.4.3	Fluorescent properties of 2-DPAN	180
3.4.4	Algal growth and acquisition of probe concentration	180

3.4.5	Wash free imaging technique with DPAS and 2-DPAN	183
3.4.6	Comparison of the lipid-specific probes	186
3.4.7	Flow cytometric analysis of lipid content	189
3.4.8	Confocal analysis of the stress-induced lipid droplets in <i>Chlamydomonas reinhardtii</i>	194
3.4.9	H ₂ O ₂ content in the <i>Chlamydomonas reinhardtii</i> cells	200
3.4.10	Fatty acid analysis	202
3.5	Discussion	204
3.6	Conclusion	210
3.7	References	211

Chapter 4: Supplementation of H₂O₂ to the Medium Enhanced Lipid Accumulation in Microalgae: Visualizing Lipid Drops with a Novel Fluorescent Probe 226

4.1	Abstract	227
4.2	Introduction	228
4.3	Materials and methods	230
4.3.1	Microalga cultivation and lipid induction	230
4.3.2	Determination of algal growth in different concentrations of TPE-BO and H ₂ O ₂	231
4.3.3	Sample preparation for fluorescent staining of lipid and H ₂ O ₂	232
4.3.4	Imaging of <i>Chlamydomonas reinhardtii</i> with confocal microscope	233
4.3.5	Flow cytometric analysis of lipid content	233
4.3.6	Lipid extraction and analysis of fatty acids	233
4.3.7	Data analysis	234
4.4	Results	235
4.4.1	Growth of <i>Chlamydomonas reinhardtii</i> in different concentrations of TPE-BO	235
4.4.2	Confocal analysis of H ₂ O ₂ activity in nutrient-starved <i>Chlamydomonas reinhardtii</i> cells	236
4.4.3	Effects of H ₂ O ₂ supplementation on <i>Chlamydomonas reinhardtii</i>	242
4.4.4	Effects of H ₂ O ₂ supplementation on lipid bioaccumulation	243
4.4.5	Effects of H ₂ O ₂ supplementation on lipid composition in <i>Chlamydomonas reinhardtii</i>	250

4.5	Discussion	252
4.6	Conclusion	256
4.7	Reference	257
Chapter 5: General Discussion, Conclusions and Future Research		266
5.1	General discussion	267
5.1.1	Identification of the lipid induction conditions in <i>Euglena gracilis</i>	269
5.1.2	Identification of the lipid induction conditions in <i>Chlamydomonas reinhardtii</i>	272
5.1.3	Effects of H ₂ O ₂ on the lipid accumulation and fatty acid composition in <i>Chlamydomonas reinhardtii</i>	274
5.2	Conclusion	276
5.3	Implications	277
5.4	Future Research	279
5.5	References	281

List of Tables **Page**

Table 1.1 **2**

Table 1.2 **16**

Table 1.3 **30**

Table 1.4 **50**

Table 1.5 **56**

Table 2.1 **138**

Table 3.1 **204**

Table 4.1 **251**

List of Figures	Page
Fig. 1.1	6
Fig. 1.2	11
Fig. 1.3	21
Fig. 1.4	23
Fig. 1.5	25
Fig. 1.6	35
Fig. 1.7	38
Fig. 1.8	41
Fig. 1.9	43
Fig. 1.10	44
Fig. 1.11	46
Fig. 1.12	48
Fig. 1.13	49
Fig. 2.1	109
Fig. 2.2	113
Fig. 2.3	116
Fig. 2.4	116
Fig. 2.5	118
Fig. 2.6	119

List of Figures	Page
Fig. 2.7	120
Fig. 2.8	122
Fig. 2.9	123
Fig. 2.10	124
Fig. 2.11	126
Fig. 2.12	127
Fig. 2.13	128
Fig. 2.14	129
Fig. 2.15	130
Fig. 2.16	131
Fig. 2.17	133
Fig. 2.18	134
Fig. 2.19	135
Fig. 2.20	137
Fig. 3.1	178
Fig. 3.2	179
Fig. 3.3	180
Fig. 3.4	181
Fig. 3.5	182

List of Figures	Page
Fig. 3.6	183
Fig. 3.7	184
Fig. 3.8	185
Fig. 3.9	187
Fig. 3.10	188
Fig. 3.11	189
Fig. 3.12	191
Fig. 3.13	192
Fig. 3.14	193
Fig. 3.15	195
Fig. 3.16	196
Fig. 3.17	197
Fig. 3.18	198
Fig. 3.19	199
Fig. 3.20	201
Fig. 3.21	202
Fig. 4.1	236
Fig. 4.2	237
Fig. 4.3	238

List of Figures	Page
Fig. 4.4	239
Fig. 4.5	240
Fig. 4.6	241
Fig. 4.7	242
Fig. 4.8	243
Fig. 4.9	244
Fig. 4.10	245
Fig. 4.11	246
Fig. 4.12	247
Fig. 4.13	248
Fig. 4.14	249
Fig. 4.15	250
Fig. 5.1	271
Fig. 5.2	273
Fig. 5.3	275
Fig. 5.4	278

Abstract

The usage of microalgal lipids is ubiquitous, ranging from bioactive compounds to biofuel production. Identification of lipid inducing conditions and underlying biochemical changes can significantly improve lipid quantity and quality in algae. However, there is a lack of an appropriate tool *in vivo* to visualize lipid drops in algae. Traditional probes for lipid studies often suffer from various dye-specific limitations, such as aggregation-caused quenching and self-decomposition phenomena that hinder the accuracy of lipid identification. The recent emergence of aggregation-induced emission (AIE)-based nanoprobes has shown a promising attribute to overcome the limitations of conventional fluorophores for bioimaging the target molecules. This thesis aims to identify the lipid producing conditions using novel AIEgens as the lipid detecting probes in microalgae. Two morphologically distinctive algae were used *Euglena gracilis*, without a cell wall, and *Chlamydomonas reinhardtii*, with a carbohydrates-based cell wall.

Three experiments were included in this thesis. Experiment 1 evaluates the effects of light ($70 \text{ mmol photons m}^{-2} \text{ s}^{-1}$), nutrient starvation and supplemented carbon source on lipid biosynthesis in *E. gracilis* cells. Cellular lipid drops (LDs) were detected with a lipid-specific AIE-probe, DPAS ($\text{C}_{20}\text{H}_{16}\text{N}_2\text{O}$). Experiment 2 determines the lipid inducing conditions with AIE-probe, 2-DPAN ($\text{C}_{24}\text{H}_{18}\text{N}_2\text{O}$), as a new tool to detect the LD formation in *C. reinhardtii*. In addition, hydrogen peroxide (H_2O_2) activity was measured as a component of the secondary messenger molecules and natural by-products. The novel H_2O_2 detection technique was established utilizing H_2O_2 -specific AIEgen, TPE-BO ($\text{C}_{38}\text{H}_{42}\text{B}_2\text{O}_4$). Finally, experiment 3 determines the effects of external H_2O_2 supplementation on the lipid composition and content in *C. reinhardtii*.

The results of experiment 1 suggest that compared to the autotrophic condition (modified Cramer-Myers medium, MCM), nutrient-starved heterotrophic condition (nitrogen and calcium starved MCM, but with glucose supplementation in the dark) increased total lipid and health beneficiary LC-PUFAs production in *E. gracilis* by ~11.93% and ~14.36%, respectively. In experiment 2, *C. reinhardtii* cultured in the nitrogen and calcium starved, but sodium acetate (2.0 g/L) supplemented Woods Hole (MBL) medium under continuous light produced 4.32% more lipid than the autotrophic condition (MBL medium). Maximum amounts of health beneficiary α -linolenic acid ($46.05 \pm 2.31\%$) and H_2O_2 ($38.57 \pm 7.01 \mu\text{M/g}$ fresh cell) were detected in the lipid-induced cells. In experiment 3, supplementation of 0.4 mM and 0.6 mM H_2O_2 in the *C. reinhardtii* culture (MBL medium; continuous light) also increased the lipid accumulation to $12.67 \pm 1.45\%$ and $13.12 \pm 1.04\%$, respectively, compared with that of the $6.77 \pm 1.92\%$ lipid in control (without H_2O_2).

Distinctive LDs labelled by DPAS in *E. gracilis* cells have confirmed the lipid enrichment conditions under confocal microscopy and flow cytometry. Confocal images labelled with 2-DPAN and TPEBO have also clearly demonstrated the LDs and H_2O_2 , respectively, in the lipid-induced *C. reinhardtii* cells. Co-staining in the presence of traditional lipid-specific BODIPY dye and chlorophyll indicates that DPAS and 2-DPAN are suitable for multicolour imaging with red and green fluorophores. 2-DPAN showed better fluorescence intensity than DPAS and BODIPY in *C. reinhardtii*. Compared to BODIPY, 2-DPAN and DPAS are better probes and are recommended as a rapid and easy lipid screening tool to detect lipid drops in microalgae.

Declaration

I certify that this thesis is an original report of my research, and the work has not been submitted in support of a degree in any other university or professional qualification. To the best of my knowledge, this thesis does not contain any material previously published by another person except those have been indicated clearly and acknowledged with due references. All the supporting literature and resources have been referred accordingly in this thesis.

A H M Mohsinul Reza

April 2022

Acknowledgements

The author would like to acknowledge the financial support of the Australian Government Research Training Program Scholarship (AGRTPS) (International) for his PhD study at Flinders University, Australia.

The author expresses his abstruse indebtedness and sincerest gratitude to his reverend teacher and research supervisor, Dr. Jianguang Qin, Professor, School of Biological Sciences, College of Science and Engineering, Flinders University, Australia, for his scholastic supervision, kindness, valuable suggestions, constant encouragement and compassionate co-operation in carrying out this research and writing up of this thesis.

The author also expresses his deepest sense of gratitude to his respected co-supervisor, Dr. Youhong Tang, Professor, Institute for NanoScale Science and Technology, College of Science and Engineering, Flinders University, Australia, for his valuable suggestions, encouragement, solitary instructions, and constructive criticism throughout the entire period of this research work.

The author feels proud to express his immense indebtedness to his other co-supervisors, Emeritus Professor Dr. Greg Barritt, College of Medicine and Public Health, Flinders University, Australia and Associate Professor Sophie Leterme, College of Science and Engineering, Flinders University, Australia, for their support and assistance during the time of his PhD study. The author also appreciates the time and effort of Professor Xiaoxu Li and Dr. Yuning Hong for being the research assessors and providing valuable comments to guide through the PhD study.

The author owes special gratefulness to all the School of Biological Sciences technical staff for their thoughtful advice and support throughout the study. Also the author would like to take the opportunity to uphold his gratefulness to all the International Student Center staffs, Flinders University, Australia, for their kind cooperation and inspiration throughout his stay in Australia.

Lastly and foremost, the author would like to thank his parents, wife and friends for their love, sacrifice, patience and encouragement during these years.

The Author

April, 2022

Chapter 1: General Introduction

1.1 Importance of microalgae

The green microalgae signify an important photosynthetic group of morphologically diverse eukaryotes that subjugate almost every photic habitat on earth. They are among the fastest-growing photosynthetic organisms in the ecosystem, playing crucial roles in energy transfer at trophic levels (Avagyan, 2008). These photosynthetic organisms encompass a diverse group, assorted from varied cellular structures and a comprehensive range of habitats conditions. Unlike terrestrial organisms, to thrive the diversified and extreme environments, these organisms produce a range of unique bioactive and complex compounds (Wells et al., 2017; Saha et al., 2018). The valuable metabolites, obtained from microalgae are essential for several nutraceutical and pharmaceutical purposes, and the market for these products is expanding rapidly. Some lipid, carotenoid, and vitamin-producing microalgae species with potential health benefits have been enlisted in Table 1.1 (Reza et al., 2021).

Table 1.1 Microalgae derived key biofunctional components and their potential health benefits

Major biofunctional components	Algae species	Bioactivities/health benefits
Lipids		
Arachidonic acid	<i>Navicula atomus</i> ; <i>Pediastrum boryanum</i> ; <i>Porphyridium sp.</i>	<ul style="list-style-type: none"> • Improves normal growth, visual and functional development in infants • Mediators for resolving inflammation and wound healing • Improve cell membrane fluidity • Regulate nerve impulses, muscle contraction, and hormone secretion by affecting ion channels • Enhance the functional activity of ligand-gated ion channels • Exhibit tumoricidal activities
Docosahexaenoic acid, Eicosapentaenoic acid	<i>Chroomonas mesostigmatica</i> ; <i>Guillardia theta</i> ; <i>Hemiselmis sp.</i> ; <i>Proteomonas sulcata</i> ; <i>Rhodomonas salina</i> ; <i>Storeatula major</i> ; <i>Teleaulax acuta</i> ; <i>Teleaulax amphioxeia</i> ;	<ul style="list-style-type: none"> • Cardiovascular benefits • Mental development • Anti-inflammatory agent • Protect against atherosclerosis • Improve nervous system development and brain functioning

	<i>Rhodomonas baltica</i> ; <i>Pavlova lutheri</i> ; <i>Isochrysis galbana</i>	
Monoacylglycerides	<i>Skeletonema marinoi</i>	<ul style="list-style-type: none"> • Due to the excellent emulsifying properties, preferential in food industries • Present antioxidant, anti-diabetic, and antiatherogenic effects
α -Linolenic acid	<i>Chlorella vulgaris</i> ; <i>Diacronema vlkianum</i> ; <i>Isochrysis galbana</i> ; <i>Haematococcus pluvialis</i> ; <i>Spirulina maxima</i>	<ul style="list-style-type: none"> • Have modest cardioprotective effects • Improve bone health • May offer modest protection against type 2 diabetes • Exhibit neuroprotective properties • Reduce intra-organ fat mass, body weight, and blood triglycerides • Associated with the cancer prevention • Reduce blood pressure; inflammatory markers • Reduce pneumonia and respiratory infections • Improve skin health
Carotenoids		
Astaxanthin;	<i>Chlorococcum</i> sp.; <i>Haematococcus pluvialis</i> ; <i>Chlorella protothecoides</i> ; <i>Scenedesmus</i> sp.; <i>Chlorella zofingiensis</i>	<ul style="list-style-type: none"> • Nutritional supplement • Antioxidant and anticancer agent • Prevent diabetes • Ameliorate cardiovascular diseases • Improve neurodegenerative disorders • Stimulates immunization
β -Carotene	<i>Botryococcus braunii</i> ; <i>Chlamydomonas nivalis</i> ; <i>Chlamydocapsa</i> sp.; <i>Chlorella sorokiniana</i> ; <i>Chlorococcum</i> sp.; <i>Chondria striolata</i> ; <i>Dunaliella salina</i> ; <i>Dunaliella tertiolecta</i> ; <i>Paeonia obovate</i>	<ul style="list-style-type: none"> • Precursor of vitamin A • Improve cognitive functions and skin health • Decrease the occurrence of type 2 diabetes • Antioxidant and antigenotoxic properties • Reduce blood pressure, • Reduce serum malondialdehyde levels and protect unsaturated lipids, thus lowering the oxidative stress • Exhibits radioprotective and antimutagenic activities • Potential chemotherapeutic substance • Inhibit atherosclerosis progression • Increase retinal functioning
Lutein	<i>Chlorella zofingiensis</i> ; <i>Chlorella protothecoides</i> ; <i>Chlorella vulgaris</i> ; <i>Muriellopsis</i> sp.; <i>Haematococcus pluvialis</i> ; <i>Scenedesmus</i> sp.; <i>Chlamydomonas</i> sp.; <i>Auxenochlorella protothecoides</i> ;	<ul style="list-style-type: none"> • Nutritional supplement • Beneficial for eye diseases • Improve age-related macular degeneration and cataract • Anti-oxidant property • Anti-cancer activity

	<i>Coelastrrella sp.</i> ; <i>Galdieria sulphuraria</i> ; <i>Vischeria stellate</i> ; <i>Parachlorella kessleri</i> ; <i>Scenedesmus almeriensis</i>	
Cantaxanthin	<i>Chlamydocapsa sp.</i> ; <i>Chlamydomonas nivalis</i> ; <i>Coelastrrella striolata var. multistriata</i> ; <i>Chlorella vulgaris</i> ; <i>Chlorella zofingiensis</i>	<ul style="list-style-type: none"> • Could be utilized as food color • Anti-oxidant property
Fucoxanthin	<i>Cyclotella cf. cryptica</i> ; <i>Cyclotella meneghiniana</i> ; <i>Cylindrotheca closterium</i> ; <i>Isochrysis aff. Galbana</i> ; <i>Mallomonas sp. SBV13</i> ; <i>Nitzschia cf. carinospeciosa</i> ; <i>Odontella aurita</i> ; <i>Paralia longispina</i> ; <i>Phaeodactylum tricornutum</i>	<ul style="list-style-type: none"> • Decrease hepatic lipid droplet accumulation • Exerts antiobesity effect • Anti-oxidant property • Anti-carcinogenic and anti-inflammatory effects
Zeaxanthin	<i>Dunaliella salina</i> ; <i>Porphyridium cruentum</i>	<ul style="list-style-type: none"> • Antioxidant effects improve skin, eye, liver, and cardiovascular health • Reduce inflammation • Decrease age-related macular degeneration and cataract
Vitamins		
Vitamin A	<i>Chlorella sp.</i> ; <i>Eisenia arborea</i> ; <i>Porphyridium cruentum</i>	<ul style="list-style-type: none"> • Improve reproduction, vision, immune function and cellular communication
Vitamin B	<i>Chlorella sp.</i> ; <i>Spirulina sp.</i> ; <i>Pavlova sp.</i> ; <i>Tetraselmis sp.</i>	<ul style="list-style-type: none"> • Anticancer activity • Reduce cholesterol and cardiovascular disease • Regenerate blood cells and repair DNA • Preserve skin and mucous membranes
Vitamin C	<i>Tetraselmis suecica</i> ; <i>Skeletonema marinoi</i>	<ul style="list-style-type: none"> • Water-soluble vitamin with antioxidant properties • Improve collagen biosynthesis and deposition • Prevent cancer and atherosclerosis
Vitamin E	<i>Dunaliella tertiolecta</i> ; <i>Tetraselmis suecica</i> ; <i>Nannochloropsis oculata</i> ; <i>Chaetoceros calcitrans</i> ; <i>Porphyridium cruentum</i>	<ul style="list-style-type: none"> • Feed supplement • Effective antioxidant and antihypertensive agents • Exhibit anticarcinogenic activities • Promising antimicrobial activities • Prevent neurodegenerative diseases • Improve endothelial function, vascular health and cell growth
Vitamin K	<i>Anabaena cylindrica</i>	<ul style="list-style-type: none"> • Protect against toxic pollutants • Prevent chronic diseases

1.2 Research of lipid drops in microalgae

1.2.1 Biosynthesis of lipid drops

Previously conceived lipids as the cytoplasmic annexation of fat (Bulger and Strum, 1974) are now considered independent organelles with key regulatory roles in energy homeostasis and signalling in multiple organisms, ranging from mammals to plants (Olzmann and Carvalho, 2019; Walther and Farese, 2012). These unique cellular organelles are non-polar, carbon-rich molecules, hydrophobic in nature, and can be stored in subcellular structures. Lipids are also termed lipid droplets (LDs), lipid bodies, oil bodies, oil globules, or oleosomes (Tzen, 2012; Huang, 2018). The biogenesis of LDs, regulation mechanisms and biological fates are still not clearly understood. In microorganisms, the lipid metabolic pathways have been branched out due to the evolutionarily diversified organisms. However, using radioactive tracer and ultrastructural analysis, as well as from the transcriptome, proteome and metabolome profiles of different fungal and higher plants (Merchant et al., 2012; Li-Beisson et al., 2015), pathways for the lipid biosynthesis in green algae have been proposed in some studies (Park et al., 2015; Liu and Benning, 2013; Li-Beisson et al., 2015; Goncalves et al., 2016). Briefly, both the endoplasmic reticulum-derived compartments and the chloroplasts are involved in TAG synthesis, which is tightly regulated by different acyltransferase isoforms (Li-Beisson et al., 2015; Goodson et al., 2011). The step starts in the chloroplast with the subsequent conversion of acetyl-CoA to malonyl-CoA and malonyl acyl carrier proteins (malonyl-ACP), catalysed by acetyl-CoA carboxylase (ACCase) and malonyl-CoA transacylase, respectively. The elongation of acyl chains from the substrates malonyl-ACP and acetyl-CoA is catalyzed by fatty-acid synthase (FAS), which consequently hydrolyze to free fatty acids (FFA) through the actions of fatty-ACP thioesterases (FAT). These fatty acids (FAs) could be used as the building blocks of diacylglycerol (DAG) and chloroplastic TAG synthesis through the acylation of glycerol-3-phosphate (G3P) to serve the

photosynthetic membrane lipids (Goodson et al., 2011). The TAG biosynthesis pathway involves several enzymes, including glycerol-3-phosphate acyltransferase (GPAT), lysophosphatidate acyltransferase and phosphatidic acid phosphatase (PAP) to catalyze G3P into lysophosphatidate (LPA), phosphatidate (PA) and DAG. The catabolic products of FAs can also be transported to cytosol and utilize coenzyme A and long-chain acyl-CoA synthetase (LACS) to synthesize acyl-CoA for more production of TAG through successive elongation and desaturation steps in the endoplasmic reticulum (Fig. 1.1) (Huerlimann and Heimann, 2013; Goncalves et al., 2016).

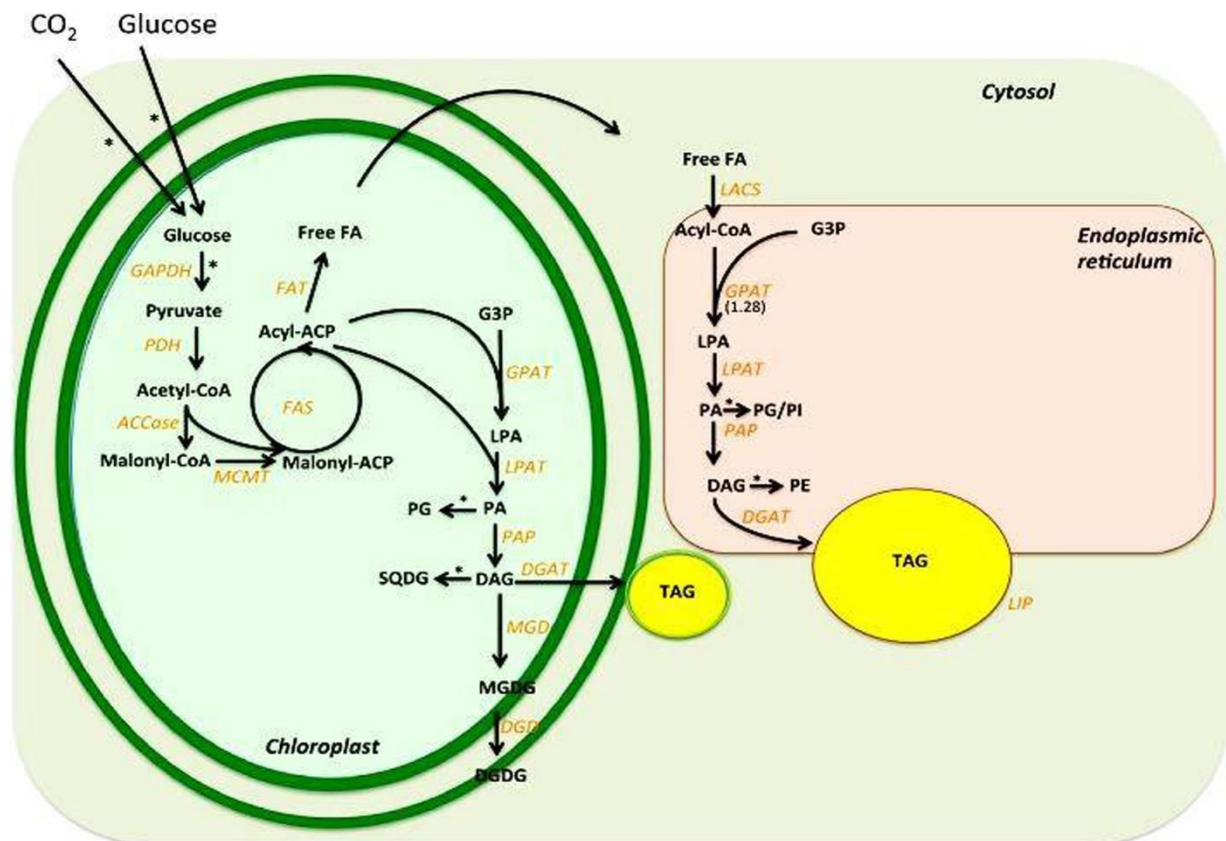


Fig. 1.1 *De novo* triacylglycerol (TAG) biosynthesis in green algae. The enzymes are represented in orange. AADA: alpha amylase domain-containing protein; ACCase: acetyl-CoA carboxylase; ACP: acyl carrier protein; CoA: coenzyme A; DAG, diacylglycerol; DGAT: diacylglycerol acyltransferase; DGD: digalactosyldiacylglycerol synthase; FAT: fatty acyl-ACP thioesterase; FAS: fatty-acid synthase; free FA: free fatty acid; G3P: glycerol 3-

phosphate; GPAT: glycerol 3-phosphate acyltransferase; LACS: long-chain acyl-CoA synthetase; LPA: lysophosphatidic acid; LPAT: lysophosphatidic acid acyltransferase; MCMT: malonyl-CoA:acyl carrier protein malonyltransferase; MGD: monogalactosyldiacylglycerol synthase; PA: phosphatidic acid; PDAT: phospholipid:diacylglycerol acyltransferase; PG: phosphatidylglycerol, SQDG: sulphoquinovosyl diacylglycerol; PI: phosphatidylinositol; PE: phosphatidylethanolamine; PDH: pyruvate dehydrogenase; PAP: phosphatidic acid phosphatase; TAG: triacylglycerol. *: Additional reactions have been omitted for clarity. References for the figure: (Park et al., 2015; Liu and Benning, 2013; Li-Beisson et al., 2015; Goncalves et al., 2016)

1.2.2 Significance of lipid drops in different organisms

LDs function as a storage depot for neutral lipids in most cell types and vary in size based on the species and growing conditions (Lin et al., 2012; Moellering and Benning, 2010). Alongside the storage roles for energy and carbon, lipids act as antioxidants and protective defence molecules to minimize the stress effects (Sun et al., 2018a; He et al., 2015). Recent proteomic advances suggest the direct involvement of several groups of functional proteins in lipid biosynthesis based on cell types (Yang et al., 2012). So far perceived, the main function of LDs is to store energy mainly in the form of highly condensed and compact structures of triacylglycerols in organisms and facilitate surplus energy during adverse and nutrient deficient environmental conditions (Walther and Farese, 2012). The possibilities of changes in buoyancy to facilitate organisms switching the adverse environment towards favourable conditions and the development of defence systems based on the polyunsaturated fatty acids (PUFAs) derived PUAs (diatom-derived polyunsaturated aldehydes) and oxylipins have also been predicted in microorganisms from different studies (Ruocco et al., 2020; Reza et al., 2020; Goncalves et al., 2016). Other complex involvements of LDs in several physiological

functions have also been reported. For example, prior to the inclusion in the dividing nuclei, accumulation of histones at LDs surface during the developmental period has been studied in eukaryotes, while ontogenetic relationships among host lipid droplets and different intracellular pathogens like hepatitis C virus, dengue virus and rotaviruses have been observed (Roingeard and Melo, 2017; Johnson et al., 2018). However, deregulations of LDs can lead to the different physiological dysfunction in organisms.

1.2.3 Lipid drops from microorganisms for human benefits

Over the last few decades, utilization of the plant-based lipids has become controversial due to food-fuel conflicts. Processing lipids from plant-based sources are also expensive and most often requires using toxic chemicals that are environmental hazards (Luterbacher et al., 2014). Therefore, over the period, oleaginous microorganisms like yeast, bacteria and microalgae have gained industrial attention owing to their advantages, such as fast-growing rates, higher oil-yielding capability, the usability of wastewaters and non-arable land, and procurement of high-valued biofunctional compounds (Singh and Olsen, 2011; Phukan et al., 2011; Jones and Mayfieldt, 2012). Generally, triacylglycerols (TAGs), wax esters (WEs), polyhydroxyalkanoates (PHAs) and polyhydroxy butyrate (PHB) from these organisms could be utilized as lipid-based biofuel sources. As an excellent genetic model organism, yeast is used for dynamic LDs research. Nearly all yeast can produce lipids. However, yeast, such as *Yarrowia lipolytica* and *Saccharomyces cerevisiae* can produce TAGs and WEs in large amounts and have been bioengineered to produce PHA/PHB (Ji et al., 2018; Du et al., 2018). Some gram-positive bacteria like *Nocardia*, *Mycobacterium*, *Rhodococcus*, *Dietzia*, and *Streptomyces*, and gram-negative bacteria like *Marinobacter*, *Pseudomonas* sp., and *Acinetobacter* can also produce TAG and WEs under nitrogen starvation and carbon supplementation (Hwangbo and Chu, 2020).

Significant parts of the biofunctional components synthesized in microalgae are identified as lipids and fatty acids. Due to the increasing interest in producing health supplements and renewable energy-, microalgal oil has been focused on intensive research (Liu and Benning, 2013; Merchant et al., 2012). All eukaryotic microalgae examined so far can synthesize lipid molecules, either prior to an impending latency period or exposed to unfavourable stressors (Hu et al., 2008). As the third generation biofuel resources, microalgae have great potential with extenuating advantages of the greenhouse gas emission, high biomass productivity and conversion efficiency of solar to chemical energy (Khan et al., 2018). Several microalgal strains, such as *Scenedesmus obliquus* (Patnaik and Mallick, 2015), *Dunaliella tertiolecta* (Arroussi et al., 2015), *Chlorella vulgaris*, *Spirulina platensis* (Farrokheh et al., 2020), *Chlorococcum parinum*, *Chlorococcum littorale* (Cabanelas et al., 2016), *Nannochloropsis oculata* (Chiu et al., 2009) and *Haematococcus pluvialis* (Hosseini et al., 2020) have been identified as good sources of TAG. Additionally, under hypoxic conditions, *E. gracilis* can produce myristic acid (C14:0) that has a lower freezing point with a good cetane number (66.2), and can be utilized for drop-in jet fuel (Yanowitz et al., 2014). The extent of unsaturation of other PUFAs with more than four double bonds can be reduced by partial catalytic hydrogenation of the oil (Chisti, 2007). The fuel properties can also be improved further by modifying the fatty ester composition for direct combustion in sensitive engines (Knothe, 2009).

The valuable metabolites obtained from these microorganisms are also important for several nutraceutical and pharmaceutical aspects. Dietary inclusion of LC-PUFAs has long been signified and associated with significantly lower risk factors for coronary heart disease and stroke (Sokoła-Wysoczańska et al., 2018; Rimm et al., 2018). This could also aid humans by cutting down the risk factors of cancer and neurodegenerative diseases by balancing the healthy ω -6/ ω -3 ratio (Freitas and Campos, 2019; Avallone et al., 2019). As the building

block precursors of distinguished prostaglandins, thromboxanes, lipoxins, leukotrienes, arachidonic acid (C20:4) and eicosapentaenoic acid (20:5, n-3) can be utilized to treat atopic diseases and asthma (Fussbroich et al., 2020; Balić et al., 2020). Palmitoleic acid (16:1n-7) consumption can also ameliorate obesity, diabetes and hepatosteatosi s (Tricò et al., 2020; Frigolet and Gutiérrez-Aguilar, 2017), whereas omega-6 polyunsaturated fatty acids and linoleic acid (18:2n-6) can prevent hair loss and assist with wound healing (Silva et al., 2018; Guo and Katta, 2017). DHA (22:6n-3) can also boost visual activities and immunity and improve human cognitive functions through the multiplexed cell membrane and cell signalling (Weiser et al., 2016; Sun et al., 2018b; Gutiérrez et al., 2019).

1.2.4 Factors affecting lipid biosynthesis and composition in microalgae

Reasons affecting the lipid biosynthesis in organisms can be classified as exogenous or endogenous factors. Exogenous factors may be relevant to the diet, physical factors, activities, and habitats of the organisms, whereas endogenous factors may associate with the genetic factors, enzymes or hormonal functioning. Generally, manipulating the stress conditions and bioengineering at the genetic level in microalgae can shift the metabolic network towards lipid accumulation (Yang et al., 2018). Nutrient composition, availability of essential carbon sources, light, and temperature are important factors that significantly influence lipid biosynthesis in algae. In addition, changing the cultural condition highly affects microalgal lipid production (Fig. 1.2).

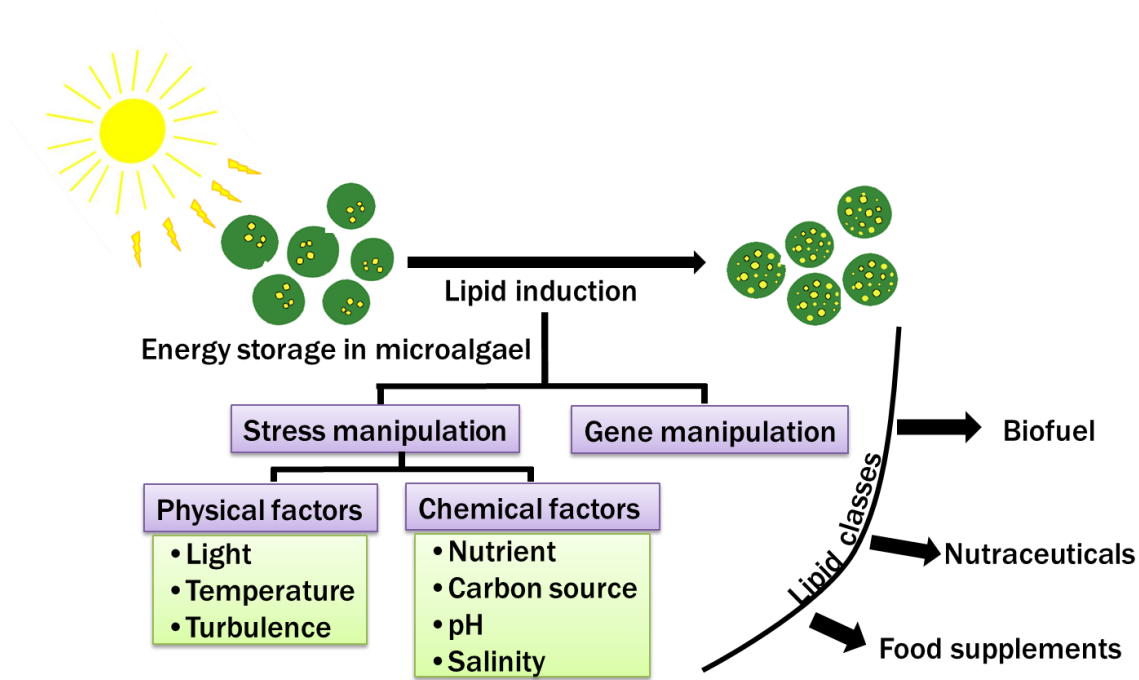


Fig. 1.2 Factors for lipid biosynthesis and lipid composition in microalgae. Depending on the lipid classes, it can be utilized as food supplements, nutraceuticals, or biofuel.

Under photo-oxidative stress or other adverse environmental conditions, the amount of synthesized triacylglycerol (TAG) in these photosynthetic organisms can vary from 20% to 50% of the dry cell weight. In nutrient replete favourable conditions, carbon flux is often directed towards synthesizing macromolecules and other cellular constituents (Szul et al., 2019; Kim et al., 2017). Conversely, in nitrogen-starved conditions, cellular carbon mostly turns to the synthesis of non-N containing compounds, especially lipids, which is expected to increase in different microalgae (Wang et al., 2019; Janssen et al., 2019; Goncalves et al., 2016). Starved conditions with other nutrients like phosphorus and sulphur have also induced lipid in *Scenedesmus* sp. and *Chlamydomonas reinhardtii*, respectively (Yang et al., 2018; Sato et al., 2014). A reflective rise in lipid content in calcium-starved cultures has also been observed in *Chlorella vulgaris* and *Scenedesmus obliquus* (Gorain et al., 2013). In contrast, inhibition in neutral lipid synthesis during nitrogen starvation has been observed due to the

exposure of voltage-gated and ligand-gated Ca²⁺ channel blockers in *Chlorella* sp. (Chen et al., 2014).

Due to the photosynthetic properties of microalgae, autotrophic growth is the most common practice for algae culture, where natural light energy and atmospheric CO₂ can be utilized as the carbon source. However, some limiting factors, such as reduced light penetrability in intensive cultures, difficulties in establishing the desired single species culture, and maintaining environmental parameters, have persuaded researchers to explore mixotrophic and heterotrophic conditions in closed and controlled conditions (Sun et al., 2018a). As the alternative carbon source to support the growth in these conditions, glucose, glycerol and acetate are frequently used for different algal species (Rohit and Venkata Mohan, 2018; Perez-Garcia et al., 2011). Therefore, the species-specific cultural parameters are critical for getting specific lipids from microalgae.

1.3 Potentials and challenges in the study of lipid droplets

The accelerated progress in LD research focuses on determining the links of LDs with prominent diseases in animal models, and triggering the synthesis in photosynthetic organisms as the beneficiary biofunctional products. Nutrient composition, environmental dynamics and hormonal functioning are the key influencers, where large networks of genes and proteins are involved in modelling lipid production. Manipulation of different nutrients, notably nitrogen, carbon, sulphur, potassium, iron and phosphorus, has been studied to increase the lipid biosynthesis in microalgae (Zhu et al., 2016a; Wang et al., 2018; Praveenkumar et al., 2012). However, the applicability of these studies is still contingent upon exploring the interacted signalling pathways, a large number of genes, and growth factors involved in lipid synthesis (Zhu, 2016b; Park et al., 2015).

1.3.1 Common methods applied in modern lipidomics analysis

Despite the challenge of lipidomics analysis due to the lipids diversity (Li et al., 2014a), recent advancements in lipid research with bioinformatics herald significant progress in the analytical chemistry area. Thin-layer chromatography (TLC) (Fuchs et al., 2011), gas chromatography (Fisk et al., 2014), liquid chromatography (Satomi et al., 2017), enzyme-linked immunosorbent assays (ELISA) (Ishihara et al., 2005), nuclear magnetic resonance (NMR) (Li et al., 2017) and mass spectrometry (MS) (Li et al., 2014b) are the most conventional techniques that are widely used to understand lipid dynamics. Although the direct infusion MS strategy does not require previous lipid separation and is relatively less time-consuming than other techniques, spectroscopic approaches do not allow visualization, which is significantly preferable for better understanding lipid synthesis involved with other dynamic biological processes (Li et al., 2014a). Other methods require biological extracts, pre-processing and storage of the samples (Seppänen-Laakso and Oresic, 2009; Furse et al., 2015) that are time-consuming, expensive, and fail to provide information about spatial distribution in *in vivo* conditions.

Electron microscopy and immunofluorescence microscopy are widely used for nanoscale analysis, visualizing LDs morphology, and distribution (Fujita et al., 2010). As the non-invasive and non-destructive methods, Raman microscopy (Abramczyk et al., 2015), coherent anti-stokes Raman scattering microscopy (Jaeger et al., 2016), and direct organelle MS (Horn et al., 2011) are also in current practices. These technologies allow studying the biophysics of LDs, but the requirement of expensive equipment, complex data processing and sample preparations often impede the proper objectives. Sometimes, cells must be fixed, or LDs need to be extracted for further analysis, sacrificing the opportunity to analyze the concurrent dynamics of LDs in integrity.

1.3.2 Common probes in lipid droplets bioimaging, their utilization and disadvantages

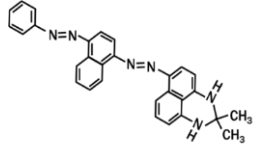
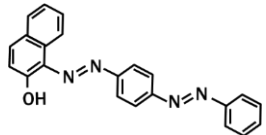
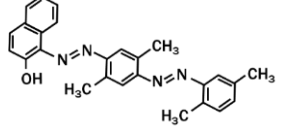
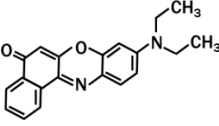
The introduction of microscopy has shaped our comprehension of fundamental research of cells as living units. To interpret dynamic functions and biological interactions at molecular level, microscopic techniques are critical. Advancements in fluorescence microscopy techniques and their large temporal resolution provide us new perception to access sensitive information about lipid organization. The availability of lipid binding probes and fluorophore-conjugated lipids is now opening up possibilities for detailed imaging of lipid drops and intracellular compartments for a superior understanding of the biophysical properties of lipid biology (Zhu et al., 2016c; Lavis, 2017; Klymchenko, 2017). Therefore, these lipid-binding probes are preferred over other techniques for rapid detection and dynamics of LDs (Tatenaka et al., 2019; Maekawa and Fairn, 2014; Daemen et al., 2015).

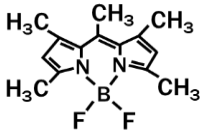
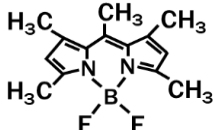
Currently, among the lipid-specific traditional dyes, Sudan Black B ((2,2-dimethyl-1,3-dihydroperimidin-6-yl)-(4-phenylazo-1-naphthyl)diazene) (Subramaniam and Chaubal, 1990), Sudan III (1-(4-(phenyldiazenyl) phenyl) azonaphthalen-2-ol) (Aoki et al., 1997), Oil Red O (1-(2,5-dimethyl-4-(2,5-dimethylphenyl) phenyldiazenyl) azonaphthalen-2-ol) (Koopman et al., 2001) are used in brightfield microscopy. Sample preparation techniques with these dyes are time-consuming and require the usage of ethanol or isopropanol as the solvent. Varying filtration conditions and alterations of LDs morphologies during fixative stages often lead to inconsistent results that are major constraints for these dyes (Ohsaki et al., 2010; Elle et al., 2010).

Nile Red (9-diethylamino-5H-benzo[a]phenoxazine-5-one) (Greenspan et al., 1985), BODIPY 493/503 (4,4-Difluoro-1,3,5,7,8-Pentamethyl-4-Bora-3a,4a-Diaza-s-Indacene) and BODIPY 505/515 (4,4-difluoro-1,3,5,7-tetramethyl-4-bora-3a,4a-diaza-s-indacene) (Thermo Fisher Scientific BODIPY 505/515, 2019; Thermo Fisher Scientific BODIPY 493/503, 2019)

are well recognized, and extensively used as commercial fluorophores for fluorescent microscopy. Depending on environment polarity, the emission of Nile Red varies greatly from deep red to strong yellow-gold colour (yellow-gold fluorescence: $\lambda_{\text{ex}} = 450\text{-}500\text{ nm}$ and $\lambda_{\text{em}} = \geq 528\text{ nm}$; red fluorescence: $\lambda_{\text{ex}} = 515\text{-}560\text{ nm}$ and $\lambda_{\text{em}} = \geq 590\text{ nm}$) (Greenspan et al., 1985). A decrease in the surrounding polarity might result in a blue-shifted emission peak for Nile Red, whereas broad absorption and emission spectra often cause overlapping of the signals between the yellow and red spectra (Else et al., 2007; Dutta et al., 1996). These properties also make the dye challenging to utilize for multicolour imaging purposes. Additionally, other proteins and nonlipid cellular structures with hydrophobic domains are often reported to affect the studies with the Nile Red (Brown et al., 1995). Compared to Nile Red, BODIPY 493/503 and BODIPY 505/515 are less affected by the surrounding polarity and pH, and are more suitable for LDs studies. However, sometimes BODIPY can bind unselectively with the mitochondrial, plasma, and nuclear membranes (Daemen et al., 2015). Additionally, dye acquisition with BODIPY and Nile Red requires extreme caution since lower concentrations can cause photobleaching issues, and a slightly higher concentration or lower-level competencies during washing steps could engender marked background signals and result in ineffective lipid studies (Spangenburg et al., 2011; Collot et al., 2018). Some commercially available lipid-specific dyes have been enlisted in Table 1.2.

Table 1.2 Properties of some commercially available lipid-specific dye

Commercial dyes for conventional bright-field microscopy				
Indicator	Chemical structure	Solubility	Notes	
Sudan Black B	 <p>Chemical formula: C₂₉H₂₄N₆ MW: 456.553</p>	C ₆ H ₅ OH, C ₂ H ₅ OH, C ₃ H ₆ O, C ₆ H ₆ , C ₇ H ₈	<ul style="list-style-type: none"> • Nonfluorescent • Can stain other materials, therefore not so lipid specific • Used to distinguish haematological disorders, fingerprint enhancement 	
Sudan III	 <p>Chemical formula: C₂₂H₁₆N₄O MW: 352.39</p>	CHCl ₃ , C ₇ H ₈ (1 mg/mL). H ₂ O (< 0.1 mg/mL) C ₂ H ₅ OH (2 mg/mL). C ₃ H ₈ O (Saturated solutions)	<ul style="list-style-type: none"> • Emit red fluorescence, therefore occasionally permit for fluorescence microscopy • Poor solubility often requires the use of ethanol or isopropanol • Might cause the disruption and fusion of lipid drops 	
Oil Red O	 <p>Chemical formula: C₂₆H₂₄N₄O MW: 408.49</p>	C ₂ H ₅ OH:CHCl ₃ (1:1)	<ul style="list-style-type: none"> • Emit red fluorescence, therefore occasionally permit for fluorescence microscopy • Poor solubility often requires the use of ethanol • Might cause the disruption and fusion of lipid drops 	
Commercial dyes for fluorescent microscopy				
Indicator	Chemical structure	$\lambda_{\text{ex}} / \lambda_{\text{em}}$ (nm)	Solubility	Notes
Nile Red	 <p>Chemical formula: C₂₀H₁₈N₂O₂ MW: 318.37</p>	λ_{ex} : 450-500, λ_{em} : > 528; λ_{ex} : 515-560, λ_{em} : > 590	MeOH, C ₂ H ₅ OH, C ₃ H ₈ O ₂ , C ₃ H ₇ NO, DMSO	<ul style="list-style-type: none"> • Due to the wide absorption and emission spectra, unsuitable for multicolor imaging • Highly sensitive to the environmental polarity • Yellow gold fluorescence in nonpolar condition; Red fluorescence in polar condition • Photobleaching might cause by self-decomposition • Unselective binding might occur with cellular structures having hydrophobic domain

BODIPY 493/503		λ_{ex} : 493; λ_{em} : 503	C ₂ H ₅ OH, DMSO	<ul style="list-style-type: none"> • Due to self-quenching and aggregation at higher concentrations, fluorescence might be diminished
BODIPY 505/515		λ_{ex} : 505; λ_{em} : 515	C ₂ H ₅ OH, DMSO	<ul style="list-style-type: none"> • Due to self-quenching and aggregation at higher concentrations, fluorescence might be diminished
Chemical formula: C ₁₄ H ₁₇ BF ₂ N ₂ MW: 262.1085				
Chemical formula: C ₁₃ H ₁₅ BF ₂ N ₂ MW: 248.0817				

1.4 Reactive oxygen species and their significance

Microalgae possess a wide range of polysaccharides, lipids, proteins, antioxidants, vitamins, and pigments. These biomolecules synthesizing machinery could be triggered by genetic manipulation, changes in environmental conditions, or exposing the organisms to different stress conditions (Gong and Bassi, 2016; Singh et al., 2016). Up to date, most of the studies are associated with the elucidation of lipid and fatty acid composition and their metabolic pathways (Sun et al., 2018a; Kumari et al., 2013; Goncalves et al., 2016; Gimpel et al., 2015). Focusing on the highly transformed molecules in these organisms during stress exposure could be a practical approach to modifying the conditions for more lipid production. The stress-based strategies are often accompanied by the formation of reactive oxygen species (ROS) that are the oxygen derivatives comprising hydrogen peroxide (H₂O₂), hydroxyl ions (OH⁻), superoxide anions (O²⁻), and their secondary reaction products (Sun et al., 2014; Zhang et al., 2019). The paradox of ROS homeostasis in organisms underlies the mechanism to preserve the cellular integrity, development, defence processes, and cell death (Rovira and Finkel, 2008; Bhattacharjee, 2012). Nonspecific and biochemical reactions of ROS with the fundamental biological molecules at higher concentrations cause cellular alteration that might

lead to oxidative damage, organelle dysfunction and mutagenesis (Tripathi et al., 2020). However, recent evidence suggests the provision of low levels of ROS as signaling molecules in several fundamental biological processes. It is also assumed that during the respiration and photosynthesis in the photosynthetic organisms, ROS produced from the electron transport reactions avail the defence measures to ameliorate the oxidative stress (Tripathi et al., 2020). Additionally, extensive quenching and scavenging mechanisms of these microorganisms also alleviate the effects of ROS (Mattila et al., 2015; Pospíšil, 2012). Regulatory roles of ROS molecules have also critically been observed in cell differentiation (Aguirre et al., 2005), immune responses (Weinberger, 2007), ion acquisition (Garg et al., 2007; Liu et al., 2007), growth and reproduction in different organisms (Armoza-Zvuloni et al., 2016; Tsukagoshi et al., 2010; Zafra et al., 2010). In order to upstream the yields of the beneficiary biomolecules from microalgae, further realizing the ROS interventions during their bioaccumulation processes could radically improve the efficiency and accuracy of these technologies.

1.5 Production of ROS in microalgae

As an integral part of the metabolic byproduct of numerous enzymatic reactions, ROS generation in different physiological and developmental processes in plants has already been well established (Vavilala et al., 2015; Ma et al., 2014; Hernández-Barrera et al., 2015). Although generated ROS could differ among organisms based on the genetic, physiological and environmental factors, as the phototrophic organisms, overlaid characteristics of plants and microalgae could make a common ground to understand the fate of ROS in photosynthetic organisms (Ugya et al., 2020). Generally, ROS is formed in the mitochondria, chloroplasts, peroxisomes, cytosol, and plasma membrane due to the inexorable electrons leakage onto molecular oxygen (Rezayian et al., 2019).

1.5.1 ROS generation from mitochondria

Equilibrium between ROS generation and cell utilization is critical to rolling out the multiplexed functioning of ROS and avoiding the toxic effects. Since mitochondria are the major sites of O₂ consumption (~90%), they are the key sources of internal ROS production (Hopkins, 2016). In a natural state, electron leakage from the mitochondrial complex I (NADH: ubiquinone oxidoreductase) and complex III (ubiquinol:cytochrome c oxidoreductase) is ~1% of the upsurge during the oxidative stress and increases ROS accumulation (Anderson et al., 2011). Being one of the leading sites of electron leakage, complex I is most accountable for the produced superoxide (O₂⁻) (Grivennikova and Vinogradov, 2006). Oxidation of NADH and succinate by Complex I and Complex II can generate electrons that reduce ubiquinone to ubiquinol in the mitochondrial membrane. In the intermembrane space, electrons are transported from ubiquinol to cytochrome c, and from cytochrome c to molecular oxygen (O₂) through the complex III and complex IV (cytochrome c oxidase), respectively (Fig. 3). During this process, O₂⁻ generates due to the reduction of O₂ into H₂O in the mitochondrial matrix (Dröse and Brandt, 2012). Subsequently, generated O₂⁻ backup the electrons in cytochrome b, accumulate semiquinone radical at the ubiquinol oxidation centre of complex III, and transfer the electron to engender O₂ from oxygen (Bleier and Dröse, 2013).

1.5.2 ROS generation from chloroplasts

To support their metabolic activities, photosynthetic organisms use sunlight to fuel energy. Chloroplasts are the explicit organelles where the conversion processes of light to chemical energy occur. In chloroplasts, most of the ROS are generated in the reaction centres of photosystem I (PSI) and photosystem II (PSII) at the time of photoreduction of oxygen (Fig. 3) (Nishiyama et al., 2011). During photosynthesis in microalgae, water photooxidizes, and NADP⁺ is reduced to NADPH, resulting in electrons transfer through PSII, cytochrome b₆t (Cyt b₆t) complex and PSI. Electrons leaked during this process react with O₂ and

consequently form O_2^- and H_2O_2 (Larosa et al., 2018; Karash and Kwon, 2018). Produced H_2O_2 subsequently reacts with the available nutrients, specifically Cu^{2+} and Fe^{3+} to form hydroxyl (OH) radicals (Karash and Kwon, 2018).

1.5.3 ROS Production in the endoplasmic reticulum

The endoplasmic reticulum (ER) is the membrane system within the cytoplasm of algal cells, where secretory, and membrane proteins are synthesized and folded (Ozgur et al., 2014). Proteins that do not fold properly can be accumulated in ER and promote catabolic processes to aid cellular homeostasis through autophagocytosis (Pérez-Martín, 2014). Although the types and quantities of proteins vary among organisms, phylogenetic analysis has revealed that proteins like PDIs (protein disulfide isomerases) synthesized in the ER are highly conserved among unicellular algae, plants, and multicellular organisms (Yang et al., 2014; Shimizu and Hendershot, 2009). This enzyme introduces disulfide bonds between cysteine residues in the course of folding of client proteins. During this process, an oxidoreductase enzyme, ER oxidoreductin 1 (ERO1) plays a critical role in keeping PDI active and oxidized in the ER. For every disulfide bond, ERO1 can reduce oxygen to produce H_2O_2 (Fig. 1.3) (Pérez-Martín, 2014; Cheng and Yang, 2011).

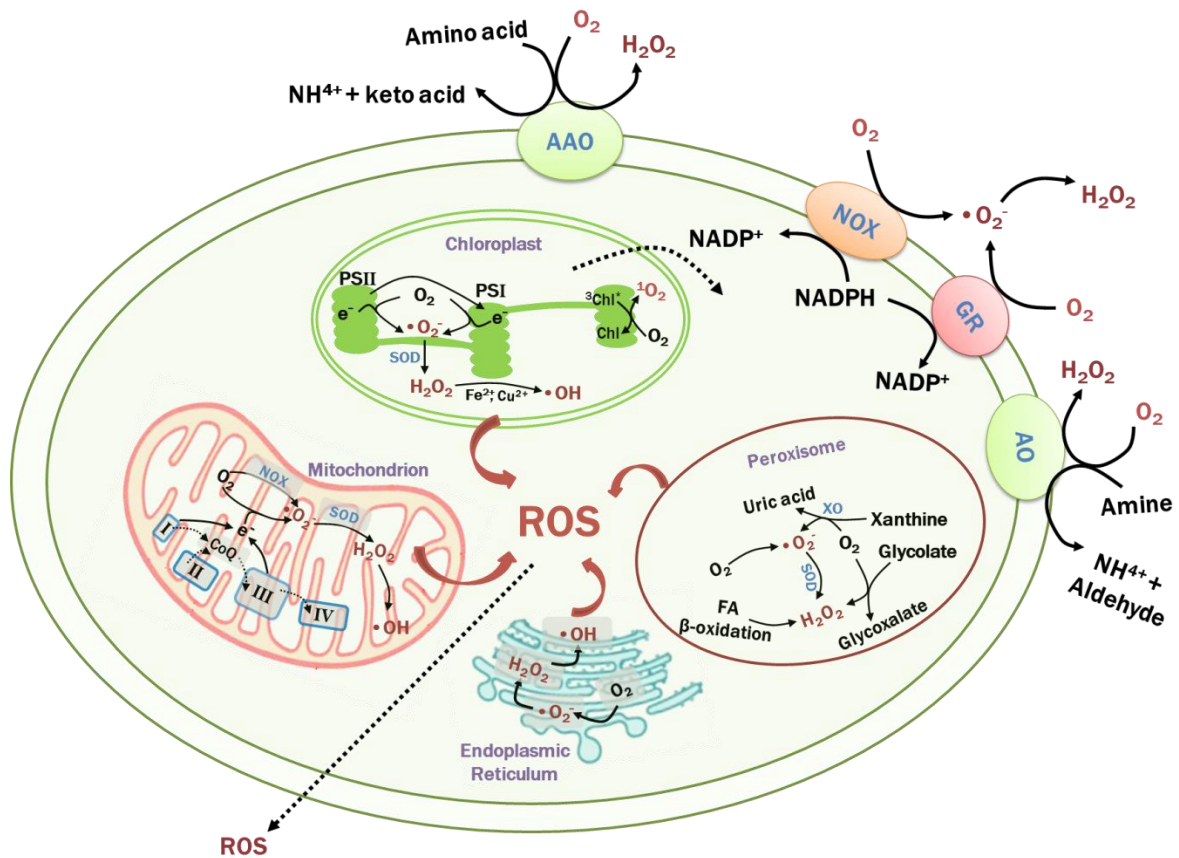


Fig. 1.3 Simplified representation of the intracellular and extracellular reactive oxygen species synthesis sites in phytoplankton. Superoxide and hydrogen peroxide form through the transmembrane and outer-membrane enzymes. Hydrogen peroxide also forms via dismutation of superoxide (solid arrows) and is transported across biological membranes. Solid arrows reflect chemical reactions; dashed arrows indicate transport. In the mitochondrion, I, II, III and IV indicate Complex I, Complex II, Complex III and Complex IV, respectively. PSI and PSII in chloroplast indicate photosystem I and photosystem II, respectively. Additional abbreviations: AAO, amino acid oxidase; AO, amine oxidase; GR, glutathione reductase; HOX, hexose oxidase; NOX, NADPH oxidase; XO, xanthine oxidase. For reference, Zhang et al. (2020a)

1.5.4 Peroxisomes, plasma membrane and cell wall as the sources of ROS

Peroxisomes are dynamic and metabolically active complex organelles involved in different cellular processes, including development, photomorphogenesis and stress responses. Due to the presence of oxidases and their parts in metabolism, H_2O_2 and several superoxide radicals are produced in these organelles (Fig. 3) (Sandalio and Romero-Puertas, 2015; del Río et al., 2006). The major pathways for the production of H_2O_2 in peroxisome are the photorespiratory reaction of glycolate oxidase (GO), fatty acid β oxidation, enzymatic dismutation of O_2^- , and the actions of flavin oxidases (FO) (Sandalio et al., 2013). ROS, such as O_2^- and H_2O_2 are also produced in the cell wall and plasma membrane of photosynthetic organisms in a highly regulated manner. Enzymes like NADPH oxidase and quinone reductase have been accredited to O_2^- formation that subsequently dismutates to H_2O_2 by superoxide dismutase (SOD) (Ugya et al., 2020).

1.6 Putative roles of ROS in biomolecules synthesis

Recently, several stress-based strategies have been adopted to induce the synthesis of essential biomolecules in microalgae (Tang et al., 2016; Sivaramakrishnan and Incharoensakdi, 2017). However, microalgae have also developed highly controlled molecular machineries to thrive in diversified environmental conditions (Lushchak, 2011). During exposure to the stressors, algal cells regulate oxidative metabolism, ROS production, and biosynthesis of several essential biomolecules to ameliorate oxidative damage (Schieber and Chandel, 2014; Imlay, 2003).

A general rise in bioaccumulation of various antioxidant components has been manifested during the exposure of microalgae to various stressors (Sun et al., 2014; Mullineaux et al., 2018). In a natural state, oxidative damage in algae is minimized by the collective activities of SOD and the enzymes, such as ascorbate peroxidase, glutathione reductase, and

dehydroascorbate reductase, as shown in Fig. 1.4. Among the non-enzymatic components, flavonoids, carotenoids, glutathione, tocopherols, ascorbate, and phenols are the essential antioxidants in the cellular defence system against ROS (Rezayian et al., 2019). Due to the absence of other catalases in chloroplasts, ascorbate peroxidase plays a critical role in removing the H_2O_2 , whereas, in other parts, it is degraded by catalases. Intracellular reduction to the functional form of glutathione (GSH) is carried out by glutathione reductase (GR) in the presence of NADPH. By transporting the electrons and transferring the excitation energy, enzymatic and non-enzymatic antioxidants can minimize the damaging effects of ROS (Xia et al., 2018; Pikula et al., 2019).

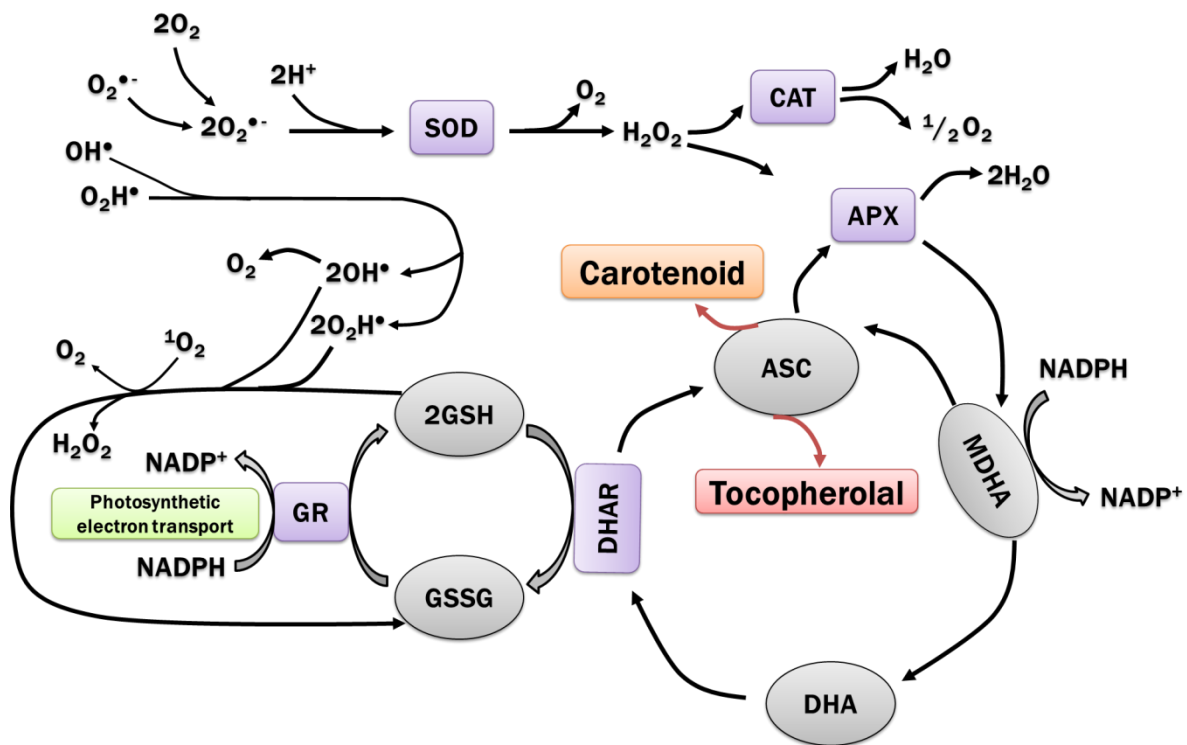


Fig. 1.4 Projected mechanistic pathway for the ROS involvement with the synthesis of enzymatic and non-enzymatic antioxidants from algae. ASC, Ascorbate; APX, Ascorbate peroxidase; CAT, Catalase; DHA, Dehydroascorbate; GSH, Glutathione; GR, Glutathione reductase; GSSG, glutathione disulfide; MDHA, Monodehydroascorbate; SOD, Superoxide

dismutase; DHA, Dehydroascorbate reductase. Part of the figure comes from Garcia et al. with modifications.

In microalgae, different stress conditions shift the metabolic network towards lipid accumulation (Yang et al., 2014; Tan and Lee, 2016). Alongside their storage roles for energy and carbon, these lipids act as antioxidants and protective defence molecules to minimize stress (Sun et al., 2018a; He et al., 2015). From previous studies, increased lipid accumulation has been associated with augmented antioxidant defence mechanisms and alleviated intracellular ROS levels (Yilancioglu et al., 2014; Sun et al., 2018b; Menon et al., 2013). Correlations among ROS, calcium (Ca^{2+})-ATPase activity (Zhang et al., 2017; Hu et al., 2007; González et al., 2010), most antioxidant components, such as superoxide dismutase 4 (SOD4), cytosolic ascorbate peroxidase (cAPX), and glutathione reductase 1 (GR1), the chloroplastic and cytosolic antioxidant enzymes, and glutathione cycle are also evident from previous studies (González et al., 2010). During stress-induced lipid synthesis, Ca^{2+} signatures are also generated by the cells from the phospholipid and chloroplast localized glycolipid precursors (Reza et al., 2021), plasma membrane-localized Ca^{2+} channels or the intracellular calcium pool through the mitochondria (Hu et al., 2007; González et al., 2010; Chen et al., 2011) (Fig. 1.5).

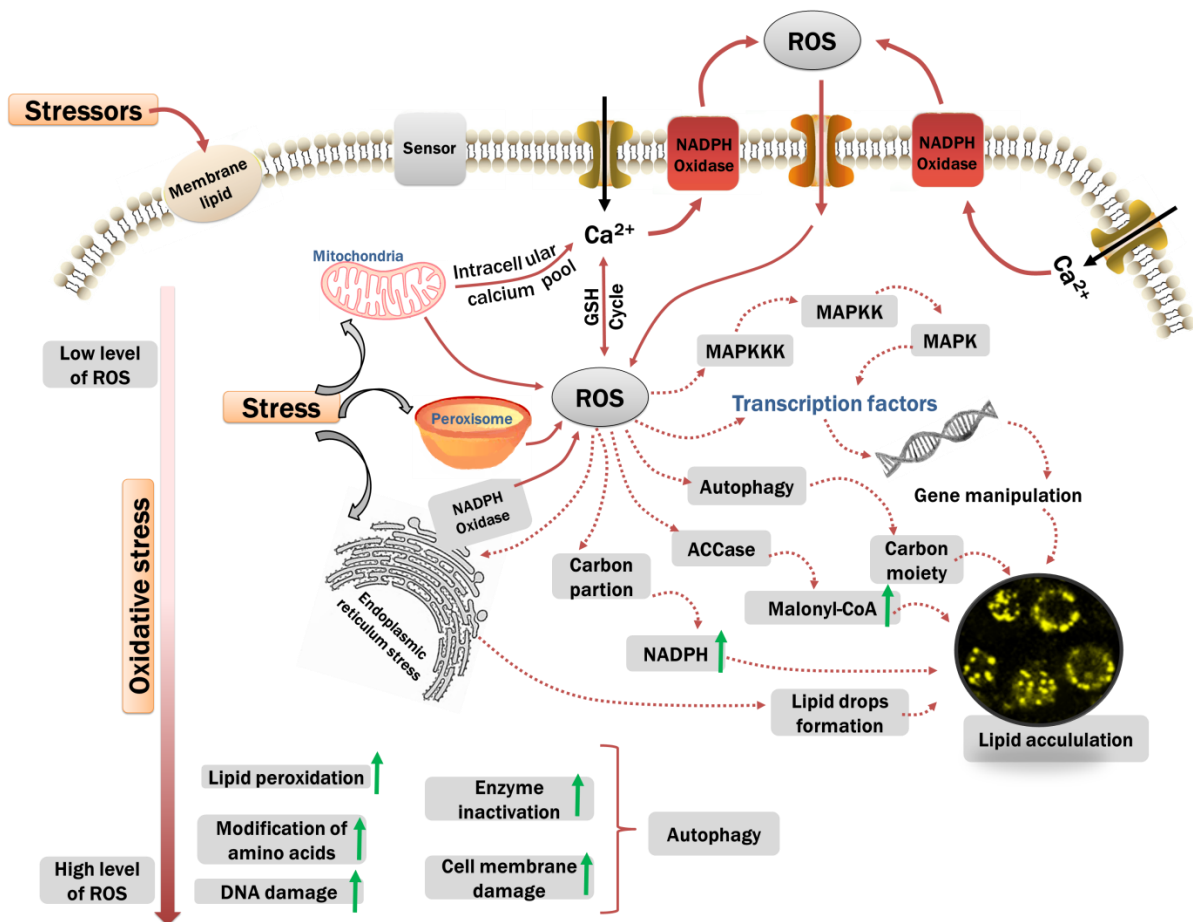


Fig. 1.5 A possible link between lipid biosynthesis, calcium signaling and reactive oxygen species (ROS)-mediated stress response in a eukaryotic cell (NADPH, nicotinamide adenine dinucleotide phosphate; ROS, reactive oxygen species; MAPK, mitogen-activated protein kinase; MAPKK, MAPK kinase; MAPKKK, TF, transcription factor; RR, response regulator; ER, endoplasmic reticulum; Green arrows, stress sensing; ACCase: acetyl-CoA carboxylase; Brown-arrows, biosynthesis of ROS; Broken brown-arrows, ROS signal transduction for ROS-induced lipid accumulation; Green arrows, induced conditions of relevant factors (Zhu, 2016; Hagiwara et al., 2016).

1.7 Current approaches for the detection of ROS molecules

1.7.1 ROS analysis with traditional technologies

Despite the importance of ROS in the biological system, their accurate measurements are very challenging owing to their intrinsic properties like lifetime, diffusion rate, ways of production and generation factors. Currently, electron spin resonance (ESR), mass spectrometry (MS), spectrophotometry, fluorescence spectroscopy, high-performance liquid chromatography (HPLC), and electrochemical techniques are in place for ROS analysis. These techniques have advantages, but none of these methods is without drawbacks. For instance, the reaction processes, sample preparation and analyzing the reaction products in chromatography are so complicated that regardless of their rapid and sensitive detectability to specific ROS, their broad utilizations are still limited. Comparatively, the spectrophotometric methods are time-efficient and have been used to semi-quantify free radicals from the absorbance differences of the substrates and products. However, sometimes the detection of the reduction products is less sensitive and selective, and low levels of the radicals are out of their detection limit.

In some cases, specific inhibitors or scavengers are required to eliminate radicals (Zhang et al., 2018; Tarpey et al., 2004). For example, electrochemical biosensors formed by the alternating layers of cytochrome *c* and poly(aniline(sulfonic acid)) on a gold wire electrode allow O_2^- quantification sensitively and selectively, but the protein for coating the electrode surface is very limited, therefore unsuitable for commercial purposes. Additionally, the number of coating layers and compositions of the proteins are experiment specific and need to be designed for a study (Zhang et al., 2018). Moreover, electron spin resonance (ESR) directly identifies oxygen free radicals by stabilizing them by creating spin traps. However, different factors, such as pH, temperature, and environmental factors, highly affect the energy

levels of radicals. Therefore, extreme caution is required to get consistent results (Berliner, 2016). Furthermore, the additional high expense of the ESR assay significantly limits the wide range of utilization of ESR.

In using redox-dependent fluorescence spectral and structural changes in proteins under oxidized conditions, several fluorescent protein-based redox probes have been designed to study the redox states of targeted organelles. These molecules could facilitate real-time recognition and active status of the redox-dependent changes through reversible reactions mediated by the radicals without permeability difficulties (Breckwoldt et al., 2015). However, fluorescent protein-based methods are also not without limitations. The preparation of these probes is often complicated, and expression levels could be affected by the target cell types, leading to inconsistent outcomes. Additionally, fluorescence from different cells could be picked up during microscopy, hindering the analysis of a large volume of cells. Using a flow cytometer or fluorescent microplate readers limits the possibilities of getting the information at cellular or subcellular levels. Considering these factors, fluorescence microscopy using ROS-specific fluorescent dyes has emerged as a powerful tool and more preferential to the researchers for rapid analysis of ROS.

1.7.2 Commercial fluorescent dyes for ROS detection

Fluorescence imaging is a non-invasive study method of biological molecules and has become prevalent due to its greater sensitivity, fast responsiveness, and higher spatial resolution. Among the traditional ROS-specific fluorescent dyes, 2',7'-dichlorodihydrofluorescein diacetate (H₂DCFDA) and its derivatives, dihydroethidium (DHE) and Amplex Red are commonly used to measure the intracellular redox states. H₂DCFDA is a nonpolar and nonionic probe hydrolyzed to the 2',7'-dichlorodihydrofluorescein (DCFH) by esterases upon crossing the cell membrane.

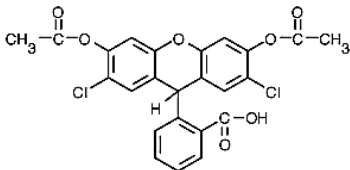
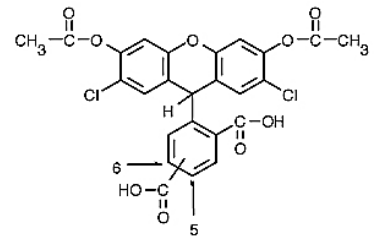
Subsequently, it is oxidized by the cellular ROS to generate the fluorescent 2',7'-dichlorofluorescein (DCF). The fluorescence intensity of DCF indicates the level of oxidative stress (Wang and Joseph, 1999). Further modifications of H₂DCFDA into its carboxylated derivatives, 6-carboxy-2',7'-dichlorodihydrofluorescein diacetate (carboxy-H₂DCFDA) and di(acetoxymethyl ester) (6-carboxy-2',7'-dichlorodihydrofluorescein diacetate) offer additional negative charges to improve its cellular retention ability. However, several complications may arise during the *in vivo* use of this probe. The specificity of the probe has already been questioned as several studies have reported interference from other free radicals, such as HOCl, NO₂⁻, ONOOH and ONOO⁻ while using this probe. Cell-specific permeability and variations of cellular esterase activities also could make it difficult to adjust the dye concentration. Additionally, reactions of the intermediary products of H₂DCFDA with oxygen and other factors like cytochrome c, hematin, peroxidases, and ferrous ions could generate ROS to give false impressions about the study (Zhang et al., 2018; Folkes et al., 2009). Therefore, experimental and analytical methods must be scrutinized to incorporate this dye in cellular ROS studies. Other cell-permeable traditional dihydro-compounds included are dihydrorhodamine 123 (DHR123) and its stable salt form dihydrorhodamine 123 dihydrochloride (Henderson and Chappell, 1993; Biotium Dihydrorhodamine 123, Dihydrochloride Salt, 2021); dihydrorhodamine 6G) (Wersto et al., 1996), and 10-acetyl-3,7-dihydroxyphenoxazine (AmplexRed) (Zhou et al., 1997).

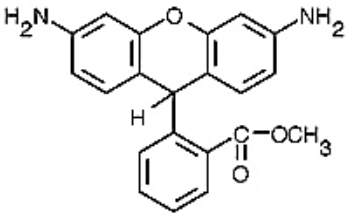
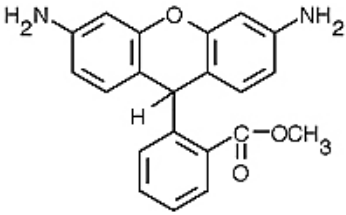
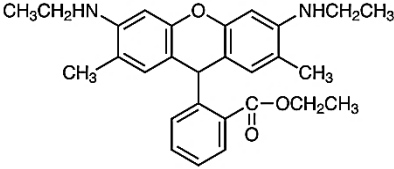
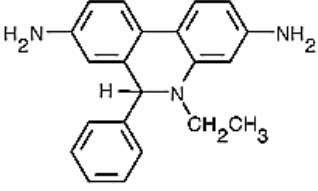
Dihydrorhodamine 123 (2-(3,6-diamino-9H-xanthen-9-yl)-benzoic acid, methyl ester) is an uncharged ROS indicator to passively diffuse through the cell membranes. After entering the cells, the cellular redox system extracts this non-fluorescent dye into fluorescent rhodamine 123. Following oxidation, rhodamine 123 accumulates in mitochondrial membranes that can be detected under fluorescent microscopy. Moreover, DHE, after entering the cells, is generally oxidized by intracellular O₂⁻ and produces 2-hydroxyethidium (2-OH-E⁺) to emit

red fluorescence (λ_{em} : 534) upon excitation at 500-530 nm. However, this fluorophore can also be non-specifically oxidized by $\cdot\text{OH}$, H_2O_2 and OONO^- and produce ethidium (E^+) to emit red fluorescence at 576 nm upon excitation at 480 nm. Therefore, the distinguished measurement of ROS often becomes difficult during *in vivo* analysis, and requires utilizing other analytical methods like HPLC and LC-MS to confirm the obtained oxidized products (Zhao et al., 2005; Fink et al., 2004). Additionally, different reaction stoichiometry between DHE and $\text{O}_2^{\cdot-}$ in different cell types often leads to the unpersuasive details of the generated 2-OH- E^+ (Zielonka et al., 2005). Although these dihydro-compound derivatives have been utilized for ROS detection, their usage can be affected by higher photosensitivity and autoxidation that might give false results (Soh, 2006; Afzal et al., 2003).

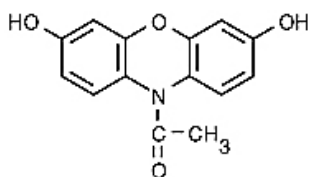
Among the traditional probes, AmplexRed is relatively more stable, H_2O_2 specific, and can detect as little as 10 picomoles of H_2O_2 . In horseradish peroxidase (HRP), this reagent reacts with H_2O_2 and produces the red-fluorescent oxidation product with an excitation and emission maxima of 571~585 nm. However, while accompanying ONOO^- or other radicals that induce the synthesis of ONOO^- , it can increase the catalysis of HRP, resulting in higher resorufin production than H_2O_2 (Dębski et al., 2016). Reactions among HRP, NADPH and reduced glutathione can also produce additional H_2O_2 , and mislead the experimental results. Moreover, the end fluorescent product resorufin could also be reduced by NADPH-CYP450 reductases to $\text{O}_2^{\cdot-}$ and H_2O_2 and loss its fluorescence, which might give a false result (Votyakova and Reynolds, 2004). Lower affinity to the cell membrane can also impede the measurement accuracy of intracellular H_2O_2 (Dikalov et al., 2007). Some commercially available ROS-specific dyes are enlisted in Table 1.3 for comparison.

Table 1.3 Properties of some commercially available ROS-specific dyes

ROS-specific commercial dyes for fluorescent microscopy				
Indicator	Chemical structure	$\lambda_{\text{ex}} / \lambda_{\text{em}}$ (nm)	Solubility	Notes
H ₂ DCFDA	 <p>Chemical formula: C₂₄H₁₆Cl₂O₇ MW: 487.29</p>	λ_{ex} : ~492-495; λ_{em} : 517-527	DMSO, DMF, C ₂ H ₅ OH	<ul style="list-style-type: none"> • Nonpolar and nonionic probe • Nonfluorescent molecule; upon hydrolysis and oxidation by esterases and ROS becomes fluorescent • Sensitive to other free radicals, such as HOCl, NO₂⁻, ONOOH and ONOO⁻ • Air sensitive; storage conditions require dry argon or nitrogen
Carboxy-H ₂ DCFDA	 <p>Chemical formula: C₂₅H₁₆Cl₂O₉ MW: 531.302</p>	λ_{ex} : ~492-495; λ_{em} : 517-527	DMSO, DMF, C ₂ H ₅ OH	<ul style="list-style-type: none"> • After hydrolyzed by esterases and oxidized by cellular ROS, the nonfluorescent probe becomes fluorescent • Better cellular retention ability than H₂DCFDA • Sensitive to other free radicals, such as HOCl, NO₂⁻, ONOOH and ONOO⁻ • Air sensitive; storage conditions require dry argon or nitrogen

Dihydrorhodamine 123		λ_{ex} : 504; λ_{em} : 534	DMSO, HCl, DMF, C ₂ H ₅ OH <ul style="list-style-type: none"> • Inappropriate for single-cell observation • More suited to detect H₂O₂ and intracellular peroxidases • Highly photosensitive and prone to autoxidation
Dihydrorhodamine 123 dihydrochloride		λ_{ex} : 500-507; λ_{em} : 529-536	DMSO, HCl, DMF, C ₂ H ₅ OH <ul style="list-style-type: none"> • Inappropriate for single-cell observation • More suited to detect H₂O₂ and intracellular peroxidases • Relatively more stable towards air oxidation and light than dihydrorhodamine 123
Dihydrorhodamine 6G		λ_{ex} : 528; λ_{em} : 551	DMSO, DMF <ul style="list-style-type: none"> • Oxidation of the probe by the cellular redox systems produces fluorescent rhodamine 6G • Air Sensitive, heat Sensitive; storage condition requires -20 °C
Dihydroethidium		λ_{ex} : 518; λ_{em} : 606	DMSO, DMF <ul style="list-style-type: none"> • Exhibit blue fluorescence in the cell cytosol upon oxidation due to DNA intercalation emitting red fluorescence • Light sensitive, storage condition requires -20 °C in nitrogen or argon • Requires additional analysis with HPLC and LC-MS to confirm the oxidized products.

AmplexRed



Chemical formula: C₁₄H₁₁NO₄

MW: 257.25

λ_{ex} : 571;

λ_{em} : 585

DMSO,

DMF

- Detect trace amounts of hydrogen peroxide (as little as 10 picomoles)
- Air sensitive, heat sensitive; storage condition requires -5 to -20 °C
- In the presence of horseradish peroxidase (HRP) it produces highly fluorescent resorufin
- ONOO⁻, or the presence of radicals that induce the synthesis of ONOO⁻ can increase the catalysis of HRP, yielding resorufin at a faster rate than H₂O₂
- HRP can react with NADPH, reduce glutathione, and produce H₂O₂ that can give a false impression
- Lower affinity to the cell membrane impede accurate measurement of the intracellular H₂O₂

1.8 Fluorophores targeting H₂O₂ in different organelles

Compared to other ROS, H₂O₂ is stable and can pass across the phospholipid bilayer via aquaporins (Reczek and Chandel, 2015). Therefore, many studies have focused on H₂O₂ as a messenger molecule and an oxidative stress marker (Miller et al., 2007; Dickinson and Chang, 2011). In higher vertebrates, many complex biological systems such as immunity, wound healing, and stem cell proliferation are linked to H₂O₂ (Niethammer et al., 2009; Haskew-Layton et al., 2010), whereas the unusual increase of this ROS can cause several health disorders (Lisanti et al., 2011; Giorgio et al., 2007; Finkel et al., 2007). A controlled

surge in the mitochondrial H_2O_2 production can improve cells' growth, differentiation, and survival (Poole and Nelson, 2008; D'Autréaux and Toledano, 2007). To understand the H_2O_2 -specific complex systems in healthy and pathological conditions, visualization techniques of H_2O_2 are crucial.

The recent development of mitochondria targeting H_2O_2 -specific dye, Mitochondria Peroxy Yellow 1 (MitoPY1) enables us to measure the amount of H_2O_2 in the mitochondria of living cells (Dickinson and Chang, 2011). A chemoselective boronate-based switch in this dye makes it more selective for H_2O_2 than other ROS species. Additionally, a mitochondrial targeting phosphonium moiety allows MitoPY1 to localize H_2O_2 in cellular mitochondria. Followed by the synthesis of Peroxyfluor-1 (PF1) (Chang et al. 2004) and Peroxy Green 1 (PG1) (Miller et al. 2007), a new class of monoboronate, cell-permeable and nontoxic H_2O_2 -specific probes with green, yellow, and orange fluorescence has been reported recently by Dickinson et al. (2010). These probes were named Peroxyfluor-2 (PF2), Peroxyfluor-3 (PF3), Peroxy Yellow 1 (PY1), and Peroxy Orange 1 (PO1). The study with PG1 allows researchers to visualize the EGF/Nox generated endogenous intracellular H_2O_2 and provides evidence for H_2O_2 signaling in nervous systems through triggered growth factors in primary neurons. However, it is not suitable for multicolour imaging with essential green-fluorescent probes. Therefore, studies have been focused on developing H_2O_2 -specific fluorescent probes suitable for multicolour imaging. The presence of common boronate switch fluorescein in PF2 and PF3, and rhodol in PY1 and PO1 preferentially makes these probes selective to H_2O_2 over other ROS classes, such as O_2^- , NO, ClO^- , and OH^- . Furthermore, the orange fluorescence of PO1 enables the utilization of the probe for multicolor imaging with the green-fluorescent ROS probe, APF. Furthermore, to visualize the responses of H_2O_2 in the immune system, a novel ratiometric H_2O_2 -specific probe, Peroxy Lucifer 1 (PL1) has been synthesised by introducing an H_2O_2 -selective boronate-based switch to the 1,8-naphthalimide dye. Reaction

with peroxide shifts the blue-colored emission of this probe to green-color by 65 nm (Srikun et al., 2008).

A highly H₂O₂-selective lysosome targeting phosphorescent probe has been recently synthesized by introducing naphthalimide and morpholine moiety in the boronate-based molecule as the fluorophore and lysosome groups, respectively (Kim et al., 2015). This biocompatible lysosome-targetable probe has successfully monitored the exogenous and endogenous H₂O₂ levels in the HeLa cells. Another fast-responsive, lysosome-targeted, two-photon H₂O₂ probe has been reported by Ren et al. (2016) by incorporating 1,8-naphthalimide and boronate as a reaction site. A rapid increase in the emission of 550 nm is observed within 60 s with this fluorophore in the presence of H₂O₂. This implies the possibility of utilizing the probe in real-time to monitor H₂O₂. Additionally, exogenous and endogenous staining of H₂O₂ in HeLa cells and living macrophage (RAW 264.7) cells suggest the promising opportunities of this fluorophore for *in vivo* H₂O₂ studies. Further colocalized labelling of Lyso-HP and LysoTracker Red suggested the implication of Lyso-HP to study exogenous and endogenous H₂O₂ in lysosomes. Under two-photon fluorescence mode (λ_{ex} : 780 nm), the detection limit of H₂O₂ has to reach 130 μm , indicating the reliability of this probe for deep tissue H₂O₂ study.

1.9 Aggregation Induced Emission-based fluorescent bioprobes

Aggregation-induced emission (AIE) is a phenomenon of certain organic luminophores introduced first by Luo et al. (2001). AIE molecules generally possess rotor-like structures and are almost non-emissive in the dissolved state due to the free intramolecular motions to consume the excited state energy and lose luminescence non-radiatively. During aggregation, propeller shape structure restricts their piling up through π - π stacking interactions and limits their molecular motion, resulting in turning off the non-radiative transitions and activating the

radiative decay channels to yield fluorescence properties (Zhao et al., 2015; Hong et al., 2009) (Fig. 1.6).

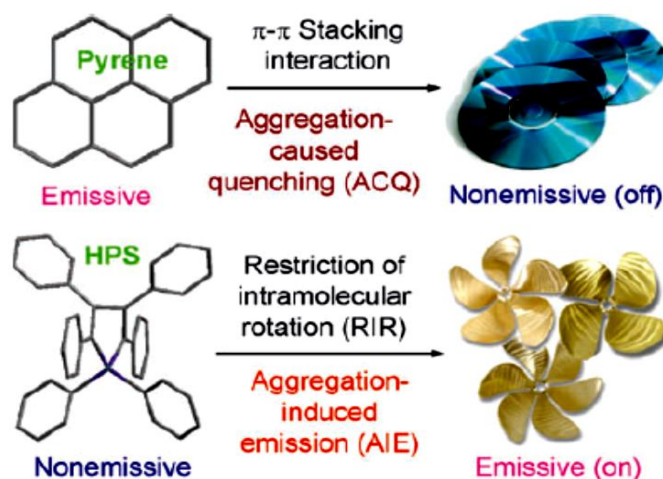


Fig. 1.6 Planar luminogens, e.g. pyrene, tend to aggregate likewise discs and pile up due to the strong π - π stacking interactions that usually stop the light emission. In contrast, nonplanar propeller-shaped luminogens such as hexaphenylsilole (HPS) show opposite characteristics and emit light by restricting intramolecular rotation through aggregation (Hong et al., 2009).

Fluorescence of the traditional dyes is most often suffered from aggregation-caused quenching (ACQ) phenomena, which impose the requirement of using these probes in dilute conditions and lead to photobleaching due to their dispersal in cells or tissues (Yu et al., 2005; Wüstner et al., 2014). However, recent advancements in the nanoaggregation of AIE bioprobes have made them more resilient and photostable by protecting inner molecules against further photobleaching and photooxidation (Wang et al., 2014). Through binding with the targeted biomolecules or influenced by the surrounding environment, the intramolecular

motions in these molecules restrict and exhibit increased emission. The incorporation of AIEgen nanoparticles also improves photostability and makes them suitable for long-term high contrast imaging in biological environments (Qian and Tang, 2017). The absence of ACQ phenomena, superior brightness, long-term *in situ* retention ability, high photostability, and low cytotoxicity have made these probes advantageous and preferable over other traditional fluorophores. Successful and specific imaging of mitochondria (Leung et al., 2013), full-range intracellular pH mapping (Chen et al., 2013), and long-term cell tracking (Wang et al., 2017a) with AIE based bioprobes have already been reported from different studies. Therefore, it is anticipated that introducing specific and stable AIEgens in lipid research could be a promising approach to advancing future lipidomics.

1.10 Recent progress of lipid-specific probes with aggregation-induced emission

The hydrophobic properties of AIE molecules make them promising for lipid studies. Due to the higher fraction of triglycerides and cholesterol esters, lipid droplets' inherent environment is hydrophobic, making them more potential for staining with AIEgens. Over the last few years, some lipid-specific AIE-probes with a diverse range of excitation and emission wavelengths have been synthesized, each of which has unique properties and could be selected effectually based on study requirements. Among these AIE-probes, some follow one-pot synthetic strategies that could be utilized to produce fluorophores in time-efficient and cost-effective manners. In addition, some of these probes could be excited at near-infrared light and are suitable for deep tissue penetration, and some have already shown their significant therapeutic properties.

1.10.1 Photostable lipid-specific probes based on simple AIEgens

Applications of AIEgens in lipidomics have been highly appreciated due to their cheap biosynthesis processes, such as lipid-specific AIEgens, FAS ($C_{20}H_{14}N_2O$) and DPAS ($C_{20}H_{16}N_2O$) are synthesized from cheap commercial products fluorenone and benzophenone, respectively (Wang et al., 2016). Previously, tetraphenylethylene (TPE) derivatives, TPE-AmAl and TPE-AC have been synthesised as bright and photostable lipid-specific AIEgens with excellent cell permeability by Wang et al. (2014) and Kang et al. (2016), respectively (Figs. 1.7A and 1.7B). The fluorescence of TPEAmAl is responsive to the environmental polarity, and emission ($\lambda_{ex} = 330-385$ nm) is red-shifted (from 525 nm to 590 nm) with the increase of water fraction from 0 to 70 vol% that consequently blue-shift with the further increase of the water percentage. Due to the responsiveness towards lower polarity by greenish-blue colour emission, aggregation of hydrophobic TPE-AmAl inside LDs can easily differentiate the LDs from the extracellular orange emission of this bioprobe. Additionally, compared to the commercial LD dyes, TPE-AmAl exhibited much lower background noise and higher sensitivity. TPE core of TPE-AmAl was further modified into a new near-infrared (NIR) AIEgen by introducing dimethylamine as the electron donor and malononitrile as the electron acceptor as TPE-AC. The absorption maximum of this newly synthesized AIE nanoprobe was recorded as 455 nm in tetrahydrofuran (THF) solution, whereas aggregation in higher water fraction caused emission at 705 nm. To minimize the issues of AIEgen, TPEAmAl that are affected by the surrounding environment polarity, utilizing the cheap commercial products fluorenone and benzophenone, Wang et al. (2014) synthesized two AIE bioprobes, FAS and DPAS, respectively (Figs. 1.7C and 1.7D). Unlike the environment sensitivity of fluoregen TPEAmAl, the fluorescence of FAS and DPAS were found stable with good resolution and high contrast in LDs. Therefore, both dyes were able to work at

significantly higher concentrations with brighter images, and resolved the concentration-associated ACQ problems of the traditional fluorescence probes.

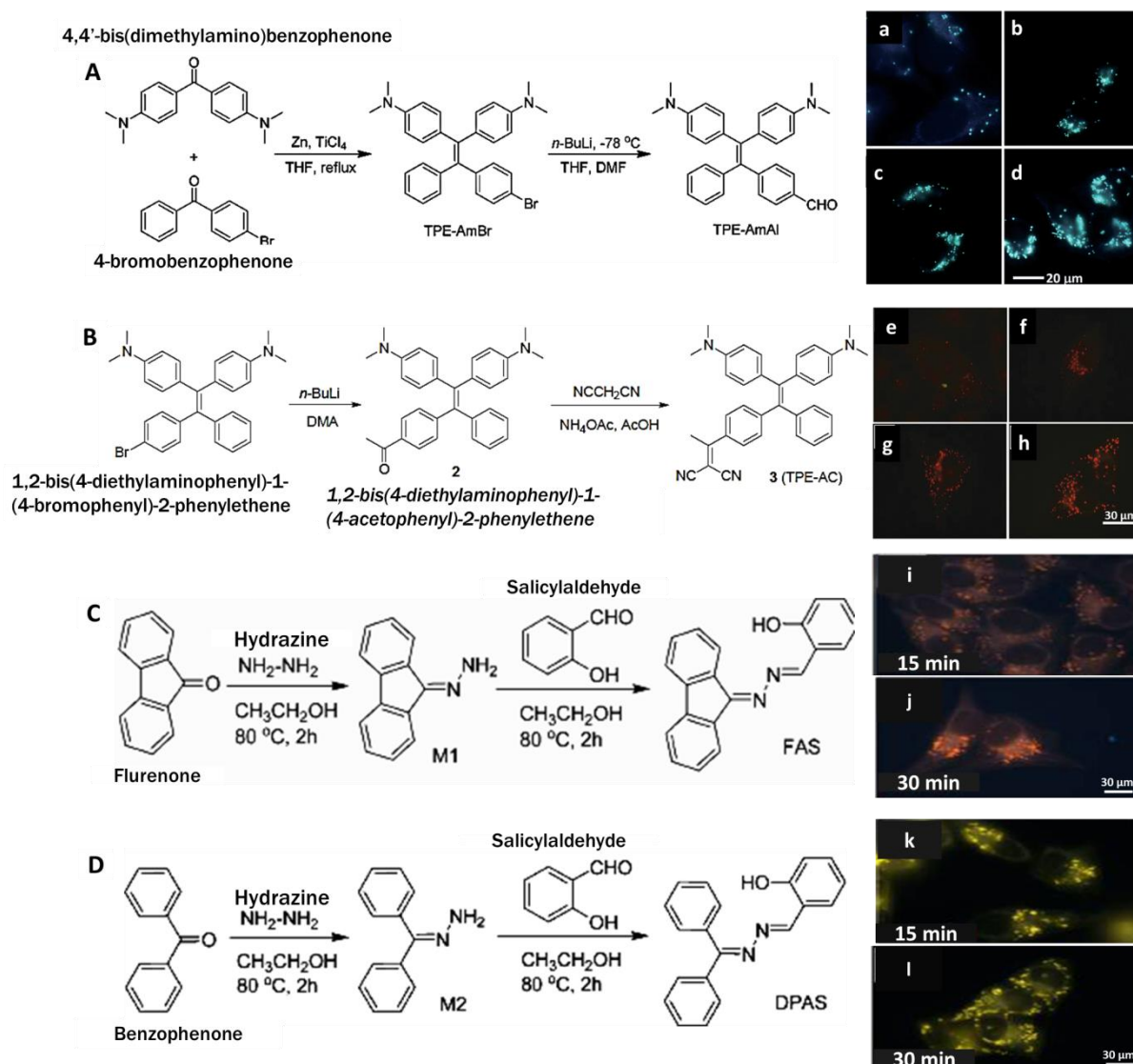


Fig. 1.7 Simple synthetic pathways and staining of oleic acid-treated lipid drops in HeLa cells with AIEgens, TPEAmAl (A), TPE-AC (B), FAS (C) and DPAS (D). (a-d) HeLa cells stained with 10 μM TPE-AmAl for 15 min after incubation in the presence of (a) 0, (b) 12.5, (c) 25 and (d) 50 μM oleic acid for 6 h (λ_{ex} : 330-385 nm); (e-h) HeLa cells stained with 10 μM TPE-AC for 15 min after incubation in the presence of (a) 0, (b) 12.5, (c) 25 and (d) 50 μM oleic acid for 6 h (λ_{ex} : 510-550 nm). (i-l) HeLa cells were stained with 7.5 μM FAS (λ_{ex} :

400–440 nm) (i, j) and DPAS (λ_{ex} : 330–385 nm) (k–l) at different times after incubation with 50 μM oleic acid for 6 h. Stained time: (i, k) 15 min; (j, l) 30 min. (Wang et al., 2016; Wang et al., 2014; Kang et al., 2016).

However, these lipid-specific AIE probes require UV excitation and mostly show short-wavelength emission, which might damage some cellular structures during a long exposure or be affected by some of the cellular autofluorescence properties. Moreover, despite the near-infrared (NIR) emission properties of TPE-AC, the excitation wavelength are merely 450 nm, which is not considered long enough to reach the optical window for optimal tissue penetration (750-950 nm) (Jiang et al., 2017). Considering these facts, the necessity of lipid-specific two-photon lipid AIEgens has emerged, on which researchers have been focused in recent years.

1.10.2 Two-photon lipid droplets specific AIE bio-probes

Multiphoton imaging generally allows lower background autofluorescence, minimal photobleaching, and higher spatial resolution. Owing to the high brightness and photostable characteristics, AIEgens have been considered more promising candidates for multiphoton-active imaging (Zhuang et al., 2019; Niu et al., 2018; Jiang et al., 2017). Additionally, near-infrared light can facilitate a lower scattering coefficient and narrower focus range, allowing more deep tissue penetration and being more suitable for biomedical diagnosis and therapy (Qin et al., 2020; Hamon et al., 2020; Collot et al., 2019). Furthermore, two-photon excitation in the fluorescent compound is critically determined by the molecular two-photon absorption strengths ($\delta_{2\text{PA}}$). A higher value of $\delta_{2\text{PA}}$ shows stronger two-photon excited fluorescence (TPEF) and a lesser deleterious thermal effect from the strong laser pulse (Lepock, 2003), therefore can provide an easier way to realize red and NIR excitations. Recently, several AIE probes have been designed for two-photon fluorescence microscopy (2 PM) and perform

better than the commercial LD staining fluorophores in terms of higher 3D resolution, lesser photobleaching, and low autofluorescence and deeper tissue penetration.

Among these probes, TPA-BI ($C_{32}H_{29}N_3O$) (Jiang et al., 2017) has shown strong solvatochromism properties and has successfully been utilized in LD imaging in several cell lines as HeLa, HepG-2 and A549, and in fixed cells. Compared to the one-photon excitation ($\lambda_{ex} = 400-440$ nm), under two-photon excitation ($\lambda_{ex} = 840$ nm, 900 nm and 980 nm) in HeLa cells, the response of TPA-BI to the TAG/LDs has been largely increased ($\lambda_{em} = 450-550$ nm), where BODIPY 493/503 ($\lambda_{em} = 500-550$ nm) showed significant signal loss (Fig. 1.8A) to allow the escaping of photothermal damage to living cells caused by the high laser power. Moreover, by decorating the nonaromatic rotor of the trifluoromethyl group (CF_3) on the π -conjugated core, another two-photon AIE compound, ABCXF ($C_{21}H_{16}F_6N_2$), has been developed with better tissue penetration during lipid imaging in guinea pig liver tissue (Figs. 1.8B-1.8D) (Park et al., 2021). Compared to the one-photon fluorescence imaging (λ_{ex} : 488 nm), under excitation of 850 nm, this probe signalled better at 500-600 nm (Fig. 1.8A). Furthermore, due to the intramolecular charge transfer effects, the solvatochromism properties of ABCXF have shown increased fluorescence intensity with the increased solvent polarity that might favour this two-photon AIE-probe in biological systems.

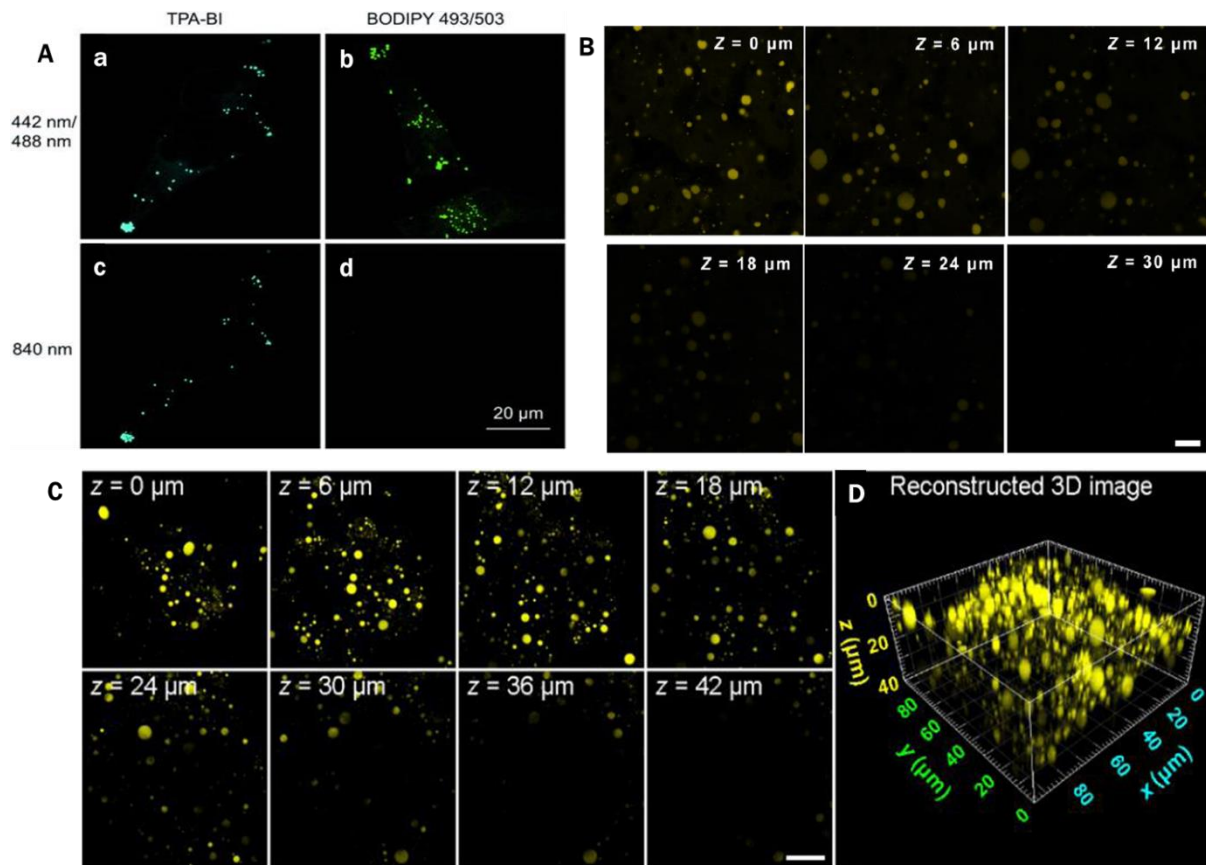


Fig. 1.8 Confocal fluorescence imaging with TPA-BI (A) and ABCXF (B-D). (A) HeLa cells stained with 5 μM of TPA-BI (a and c) and 5 μM of BODIPY 493/503 for 20 min (b and d). Conditions: one-photon excitation (a and b) (a) $\lambda_{\text{ex}} = 442 \text{ nm}$ and $\lambda_{\text{em}} = 450\text{-}550 \text{ nm}$, (b) $\lambda_{\text{ex}} = 488 \text{ nm}$ and $\lambda_{\text{em}} = 500\text{-}600 \text{ nm}$; two-photon excitation (c and d) (c) $\lambda_{\text{ex}} = 840 \text{ nm}$ and $\lambda_{\text{em}} = 450\text{-}550 \text{ nm}$, (d) $\lambda_{\text{ex}} = 840 \text{ nm}$ and $\lambda_{\text{em}} = 500\text{-}600 \text{ nm}$. Two-photon excitation resulted in increased fluorescence of TPA-BI in TAG/LD, while BODIPY 493/503 showed significant signal loss under two-photon excitation (Jiang et al., 2017). (B-D) Deep tissue imaging of lipid drops in the liver tissue of high-fat feeding guinea pig stained with ABCXF (2 μM) at different penetration depths (Scale bar: 20 μm). (B) One-photon ($\lambda_{\text{ex}} = 488 \text{ nm}$) images; (C) Two-photon ($\lambda_{\text{ex}} = 850 \text{ nm}$) fluorescent images; (D) Reconstructed 3D two-photon fluorescent images. The spherical LDs in the tissue sample were observed along the z-axis up to a depth of 42 μm). A High-resolution 3D two-photon fluorescent image was

successfully constructed with ABCXF under two-photon excitation one-photon fluorescence imaging only showed a shallow penetration depth of less than 30 μm .

In 2018, a novel family of two-photon donor-acceptor AIEgens was developed by Niu et al. (2018) by utilizing naphthalene as the core and termed as NAP AIEgens. This family of two-photon probes includes NAP-Ph ($\text{C}_{28}\text{H}_{25}\text{N}_2\text{O}$), NAP-Br ($\text{C}_{22}\text{H}_{19}\text{BrN}_2\text{O}$), NAP- CF_3 ($\text{C}_{24}\text{H}_{18}\text{F}_6\text{N}_2\text{O}$), and NAP-Py ($\text{C}_{27}\text{H}_{23}\text{N}_3\text{O}$) and showed successful LDs staining performance in HeLa cells at ultra-low concentration (50-100 nM) (Fig. 1.9A). Due to the high hydrophobic nature of lipid drops, organic dyes with high hydrophobicity potentially show more specificity for lipid droplet staining. The calculated partition coefficient (P) (ClogP) values of NAP-Ph, NAP-Br, NAP- CF_3 , and NAP-Py have been reported as 6.681, 5.656, 6.559 and 5.184, respectively, which is higher than the traditional lipid specific dyes Nile Red (4.618) and BODIPY 493/503 (5.028) (Fig. 1.9B). The partition coefficient (P) describes the dissolving ability in an immiscible biphasic system of lipid (fats, oils, organic solvents) and water. Therefore, the higher ClogP values of the NAP AIEgens indicate more hydrophobicity than Nile Red and BODIPY 493/503, and potentially one reason for better performance at ultra-low concentration. Higher dye concentration could have detrimental effects on the normal physiological activities of the cells. Hence the effective applications of these two-photon dyes at lower concentrations could be helpful and serve better for lipid research than other AIE-gens.

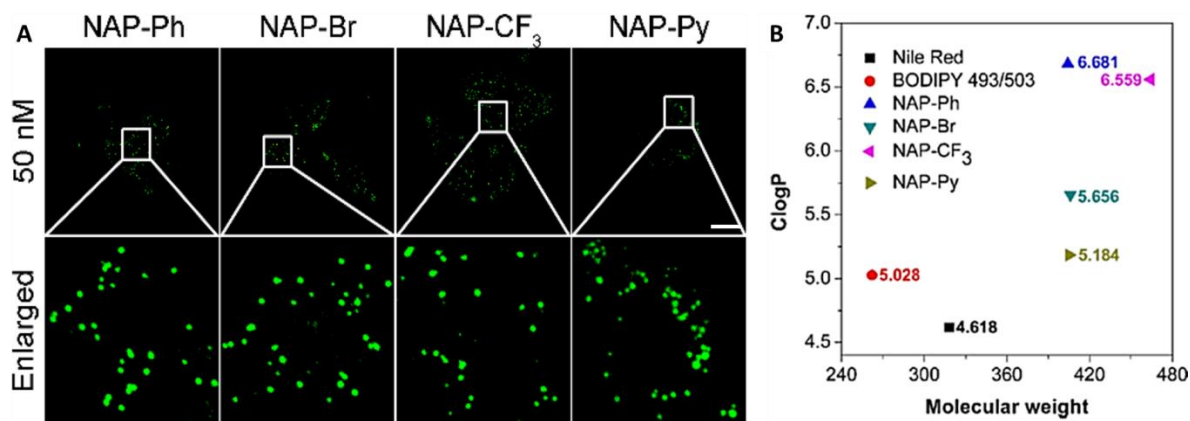


Fig. 1.9 Confocal laser scanning microscopy of lipid drops with ultra-low concentration (50 nM) of NAP-AIEgens (A) and ClogP values of NAP-AIEgens (B). (A) Images of HeLa cells stained with NAP-Ph, NAP-Br, NAP-CF₃, NAP-Py. Scale bar: 20 μm. (B) ClogP of Nile Red, BODIPY 493/503, NAP-Ph, NAP-Br, NAP-CF₃, and NAP-Py. Higher values indicate better lipid droplet staining performance (Niu et al., 2018).

1.10.3 AIE-based fluorophore to visualize LD-lysosome interplay

The unique labelling behaviours and distinguished emission properties of certain AIE probes can create new possibilities to visualize *in vivo* lipophagic triacylglycerol catabolism. As an integral part of cellular metabolism, the interaction between cytoplasmic LDs and lysosomes can be associated with several inflammations and metabolic disorders (Dugail, 2014; Dong and Czaja, 2011). Recently, an encapsulated polymeric matrix (DSPE-PEG₂₀₀₀) of AIE-based fluorophore TPA-BTTDO (C₅₄H₃₈N₂O₂S₂) has been synthesized and shows dual emission with red and cyan fluorescence in the lysosome and LDs, respectively (Hu et al., 2019). The molecular structure of TPA-BTTDO encompasses an electron-withdrawing thieno[3,2-b]thiophene S,S-dioxide (TTDO) core and electron-donating triphenylamine (TPA) groups to induce the molecule for the twisted intramolecular charge transfer (TICT) between TTDO and

TPA, particularly in a high polar environment. Due to the poor solubility in water, to increase the water dispersibility in the biological condition, the AIEgen has been encapsulated in DSPE-PEG₂₀₀₀. After the internalization through the cell membrane via endocytosis, the probe shows high polarity dependant red emission (614 nm) during the localization in the lysosome. Following enzymatic degradation, DSPE-PEG₂₀₀₀ matrix exposes the hydrophobic TPA-BTTDO to the less polar hydrophobic LDs and results in cyan emission (498 nm) that enables us to conceptualize LD components degradation by lysosomal enzymes (Fig. 1.10). These unique properties could hold significant prospects for investigating LDs-lysosome-related metabolic disorders.

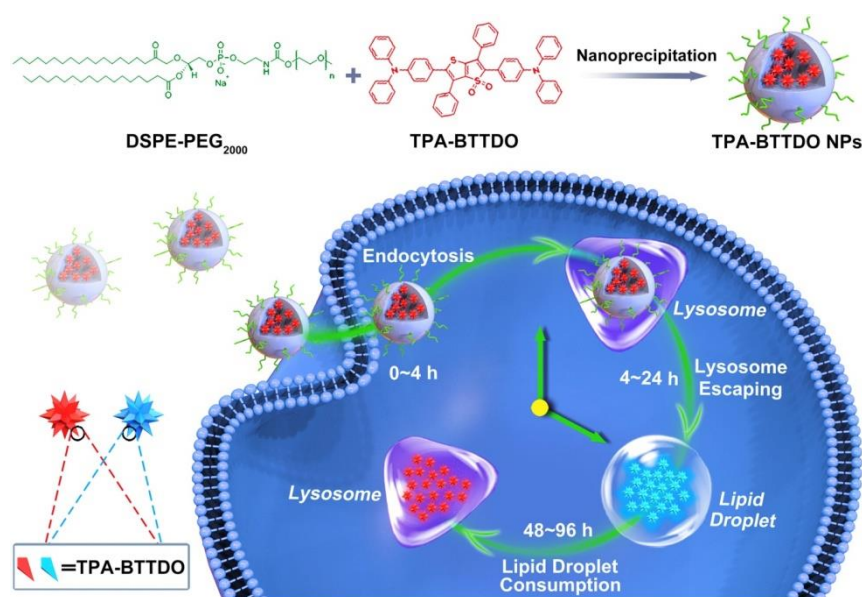


Fig. 1.10 Systematic diagram of the internalization and consumption processes of TPA-BTTDO NPs in cells (Hu et al., 2019).

1.10.4 Lipid-specific AIEgens system with wide emission tenability

Recently, designing AIE materials with red/NIR emissive properties has become of significant interest to AIE researchers. Being one of the three primary colours (Red, Yellow,

and Blue), red is the crucial element in the full-color display systems and has been utilized in a wide range of optoelectronic devices. Due to the considerable penetration depth, lower background autofluorescence and minimal cellular damage, fluorescence materials emitted at red/NIR regions are more preferential for biological studies. Nanoparticles based on red/NIR emissive AIE materials are also privileged for inorganic quantum dots due to the lower toxicity, higher emission and photobleaching resistance. However, due to the tedious synthesis process and complex structures, not so many lipid-specific probes with red/NIR emissive properties have been reported despite significant efforts. Recently, by installing different rotors (phenol, diphenylamine and ethene-1,1,2-triyltribenzene) in the ACQ compound, Zhang et al. (2020b) stepwise enhanced the donor (D) - acceptor (A) interactions to construct an AIE-system that covers almost all regions of visible light, pursuing maximum emission wavelength in the NIR region (Figs. 1.11A and 1.11B). In the study, structures with intramolecular motions, such as oxydibenzene, triphenylamine (TPA), and tetraphenylethene (TPE) were (D), the carbon-carbon double bond acted as the π bridge, and cyanogroup, trifluoromethyl, as well as the benzene ring, attached to the nitro group acted as the (A). These AIEgens showed negligible cytotoxicity and excellent LDs-specificity. AIEgen, B3 showed high sensitivity to triolein and distinguished the blood of hyperlipidemia patients from ordinary people (Figs. 1.11C and 1.11D). Therefore, this could be a new tool for potential biomedical research.

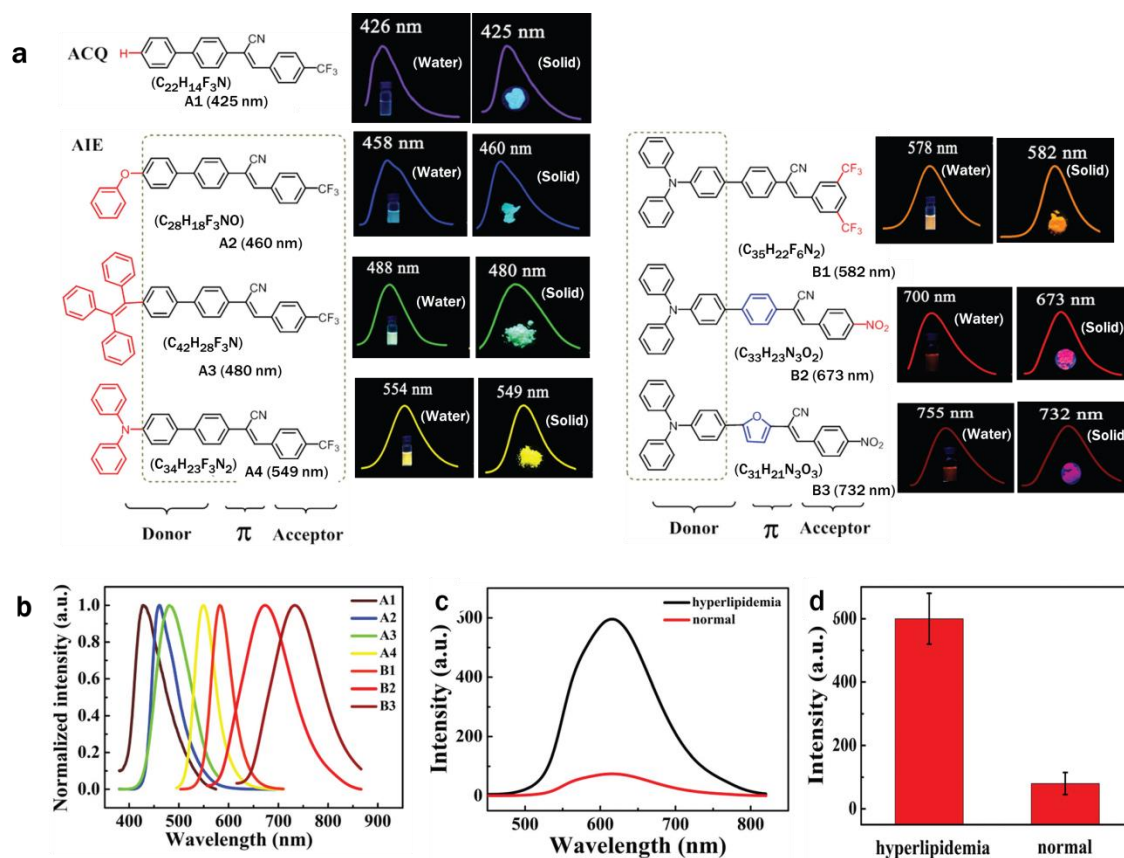


Fig. 1.11 Chemical structures of the tunable AIE system from an ACQ compound (A1) to AIEgens (A1, A2, A3, A4, B1, B2 and B3) and their emissions. (a) Tuning AIEgens (A1, A2, A3, A4, B1, B2 and B3) from compound (A1), and respective photographs of in water and the solid-state were taken under 365 nm UV light. Installing a phenol rotor to the ACQ compound, A1 constructs the AIE-active compound A2, while introducing diphenylamine and ethene-1,1,2-triyltribenzene rotors constructed AIEgens A3 and A4, respectively. Subsequently, the electron-withdrawing group of A4 was modified to get compounds B1, B2 and B3 and the emission reached in NIR region. (b) Normalized PL spectra of A1 (λ_{em} : 425 nm), A2 (λ_{em} : 460 nm), A3 (λ_{em} : 480 nm), A4 (λ_{em} : 549 nm), B1 (λ_{em} : 582 nm), B2 (λ_{em} : 673 nm) and B3 (λ_{em} : 732 nm) in the solid state. (c) Emission spectra of B3 (1.0×10^{-6} M, λ_{ex} : 423 nm) in the serum of hyperlipidemia and normal people. (d) Bar graph of fluorescence intensities in the serum of hyperlipidemia and normal people (n = 6).

1.10.5 Biocompatible AIEgen from natural resources

Fluorogenic compounds derived from natural resources could be more environmentally friendly, biodegradable and cost-effective, which might increase their opportunities for applications. Additionally, exploration of water-soluble AIEgens can hold fundamental advantages for biological studies. For example, a natural isoquinoline alkaloid, berberine chloride (BBR chloride), isolated from Chinese herbal plants, has recently been reported to hold an unconventional rotor-free AIEgen characteristic with water-soluble properties (Gu et al., 2018).

In dilute water solution, BBR chloride shows weak emission, probably due to the active intramolecular vibration behaviour and the twisted intramolecular charge transfer (TICT) effect that opens the access to non-radiative decay. In the aggregates or solid state, the non-radiative decay pathway in this AIEgen is suppressed, resulting in bright fluorescence. With the increasing solvent polarity, the absorption of BBR chloride remains almost unchanged while the fluorescence intensity decreases significantly, followed by red shifting of the emission maximum from 525 nm to 550 nm, which suggests the TICT effect in this AIEgen. However, BBR chloride is also sensitive to viscosity and temperature. Upon exposure to the more viscous environment and lower temperature, the fluorescence intensity of BBR chloride shows a sharp increase, which signifies the influence of the intramolecular vibration in this AIEgen. This biocompatible fluorophore can successfully stain lipid drops in different cells, such as HeLa, A549 and MCF-10A cells. Compared to the green fluorescent protein (GFP), after 20 scans, BBR chloride retained 30% more fluorescence intensity, which proves the photostable character of this probe over the traditional fluorophore, GFP (Fig. 1.12). These characteristics make this naturally obtained LDs specific AIEgen a promising candidate for LD imaging and associated disease diagnosis.

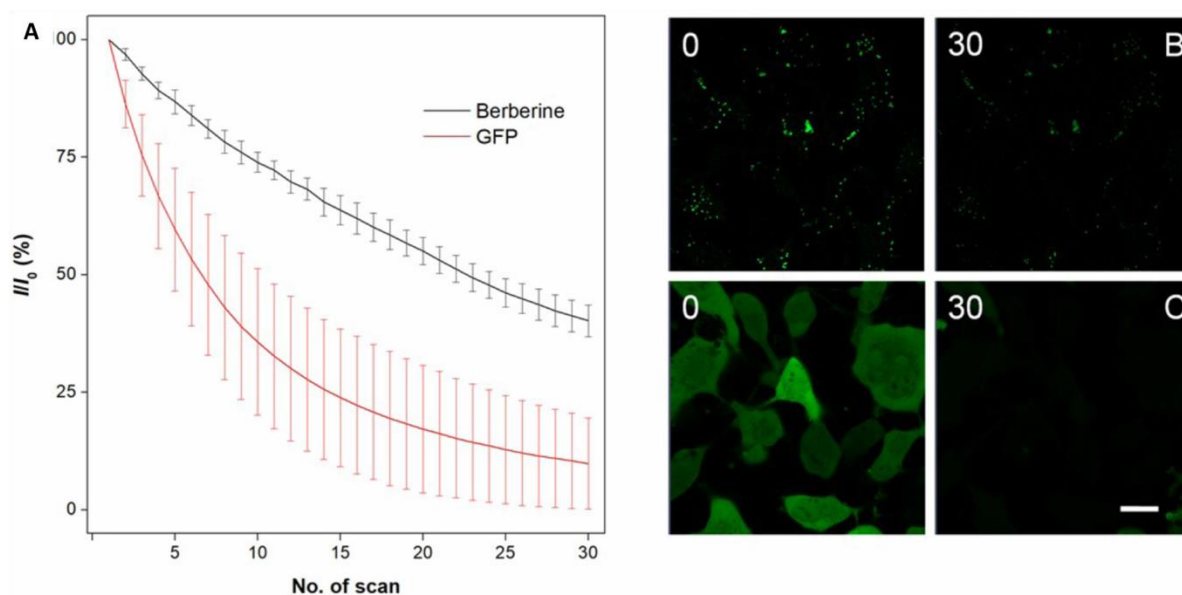


Fig. 1.12 Photostability of berberine chloride (BBR Chloride) and green fluorescent protein (GFP). (A) BBR Chloride and GFP under continuous scanning at 488 nm (2.3 μ W). I_0 is the initial PL intensity, while I is that of the corresponding sample after a designated number of scans. (B) Confocal images of HeLa cells stained with BBR Chloride (10 μ M) and (C) 786-O cells containing GFP gene before and after 30 scans of light irradiation; λ_{ex} : 488 nm; All the images share the same scale bar: 20 μ m. Error bars are \pm relative standard deviations, $n = 6$.

1.10.6 Lipid specific AIEgens in algae research

Due to the utilization of non-arable land, ability to reduce pollution and rapid growth rate, microalgae have high prospective and various benefits for lipid production. Green microalgae could be utilized more effectually for biofuel and health beneficiary food supplementation than land-based plants. Over the years of AIE research, many studies have been reported to illustrate different lipid-specific AIE probes for disease diagnosis and photodynamic therapy in animal cell models. However, in comparison to the higher organisms, reports on AIE molecules introduced to microalgae are very few and still a significant area to explore. A

recent study of an algal model of *Nannochloropsis* sp. by Wang et al. (2014) revealed greenish-blue emission upon aggregation of the TPE-AmAl probe in lipid drops (Fig. 1.13).

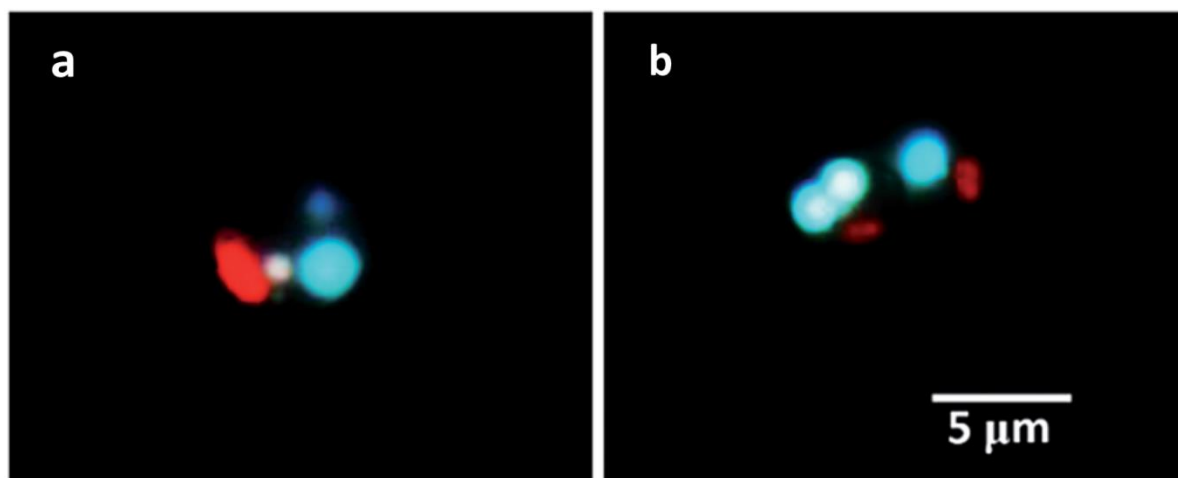
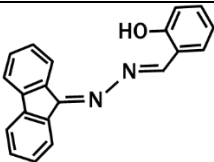
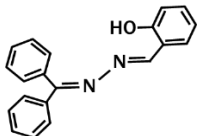
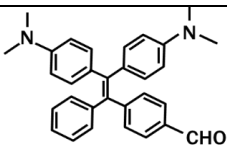
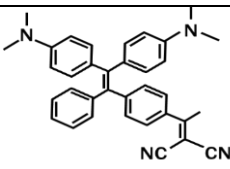
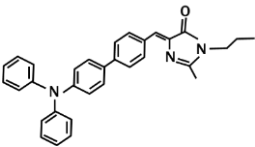
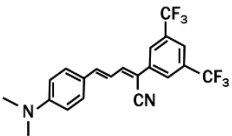


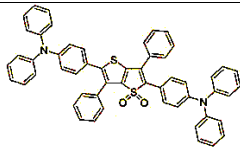
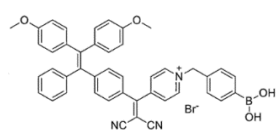
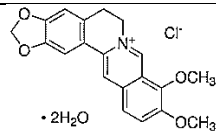
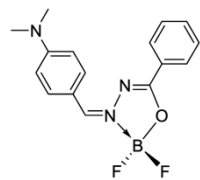
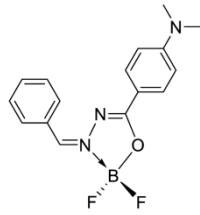
Fig. 1.13 Fluorescent images of green algae stained with 2.5 mM TPE-AmAl in (a) 10 vol% and (b) 20 vol% DMSO at 40 °C for 10 min. λ_{ex} : 330-385 nm. The blue emission is from the LDs; the red emission is from the chloroplast.

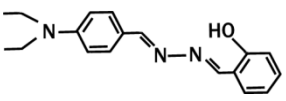
To facilitate the probe's diffusion, different DMSO fractions containing the same concentration of TPEAmAl were used in culture media, whereas high contents of DMSO showed shorter diffusion times for the AIE probe to enter through the algal cell wall. Since different microalgae have unique cell types and auto-fluorescence characteristics, the requirement for appropriate selection of AIEgens and their acquisition techniques is crucial for studying lipid drops in microalgae.

A summary of the lipid-specific AIE-probes is given in Table 1.4.

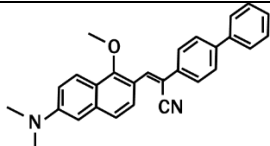
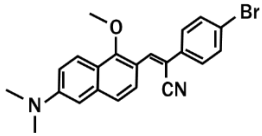
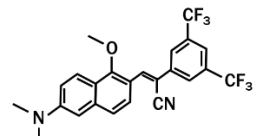
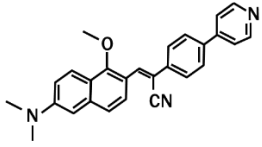
Table 1.4 Properties of some recently synthesized LDs specific AIE fluorescent probes.

Probes	Chemical structure	$\lambda_{\text{ex}} / \lambda_{\text{em}}$ (nm)	Solubility	Notes
FAS	 <p>Chemical formula: $\text{C}_{20}\text{H}_{14}\text{N}_2\text{O}$ Calculated MW: 298.33</p>	λ_{ex} : 400-440, λ_{em} : 595	DMSO	<ul style="list-style-type: none"> • Lesser background noises • Higher photostability • Biocompatible and almost no cytotoxicity (Wang et al., 2014)
DPAS	 <p>Chemical formula: $\text{C}_{20}\text{H}_{16}\text{N}_2\text{O}$ Calculated MW: 300.35</p>	λ_{ex} : 330-385, λ_{em} : 565	DMSO	<ul style="list-style-type: none"> • Much lower background noises • No noticeable cytotoxicity • Photostable and biocompatible (Wang et al., 2014)
TPE-AmAl	 <p>Chemical formula: $\text{C}_{31}\text{H}_{30}\text{N}_2\text{O}$ Calculated MW: 446.2358</p>	λ_{ex} : 330-385, λ_{em} : ≥ 420	<ul style="list-style-type: none"> • DMSO • THF • CHCl_3 • CH_2Cl_2 • DMF 	<ul style="list-style-type: none"> • Sensitive to the environment polarity • Higher photostability • Lower background noise • Biocompatible and almost no cytotoxicity (Wang et al., 2014)
TPE-AC	 <p>Calculated MW: 508.2627</p>	λ_{ex} : 455 in THF; 510-550 in DMSO. λ_{em} : ≥ 705	<ul style="list-style-type: none"> • DMSO • THF 	<ul style="list-style-type: none"> • Bright near-infrared emission • Higher photostability • Biocompatible and very low cytotoxicity (Kang et al., 2016)
TPA-BI	 <p>Chemical formula: $\text{C}_{32}\text{H}_{29}\text{N}_3\text{O}$ Calculated MW: 471.2311</p>	λ_{ex} : 400-440 and 840 λ_{em} : 450-550	DMSO and other polar solvents	<ul style="list-style-type: none"> • Competent in both one-photon and two-photon imaging • Reduced photobleaching • Deeper tissue penetration • Photophysical properties intensely depend on solvent polarity (Jiang et al., 2017)
ABCXF	 <p>Chemical formula: $\text{C}_{21}\text{H}_{16}\text{F}_6\text{N}_2$ Calculated MW: 410.1218</p>	λ_{ex} : 488 and 850 λ_{em} : 500-600	DMSO, DCM, Acetonitrile Acetone EtOH, DMF MeOH, THF Toluene Chloroform Ethyl ether	<ul style="list-style-type: none"> • Competent in both one-photon and two-photon imaging • Deeper tissue penetration up to 42 μm in two-photon imaging • Reduced photobleaching • Increased fluorescence intensity with increased polarity • More suitable in the biological system (Park et al., 2021)

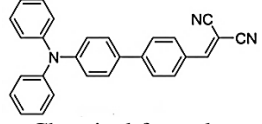
TPA-BTTDO	 <p>Chemical formula: C₅₄H₃₈N₂O₂S₂ Calculated MW: 810.2375</p>	<p>λ_{ex}: 405, λ_{em}: 450-725</p>	<p>THF, CH₂Cl₂, DMF and other organic solvents</p>	<ul style="list-style-type: none"> • Sensitive to the environment polarity • Cyan emission (498 nm) in lipid droplet; red emission (614 nm) in the lysosome • Photostable and biocompatible (Hu et al., 2019)
TPECNPB	 <p>Chemical formula: C₄₄H₃₅BN₃O₄⁺ Calculated MW: 680.2715</p>	<p>λ_{ex}: 450 λ_{em}: 625</p>	<p>THF</p>	<ul style="list-style-type: none"> • Sensitive to H₂O₂, enable cancer cell ablation efficiently through ROS generation • Photostable, supports long-term visualization of the photodynamic therapy efficiently <i>in vitro</i> and <i>in vivo</i> (Jiang et al., 2020)
Berberine chloride	 <p>Chemical formula: C₂₀H₁₈ClNO₄ Calculated MW: 371.81</p>	<p>λ_{ex}: 488 λ_{em}: 500-580</p>	<p>H₂O</p>	<ul style="list-style-type: none"> • Water soluble, more suitable for biological studies • Photostable and biocompatible • Sensitive to the viscosity and temperature (Gu et al., 2018)
DMA-POABP	 <p>Chemical formula: C₁₆H₁₆BF₂N₃O Calculated MW: 316.1354</p>	<p>λ_{ex}: 330-385 λ_{em}: 448-548</p>	<p>Hexane, Toluene, DCM, 1,4-dioxane, Chloroform, THF, ACN, DMF, EtOH, MeOH, IPA, DMSO</p>	<ul style="list-style-type: none"> • Organoboron isomer • In HeLa cells showed better resolution and higher contrast in comparison with Nile Red • Bright-blue fluorescence • Biocompatible, no noticeable repressive effect on cell • More photostable than Nile Red • Strong emission in a viscous medium • In solution, exhibited bluer but weaker emission than POABP-DMA (Ni et al., 2018)
POABP-DMA	 <p>Chemical formula: C₁₆H₁₆BF₂N₃O Calculated MW: 315.1354</p>	<p>λ_{ex}: 330-385 λ_{em}: 448-548</p>	<p>Hexane, Toluene, DCM, 1,4-dioxane, Chloroform, THF, ACN, DMF, EtOH, MeOH, IPA,</p>	<ul style="list-style-type: none"> • Organoboron isomer • In HeLa cells showed better resolution and higher contrast in comparison with Nile Red • Bright-blue fluorescence • Biocompatible, no noticeable repressive effect on cell • More photostable than Nile Red • Strong emission in a viscous medium

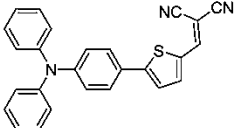
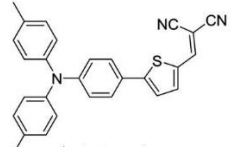
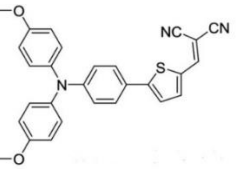
			DMSO	<ul style="list-style-type: none"> In solution, exhibited less blue but stronger emission than DMA-POABP (Ni et al., 2018)
AP-DEA	 <p>Chemical formula: C₁₈H₂₁N₃O Calculated MW: 295.1685</p>	λ_{ex} : 405 λ_{em} : 448–548	THF, DMSO	<ul style="list-style-type: none"> High colocalization with Nile Red in HeLa cells Superior photostability Can generate reactive oxygen species very fast and effectively, therefore much suitable for photodynamic therapy No noticeable repressive effect on HeLa cell growth (Ni et al., 2019)

NAP-AIEGens: NAP-Ph, NAP-Br, NAP-CF₃, NAP-Py (Niu et al., 2018)

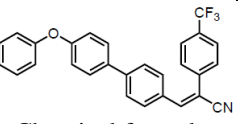
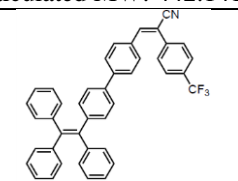
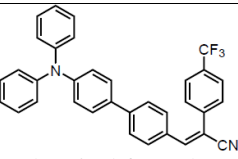
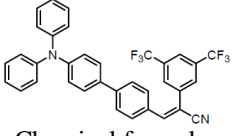
NAP-Ph	 <p>Chemical formula: C₂₈H₂₅N₂O Calculated MW: 405.1961</p>			
NAP-Br	 <p>Chemical formula: C₂₂H₁₉BrN₂O Calculated MW: 406.0691</p>	λ_{ex} : 405 and 860 λ_{em} : 480-560	THF, CH ₃ CN, toluene, diethyl ether, acetone, DMSO	<ul style="list-style-type: none"> Competent in both one-photon and two-photon imaging Deeper tissue penetration up to 70 μm in two-photon imaging has been recorded for NAP-CF₃ Reduced photobleaching Could be used at an ultra-low concentration (50-100 nM)
NAP-CF ₃	 <p>Chemical formula: C₂₄H₁₈F₆N₂O Calculated MW: 464.1323</p>			
NAP-Py	 <p>Chemical formula: C₂₇H₂₃N₃O Calculated MW: 405.1841</p>			

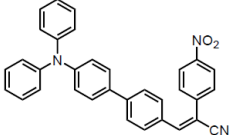
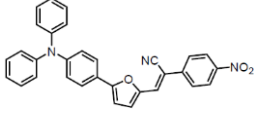
One-pot synthesised AIEGens: TPMN, TTMN, MeTTMN, and MeOTTMN (Wang et al., 2017b)

TPMN	 <p>Chemical formula: C₂₈H₁₉N₃ Calculated MW: 397.1579</p>	λ_{ex} : 441 λ_{em} : 637	Toluene, Ethyl acetate, THF, Chloroform DMSO,	<ul style="list-style-type: none"> Red/NIR AIE luminogens Simple structures Photostable and bright emission Suitable for photodynamic therapy
------	--	--	---	---

TTMN	 <p>Chemical formula: C₂₆H₁₇N₃S Calculated MW: 403.1143</p>	λ_{ex} : 483 λ_{em} : 672	Acetone, DCM, Acetonitrile, MeOH	<ul style="list-style-type: none"> • Low toxicity in dark
MeTTMN	 <p>Chemical formula: C₂₈H₂₁N₃S Calculated MW: 431.5570</p>	λ_{ex} : 492 λ_{em} : 681		
MeOTTMN	 <p>Chemical formula: C₂₈H₂₁N₃O₂S Calculated MW: 463.1354</p>	λ_{ex} : 499 λ_{em} : 701		

AIE system of A2, A3, A4, B1, B2 and B3 with wide tunable emissions (Zhang et al., 2020b)

A2	 <p>Chemical formula: C₂₈H₁₈F₃NO Calculated MW: 442.1413</p>	λ_{ex} : 405 λ_{em} : 420-480		
A3	 <p>Chemical formula: C₄₂H₂₈F₃N Calculated MW: 604.2247</p>	λ_{ex} : 458 λ_{em} : 580-650	DMSO	<ul style="list-style-type: none"> • Tunable AIEgens with wide visible spectra (400-780 nm) • High photostability and bright emission • Low toxicity • B3 achieved far-red emission • B3 is sensitive to trioctanoin, therefore can distinguish hyperlipidemia patient blood
A4	 <p>Chemical formula: C₃₄H₂₃F₃N₂ Calculated MW: 517.1886</p>	λ_{ex} : 514 λ_{em} : 520-570		
B1	 <p>Chemical formula: C₃₅H₂₂F₆N₂ Calculated MW: 585.1760</p>	λ_{ex} : 514 λ_{em} : 540-620		

B2	 <p>Chemical formula: C₃₃H₂₃N₃O₂ Calculated MW: 494.1863</p>	λ_{ex} : 514 λ_{em} : 590-680
B3	 <p>Chemical formula: C₃₁H₂₁N₃O₃ Calculated MW: 484.1656</p>	λ_{ex} : 488 λ_{em} : 600-750

1.11 AIE-based molecules for H₂O₂ detection

Due to the high hydrophobic nature, organic molecules tend to aggregate in natural states. The introduction of AIE-based technologies has significantly improved the fluorescence bioimaging techniques for the *in vivo* studies of essential biomolecules. However, despite the significant focus on AIE research, only a few H₂O₂-specific AIEgens have been reported. The recent report of a novel ratiometric AIE-probe, TPE-TLE shows excellent fluorescent properties (Liu et al., 2017). Ratiometric fluorescence sensing is a specific setting owing to its excellent sensitivity, inherent reliability, and self-calibration properties, enabling them to analyze the biological molecules precisely. TPE-TLE is an excellent H₂O₂-specific photostable probe with better cellular permeability, distinct emission peaks, higher sensitivity, and lower cytotoxicity. By incorporating a thiazole group and a borate moiety on the tetraphenylethene (TPE)-core of the structure of AIE luminogen, TPE has been modified towards H₂O₂ selectivity that allows it to distinguish much more endogenous H₂O₂ in cancer cells than the macrophages. A low micromolar concentration of H₂O₂ detectability of TPE-TLE has also made this AIE-probe very promising for future biomedical endeavours.

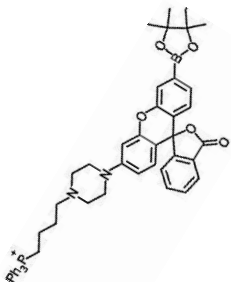
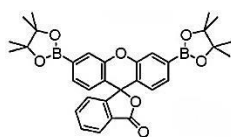
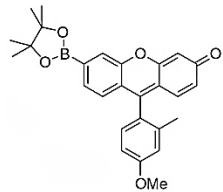
Another novel sugar-boronic acid complex, TPE-DABF, exhibits dual AIE and intramolecular charge transfer (ICT) mechanisms that allow detection of glucose and H₂O₂ through signal “on-off-on” processes (Liu et al., 2016). The presence of dialdehyde-

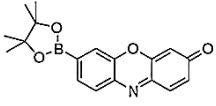
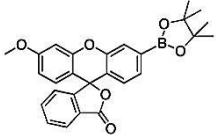
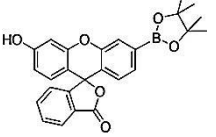
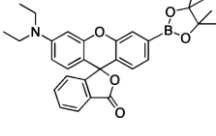
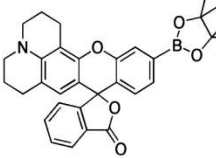
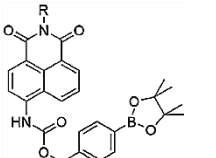
diboronic acid-functionalized tetraphenylethene, TPE-DABA (4,4'-(1,2-bis(4-formylphenyl)-1,2-ethenylene) diphenylboronic acid) in the complex TPE-DABF increases the water solubility and lowers the background fluorescence. Upon oxidation in the presence of H_2O_2 , the product of TPE-DAP (4,4'-(1,2-bis(4-hydroxyphenyl)-1,2-ethenylene)dibenzaldehyde) can induce the formation of aggregates, hence increase the fluorescence emission at 576 nm. The significant sensitivity of TPE-DABF allows it to detect H_2O_2 concentration even at a micromolar range, while in the neutral condition, it can also detect glucose. Therefore, this dual-functional probe can show significant promises in the study of H_2O_2 in physiological conditions. Moreover, glucose and acetylcholine's catalytic and oxidation reaction can induce H_2O_2 production in cells during oxidative stress. Therefore, accurate and rapid detection of these biomolecules and enzymes involved with these processes could improve health care with early disease diagnosis. Recently, a fluorescent “turn on” AIE-active bioprobe, TPE-HPro ($C_{46}H_{42}BNO_3$), was designed by Song et al. (2016) for quick and easy detection of H_2O_2 and D-glucose with high selectivity. By incorporating TPE, imine group, and phenylboronic ester, this H_2O_2 -specific AIEgen has been modulated to sense GOx catalyzed D-glucose and H_2O_2 at the micromolar range, therefore considered promising for developing rapid test strips for diabetes diagnosis and clinical research.

AIE- probe with the increased polarity of C-B bonds can be selective to H_2O_2 and allow prompt monitoring of this ROS. Such a well-designed probe is TPE-BO ($C_{38}H_{42}B_2O_4$), which has effectively been utilized for monitoring the levels in living mice macrophage (RAW264.7) cells (Zhang et al., 2015). The simple structure of this probe contains phenylboronic ester moiety that transforms into the phenol group in the presence of H_2O_2 . The transformation causes the restriction of the intramolecular rotation, turns on the fluorescence, and enables the detection of H_2O_2 . While mice macrophage cells were treated with phorbol-12-myristate-13-acetate (PMA), they can induce the production of H_2O_2 due to

the cellular inflammation response. Therefore, these endogenous ROS could easily be detected (λ_{ex} : 405 nm; λ_{em} : 488 nm) within seconds of TPE-BO exposure, indicating that the probe is a rapid H_2O_2 diagnosis tool. Additionally, more than 95% cell viability has indicated TPE-BO as a very low toxic, photostable, highly effective, and first AIEgen for *in vivo* H_2O_2 research. Properties of some currently available H_2O_2 -specific dyes are listed in Table 1.5.

Table 1.5. Properties of some H_2O_2 -specific fluorescent dyes

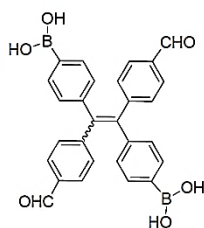
H_2O_2-specific dyes for fluorescent microscopy				
Indicator	Chemical structure	$\lambda_{\text{ex}}, \lambda_{\text{em}}$ (nm)	Solubility	Notes
MitoPY1		λ_{ex} : 510; λ_{em} : 527-580	DMSO	<ul style="list-style-type: none"> • Mitochondria targeting, H_2O_2 imaging probe • Biocompatible cell lines were HeLa, Cos-7, HEK293, and CHO.K1 (Dickinson and Chang, 2011)
	MW: 827.3781			
Peroxyfluor-1 (PF1)		λ_{ex} : 488; λ_{em} : 505-580	H_2O	<ul style="list-style-type: none"> • >500-fold higher selectivity for H_2O_2 than O_2^-, NO, and $-\text{OCl}$ • Membrane permeable, able to detect micromolar changes of H_2O_2 concentrations in living cells (Chang et al., 2004)
	MW: 553.2569			
Peroxy Green 1, PG1		λ_{ex} : 488; λ_{em} : 495-559	H_2O	<ul style="list-style-type: none"> • Mono-boronate reagent • Specific detection of H_2O_2 in aqueous solution, in living cells, and EGF/Nox generated endogenous intracellular H_2O_2 • Provide evidence for H_2O_2 signaling in brain systems through triggered growth factors in primary neurons • Unsuitable for multicolour imaging with green-fluorescent highly reactive oxygen species (hROS) probe, APF (Miller et al., 2007)
	MW: 443.2033			

Peroxy Crimson 1, PC1		λ_{ex} : 543; λ_{em} : 548-644	H ₂ O	Like PG1, PC1 cannot detect peroxide bursts at basal levels (Miller et al., 2007)
MW: 324.1428				
Peroxyfluor-2 (PF2)		λ_{ex} : 488; λ_{em} : 495-581	H ₂ O	<ul style="list-style-type: none"> • Fluorescein derivatives • Green fluorescence • Cell permeable and nontoxic
MW: 457.1822				
Peroxyfluor-3 (PF3)				(Dickinson et al., 2010)
MW: 443.1676				
Peroxy Yellow 1 (PY1)		λ_{ex} : 514; λ_{em} : 516-581	H ₂ O	<ul style="list-style-type: none"> • Rhodol derivative • Yellow fluorescence • Cell permeable and nontoxic
MW: 498.2452				(Dickinson et al., 2010)
Peroxy Orange 1 (PO1)		λ_{ex} : 540; λ_{em} : 548-613	H ₂ O	<ul style="list-style-type: none"> • Orange fluorescence; suitable for multicolor imaging with green-fluorescent ROS probe, APF • Allows selective discrimination between changes in H₂O₂ and HOCl levels • Labelling macrophages with both PO1 and APF could stimulate an immune response • Cell permeable and nontoxic
MW: 522.2456				(Dickinson et al., 2010)
Peroxy Lucifer 1 (PL1)		λ_{ex} : 820; λ_{em} : 430-495 and 535-600	DMSO	<ul style="list-style-type: none"> • Generation of H₂O₂ results in increased green-to-blue emission ratios • Biocompatible probe; enables live-cell imaging of H₂O₂ at natural immune response levels • Ratiometric data allows visual analysis of changing the concentration of H₂O₂ at phagocytic sites along with the variations of H₂O₂ throughout the cytoplasm
MW: 603.2436				(Srikun et al., 2008)

Probe 1		λ_{ex} : 405; λ_{em} : 490-590	H ₂ O	<ul style="list-style-type: none"> • Lysosome-targetable H₂O₂ indicator • Efficient for monitoring the exogenous and endogenous H₂O₂ levels <i>in vivo</i> • Better water solubility enhance the applicability • Highly selective for H₂O₂ in comparison to other ROS, such as $\cdot\text{OH}$, ONOO\cdot, OOR, NO, ClO\cdot, and t-ROOH (Kim et al., 2015)
	MW: 655.33			
Lyso-HP		λ_{ex} : 450 and 780; λ_{em} : 500-550	DMF	<ul style="list-style-type: none"> • Two-photon fluorescent probe enables deep tissue analysis for H₂O₂ up to 130 μm • H₂O₂ detection limit of the probe in living tissue is around 10 μM • Lysosome-targeted, biocompatible probe with a significant turn-on fluorescence signal (~80-fold fluorescence enhancement) • Lower toxicity, able to detect exogenous and endogenous H₂O₂ <i>in vivo</i> condition (Ren et al., 2016)
	MW: 437.2252			
H₂O₂-specific AIE probes				
TPE-TLE		λ_{ex} : 405; λ_{em} : 425-475 and λ_{em} : 570-620	DMF, DMSO, EtOH, CHCl ₃ , H ₂ O, PBS	<ul style="list-style-type: none"> • Enable ratiometric imaging of endogenous H₂O₂ in RAW264.7 macrophages and cancer cells HepG2 • Can detect H₂O₂ at micromolar level; strong fluorescence in the red channel ($\lambda_{\text{ex}} = 405 \text{ nm}$, $\lambda_{\text{em}} = 570\text{-}620 \text{ nm}$) in the presence of H₂O₂ • Exhibits higher sensitivity (detection limit: 1 μM) in PBS buffer solution containing 10% DMF • Probe performances do not influence much by pH • High selectivity, very little to no toxicity, great cell permeability (Liu et al., 2017)
	MW: 698.30			

TPE-DABA

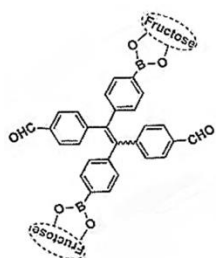
(MW: 477.1685)



TPE-
DABA
TPE-
DABF

↓ D-fructose

TPE-DABF

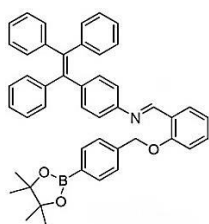


λ_{ex} : 430;
 λ_{em} : 576

H₂O,
PBS,
DMSO

- Photostable, dual functional probe for glucose and H₂O₂
 - Optimum changes in fluorescence occur within 60 min of reaction of the probe with H₂O₂
 - Sensitive detection of H₂O₂ ranging from ~3.2 μ M to 300 μ M
 - In the presence of D-fructose loses fluorescence due to the activation of intramolecular motions
 - Can detect glucose in a neutral condition
- (Liu et al., 2016)

TPE-
HPro



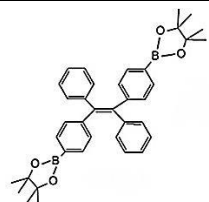
MW: 667.3258

λ_{ex} : 373;
 λ_{em} : 540

Acetonitrile
PBS

- Photostable, dual functional AIEgen for the study of H₂O₂ and D-glucose
 - H₂O₂ detection range is 0-100 μ M
 - In the presence of glucose oxidase, probe shows selectively towards glucose within the range of 0-200 μ M
 - Serum glucose level could be efficiently analyzed, therefore promising for diabetics' diagnosis and rapid detection of glucose and H₂O₂ in test strips
- (Song et al., 2016)

TPE-BO



MW: 585.3354

λ_{ex} : 405;
 λ_{em} : ~500

DMSO

- Photostable, rapid H₂O₂ monitoring tool, show maximum fluorescence within seconds
 - Very low toxicity with more than 95% cell viability
- (Zhang et al., 2015)
-

1.12 Study objectives

Lipid content and lipid composition in microalgae vary from species to species. It is also highly dependent on cultural conditions. Therefore, many challenges must be overcome for mass scale and cost-effective production of necessity-based specific lipids from microalgae. A better understanding of the physiological conditions required to coordinate and accumulate these lipids may improve comprehension of lipid-associated physiological changes in different cellular structures, including microalgae. Since large networks of genes and proteins are responsible for the remodelling of lipid biosynthesis under nutrient-limiting conditions in photosynthetic organisms (Boyle et al., 2012; Guarnieri et al., 2011; Hockin et al., 2012; Li-Beisson et al., 2015), despite a large number of studies, signaling pathways involved with lipid induction, and the interactions between growth factors and lipid content under stress conditions are still perplexed (Adams et al., 2013; Park et al., 2015; Schmollinger et al., 2014). Alongside the advanced research at the molecular level, it is also important to visualize LDs and important components that might involve their synthesis to understand the mechanisms of lipid biosynthesis and their fate during cellular metabolism. Clear links between lipid accumulation, augmented antioxidant defence and alleviated intracellular ROS levels have been demonstrated in different studies. Among the ROS molecules, H_2O_2 is more stable and can cross the phospholipid bilayer. Recently, H_2O_2 research has focused on the messenger molecule and an oxidative stress marker (Reczek and Chandel, 2015; Dickinson, 2011). Therefore, studying the lipid metabolic pathways, associated genes, reactive oxygen species, and signaling systems in different cell types is still a significant area to improve the understanding of the metabolic pathways and lipid accumulation, specifically in microalgae. Additionally, early prediction of the lipid-inducing conditions can help take necessary actions towards desired outcomes. Therefore, commercial production of LDs from microalgae

requires easy and rapid detection of the lipid-inducing conditions for which rapid and reliable LDs detection tools are in great demand.

This thesis studied two algal species based on cell wall structures: *Euglena gracilis* without a cell wall and *Chlamydomonas reinhardtii* with a carbohydrates-based cell wall. The lipid-inducing conditions and FAs composition at the different cultural conditions in these two algal species have been studied. As a novel analytical approach, AIE-based techniques have been established as the rapid, easy, biocompatible and photostable methods for studying LDs enriched conditions in two different algal cell types. Five aims are proposed to achieve the objectives:

- (1) identify lipid-inducing conditions in *E. gracilis* and *C. reinhardtii*;
- (2) develop AIE-based multicolor fluorescence imaging techniques for rapid detection of lipid drops in these two species of microalgae with different cell wall structures;
- (3) compare the performances of AIE bioprobes with traditional techniques;
- (4) determine the H_2O_2 activity as the natural by-products and component of secondary messengers in *C. reinhardtii* during lipid-induced conditions; and
- (5) determine the effects of direct H_2O_2 supplementation on the lipid production in *C. reinhardtii*.

This thesis consists of three studies to address these objectives. Study 1 and Study 2 address objectives 1, 2 and 3, focusing on the *E. gracilis* cells, and *C. reinhardtii* cells, respectively. Study 3 addresses objectives 4 and 5.

1.12.1 Study 1: Stress-induced lipid droplets conditions in a cell wall deficient alga, Euglena gracilis with aggregation induced emission (AIE) fluorophore

This study aims to identify the effects of light, nutrient starvation and supplemented carbon source on lipid accumulation in *E. gracilis* cells. LDs in this cell wall deficient microalga have been detected with lipid-specific AIE-probe, DPAS (C₂₀H₁₆N₂O). Colocalization studies have been performed with traditional lipid-specific dye, BODIPY, and the performances have been compared with DPAS. The fluorescence measurement of LDs has been cross-checked with the gravimetric analysis, and the major lipid classes have been identified. This study contributes to the knowledge of *E. gracilis* culture conditions for increased production of healthy lipids. The AIE-based LDs visualization technique has provided new opportunities to study LDs in *E. gracilis* with less effort and high efficiency.

1.12.2 Study 2: Stress-induced lipid droplet conditions with aggregation induced emission fluorophores in a flagellate microalga Chlamydomonas reinhardtii with carbohydrate cell walls

In this study, the effects of light, nutrient starvation and supplemented carbon source on lipid bioaccumulation in *C. reinhardtii* have been monitored *in vivo* with a new lipid-specific AIE probe, 2-DPAN (C₂₄H₁₈N₂O). The performances of 2-DPAN have been compared to the AIE probe, DPAS and the traditional dye, BODIPY, in this microalga with a carbohydrates-based cell wall structure. In addition, FAs composition and H₂O₂ content in the cells of different cultural conditions have also been analyzed. The outcome of this study provides information on optimized lipid enrichment conditions in *C. reinhardtii*. This study also demonstrates a

novel technique of utilizing a new AIE probe as the reliable *in vivo* lipid detection tool in a complex carbohydrates-based cell wall containing microalga. Additionally, this study also suggests the involvement of H₂O₂ in the regulation of LDs biosynthesis in microalgae.

1.13.3 Study 3: Supplementation of H₂O₂ to the medium enhanced lipid accumulation in microalgae: visualizing lipid drops with a novel fluorescent probe

Following the association of the H₂O₂ in lipid induction identified in Study 2, the effects of direct supplementation of H₂O₂ on growth, lipid biosynthesis and FAs composition were studied in *C. reinhardtii*. H₂O₂ activity in the nutrient-altered conditions has been determined *in vivo* with a new H₂O₂-specific AIEgen, TPE-BO (C₃₈H₄₂B₂O₄). In addition, lipid accumulation in different conditions has also been analyzed with lipid-specific AIE probe 2-DPAN. This study provides new insights into the effects of H₂O₂ as the messenger molecule and stressed marker in lipid induction in *C. reinhardtii*. Additionally, a novel AIE-based strategy of wash free, biocompatible, photostable, multicolour imaging of H₂O₂ activities during lipid biosynthesis in *C. reinhardtii* has been established to further screen the LDs production capacity in other algal species for human benefits.

1.13 Thesis organization

The present thesis consists of five chapters to illustrate specific research aims, methods, and results, ultimately contributing to algal lipid research by establishing the lipid-inducing conditions and developing rapid, easy, and reliable *in vivo* LDs and H₂O₂ monitoring techniques.

Chapter 1 briefly introduces the importance of microalgae, ROS molecules, and some key features of lipid and H₂O₂ detection techniques in microalgae. Then, a brief background provides the current constraints and knowledge gaps in lipid research in microalgae.

Three data chapters (2, 3, and 4) represent three major experiments in this thesis. The experiments have been designed consecutively based on the outcomes of the chapters. Therefore, some repetitions could be noticed in the background and method sections. All the chapters have been formatted as manuscripts for journal publications. The studies were performed by the author of the present thesis under the supervision of the principal supervisor and co-supervisors. Therefore, in the published manuscripts of the peer-reviewed journals, the author of this thesis has been enlisted as a principal author.

Chapter 5 generally discusses the main results found in the thesis research with a provision for future research.

Published papers in each chapter

Chapter 1: General introduction

Published as two review articles and one book chapter as follows:

Reza, A.H.M.M., Tavakoli, J., Zhou, Y., Qin, J., & Tang, Y. (2020). Synthetic fluorescent probes to apprehend calcium signalling in lipid droplet accumulation in microalgae—an updated review. *Science China Chemistry*, 63. <https://doi.org/10.1007/s11426-019-9664-7>

Reza, A.H.M.M., Zhu, X., Qin, J., & Tang, Y. (2021). Microalgae-derived health supplements to therapeutic shifts: Redox-based study opportunities with AIE-based technologies. *Advanced Healthcare Materials*, 10(24):e2101223 <https://doi.org/10.1002/adhm.202101223>

Reza, A.H.M.M., Zhou, Y., Qin, J. & Tang, Y. (2021). Aggregation-induced emission luminogens for lipid droplet imaging. In book: *Progress in Molecular Biology and Translational Science* Publisher: Elsevier B.V. ISSN (Print): 1877-1173. <https://doi.org/10.1016/bs.pmbts.2021.06.009>

Chapter 2: Stress-induced lipid droplets conditions in a cell wall deficient alga, *Euglena gracilis* with aggregation induced emission (AIE) fluorophore

Published as **Reza, A.H.M.M.**, Zhou, Y., Tavakoli, J., Tang, Y., & Qin, J. (2021). Understanding the lipid production mechanism in *Euglena gracilis* with a fast-response AIEgen bioprobe, DPAS. *Materials Chemistry Frontiers*, 5, 268-283. <https://doi.org/10.1039/d0qm00621a>

Chapter 3: Stress-induced lipid droplet conditions with aggregation induced emission fluorophores in a flagellate microalga *Chlamydomonas reinhardtii* with carbohydrate cell walls

Chapter 4: Supplementation of H₂O₂ to the medium enhanced lipid accumulation in microalgae: visualizing lipid drops with a novel fluorescent probe

Chapter 3 and Chapter 4 have been combined and published in *Biosensors* as **Reza, A.H.M.M.**, Rakhi, S.F., Zhu, X., Qin, J., & Tang, Y. (2022). Visualizing the emerging platform of using microalgae as a sustainable bio-factory for healthy lipid production through biocompatible AIE probes. *Biosensors*, 12(4): 208. <https://doi.org/10.3390/bios12040208>

Chapter 5: General discussion, conclusions and future research.

1.14 References

Abramczyk, H., Surmacki, J., Kopeć, M., Olejnik, A. K., Lubecka-Pietruszewska, K., & Fabianowska-Majewska, K. (2015). The role of lipid droplets and adipocytes in cancer. Raman imaging of cell cultures: MCF10A, MCF7, and MDA-MB-231 compared to adipocytes in cancerous human breast tissue. *The Analyst*, 140(7), 2224-2235. <https://doi.org/10.1039/c4an01875c>

Adams, C., Godfrey, V., Wahlen, B., Seefeldt, L. & Bugbee, B. (2013). Understanding precision nitrogen stress to optimize the growth and lipid content trade-off in oleaginous green microalgae. *Bioresource Technology*, 131, 188-194. <https://doi.org/10.1016/j.biortech.2012.12.143>

Afzal, M., Matsugo, S., Sasai, M., Xu, B., Aoyama, K., & Takeuchi, T. (2003). Method to overcome photoreaction, a serious drawback to the use of dichlorofluorescein in evaluation of reactive oxygen species. *Biochemical and Biophysical Research Communications*, 304(4), 619-624. [https://doi.org/10.1016/s0006-291x\(03\)00641-7](https://doi.org/10.1016/s0006-291x(03)00641-7)

Aguirre, J., Ríos-Momberg, M., Hewitt, D., & Hansberg, W. (2005). Reactive oxygen species and development in microbial eukaryotes. *Trends in Microbiology*, 13(3), 111-118. <https://doi.org/10.1016/j.tim.2005.01.007>

Aoki, T., Hagiwara, H., & Fujimoto, T. (1997). Peculiar distribution of fodrin in fat-storing cells. *Experimental Cell Research*, 234(2), 313-320. <https://doi.org/10.1006/excr.1997.3645>

Anderson, A., Bothwell, J. H., Laohavisit, A., Smith, A. G., & Davies, J. M. (2011). NOX or not? Evidence for algal NADPH oxidases. *Trends in Plant Science*, 16(11), 579-581. <https://doi.org/10.1016/j.tplants.2011.09.003>

- Armoza-Zvuloni, R., Schneider, A., Sher, D., & Shaked, Y. (2016). Rapid Hydrogen Peroxide release from the coral *Stylophora pistillata* during feeding and in response to chemical and physical stimuli. *Scientific Reports*, 6, 21000. <https://doi.org/10.1038/srep21000>
- Arroussi, H. E. I., Benhima, R., Iman, B., Mernissi, N. E. I., & Wahby, I. (2015). Improvement of the potential of *Dunaliella tertiolecta* as a source of biodiesel by auxin treatment coupled to salt stress, *Renewable Energy*, 77, 15-19. <https://doi.org/10.1016/j.renene.2014.12.010>
- Avagyan, A. B. (2008). A contribution to global sustainable development: inclusion of microalgae and their biomass in production and bio cycles. *Clean Technologies and Environmental Policy*, 10(4), 313-317. <https://doi.org/10.1007/s10098-008-0180-5>
- Avallone, R., Vitale, G., & Bertolotti, M. (2019). Omega-3 fatty acids and neurodegenerative diseases: New evidence in clinical trials. *International Journal of Molecular Sciences*, 20(17), 4256. <https://doi.org/10.3390/ijms20174256>
- Balić, A., Vlašić, D., Žužul, K., Marinović, B., & Bukvić Mokos, Z. (2020). Omega-3 versus omega-6 polyunsaturated fatty acids in the prevention and treatment of inflammatory skin diseases. *International Journal of Molecular Sciences*, 21(3), 741. <https://doi.org/10.3390/ijms21030741>
- Berliner, L. J. (2016). The evolution of biomedical EPR (ESR), *Biomedical Spectroscopy and Imaging*, 5, 5-26. <https://doi.org/10.3233/BSI-150128>
- Bhattacharjee S. (2012). "The language of reactive oxygen species signaling in plants", *Journal of Botany*, Article ID 985298, 22. <https://doi.org/10.1155/2012/985298>

Bleier, L., & Dröse, S. (2013). Superoxide generation by complex III: from mechanistic rationales to functional consequences. *Biochimica et Biophysica Acta*, 1827(11-12), 1320-1331. <https://doi.org/10.1016/j.bbabi.2012.12.002>

Boyle, N. R., Page, M. D., Liu, B., Blaby, I. K., Casero, D., Kropat, J., Cokus, S. J., Hong-Hermesdorf, A., Shaw, J., Karpowicz, S. J., Gallaher, S. D., Johnson, S., Benning, C., Pellegrini, M., Grossman, A. & Merchant, S. S. (2012). Three acyltransferases and nitrogen-responsive regulator are implicated in nitrogen starvation-induced triacylglycerol accumulation in *Chlamydomonas*. *Journal of Biological Chemistry*, 287(19), 15811-15825. <https://doi.org/10.1074/jbc.M111.334052>

Breckwoldt, M. O., Wittmann, C., Misgeld, T., Kerschensteiner, M., & Grabher, C. (2015). Redox imaging using genetically encoded redox indicators in zebrafish and mice. *Biological Chemistry*, 396(5), 511-522. <https://doi.org/10.1515/hsz-2014-0294>

Brown, M. B., Miller, J. N. & Seare, N. J. (1995). An investigation of the use of Nile red as a long-wavelength fluorescent probe for the study of alpha 1-acid glycoprotein-drug interactions. *Journal of Pharmaceutical and Biomedical Analysis*, 13(8), 1011-7. [https://doi.org/10.1016/0731-7085\(95\)01524-O](https://doi.org/10.1016/0731-7085(95)01524-O)

Bulger R.E., & Strum J.M. (1974). The machinery of the cytoplasm. In: The functioning cytoplasm. Springer, Boston, MA. https://doi.org/10.1007/978-1-4615-8717-0_3

Cabanelas, I. T., van der Zwart, M., Kleinegris, D. M., Wijffels, R. H., & Barbosa, M. J. (2016). Sorting cells of the microalga *Chlorococcum littorale* with increased triacylglycerol productivity. *Biotechnology for Biofuels*, 9(1), 183. <https://doi.org/10.1186/s13068-016-0595->

x

- Chen, S., Hong, Y., Liu, Y., Liu, J., Leung, C. W., Li, M., Kwok, R. T., Zhao, E., Lam, J. W., Yu, Y. & Tang, B. Z. (2013). Full-range intracellular pH sensing by an aggregation-induced emission-active two-channel ratiometric fluorogen. *Journal of the American Chemical Society*, 135(13), 4926-9. [https://doi.org/ 10.1021/ja400337p](https://doi.org/10.1021/ja400337p)
- Chen, H., Chen, S. L., & Jiang, J. G. (2011). Effect of Ca²⁺ channel block on glycerol metabolism in *Dunaliella salina* under hypoosmotic and hyperosmotic stresses. *PLoS One*, 6(12), e28613. <https://doi.org/10.1371/journal.pone.0028613>
- Cheng, Y., & Yang, J. M. (2011). Survival and death of endoplasmic-reticulum-stressed cells: Role of autophagy. *World Journal of Biological Chemistry*, 2(10), 226-231. <https://doi.org/10.4331/wjbc.v2.i10.226>
- Chisti, Y. (2007). Biodiesel from microalgae. *Biotechnology Advances*, 25(3), 294-306. <https://doi.org/10.1016/j.biotechadv.2007.02.001>
- Chen, H., Zhang, Y., He, C., & Wang, Q. (2014). Ca²⁺ signal transduction related to neutral lipid synthesis in an oil-producing green alga *Chlorella* sp. C2. *Plant and Cell Physiology*, 55(3), 634-44. [https://doi.org/ 10.1093/pcp/pcu015](https://doi.org/10.1093/pcp/pcu015)
- Chiu, S. Y., Kao, C. Y., Tsai, M. T., Ong, S. C., Chen, C. H., & Lin, C. S. (2009). Lipid accumulation and CO₂ utilization of *Nannochloropsis oculata* in response to CO₂ aeration. *Bioresource Technology*, 100(2), 833-838. <https://doi.org/10.1016/j.biortech.2008.06.061>
- Collot, M., Ashokkumar, P., Anton, H., Boutant, E., Faklaris, O., Galli, T., Mély, Y., Danglot, L., & Klymchenko, A. S. (2019). MemBright: A family of fluorescent membrane probes for advanced cellular imaging and neuroscience. *Cell Chemical Biology*, 26(4), 600-614.e7. <https://doi.org/10.1016/j.chembiol.2019.01.009>

Collot, M., Fam, T. K., Ashokkumar, P., Faklaris, O., Galli, T., Danglot, L. & Klymchenko, A. S. (2018). Ultrabright and Ffluorogenic probes for multicolor imaging and tracking of lipid droplets in cells and tissues. *Journal of the American Chemical Society*, *140*(16), 5401-5411. <https://doi.org/10.1021/jacs.7b12817>

Daemen, S., van Zandvoort, M., Parekh, S. H., & Hesselink, M. (2015). Microscopy tools for the investigation of intracellular lipid storage and dynamics. *Molecular Metabolism*, *5*(3), 153-163. <https://doi.org/10.1016/j.molmet.2015.12.005>

Dębski, D., Smulik, R., Zielonka, J., Michałowski, B., Jakubowska, M., Dębowska, K., Adamus, J., Marcinek, A., Kalyanaraman, B., & Sikora, A. (2016). Mechanism of oxidative conversion of Amplex® Red to resorufin: Pulse radiolysis and enzymatic studies. *Free Radical Biology & Medicine*, *95*, 323-332. <https://doi.org/10.1016/j.freeradbiomed.2016.03.027>

del Río, L. A., Sandalio, L. M., Corpas, F. J., Palma, J. M., & Barroso, J. B. (2006). Reactive oxygen species and reactive nitrogen species in peroxisomes. Production, scavenging, and role in cell signaling. *Plant Physiology*, *141*(2), 330-335. <https://doi.org/10.1104/pp.106.078204>

Dickinson, B. C., & Chang, C. J. (2011). Chemistry and biology of reactive oxygen species in signaling or stress responses. *Nature Chemical Biology*, *7*(8), 504-511. <https://doi.org/10.1038/nchembio.607>

Dickinson, B. C., Huynh, C., & Chang, C. J. (2010). A palette of fluorescent probes with varying emission colors for imaging hydrogen peroxide signaling in living cells. *Journal of the American Chemical Society*, *132*(16), 5906-5915. <https://doi.org/10.1021/ja1014103>

- Dikalov, S., Griendling, K. K., & Harrison, D. G. (2007). Measurement of reactive oxygen species in cardiovascular studies. *Hypertension (Dallas, Tex.: 1979)*, 49(4), 717-727. <https://doi.org/10.1161/01.HYP.0000258594.87211.6b>
- Dong, H., & Czaja, M. J. (2011). Regulation of lipid droplets by autophagy. *Trends in Endocrinology and Metabolism: TEM*, 22(6), 234-240. <https://doi.org/10.1016/j.tem.2011.02.003>
- Dröse, S., & Brandt, U. (2012). Molecular mechanisms of superoxide production by the mitochondrial respiratory chain. *Advances in Experimental Medicine and Biology*, 748, 145-169. https://doi.org/10.1007/978-1-4614-3573-0_6
- Du, Z. Y., Alvaro, J., Hyden, B., Zienkiewicz, K., Benning, N., Zienkiewicz, A., Bonito, G., & Benning, C. (2018). Enhancing oil production and harvest by combining the marine alga *Nannochloropsis oceanica* and the oleaginous fungus *Mortierella elongata*. *Biotechnology for Biofuels*, 11, 174. <https://doi.org/10.1186/s13068-018-1172-2>
- Dugail I. (2014). Lysosome/lipid droplet interplay in metabolic diseases. *Biochimie*, 96, 102-105. <https://doi.org/10.1016/j.biochi.2013.07.008>
- Dutta, A. K., Kamada, K. & Ohta, K. (1996). Spectroscopic studies of Nile red in organic solvents and polymers. *Journal of Photochemistry and Photobiology A: Chemistry*, 93(1), 57-64. [https://doi.org/10.1016/1010-6030\(95\)04140-0](https://doi.org/10.1016/1010-6030(95)04140-0)
- Elle, I. C., Olsen, L. C., Pultz, D., Rodkaer, S. V. & Faergeman, N. J. (2010). Something worth dyeing for: molecular tools for the dissection of lipid metabolism in *Caenorhabditis elegans*. *FEBS Letters*, 584(11), 2183-2193. <https://doi.org/10.1016/j.febslet.2010.03.046>

Elsey, D., Jameson, D., Raleigh, B. & Cooney, M. J. (2007). Fluorescent measurement of microalgal neutral lipids. *Journal of Microbiological Methods*, 68(3), 639-42. <https://doi.org/10.1016/j.mimet.2006.11.008>

Farrokheh, A., Tahvildari, K. & Nozari, M. (2020). Biodiesel production from the *Chlorella vulgaris* and *Spirulina platensis* microalgae by electrolysis using CaO/KOH-Fe₃O₄ and KF/KOH-Fe₃O₄ as magnetic nanocatalysts. *Biomass Conversion and Biorefinery*, <https://doi.org/10.1007/s13399-020-00688-z>

Fink, B., Laude, K., McCann, L., Doughan, A., Harrison, D. G., & Dikalov, S. (2004). Detection of intracellular superoxide formation in endothelial cells and intact tissues using dihydroethidium and an HPLC-based assay. *American Journal of Physiology. Cell Physiology*, 287(4), C895-C902. <https://doi.org/10.1152/ajpcell.00028.2004>

Fisk, H. L., West, A. L., Childs, C. E., Burdge, G. C., & Calder, P. C. (2014). The use of gas chromatography to analyze compositional changes of fatty acids in rat liver tissue during pregnancy. *Journal of Visualized Experiments: JoVE*, 85, 51445. <https://doi.org/10.3791/51445>

Folkes, L. K., Patel, K. B., Wardman, P., & Wrona, M. (2009). Kinetics of reaction of nitrogen dioxide with dihydrorhodamine and the reaction of the dihydrorhodamine radical with oxygen: implications for quantifying peroxynitrite formation in cells. *Archives of Biochemistry and Biophysics*, 484(2), 122-126. <https://doi.org/10.1016/j.abb.2008.10.014>

Freitas, R., & Campos, M. M. (2019). Protective effects of omega-3 fatty acids in cancer-related complications. *Nutrients*, 11(5), 945. <https://doi.org/10.3390/nu11050945>

- Frigolet, M. E., & Gutiérrez-Aguilar, R. (2017). The role of the novel lipokine palmitoleic acid in health and disease. *Advances in Nutrition* (Bethesda, Md.), 8(1), 173S-181S. <https://doi.org/10.3945/an.115.011130>
- Fuchs, B., Süss, R., Teuber, K., Eibisch, M., & Schiller, J. (2011). Lipid analysis by thin-layer chromatography--a review of the current state. *Journal of Chromatography. A*, 1218(19), 2754-2774. <https://doi.org/10.1016/j.chroma.2010.11.066>
- Fujita, A., Cheng, J., & Fujimoto, T. (2010). Quantitative electron microscopy for the nanoscale analysis of membrane lipid distribution. *Nature Protocols*, 5(4), 661-669. <https://doi.org/10.1038/nprot.2010.20>
- Furse, S., Egmond, M. R., & Killian, J. A. (2015). Isolation of lipids from biological samples. *Molecular Membrane Biology*, 32(3), 55-64. <https://doi.org/10.3109/09687688.2015.1050468>
- Fussbroich, D., Colas, R. A., Eickmeier, O., Trischler, J., Jerkic, S. P., Zimmermann, K., Göpel, A., Schwenger, T., Schaible, A., Henrich, D., Baer, P., Zielen, S., Dalli, J., Beermann, C., & Schubert, R. (2020). A combination of LCPUFA ameliorates airway inflammation in asthmatic mice by promoting pro-resolving effects and reducing adverse effects of EPA. *Mucosal Immunology*, 13(3), 481-492. <https://doi.org/10.1038/s41385-019-0245-2>
- Garcia A. C., Arispuro I. V., Hernandez E. A. and Tellez M. A. A. M. (2012). Oligoglucan elicitor effects during plant oxidative stress, Cell Metabolism - Cell Homeostasis and Stress Response, Paula Bubulya, IntechOpen, <https://doi.org/10.5772/26057>.
- Garg, S., Rose, A. L., Godrant, A., & Waite, T. D. (2007) Iron uptake by the ichthyotoxic *Chattonella marina* (Raphidophyceae): impact of superoxide generation. *Journal of Phycology*, 43, 978-991. <https://doi.org/10.1111/j.1529-8817.2007.00394.x>

- Gimpel, J. A., Henríquez, V. & Mayfield, S. P. (2015). In Metabolic Engineering of eukaryotic microalgae: Potential and challenges come with great diversity. *Frontiers in Microbiology*, 6, 1376. <https://doi.org/10.3389/fmicb.2015.01376>
- Goncalves, E. C., Wilkie, A. C., Kirst, M., & Rathinasabapathi, B. (2016). Metabolic regulation of triacylglycerol accumulation in the green algae: identification of potential targets for engineering to improve oil yield. *Plant Biotechnology Journal*, 14(8), 1649-1660. <https://doi.org/10.1111/pbi.12523>
- Gong, M., & Bassi, A. (2016). Carotenoids from microalgae: A review of recent developments. *Biotechnology Advances*, 34(8), 1396-1412. <https://doi.org/10.1016/j.biotechadv.2016.10.005>
- González, A., Trebotich, J., Vergara, E., Medina, C., Morales, B., & Moenne, A. (2010). Copper-induced calcium release from ER involves the activation of ryanodine-sensitive and IP(3)-sensitive channels in *Ulva compressa*. *Plant Signaling & Behavior*, 5(12), 1647-1649. <https://doi.org/10.4161/psb.5.12.13977>
- Goodson, C., Roth, R., Wang, Z. T., & Goodenough, U. (2011). Structural correlates of cytoplasmic and chloroplast lipid body synthesis in *Chlamydomonas reinhardtii* and stimulation of lipid body production with acetate boost. *Eukaryotic Cell*, 10(12), 1592-1606. <https://doi.org/10.1128/EC.05242-11>
- Gorain, P. C., Bagchi, S. K., & Mallick, N. (2013). Effects of calcium, magnesium and sodium chloride in enhancing lipid accumulation in two green microalgae. *Environmental Technology*, 34(13-16), 1887-94. <https://doi.org/10.1080/09593330.2013.812668>

- Greenspan, P., Mayer, E. P., & Fowler, S. D. (1985). Nile red: a selective fluorescent stain for intracellular lipid droplets. *Journal of Cell Biology*, 1985(100), 965-973. <https://doi.org/10.1083/jcb.100.3.965>
- Grivennikova, V. G., & Vinogradov, A. D. (2006). Generation of superoxide by the mitochondrial Complex I. *Biochimica et Biophysica Acta*, 1757(5-6), 553-561. <https://doi.org/10.1016/j.bbabi.2006.03.013>
- Gu, Y., Zhao, Z., Su, H., Zhang, P., Liu, J., Niu, G., Li, S., Wang, Z., Kwok, R., Ni, X. L., Sun, J., Qin, A., Lam, J., & Tang, B. Z. (2018). Exploration of biocompatible AIEgens from natural resources. *Chemical Science*, 9(31), 6497-6502. <https://doi.org/10.1039/c8sc01635f>
- Guarnieri, M. T., Nag, A., Smolinski, S. L., Darzins, A., Seibert, M. & Pienkos, P. T. (2011). Examination of triacylglycerol biosynthetic pathways via de novo transcriptomic and proteomic analyses in an unsequenced microalga. *PLoS ONE*, 6, e25851. <https://doi.org/10.1371/journal.pone.0025851>
- Guo, E. L., & Katta, R. (2017). Diet and hair loss: effects of nutrient deficiency and supplement use. *Dermatology Practical & Conceptual*, 7(1), 1-10. <https://doi.org/10.5826/dpc.0701a01>
- Gutiérrez, S., Svahn, S. L., & Johansson, M. E. (2019). Effects of omega-3 fatty acids on immune cells. *International Journal of Molecular Sciences*, 20(20), 5028. <https://doi.org/10.3390/ijms20205028>
- Hagiwara, D., Sakamoto, K., Abe, K., & Gomi, K. (2016). Signaling pathways for stress responses and adaptation in *Aspergillus* species: stress biology in the post-genomic era. *Bioscience, Biotechnology, and Biochemistry*, 80(9), 1667-1680. <https://doi.org/10.1080/09168451.2016.1162085>

Hamon, N., Roux, A., Beyler, M., Mulatier, J. C., Andraud, C., Nguyen, C., Maynadier, M., Bettache, N., Duperray, A., Grichine, A., Brasselet, S., Gary-Bobo, M., Maury, O., & Tripier, R. (2020). Pycnen-based Ln(III) complexes as highly luminescent bioprobes for *in vitro* and *in vivo* one- and two-photon bioimaging applications. *Journal of the American Chemical Society*, *142*(22), 10184-10197. <https://doi.org/10.1021/jacs.0c03496>

He, Q., Yang, H., Wu, L., & Hu, C. (2015). Effect of light intensity on physiological changes, carbon allocation and neutral lipid accumulation in oleaginous microalgae. *Bioresource Technology*, *191*, 219-228. <https://doi.org/10.1016/j.biortech.2015.05.021>

Hockin, N. L., Mock, T., Mulholland, F., Kopriva, S. & Malin, G. (2012). The response of diatom central carbon metabolism to nitrogen starvation is different from that of green algae and higher plants. *Plant Physiology*, *158*(1), 299-312. <https://doi.org/10.1104/pp.111.184333>

Hong, Y., Lam, J. W. & Tang, B. Z. (2009). Aggregation-induced emission: phenomenon, mechanism and applications. *Chemical Communications*, *29*, 4332-53. <https://doi.org/10.1039/b904665h>

Hopkins, R. Z. (2016). Superoxide in biology and medicine: an overview. *Reactive Oxygen Species*, *1*, 99-109. <https://doi.org/10.20455/ros.2016.825>

Hosseini, A., Jazini, M., Mahdih, M., & Karimi, K. (2020). Efficient superantioxidant and biofuel production from microalga *Haematococcus pluvialis* via a biorefinery approach. *Bioresource Technology*, *306*, 123100. <https://doi.org/10.1016/j.biortech.2020.123100>.

He, Y. K., Tang, R. H., Hao, Y., Stevens, R. D., Cook, C. W., Ahn, S. M., Jing, L., Yang, Z., Chen, L., Guo, F., Fiorani, F., Jackson, R. B., Crawford, N. M. & Pei, Z. M. (2004). Nitric oxide represses the *Arabidopsis* floral transition. *Science*, *305*(5692), 1968-1971. <https://doi.org/10.1126/science.1098837>

- Hernández-Barrera, A., Velarde-Buendía, A., Zepeda, I., Sanchez, F., Quinto, C., Sánchez-Lopez, R., Cheung, A. Y., Wu, H. M., & Cardenas, L. (2015). Hyper, a hydrogen peroxide sensor, indicates the sensitivity of the Arabidopsis root elongation zone to aluminum treatment. *Sensors (Basel, Switzerland)*, *15*(1), 855-867. <https://doi.org/10.3390/s150100855>
- Horn, P. J., Ledbetter, N. R., James, C. N., Hoffman, W. D., Case, C. R., Verbeck, G. F., & Chapman, K. D. (2011). Visualization of lipid droplet composition by direct organelle mass spectrometry. *The Journal of Biological Chemistry*, *286*(5), 3298-3306. <https://doi.org/10.1074/jbc.M110.186353>
- Hu, R., Chen, B., Wang, Z., Qin, A., Zhao, Z., Lou, X., & Tang, B. Z. (2019). Intriguing "chameleon" fluorescent bioprobes for the visualization of lipid droplet-lysosome interplay. *Biomaterials*, *203*, 43-51. <https://doi.org/10.1016/j.biomaterials.2019.03.002>
- Hu, Q., Sommerfeld, M., Jarvis, E., Ghirardi, M., Posewitz, M., Seibert, M. & Darzins, A. (2008). Microalgal triacylglycerols as feedstocks for biofuel production: perspectives and advances. *The Plant Journal*, *54*(4), 621-639. <https://doi.org/10.1111/j.1365-313X.2008.03492.x>
- Hu, X., Jiang, M., Zhang, J., Zhang, A., Lin, F., & Tan, M. (2007). Calcium-calmodulin is required for abscisic acid-induced antioxidant defense and functions both upstream and downstream of H₂O₂ production in leaves of maize (*Zea mays*) plants. *The New Phytologist*, *173*(1), 27-38. <https://doi.org/10.1111/j.1469-8137.2006.01888.x>
- Huerlimann, R., & Heimann, K. (2013). Comprehensive guide to acetyl-carboxylases in algae. *Critical Reviews in Biotechnology*, *33*(1), 49-65. <https://doi.org/10.3109/07388551.2012.668671>

- Hwangbo, M., & Chu, K. H. (2020). Recent advances in production and extraction of bacterial lipids for biofuel production. *The Science of the Total Environment*, 734, 139420. <https://doi.org/10.1016/j.scitotenv.2020.139420>
- Imlay J. A. (2003). Pathways of oxidative damage. *Annual Review of Microbiology*, 57, 395-418. <https://doi.org/10.1146/annurev.micro.57.030502.090938>
- Ishihara, M., Kujiraoka, T., Iwasaki, T., Nagano, M., Takano, M., Ishii, J., Tsuji, M., Ide, H., Miller, I. P., Miller, N. E., & Hattori, H. (2005). A sandwich enzyme-linked immunosorbent assay for human plasma apolipoprotein A-V concentration. *Journal of Lipid Research*, 46(9), 2015-2022. <https://doi.org/10.1194/jlr.D500018-JLR200>
- Jaeger, D., Pilger, C., Hachmeister, H., Oberländer, E., Wördenweber, R., Wichmann, J., Mussnug, J. H., Huser, T., & Kruse, O. (2016). Label-free in vivo analysis of intracellular lipid droplets in the oleaginous microalga *Monoraphidium neglectum* by coherent Raman scattering microscopy. *Scientific Reports*, 6, 35340. <https://doi.org/10.1038/srep35340>
- Janssen, J. H., Wijffels, R. H., & Barbosa, M. J. (2019). Lipid production in *Nannochloropsis gaditana* during nitrogen starvation. *Biology*, 8(1), 5. <https://doi.org/10.3390/biology8010005>
- Ji, R. Y., Ding, Y., Shi, T. Q., Lin, L., Huang, H., Gao, Z., & Ji, X. J. (2018). Metabolic engineering of yeast for the production of 3-hydroxypropionic acid. *Frontiers in Microbiology*, 9, 2185. <https://doi.org/10.3389/fmicb.2018.02185>
- Jiang, G., Li, C., Liu, X., Chen, Q., Li, X., Gu, X., Zhang, P., Lai, Q., & Wang, J. (2020). Lipid droplet-targetable fluorescence guided photodynamic therapy of cancer cells with an activatable AIE-active fluorescent probe for hydrogen peroxide. *Advanced Optical Materials*, 8, 20, 2001119. <https://doi.org/10.1002/adom.202001119>

- Jiang, M., Gu, X., Lam, J., Zhang, Y., Kwok, R., Wong, K. S., & Tang, B. Z. (2017). Two-photon AIE bio-probe with large Stokes shift for specific imaging of lipid droplets. *Chemical Science*, 8(8), 5440-5446. <https://doi.org/10.1039/c7sc01400g>
- Johnson, M. R., Stephenson, R. A., Ghaemmaghami, S., & Welte, M. A. (2018). Developmentally regulated H2Av buffering via dynamic sequestration to lipid droplets in *Drosophila* embryos. *eLife*, 7, e36021. <https://doi.org/10.7554/eLife.36021>
- Jones, C. S., & Mayfieldt, S. P. (2012). Algae biofuels: versatility for the future of bioenergy. *Current Opinion in Biotechnology*, 23, 346-351. <https://doi.org/10.1016/j.copbio.2011.10.013>
- Kang, M., Gu, X., Kwok, R. T., Leung, C. W., Lam, J. W., Li, F. & Tang, B. Z. (2016). A near-infrared AIEgen for specific imaging of lipid droplets. *Chemical Communications*, 52(35), 5957-60. <https://doi.org/10.1039/c6cc01797e>
- Karash, S., & Kwon, Y. M. (2018). Iron-dependent essential genes in *Salmonella Typhimurium*. *BMC Genomics*, 19(1), 610. <https://doi.org/10.1186/s12864-018-4986-1>
- Khan, M. I., Shin, J. H., & Kim, J. D. (2018). The promising future of microalgae: current status, challenges, and optimization of a sustainable and renewable industry for biofuels, feed, and other products. *Microbial Cell Factories*, 17(1), 36. <https://doi.org/10.1186/s12934-018-0879-x>
- Kim, J., Brown, C. M., Kim, M. K., Burrows, E. H., Bach, S., Lun, D. S., & Falkowski, P. G. (2017). Effect of cell cycle arrest on intermediate metabolism in the marine diatom *Phaeodactylum tricornutum*. *Proceedings of the National Academy of Sciences of the United States of America*, 114(38), E8007-E8016. <https://doi.org/10.1073/pnas.1711642114>

Kim, D., Kim, G., Nam, S. J., Yin, J., & Yoon, J. (2015). Visualization of endogenous and exogenous hydrogen peroxide using a lysosome-targetable fluorescent probe. *Scientific Reports*, 5, 8488. <https://doi.org/10.1038/srep08488>

Klymchenko A. S. (2017). Solvatochromic and fluorogenic dyes as environment-sensitive probes: Design and biological applications. *Accounts of Chemical Research*, 50(2), 366-375. <https://doi.org/10.1021/acs.accounts.6b00517>

Knothe G. (2009). Improving biodiesel fuel properties by modifying fatty ester composition. *Energy & Environmental Science*. 2(7), 759-766. <https://doi.org/10.1039/B903941D>

Koopman, R., Schaart, G., & Hesselink, M. K. (2001). Optimisation of oil red O staining permits combination with immunofluorescence and automated quantification of lipids. *Histochemistry and Cell Biology*, 116(1), 63-68. <https://doi.org/10.1007/s004180100297>

Kumari, P., Kumar, M., Reddy, C. R. K. & Jha, B. (2013). Algal lipids, fatty acids and sterols. Functional ingredients from algae for foods and nutraceuticals, Edition: First Chapter: algal lipids, fatty acids and sterols. *Woodhead Publishing Series in Food Science, Technology and Nutrition*, pp. 87-134

Larosa, V., Meneghesso, A., La Rocca, N., Steinbeck, J., Hippler, M., Szabò, I., & Morosinotto, T. (2018). Mitochondria affect photosynthetic electron transport and photosensitivity in a green alga. *Plant Physiology*, 176(3), 2305-2314. <https://doi.org/10.1104/pp.17.01249>

Lavis L. D. (2017). Teaching old dyes new tricks: Biological probes built from fluoresceins and rhodamines. *Annual Review of Biochemistry*, 86, 825-843. <https://doi.org/10.1146/annurev-biochem-061516-04483>

- Lepock J. R. (2003). Cellular effects of hyperthermia: relevance to the minimum dose for thermal damage. *International Journal of Hyperthermia: the Official Journal of European Society for Hyperthermic Oncology, North American Hyperthermia Group*, 19(3), 252-266. <https://doi.org/10.1080/0265673031000065042>
- Leung, C. W., Hong, Y., Chen, S., Zhao, E., Lam, J. W. & Tang, B. Z. (2013). A photostable AIE luminogen for specific mitochondrial imaging and tracking. *Journal of the American Chemical Society*, 135(1), 62-5. <https://doi.org/10.1021/ja310324q>
- Li, J., Vosegaard, T., & Guo, Z. (2017). Applications of nuclear magnetic resonance in lipid analyses: An emerging powerful tool for lipidomics studies. *Progress in Lipid Research*, 68, 37-56. <https://doi.org/10.1016/j.plipres.2017.09.003>
- Li, M., Yang, L., Bai, Y., & Liu, H. (2014a). Analytical methods in lipidomics and their applications. *Analytical Chemistry*, 86(1), 161-175. <https://doi.org/10.1021/ac403554h>
- Li, L., Han, J., Wang, Z., Liu, J., Wei, J., Xiong, S., & Zhao, Z. (2014b). Mass spectrometry methodology in lipid analysis. *International Journal of Molecular Sciences*, 15(6), 10492-10507. <https://doi.org/10.3390/ijms150610492>
- Li-Beisson, Y., Beisson, F. & Riekhof, W. (2015). Metabolism of acyl-lipids in *Chlamydomonas reinhardtii*. *The Plant Journal*, 82(3), 504-522. <https://doi.org/10.1111/tpj.12787>
- Lin, I. P., Jiang, P. L., Chen, C. S. & Tzen, J. T. C. (2012). A unique caleosin serving as the major integral protein in oil bodies isolated from *Chlorella* sp. cells cultured with limited nitrogen. *Plant Physiology and Biochemistry*, 61, 80-87. <https://doi.org/10.1016/j.plaphy.2012.09.008>

- Liu, Y., Nie, J., Niu, J., Meng, F., & Lin, W. (2017). Ratiometric fluorescent probe with AIE property for monitoring endogenous hydrogen peroxide in macrophages and cancer cells. *Scientific Reports*, 7(1), 7293. <https://doi.org/10.1038/s41598-017-07465-5>
- Liu, G. J., Long, Z., Lv, H. J., Li, C. Y., & Xing, G. W. (2016). A dialdehyde-diboronate-functionalized AIE luminogen: design, synthesis and application in the detection of hydrogen peroxide. *Chemical Communications (Cambridge, England)*, 52(67), 10233-10236. <https://doi.org/10.1039/c6cc05116b>
- Liu, B. & Benning, C. (2013). Lipid metabolism in microalgae distinguishes itself. *Current Opinion in Biotechnology*, 24(2), 300-309. <https://doi.org/10.1016/j.copbio.2012.08.008>
- Liu, W., Au, D. W. T., Anderson, D. M., Lam, P. K. S., & Wu, R. S. S. (2007). Effects of nutrients, salinity, pH and light: dark cycle on the production of reactive oxygen species in the alga *Chattonella marina*. *Journal of Experimental Marine Biology and Ecology*, 346, 76-86. <https://doi.org/10.1016/j.jembe.2007.03.007>
- Luo, J., Xie, Z., Lam, J. W., Cheng, L., Chen, H., Qiu, C., Kwok, H. S., Zhan, X., Liu, Y., Zhu, D. & Tang, B. Z. (2001). Aggregation-induced emission of 1-methyl-1,2,3,4,5-pentaphenylsilole. *Chemical Communications*, 381(18), 1740-1. <https://doi.org/10.1039/B105159H>
- Lushchak V. I. (2011). Adaptive response to oxidative stress: Bacteria, fungi, plants and animals. *Comparative biochemistry and physiology. Toxicology & Pharmacology: CBP*, 153(2), 175-190. <https://doi.org/10.1016/j.cbpc.2010.10.004>
- Luterbacher, J. S., Martin Alonso, D., Dumesic, J. A. (2014). Targeted chemical upgrading of lignocellulosic biomass to platform molecules. *Green Chemistry*, 16, 4816-38. <https://doi.org/10.1039/C4GC01160K>

Ma, H., Zhao, C., Meng, H., Li, R., Mao, L., Hu, D., Tian, M., Yuan, J., & Wei, Y. (2021). Multifunctional organic fluorescent probe with aggregation-induced emission characteristics: ultrafast tumor monitoring, two-photon imaging, and image-guide photodynamic therapy. *ACS Applied Materials & Interfaces*, *13*(7), 7987-7996. <https://doi.org/10.1021/acsami.0c21309>

Maekawa, M., & Fairn, G. D. (2014). Molecular probes to visualize the location, organization and dynamics of lipids. *Journal of Cell Science*, *127*(22), 4801-4812. <https://doi.org/10.1242/jcs.150524>

Mattila, H., Khorobrykh, S., Havurinne, V., & Tyystjärvi, E. (2015). Reactive oxygen species: Reactions and detection from photosynthetic tissues. *Journal of Photochemistry and Photobiology. B, Biology*, *152*(Pt B), 176-214. <https://doi.org/10.1016/j.jphotobiol.2015.10.001>

Menon, K. R., Balan, R., & Suraishkumar, G. K. (2013). Stress induced lipid production in *Chlorella vulgaris*: relationship with specific intracellular reactive species levels. *Biotechnology and Bioengineering*, *110*(6), 1627-1636. <https://doi.org/10.1002/bit.24835>

Merchant, S. S., Kropat, J., Liu, B., Shaw, J. & Warakanont, J. (2012). TAG, You are it! *Chlamydomonas* as a reference organism for understanding algal triacylglycerol accumulation. *Current Opinion in Biotechnology*, *23*(3), 352-363. <https://doi.org/10.1016/j.copbio.2011.12.001>

Miller, E. W., Tulyathan, O., Isacoff, E. Y., & Chang, C. J. (2007). Molecular imaging of hydrogen peroxide produced for cell signaling. *Nature Chemical Biology*, *3*(5), 263-267. <https://doi.org/10.1038/nchembio871>

Mullineaux, P. M., Exposito-Rodriguez, M., Laissue, P. P., & Smirnov, N. (2018). ROS-dependent signalling pathways in plants and algae exposed to high light: Comparisons with other eukaryotes. *Free Radical Biology & Medicine*, *122*, 52-64. <https://doi.org/10.1016/j.freeradbiomed.2018.01.033>

Ni, J. S., Liu, H., Liu, J., Jiang, M., Zhao, Z., Chen, Y., Kwok, R. T. K., Lam, J., W. Y., Peng Q., & Tang, B. Z. (2018). The unusual aggregation-induced emission of coplanar organoboron isomers and their lipid droplet-specific applications. *Materials Chemistry Frontiers*, *2018*, 2, 1498-1507. <https://doi.org/10.1039/C8QM00184G>

Ni, J. S., Lee, M., Zhang, P., Gui, C., Chen, Y., Wang, D., Yu, Z. Q., Kwok, R., Lam, J., & Tang, B. Z. (2019). Swiss knife-inspired multifunctional fluorescence probes for cellular organelle targeting based on simple AIEgens. *Analytical chemistry*, *91*(3), 2169-2176. <https://doi.org/10.1021/acs.analchem.8b04736>

Nishiyama, Y., Allakhverdiev, S. I., & Murata, N. (2011). Protein synthesis is the primary target of reactive oxygen species in the photoinhibition of photosystem II. *Physiologia Plantarum*, *142*(1), 35-46. <https://doi.org/10.1111/j.1399-3054.2011.01457.x>

Niu, G., Zhang, R., Kwong, J. P. C., Lam, J. W. Y., Chen, C., Wang, J., Chen, Y., Feng, X., Kwok, R. T. K., Sung, H. H.-Y., Williams, I. D., Elsegood, M. R. J., Qu, J., Ma, C., Wong, K. S., Yu, X., & Tang, B. Z. (2018). Specific two-photon imaging of live cellular and deep-tissue lipid droplets by lipophilic AIEgens at ultralow concentration. *Chemistry of Materials*, *30*(14), 4778-4787. <https://doi.org/10.1021/acs.chemmater.8b01943>

Ohsaki, Y., Shinohara, Y., Suzuki, M. & Fujimoto T. (2010). A pitfall in using BODIPY dyes to label lipid droplets for fluorescence microscopy. *Histochemistry and Cell Biology*, *133*(4), 477-480. <https://doi.org/10.1007/s00418-010-0678-x>

Ozgur, R., Turkan, I., Uzilday, B., & Sekmen, A. H. (2014). Endoplasmic reticulum stress triggers ROS signalling, changes the redox state, and regulates the antioxidant defence of *Arabidopsis thaliana*. *Journal of Experimental Botany*, *65*(5), 1377-1390. <https://doi.org/10.1093/jxb/eru034>

Park, H., Li, S., Niu, G., Zhang, H., Song, Z., Lu, Q., Zhang, J., Ma, C., Kwok, R. T. K., Lam, J. W. Y., Wong, K. S., Yu, X., Xiong, Q., & Tang, B. Z. (2021). Diagnosis of fatty liver disease by a multiphoton-active and lipid-droplet-specific AIEgen with nonaromatic rotors. *Materials Chemistry Frontiers*, *2021*, *5*, 1853-1862. <https://doi.org/10.1039/D0QM00877J>

Park, J. J., Wang, H., Gargouri, M., Deshpande, R. R., Skepper, J. N., Holguin, F. O., Juergens, M. T., Shachar-Hill, Y., Hicks, L. M. & Gang, D. R. (2015). The response of *Chlamydomonas reinhardtii* to nitrogen deprivation: a systems biology analysis. *The Plant Journal*, *81*(4), 611-624. <https://doi.org/10.1111/tpj.12747>

Patnaik, R., & Mallick, N. (2015). Utilization of *Scenedesmus obliquus* biomass as feedstock for biodiesel and other industrially important co-products: An integrated paradigm for microalgal biorefinery. *Algal Research*, *12*, 328-336. <https://doi.org/10.1016/j.algal.2015.09.009>

Perez-Garcia, O., Escalante, F. M., de-Bashan, L. E., & Bashan, Y. (2011). Heterotrophic cultures of microalgae: metabolism and potential products. *Water Research*, *45*, 11-36. <https://doi.org/10.1016/j.watres.2010.08.037>.

Pérez-Martín, M., Pérez-Pérez, M. E., Lemaire, S. D., & Crespo, J. L. (2014). Oxidative stress contributes to autophagy induction in response to endoplasmic reticulum stress in

Chlamydomonas reinhardtii. *Plant Physiology*, 166(2), 997-1008. <https://doi.org/10.1104/pp.114.243659>

Phukan, M. M., Chutia, R. S., Konwar, B. K., Kataki, R. (2011). Microalgae *Chlorella* as a potential bio-energy feedstock. *Applied Energy*, 8(10): 3307-12. <https://doi.org/10.1016/j.apenergy.2010.11.026>

Pikula, K. S., Zakharenko, A. M., Aruoja, V., Golokhvast, K. S., Tsatsakis, A. M. (2019). Oxidative stress and its biomarkers in microalgal ecotoxicology-A minireview. *Current Opinion in Toxicology*, 13, 8-15. <https://doi.org/10.1016/j.cotox.2018.12.006>

Pospíšil P. (2012). Molecular mechanisms of production and scavenging of reactive oxygen species by photosystem II. *Biochimica et Biophysica Acta*, 1817(1), 218-231. <https://doi.org/10.1016/j.bbabi.2011.05.017>

Praveenkumar, R., Shameera, K., Mahalakshmi, G., Akbarsha, M.A., & Thajuddin, N. (2012). Influence of nutrient deprivations on lipid accumulation in a dominant indigenous microalga *Chlorella* sp.. *Biomass and Bioenergy*, 37, 60-66. <https://doi.org/10.1016/j.biombioe.2011.12.035>

Qian, J., & Tang, B. Z. (2017). AIE luminogens for bioimaging and theranostics: from organelles to animals. *Chem*, 3(1), 56-91 <https://doi.org/10.1016/j.chempr.2017.05.010>

Qin, W., Alifu, N., Lam, J., Cui, Y., Su, H., Liang, G., Qian, J., & Tang, B. Z. (2020). Facile synthesis of efficient luminogens with AIE features for three-photon fluorescence imaging of the brain through the intact skull. *Advanced Materials (Deerfield Beach, Fla.)*, 32(23), e2000364. <https://doi.org/10.1002/adma.202000364>

Reza, A. H. M. M., Zhu, X., Qin, J., & Tang, Y. (2021). Microalgae-derived health supplements to therapeutic shifts: Redox-based study opportunities with AIE-Based

technologies. *Advanced healthcare materials*, e2101223. *Advanced Healthcare Materials*, 10(24), e2101223. <https://doi.org/10.1002/adhm.202101223>

Reza, A. H. M. M., Zhou, Y. Tavakoli, J., Tang, Y. & Qin J. (2020) Understanding the lipid production mechanism in *Euglena gracilis* with a fast-response AIEgen bioprobe, DPAS. *Materials Chemistry Frontiers*. <https://doi.org/10.1039/D0QM00621A>

Rezayian, M., Niknam, V., & Ebrahimzadeh, H. (2019). Oxidative damage and antioxidative system in algae. *Toxicology Reports*, 6, 1309-1313. <https://doi.org/10.1016/j.toxrep.2019.10.00>

Rimm, E. B., Appel, L. J., Chiuve, S. E., Djoussé, L., Engler, M. B., Kris-Etherton, P. M., Mozaffarian, D., Siscovick, D. S., Lichtenstein, A. H., & American Heart Association Nutrition Committee of the Council on Lifestyle and Cardiometabolic Health; Council on Epidemiology and Prevention; Council on Cardiovascular Disease in the Young; Council on Cardiovascular and Stroke Nursing; and Council on Clinical Cardiology (2018). Seafood long-chain n-3 polyunsaturated fatty acids and cardiovascular disease: A science advisory from the American Heart Association. *Circulation*, 138(1), e35-e47. <https://doi.org/10.1161/CIR.0000000000000574>

Reczek, C. R., & Chandel, N. S. (2015). ROS-dependent signal transduction. *Current Opinion in Cell Biology*, 33, 8-13. <https://doi.org/10.1016/j.ceb.2014.09.010>

Ren, M., Deng, B., Wang, J. Y., Kong, X., Liu, Z. R., Zhou, K., He, L., & Lin, W. (2016). A fast responsive two-photon fluorescent probe for imaging H₂O₂ in lysosomes with a large turn-on fluorescence signal. *Biosensors & Bioelectronics*, 79, 237-243. <https://doi.org/10.1016/j.bios.2015.12.046>

- Rohit, M. V., & Venkata Mohan, S. (2018). Quantum yield and fatty acid profile variations with nutritional mode during microalgae cultivation. *Frontiers in Bioengineering and Biotechnology*, 6, 111. <https://doi.org/10.3389/fbioe.2018.00111>
- Roingard, P., & Melo, R. C. (2017). Lipid droplet hijacking by intracellular pathogens. *Cellular Microbiology*, 19(1), 10.1111/cmi.12688. <https://doi.org/10.1111/cmi.12688>
- Rovira I.I., Finkel T. (2008). Reactive Oxygen Species as Signaling Molecules. In: Miwa S., Beckman K.B., Muller F.L. (eds) Oxidative stress in aging. *Aging Medicine*. Humana Press. https://doi.org/10.1007/978-1-59745-420-9_16
- Ruocco, N., Albarano, L., Esposito, R., Zupo, V., Costantini, M., & Ianora, A. (2020). Multiple roles of diatom-derived oxylipins within marine environments and their potential biotechnological applications. *Marine Drugs*, 18(7), 342. <https://doi.org/10.3390/md18070342>
- Saha, M., Goecke, F. & Bhadury, P. (2018). Minireview: algal natural compounds and extracts as antifoulants. *Journal of Applied Phycology*, 30(3), 1859-1874. <https://doi.org/10.1007/s10811-017-1322-0>
- Sandalio, L. M., & Romero-Puertas, M. C. (2015). Peroxisomes sense and respond to environmental cues by regulating ROS and RNS signalling networks. *Annals of Botany*, 116(4), 475-485. <https://doi.org/10.1093/aob/mcv074>
- Sandalio, L. M., Rodríguez-Serrano, M., Romero-Puertas, M. C., & del Río, L. A. (2013). Role of peroxisomes as a source of reactive oxygen species (ROS) signaling molecules. *Sub-cellular Biochemistry*, 69, 231-255. https://doi.org/10.1007/978-94-007-6889-5_13

- Sato, A., Matsumura, R., Hoshino, N., Tsuzuki, M., & N. Sato (2014). Responsibility of regulatory gene expression and repressed protein synthesis for triacylglycerol accumulation on sulfur-starvation in *Chlamydomonas reinhardtii*. *Frontiers in Plant Science*, 5, 444. <https://doi.org/10.3389/fpls.2014.00444>
- Satomi, Y., Hirayama, M., & Kobayashi, H. (2017). One-step lipid extraction for plasma lipidomics analysis by liquid chromatography mass spectrometry. *Journal of Chromatography. B, Analytical Technologies in the Biomedical and Life Sciences*, 1063, 93-100. <https://doi.org/10.1016/j.jchromb.2017.08.020>
- Schieber, M., & Chandel, N. S. (2014). ROS function in redox signaling and oxidative stress. *Current Biology : CB*, 24(10), R453-R462. <https://doi.org/10.1016/j.cub.2014.03.034>
- Schmollinger, S., Muhlhaus, T., Boyle, N.R., Blaby, I. K., Casero, D., Mettler, T., Moseley, J. L., Kropat, J., Sommer, F., Strenkert, D., Hemme, D., Pellegrini, M., Grossman, A.R., Stitt, M., Schroda, M., Merchant, S. S. (2014). Nitrogen-sparing mechanisms in *Chlamydomonas* affect the transcriptome, the proteome, and photosynthetic metabolism. *The Plant Cell*, 26(4), 1410-1435. <https://doi.org/10.1105/tpc.113.122523>
- Seppänen-Laakso, T., & Oresic, M. (2009). How to study lipidomes. *Journal of molecular endocrinology*, 42(3), 185-190. <https://doi.org/10.1677/JME-08-0150>
- Shimizu, Y., & Hendershot, L. M. (2009). Oxidative folding: cellular strategies for dealing with the resultant equimolar production of reactive oxygen species. *Antioxidants & Redox Signaling*, 11(9), 2317-2331. <https://doi.org/10.1089/ars.2009.2501>
- Silva, J. R., Burger, B., Kühl, C., Candreva, T., Dos Anjos, M., & Rodrigues, H. G. (2018). Wound healing and omega-6 fatty acids: From inflammation to repair. *Mediators of Inflammation*, 2018, 2503950. <https://doi.org/10.1155/2018/2503950>

- Singh, P., Kumari, S., Guldhe, A., Misra, R., Rawat, I., & Bux, F. (2016). Trends and novel strategies for enhancing lipid accumulation and quality in microalgae. *Renewable and Sustainable Energy Reviews*, 55, 1-16. [https://doi.org/ 10.1016/j.rser.2015.11.001](https://doi.org/10.1016/j.rser.2015.11.001)
- Singh, A., & Olsen, S. I. (2011). A critical review of biochemical conversion, sustainability and life cycle assessment of algal biofuels. *Applied Energy*, 88(10): 3548-55. [https://doi.org/ 10.1016/j.apenergy.2010.12.012](https://doi.org/10.1016/j.apenergy.2010.12.012)
- Sivaramakrishnan, R., & Incharoensakdi, A. (2017). Enhancement of lipid production in *Scenedesmus* sp. by UV mutagenesis and hydrogen peroxide treatment. *Bioresource Technology*, 235, 366-370. [https://doi.org/ 10.1016/j.biortech.2017.03.102](https://doi.org/10.1016/j.biortech.2017.03.102)
- Soh, N. (2006). Recent advances in fluorescent probes for the detection of reactive oxygen species. *Analytical and Bioanalytical Chemistry*, 386(3), 532-543. <https://doi.org/10.1007/s00216-006-0366-9>
- Sokoła-Wysoczańska, E., Wysoczański, T., Wagner, J., Czyż, K., Bodkowski, R., Lochyński, S., & Patkowska-Sokoła, B. (2018). Polyunsaturated fatty acids and their potential therapeutic role in cardiovascular system disorders-A review. *Nutrients*, 10(10), 1561. <https://doi.org/10.3390/nu10101561>
- Song, Z., Kwok, R. T., Ding, D., Nie, H., Lam, J. W., Liu, B., & Tang, B. Z. (2016). An AIE-active fluorescence turn-on bioprobe mediated by hydrogen-bonding interaction for highly sensitive detection of hydrogen peroxide and glucose. *Chemical Communications (Cambridge, England)*, 52(65), 10076-10079. <https://doi.org/10.1039/c6cc05049b>
- Spangenburg, E. E., Pratt, S. J., Wohlers, L. M. & Lovering, R. M. (2011). Use of BODIPY (493/503) to visualize intramuscular lipid droplets in skeletal muscle. *Journal of Biomedicine and Biotechnology*, Article ID 598358, 8. [https://doi.org/ 10.1155/2011/598358](https://doi.org/10.1155/2011/598358)

- Srikun, D., Miller, E. W., Domaille, D. W., & Chang, C. J. (2008). An ICT-based approach to ratiometric fluorescence imaging of hydrogen peroxide produced in living cells. *Journal of the American Chemical Society*, *130*(14), 4596-4597. <https://doi.org/10.1021/ja711480f>
- Subramaniam, H.N., & Chaubal, K. A. (1990) Evaluation of intracellular lipids by standardized staining with a Sudan black B fraction. *Journal of Biochemical and Biophysical Methods*, *21*, 9-16. [https://doi.org/10.1016/0165-022X\(90\)90040-J](https://doi.org/10.1016/0165-022X(90)90040-J)
- Sun, X. M., Ren, L. J., Zhao, Q. Y., Ji, X. J. & Huang, H. (2018a). Microalgae for the production of lipid and carotenoids: a review with focus on stress regulation and adaptation. *Biotechnology for Biofuels*, *11*, 272. <https://doi.org/10.1186/s13068-018-1275-9>
- Sun, G. Y., Simonyi, A., Fritsche, K. L., Chuang, D. Y., Hannink, M., Gu, Z., Greenlief, C. M., Yao, J. K., Lee, J. C., & Beversdorf, D. Q. (2018b). Docosahexaenoic acid (DHA): An essential nutrient and a nutraceutical for brain health and diseases. *Prostaglandins, Leukotrienes, and Essential Fatty Acids*, *136*, 3-13. <https://doi.org/10.1016/j.plefa.2017.03.006>
- Sun, X., Zhong, Y., Huang, Z., & Yang, Y. (2014). Selenium accumulation in unicellular green alga *Chlorella vulgaris* and its effects on antioxidant enzymes and content of photosynthetic pigments. *PloS one*, *9*(11), e112270. <https://doi.org/10.1371/journal.pone.0112270>
- Szul, M. J., Dearth, S. P., Campagna, S. R., & Zinser, E. R. (2019). Correction for Szul et al., "Carbon fate and flux in *Prochlorococcus* under nitrogen limitation". *mSystems*, *4*(2), e00204-19. <https://doi.org/10.1128/mSystems.00204-19>

- Tan, K. W., & Lee, Y. K. (2016). The dilemma for lipid productivity in green microalgae: importance of substrate provision in improving oil yield without sacrificing growth. *Biotechnology for Biofuels*, 9, 255. <https://doi.org/10.1186/s13068-016-0671-2>
- Tang, X., Zan, X., Zhao, L., Chen, H., Chen, Y. Q., Chen, W., Song, Y., & Ratledge, C. (2016). Proteomics analysis of high lipid-producing strain *Mucor circinelloides* WJ11: an explanation for the mechanism of lipid accumulation at the proteomic level. *Microbial Cell Factories*, 15, 35. <https://doi.org/10.1186/s12934-016-0428-4>
- Tarpey, M. M., Wink, D. A., & Grisham, M. B. (2004). Methods for detection of reactive metabolites of oxygen and nitrogen: in vitro and in vivo considerations. *American Journal of Physiology, Regulatory, Integrative and Comparative Physiology*, 286(3), R431-R444. <https://doi.org/10.1152/ajpregu.00361.2003>
- Tatenaka, Y., Kato, H., Ishiyama, M., Sasamoto, K., Shiga, M., Nishitoh, H., & Ueno, Y. (2019). Monitoring lipid droplet dynamics in living cells by using fluorescent probes. *Biochemistry*, 58(6), 499-503. <https://doi.org/10.1021/acs.biochem.8b01071>
- Thermo Fisher Scientific BODIPY 505/515. (accessed on 08 July 2019), Available from: <https://www.thermofisher.com/order/catalog/product/D3921>.
- Thermo Fisher Scientific BODIPY 493/503. (accessed on 08 July 2019), Available from: <https://www.thermofisher.com/order/catalog/product/D3922>.
- Tripathi, D., Nam, A., Oldenburg, D. J., & Bendich, A. J. (2020). Reactive oxygen species, antioxidant agents, and DNA damage in developing maize mitochondria and plastids. *Frontiers in Plant Science*, 11, 596. <https://doi.org/10.3389/fpls.2020.00596>
- Tricò, D., Mengozzi, A., Nesti, L., Hatunic, M., Gabriel Sanchez, R., Konrad, T., Lalić, K., Lalić, N. M., Mari, A., Natali, A., & EGIR-RISC Study Group (2020). Circulating

palmitoleic acid is an independent determinant of insulin sensitivity, beta cell function and glucose tolerance in non-diabetic individuals: a longitudinal analysis. *Diabetologia*, 63(1), 206-218. <https://doi.org/10.1007/s00125-019-05013-6>

Tsukagoshi, H., Busch, W., & Benfey, P. N. (2010). Transcriptional regulation of ROS controls transition from proliferation to differentiation in the root. *Cell*, 143(4), 606-616. <https://doi.org/10.1016/j.cell.2010.10.020>

Ugya, A. Y., Imam, T. S., Li, A., Ma, J., & Hua, X. (2020). Antioxidant response mechanism of freshwater microalgae species to reactive oxygen species production: a mini review, *Chemistry and Ecology*, 36(2), 174-193. <https://doi.org/10.1080/02757540.2019.1688308>

Vavilala, S. L., Gawde, K. K., Sinha, M., & D'Souza, J. S. (2015). Programmed cell death is induced by hydrogen peroxide but not by excessive ionic stress of sodium chloride in the unicellular green alga *Chlamydomonas reinhardtii*. *European Journal of Phycology*, 50, 422-438. <https://doi.org/10.1080/09670262.2015.1070437>

Votyakova, T. V., & Reynolds, I. J. (2004). Detection of hydrogen peroxide with Amplex Red: interference by NADH and reduced glutathione auto-oxidation. *Archives of Biochemistry and Biophysics*, 431(1), 138-144. <https://doi.org/10.1016/j.abb.2004.07.025>

Walther, T. C., & Farese, R. V., Jr (2012). Lipid droplets and cellular lipid metabolism. *Annual Review of Biochemistry*, 81, 687-714. <https://doi.org/10.1146/annurev-biochem-061009-102430>

Wang, X., Fosse, H.K., Li, K., Chauton, M.S., Vadstein, O., & Reitan, K.I. (2019). Influence of nitrogen limitation on lipid accumulation and EPA and DHA content in four marine

microalgae for possible use in aquafeed. *Frontiers in Marine Science*, 6, 95. <https://doi.org/10.3389/fmars.2019.00095>

Wang, H., Zhang, Y., Zhou, W., Noppol, L., & Liu, T. (2018). Mechanism and enhancement of lipid accumulation in filamentous oleaginous microalgae *Tribonema minus* under heterotrophic condition. *Biotechnology for Biofuels*, 11, 328. <https://doi.org/10.1186/s13068-018-1329-z>

Wang, Z., Yang, L., Liu, Y., Huang, X., Qiao, F., Qin, W., Hu, Q. & Tang, B. Z. (2017a). Ultra long-term cellular tracing by a fluorescent AIE bioconjugate with good water solubility over a wide pH range. *Journal of Materials Chemistry B*, 5(25), 4981-4987. <https://doi.org/10.1039/C7TB00861A>

Wang, D., Su, H., Kwok, R. T. K., Shan, G., Leung, A. C. S., Lee, M. M. S., Sung, H. H. Y., Williams, I. D., & Lam, J. W. Y., & Tang, B. Z. (2017b). Facile synthesis of Red/NIR AIE luminogens with simple structures, bright emissions, and high photostabilities, and their applications for specific imaging of lipid droplets and image-guided photodynamic therapy. *Advanced Functional Materials*, 27, 46, 1704039. <https://doi.org/10.1002/adfm.201704039>

Wang, Z., Gui, C., Zhao, E., Wang, J., Li, X., Qin, A., Zhao, Z., Yu, Z. & Tang, B. Z. (2016). Specific fluorescence probes for lipid droplets based on simple AIEgens. *ACS Applied Materials & Interfaces*, 8(16), 10193-10200. <https://doi.org/10.1021/acsami.6b01282>

Wang, E., Zhao, E., Hong, Y., Lam, J. W. Y. & Tang, B. Z. (2014). A highly selective AIE fluorogen for lipid droplet imaging in live cells and green algae. *Journal of Materials Chemistry B*, 2, 2013-2019. <https://doi.org/10.1039/C3TB21675F>

- Wang, H., & Joseph, J. A. (1999). Quantifying cellular oxidative stress by dichlorofluorescein assay using microplate reader. *Free Radical Biology & Medicine*, 27(5-6), 612-616. [https://doi.org/10.1016/s0891-5849\(99\)00107-0](https://doi.org/10.1016/s0891-5849(99)00107-0)
- Wersto, R. P., Rosenthal, E. R., Crystal, R. G., & Spring, K. R. (1996). Uptake of fluorescent dyes associated with the functional expression of the cystic fibrosis transmembrane conductance regulator in epithelial cells. *Proceedings of the National Academy of Sciences of the United States of America*, 93(3), 1167-1172. <https://doi.org/10.1073/pnas.93.3.1167>
- Weinberger F. (2007). Pathogen-induced defense and innate immunity in macroalgae. *The Biological Bulletin*, 213(3), 290-302. <https://doi.org/10.2307/25066646>
- Weiser, M. J., Butt, C. M., & Mohajeri, M. H. (2016). Docosahexaenoic acid and cognition throughout the lifespan. *Nutrients*, 8(2), 99. <https://doi.org/10.3390/nu8020099>
- Wells, M. L., Potin, P., Craigie, J. S., Raven, J. A., Merchant, S. S., Helliwell, K. E., Smith, A. G., Camire, M. E. & Brawley, S. H. (2017). Algae as nutritional and functional food sources: revisiting our understanding. *Journal of Applied Phycology*, 29(2), 949-982. <https://doi.org/10.1007/s10811-016-0974-5>
- Wüstner, D., Christensen, T., Solanko, L. & Sage, D. (2014). Photobleaching kinetics and time-integrated emission of fluorescent probes in cellular membranes. *Molecules*, 19(8), 11096-11130. <https://doi.org/10.3390/molecules190811096>
- Xia, T., Kovichich, M., Liong, M., Mädler, L., Gilbert, B., Shi, H., Yeh, J. I., Zink, J. I., & Nel, A. E. (2008). Comparison of the mechanism of toxicity of zinc oxide and cerium oxide nanoparticles based on dissolution and oxidative stress properties. *ACS Nano*, 2(10), 2121-2134. <https://doi.org/10.1021/nn800511k>

Yang, L., Chen, J., Qin, S., Zeng, M., Jiang, Y., Hu, L., Xiao, P., Hao, W., Hu, Z., Lei, A. & Wang, J. (2018). Growth and lipid accumulation by different nutrients in the microalga *Chlamydomonas reinhardtii*. *Biotechnology for Biofuels*, 11, 40. <https://doi.org/10.1186/s13068-018-1041-z>

Yang, Z. K., Ma, Y. H., Zheng, J. W., Yang, W. D., Liu, J. S., & Li, H. Y. (2014). Proteomics to reveal metabolic network shifts towards lipid accumulation following nitrogen deprivation in the diatom *Phaeodactylum tricornutum*. *Journal of Applied Phycology*, 26(1), 73-82. <https://doi.org/1007/s10811-013-0050-3>

Yang, L., Ding, Y., Chen, Y., Zhang, S., Huo, C., Wang, Y., Yu, J., Zhang, P., Na, H., Zhang, H., Ma, Y., & Liu, P. (2012). The proteomics of lipid droplets: structure, dynamics, and functions of the organelle conserved from bacteria to humans. *Journal of Lipid Research*, 53(7), 1245-1253. <https://doi.org/10.1194/jlr.R024117>

Yanowitz, J., Ratcliff, M. A., McCormick, R. L., Taylor, J. D. & Murphy, M. J. (2014). Compendium of experimental cetane numbers. In: Technical Report. National Renewable Energy Laboratory. Available from: <https://www.nrel.gov/docs/fy17osti/67585.pdf> (accessed September, 2020)

Yilancioglu, K., Cokol, M., Pastirmaci, I., Erman, B., & Cetiner, S. (2014). Oxidative stress is a mediator for increased lipid accumulation in a newly isolated *Dunaliella salina* strain. *PloS One*, 9(3), e91957. <https://doi.org/10.1371/journal.pone.0091957>

Yu, S. J., Kang, M. W., Chang, H. C., Chen, K. M. & Yu, Y. C. (2005). Bright fluorescent nanodiamonds: No photobleaching and low cytotoxicity. *Journal of the American Chemical Society*, 127(50), 17604-17605. <https://doi.org/10.1021/ja0567081>

Zafra, A., Rodríguez-García, M. I., & Alché, J. (2010). Cellular localization of ROS and NO in olive reproductive tissues during flower development. *BMC Plant Biology*, *10*, 36. <https://doi.org/10.1186/1471-2229-10-36>

Zhang, S., He, Y., Sen, B., & Wang, G. (2020a). Reactive oxygen species and their applications toward enhanced lipid accumulation in oleaginous microorganisms. *Bioresource Technology*, *307*, 123234. <https://doi.org/10.1016/j.biortech.2020.123234>

Zhang, F., Li, Z., Liu, Y., Yang, B., Qiao, H., Chai, J., Wen, G., & Liu, B. (2020b). Rational construction of AIEgens with wide color tunability and their specific lipid droplet imaging applications. *Journal of Materials Chemistry. B*, *8*(41), 9533-9543. <https://doi.org/10.1039/d0tb01806f>

Zhang, L., Liao, C., Yang, Y., Wang, Y. Z., Ding, K., Huo, D., & Hou, C. (2019). Response of lipid biosynthesis in *Chlorella pyrenoidosa* to intracellular reactive oxygen species level under stress conditions. *Bioresource Technology*, *287*, 121414. <https://doi.org/10.1016/j.biortech.2019.121414>

Zhang, Y. F., Dai, M. H., & Yuan Z.H. (2018). Methods for detection of reactive oxygen species. *Analytical Methods*, *10*, 4625-4638. <https://doi.org/10.1039/c8ay01339j>

Zhang, X., Tang, X., Wang, M., Zhang, W., Zhou, B., & Wang, Y. (2017). ROS and calcium signaling mediated pathways involved in stress responses of the marine microalgae *Dunaliella salina* to enhanced UV-B radiation. *Journal of Photochemistry and Photobiology. B, Biology*, *173*, 360-367. <https://doi.org/10.1016/j.jphotobiol.2017.05.038>

Zhang, W., Liu, W., Li, P., Huang, F., Wang, H., & Tang, B. (2015). Rapid-response fluorescent probe for hydrogen peroxide in living cells based on increased polarity of C-B

bonds. *Analytical Chemistry*, 87(19), 9825-9828. <https://doi.org/10.1021/acs.analchem.5b02194>

Zhao, Z., He, B. & Tang, B. Z. (2015). Aggregation-induced emission of siloles. *Chemical Science*, 6(10), 5347-5365. <https://doi.org/10.1039/c5sc01946j>

Zhao, H., Joseph, J., Fales, H. M., Sokoloski, E. A., Levine, R. L., Vasquez-Vivar, J., & Kalyanaraman, B. (2005). Detection and characterization of the product of hydroethidine and intracellular superoxide by HPLC and limitations of fluorescence. *Proceedings of the National Academy of Sciences of the United States of America*, 102(16), 5727-5732. <https://doi.org/10.1073/pnas.0501719102>

Zhou, M., Diwu, Z., Panchuk-Voloshina, N., & Haugland, R. P. (1997). A stable nonfluorescent derivative of resorufin for the fluorometric determination of trace hydrogen peroxide: applications in detecting the activity of phagocyte NADPH oxidase and other oxidases. *Analytical Biochemistry*, 253(2), 162-168. <https://doi.org/10.1006/abio.1997.2391>

Zhu J. K. (2016). Abiotic stress signaling and responses in plants. *Cell*, 167(2), 313-324. <https://doi.org/10.1016/j.cell.2016.08.029>

Zhu, L. D., Li, Z. H., & Hiltunen, E. (2016a). Strategies for lipid production improvement in microalgae as a biodiesel feedstock. *BioMed Research International*, 2016, 8792548. <https://doi.org/10.1155/2016/8792548>

Zhu J. K. (2016b). Abiotic stress signaling and responses in plants. *Cell*, 167(2), 313-324. <https://doi.org/10.1016/j.cell.2016.08.029>

Zhu, H., Fan, J., Du, J., & Peng, X. (2016c). Fluorescent probes for sensing and imaging within specific cellular organelles. *Accounts of Chemical Research*, 49(10), 2115-2126. <https://doi.org/10.1021/acs.accounts.6b00292>

Zhuang, W., Yang, L., Ma, B., Kong, Q., Li, G., Wang, Y., & Tang, B. Z. (2019). Multifunctional two-photon AIE luminogens for highly mitochondria-specific bioimaging and efficient photodynamic therapy. *ACS Applied Materials & Interfaces*, *11*(23), 20715-20724. <https://doi.org/10.1021/acsami.9b04813>

Zielonka, J., Zhao, H., Xu, Y., & Kalyanaraman, B. (2005). Mechanistic similarities between oxidation of hydroethidine by Fremy's salt and superoxide: stopped-flow optical and EPR studies. *Free Radical Biology & Medicine*, *39*(7), 853-863. <https://doi.org/10.1016/j.freeradbiomed.2005.05.001>

**Chapter 2: Stress-Induced Lipid Droplets Conditions in a
Cell Wall Deficient Alga, *Euglena gracilis* with
Aggregation Induced Emission (AIE) Fluorophore**

2.1 Abstract

Lipid bodies are lipid-rich organelles that can regulate the storage of neutral lipids as energy sources in organisms. Visualization of lipid droplets is a practical approach to understanding lipid dynamics in microalgae. This study explores the required environmental conditions to yield lipid in a microalgal species *Euglena gracilis* as the biofunctional component using the lipid-specific aggregation-induced emission fluorogen, DPAS (C₂₀H₁₆N₂O) and compares it to the commercial lipid staining probe BODIPY for visualizing lipid production *in vivo*. Five treatments were investigated for lipid production: (1) modified Cramer-Myers medium (MCM), (2) MCM without nitrogen (-), (3) MCM without nitrogen (-) and calcium (-), (4) MCM without nitrogen (-) and calcium (-), but with glucose (+), and (5) MCM without nitrogen (-) and calcium (-), but with glucose (+). Illumination was continually at 70 mmol photons per m⁻² s⁻¹ in all treatments except no light in Treatment 5. Distinctive lipid droplets were labelled by DPAS and detected with confocal microscopy and flow cytometry to clarify the understanding of lipid enrichment mechanism in various conditions. Treatment 1 indicates low lipid production in *E. gracilis* in an autotrophic condition. DPAS benefits from a very low background signal, and therefore is more sensitive than BODIPY for semiquantitative *in vivo* fluorescence measurements. Co-staining in the presence of BODIPY and chlorophyll also indicates that DPAS is suitable for multicolour imaging with red and green fluorophores. The present study demonstrates that DPAS is a highly effective biocompatible and photostable fluorophore for rapid and sensitive visualization of lipid droplets. This novel staining method could be used to screen microalgae that have the potential to produce lipid droplets as a health supplement for humans.

Keywords: Aggregation-induced emission; DPAS; *Euglena gracilis*; Lipid droplets; Traditional fluorophores

2.2 Introduction

With the challenges of the population growth projection of over 10.9 billion by the end of the 21st Century (World Population Prospects, 2019), microalgae research has been significantly focused due to their inherent renewable, eco-friendly, and biofunctional attributes. The valuable metabolites obtained from microalgae are important for a number of nutraceutical and pharmaceutical purposes, and the market for these products is expanding rapidly. Owing to the advantages of fast growth rates and higher oil yielding capabilities, these organisms have the potential to serve the world not only as the alternative sources of third-generation biofuel (Jones and Mayfield, 2012; Singh and Olsen, 2011) but also for the procurement of high-valued balanced dietary constituents of antioxidants, vitamins, PUFAs and other health beneficiary bioactive compounds (Galasso et al., 2019). The importance of dietary incorporation of n-3 fatty acids has long been signified, since people habituated with more LC-PUFAs intake are studied with significantly lower risk factors associated with coronary heart disease and stroke than those with more C₁₈ fatty acids consumption (Rimm et al., 2018). Currently, most human ω -3 LC-PUFA requirements are sourced from marine fish, which is under the threat of dwindling supplies because of environmental factors and pollutants contamination (Khozin-Goldberg et al., 2011). Therefore, all efforts to enrich the oilseed plants with LC-PUFAs through metabolic engineering are ongoing (Venegas-Calación, 2010), whereas microalgae are more useful due to their superior growth and abilities to utilize the wastewater and non-arable lands.

Among the microalgae, *Euglena* is a well-known representative of the single-cell flagellate eukaryotes and a member of the class Euglenoidea. The habitats of different species of *Euglena* are often diversified from freshwater to marine water (Woloski, 2002). Most species of the *Euglena* possess both autotrophic and heterotrophic characteristics using chloroplasts, and animal-like nourishment, respectively. Under sufficient sunlight, it uses the

chloroplasts containing the pigments chlorophyll a and chlorophyll b to produce sugars by photosynthesis. *Euglena gracilis* is one of the previously studied euglenids in cell biology and biochemistry (Gissibl et al., 2019). This organism contains chloroplasts, like plants, and has flagella but does not have a cell wall. This cell wall structure of euglenids is typical of animal cells (Bailey, 2019).

The *de novo* transcriptome sequencing of *E. gracilis*, has revealed enormous metabolic extents in these organisms, involving more genes than that are evident in the human genome. It has also been reported that *Euglena* has the genes for the biosynthesis of glycosylphosphatidylinositol (GPI) membrane anchors, which might be involved in anchoring these glycans to internal membranes or the cell surface, and enable these organisms to form cysts, encased in a carbohydrate sheath (O'Neill et al., 2017; O'Neill et al., 2015). To adapt the diversified environmental factors, the vast majority of algal cells are evolved with extracellular cell structures, which are also diversified and the products of complex biosynthetic machinery. These structures are the fundamental parts of these organisms to grow and develop efficiently and offer the cells different physiological processes, including protection and defence against foreign particles and microbes (Domozych et al., 2012). This unicellular, photosynthetic protist can harness multiple bioactive compounds like protein, vitamins, lipids, and the unique β -1,3-glucan paramylon. Among these, paramylon has already been commercialized as an immunostimulatory, anti-tumor, and anti-HIV agent in nutraceuticals (Rodríguez-Zavala et al., 2010; Luo et al., 2015; Grimm et al., 2015). *Euglena* can also utilize CO₂ and water to produce macromolecular organic matters in lipids, the composition of which also varies depending on cultural conditions (Hu et al., 2008; Scott et al., 2010). While aerobically grown *E. gracilis* cells are transferred into anaerobic conditions, they can degrade paramylon to synthesize and accumulate wax esters that consist of medium-chain fatty acids and alcohols with 14:0 carbon

chains as the major constituent (Tomiyaama et al., 2019). Because of the lower freezing point and having a good cetane number (66.2), myristic acid (C14:0) is more suitable as a drop-in jet fuel than other algae produced medium-length fatty acids such as palmitic acid (C16:0) and stearic acid (C18:0) (Yanowitz et al., 2014). Apart from this, *E. gracilis* cells allow growth in photoautotrophic, photomixotrophic and heterotrophic conditions. The membrane lipid composition, especially thylakoid glycolipids monogalactosyldiacylglycerol (MGDG), digalactosyldiacylglycerol (DGDG) and sulfoquinovosyldiacylglycerol (SQDG), can also be different (Shibata et al., 2018). Apparently, the production of various lipids in this species greatly depends on cultural conditions and the implemented technologies. Therefore, it is necessary to identify the appropriate cultural condition to get the desired lipid composition.

To date, despite knowing different cultivation techniques of microalgae, research on algal lipid has not been fully exploited because of the limitation of the visualization tools that could allow rapid and non-invasive evaluation of the lipid conditions. It is critical to perceive the different physiological roles of LDs in microalgae and their interfaces with other cellular organelles using reliable imaging tools, which could expand the opportunities for algal lipid production by elucidating the structural changing mechanisms during different environmental stimuli (Reza et al., 2020). Currently, lipid compositions and amount are generally determined by thin-layer chromatography (TLC) (Fuchs et al., 2011), gas chromatography (GC) (Volin, 2001), liquid chromatography (LC) (Nygren et al., 2017), enzyme-linked immunosorbent assays (ELISA) (Ishihara et al., 2005), nuclear magnetic resonance (NMR) (Li et al., 2017), flow cytometry (Peng et al., 2019) and mass spectrometry (MS) (Li et al., 2014), which are expensive, time consuming and inappropriate for visualizing spatial distribution in living cells. Some visualization techniques for nanoscale analysis of LDs available are electron microscopy and immunofluorescence microscopy (Fujita et al., 2010), Raman microscopy (Abramczyk et al., 2015), coherent anti-stokes Raman scattering

microscopy (Jaeger et al., 2016) and direct organelle mass spectrometry (Horn et al., 2011). Comprehensively, these advanced techniques require complex data analysis and sample preparations with LDs extraction and cell fixation (Fam et al., 2018) that hinder the further studies of the LDs dynamics in their native state.

The researchers have also used cost-effective rapid imaging and semiquantitative analysis of neutral lipids in microalgae lipid-specific dyes (Rumin et al., 2015; Reza et al., 2020). One of the most common problems of using these dyes is adjusting the dye acquisition and penetration techniques in microalgae. Severe aggregation-caused quenching (ACQ) in higher concentration and self-decomposition phenomenon in a dilute stage can reduce the photostability and most often make their usage difficult for fluorescence imaging (Yu et al., 2005; Spangenburg et al., 2011; Spandl et al., 2009; Collot et al., 2018). Among the lipid-specific fluorescent dyes, Nile Red (9-diethylamino-5H-benzo[a]phenoxazine-5-one) (Greenspan et al., 1985), BODIPY 493/503 (4,4-Difluoro-1,3,5,7,8-Pentamethyl-4-Bora-3a,4a-Diaza-s-Indacene) and BODIPY 505/515 (4,4-difluoro-1,3,5,7-tetramethyl-4-bora-3a,4a-diaza-s-indacene) (Thermo Fisher Scientific BODIPY 505/515, 2019; Thermo Fisher Scientific BODIPY 493/503, 2019) are most frequently used fluorophores in fluorescent microscopy. However, despite having some advantages, Nile Red has several limitations that make the frequent usage of this dye tricky. The broad absorption and emission spectra of Nile Red often produce overlapping signals between the yellow and red spectrum, while the higher sensitivity towards the environmental polarity sometimes results in the blueshifting of peak emission during lower surrounding polarity (Elsey et al., 2007). Penetration of this dye in microalgae also requires pre-treatment that affects the cellular viability (Mutanda et al., 2011; Chen et al., 2011), whereas interactions with other low-density proteins and cellular structures with hydrophobic domain have also been reported (Brown et al., 1995; Brown et al., 1992). Additionally, limitations of the long-time preservation, aggregation of the excess

dye and relative interference with the red channel of chlorophyll autofluorescence make the application of this dye challenging in algal studies (Rumin et al., 2015; Pick and Rachutin-Zalagin, 2012). Compared to the Nile Red, BODIPY is more LDs specific, relatively insensitive to the surrounding polarity and more cell-permeable, though BODIPY 505/515 is more photostable than its close analogue BODIPY 493/503 (Spangenburg et al., 2011; Mutanda, 2011; Koreivienė, 2017). However, the non-fluorogenic nature of BODIPY can produce a strong background signal, while the weak correlation between lipid content and BODIPY fluorescence intensity has also been reported (Siegler et al., 2012; Daemen et al., 2015).

Focusing on the complications of the ACQ and self-decomposition phenomena of the traditional lipid specific dyes, several lipid specific dyes with aggregation-induced emission (AIE) properties have been introduced in different studies (Reza et al., 2020). DPAS ($C_{20}H_{16}N_2O$), a new class of AIE fluorophore, has been successfully used in a recent study to label lipid droplets at significantly higher concentrations and produce brighter images, which is very promising to resolve the ACQ problems in fluorescence microscopy (Wang et al., 2016). However, the dye was used in animal cells. To ensure its universality, it is required to analyze its penetrability and lipid labelling efficacy in multiple cell types with different cellular compositions.

In the present study, we have used a different cell type *E. gracilis*, which has plant and animal characteristics. Unlike other algae with a carbohydrate-based cell wall, this microalgae species has an unusual cell membrane complex "pellicle" comprising glucose, galactose, mannose, fucose, xylose, and rhamnose (O'Neill et al., 2017). Furthermore, as a new approach, different culture conditions have been used to induce lipid in the algae to test further the performance of lipid-specific AIE bioprobe, DPAS, in *E. gracilis*.

2.3 Materials and Methods

2.3.1 Establishment of *Euglena gracilis* culture and lipid induction

The *E. gracilis* specimens were collected from the College of Science and Engineering, Flinders University, Australia, from which pure culture of *E. gracilis* (length: 55.6 ± 4.63 μm and diameter: 8-10 μm) was established in 1-L medium containing 30 wheat grains, 25 rice grains and 5 g skim milk powder. After autoclaving at 121 °C for 5 min, the culture medium was stored at 4 °C. *E. gracilis* was inoculated into the culture medium at 10% (v/v) and cultured in 250-mL Erlenmeyer flasks at 24 °C in a temperature-controlled room under continuous light (70 mmol photons per $\text{m}^{-2} \text{s}^{-1}$). The flask was stirred manually twice a day to prevent algal settlement.

For the study in controlled conditions, cultures of the *E. gracilis* were established in culture flasks with each working volume of 20 mL under 24 h cycle illumination (130-150 $\mu\text{mol}/\text{m}^2/\text{s}$) at 25 °C. For all examinations, the stock culture of *E. gracilis* was grown in modified Cramer-Myers medium (1.0 g/L of $(\text{NH}_4)_2\text{HPO}_4$, 1.0 g/L of KH_2PO_4 , 0.2 g/L of $\text{MgSO}_4 \cdot 7\text{H}_2\text{O}$, 0.02 g/L of $\text{CaCl}_2 \cdot 2\text{H}_2\text{O}$, 3 mg/L of $\text{FeSO}_4 \cdot 7\text{H}_2\text{O}$, 1.8 mg/L of $\text{MnCl}_2 \cdot 4\text{H}_2\text{O}$, 1.5 mg/L of $\text{CoSO}_4 \cdot 7\text{H}_2\text{O}$, 0.4 mg/L of $\text{ZnSO}_4 \cdot 7\text{H}_2\text{O}$, 0.2 mg/L of $\text{Na}_2\text{MoO}_4 \cdot 2\text{H}_2\text{O}$, 0.02 mg/L of $\text{CuSO}_4 \cdot 5\text{H}_2\text{O}$, 0.1 mg/L of thiamine hydrochloride (vitamin B₁), and cyanocobalamin (vitamin B₁₂) at pH 3.5.

The *E. gracilis* cells were counted on a haemocytometer (Improved Marienfeld Neubauer, Germany) to determine cell density. The growth of *E. gracilis* was also measured at 780 nm using a spectrophotometer (LKB Biochrom 4050 Ultrospec II UV/Vis). Since a linear co-relationship between OD₇₈₀ and cell density has been observed (Fig. 2.1), OD₇₈₀ was used for measuring growth in the manuscript. For induction of lipid accumulation, *E. gracilis* cells

were taken from the exponential growth phase and consequently were cultured for 10 days in five (5) different treatments.

To find the optimum conditions for stress-induced lipid biosynthesis in *E. gracilis* cells, five treatments were used to manipulate the availability of nutrient and light: (1) modified Cramer-Myers medium (MCM) (24 h, 70 mmol photons per $\text{m}^{-2} \text{s}^{-1}$); (2) MCM, nitrogen (-) (24 h, 70 mmol photons per $\text{m}^{-2} \text{s}^{-1}$); (3) MCM, nitrogen (-), calcium (-) (24 h, 70 mmol photons per $\text{m}^{-2} \text{s}^{-1}$); (4) MCM, nitrogen (-), calcium (-), glucose (+) (24 h, 70 mmol photons per $\text{m}^{-2} \text{s}^{-1}$), and (5) MCM, nitrogen (-), calcium (-), glucose (+) (Dark). The modified Cramer-Myers medium was considered nutrient sufficient, whereas cells in other treatments were considered a stressed condition.

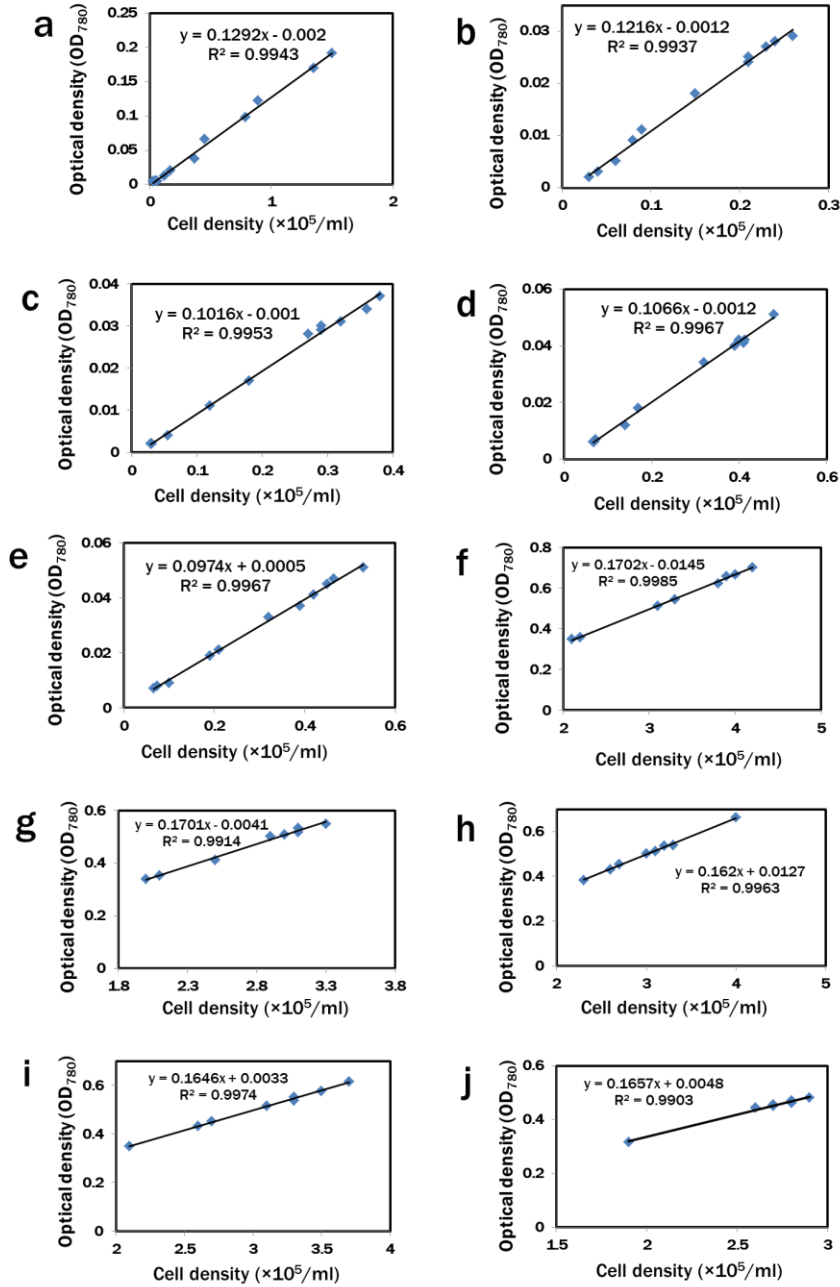


Fig. 2.1 Linear relationship between OD_{780} and cell density cultured in (a, f) Treatment 1: modified Cramer-Myers medium (MCM); (b, g) Treatment 2: MCM, (-) N_2 ; (c, h) Treatment 3: MCM, (-) N_2 , (-) Ca^{2+} ; (d, i) Treatment 4: MCM, (-) N_2 , (-) Ca^{2+} , (+) Glucose (24 h light); (e, j) Treatment 5: MCM, (-) N_2 , (-) Ca^{2+} , (+) Glucose (24 h Dark) conditions. (a-e) culture initiated with $0.05 \pm 0.02 (\times 10^5)$ cells/ml; (f-j) culture started for lipid induction with $2.08 \pm 0.14 (\times 10^5)$ cells/ml.

2.3.2 Determination of autofluorescence properties of *Euglena gracilis*

Since photosynthetic organisms can biosynthesize various molecules with autofluorescence properties (e.g. different chlorophyll and accessory pigments), the autofluorescence properties of *E. gracilis* was determined at different excitation-emission wavelengths. The analysis was conducted on a fluorescence spectrophotometer (Cary Eclipse, MY17180002, Agilent Technologies, CA, USA) and Zeiss LSM 880 Airyscan confocal microscope using ZEN 2.6 software (Carl Zeiss, Australia). A spectrophotometer detected the autofluorescence of chlorophyll from different treatments and heat-killed *E. gracilis* cells with excitation at 488 nm. Microalgae were collected by centrifugation (2,000 g, 60 sec) to ensure the lethal result and resuspended in a centrifuge tube with deionized water. Subsequently, the tube was set in a beaker, filled with water, and placed in a heater. The samples were then kept at 100 °C for 2 min, and the solution containing the microalgae was allowed to cool down at room temperature. The cells were then examined once every 2 h up to 24 h under a light microscope for any movement to confirm dead (Wang et al., 2013).

2.3.3 Lipid extraction and analysis of fatty acids

Total lipid was extracted using the adapted method of Bligh and Dyer (1959). Briefly, a sample volume was taken from the growing *E. gracilis* culture to provide approximately 500 mg of dry algal biomass. The algal culture was then centrifuged at $10000 \times g$ and 4 °C for 10 min. The supernatant was discarded, and the pellet was washed three times with an equal volume of potassium phosphate buffer adjusted to the same pH of the culture medium. Subsequently, the pellet was re-suspended in deionized water and consequently was transferred and weighed with a weighing dish. After that, the samples were dried at 60 °C for 48 h, and were stored at -20 °C for further use. Subsequently, approximately 50 mg of dried algal biomass was measured and was transferred to a mortar pre-washed with hexane. The

weighing dish was also washed with a small amount (1 ml) of hexane using a Pasteur pipette in the fume hood to completely transfer the biomass to the mortar. Consequently, the algal biomass was grounded for 5 min into a fine and smooth paste using a pestle. In the case of evaporation of hexane during grinding, hexane was added to the mortar and the resulting slurry was mixed with the pestle until it was homogenized. After that, the hexane-cell mass mixture was centrifuged at 4 °C for 20 min at 10,000 × g, and the supernatant was isolated in a pre-weighed vial. This step was followed by the addition 3 ml of hexane to the pellet and vigorous vortexing for 1 min, and centrifuged at 4 °C for 30 min at 10,000 × g to ensure all cell debris fully settled. The extracted oil mass was then determined gravimetrically after the completely evaporation of hexane. All lipid extracts were then stored at −20 °C for further analysis. Quantitative analysis of fatty acids was undertaken using a Perkin Elmer GC-MS (Clarus 500 and 560S) with internal standards. Crude lipids were extracted from the sample using solvents. The lipids were transmethylated, and the profiles of different fatty acids were obtained using gas chromatography. Results were expressed as % of fatty acid methyl esters (Christie, 1993).

2.3.4 Determination of fluorescent properties of DPAS in DMSO/water mixtures

DPAS was obtained from the Hong Kong University of Science and Technology, China (Wang et al., 2016). The absorption and photoluminescence (PL) spectra of DPAS in DMSO/water mixtures were determined using a fluorescence spectrophotometer (Cary Eclipse, MY17180002) with quartz cuvettes of 1 cm pathlength. Fluorescence spectra of 10 μM DPAS in DMSO (Sigma-Aldrich, Australia) and 40-90% water fractions (fw) were measured. The image of the aggregated DPAS in 2% in commercial sunflower oil was taken with Zeiss LSM 880 Airyscan confocal microscope using an excitation filter of 405 nm (2% laser power), emission filter of 560 nm at room temperature.

2.3.5 Determination of algal growth in different concentrations of DPAS

The *E. gracilis* at the density of $6.0 \pm 1.0 (\times 10^3)$ cells / mL (Abs_{780} : 0.0145 ± 0.0033) were introduced to different concentrations (10, 50, and 100 μ M) of DPAS in the CM medium and cultured under the previously described condition. The growth rate was determined by measuring absorbance at 780 nm at regular intervals up to 18 days with a spectrometer. Algal cells treated with 100 μ M of DPAS were observed on an optical microscope (Leica, USA) at different time intervals (0, 30, and 60 min).

2.3.6 Preparation of *Euglena gracilis* samples for BODIPY and DPAS staining

A stock solution of 1.0 mM BODIPYTM 505/515 (Thermo Fisher Scientific Inc.) was prepared in DMSO, and was stored in the dark at -20 °C. The stock solution was diluted to 10 μ M in DI water before use. For each sample, the final concentration of the DMSO was adjusted at 0.1%. The fluorometric quantification of lipids was done according to the modified method of Cooper et al. (2010). Briefly, algal cells were cultured and adjusted at 10^6 cells/ml as noted earlier. The cells were then centrifuged at 2000 g for 60 sec, and re-suspended in 200 μ L DI water. Subsequently, 200 μ L of the prepared 10 μ M BODIPYTM 505/515 solution was gently mixed with the cell suspension and incubated for 5 min in the dark. Consequently, the cells were frequently washed three times with DI water by centrifuging at 2,000 g for 60 sec and re-suspended in water. The stained cells were protected from light until further use.

For the study with DPAS, a relatively simple technique has been followed (Fig. 2.2). Stock solution of 1.0 mM DPAS in DMSO was prepared and was stored in the dark at 4 °C. The fluorescence intensities at different time intervals (10 min, 30 min, 60 min, and 120 min) were determined using Fluorescence Spectrophotometer (Cary Eclipse, MY17180002) with quartz cuvettes of 1 cm pathlength. The *E. gracilis* cells (10^5) from Treatment 5 were stained

with 10 μM DPAS. For the fluorometric quantification of lipids in *E. gracilis* cells with confocal microscopy, the cells from different treatments were adjusted at 10^6 cells/ml. The volume of 10 μM DPAS was added, and the samples were vortexed at 100 rpm for 30 sec and stored in the dark for 30 min. The final concentration of the DMSO was adjusted at 0.1% for all the studies.

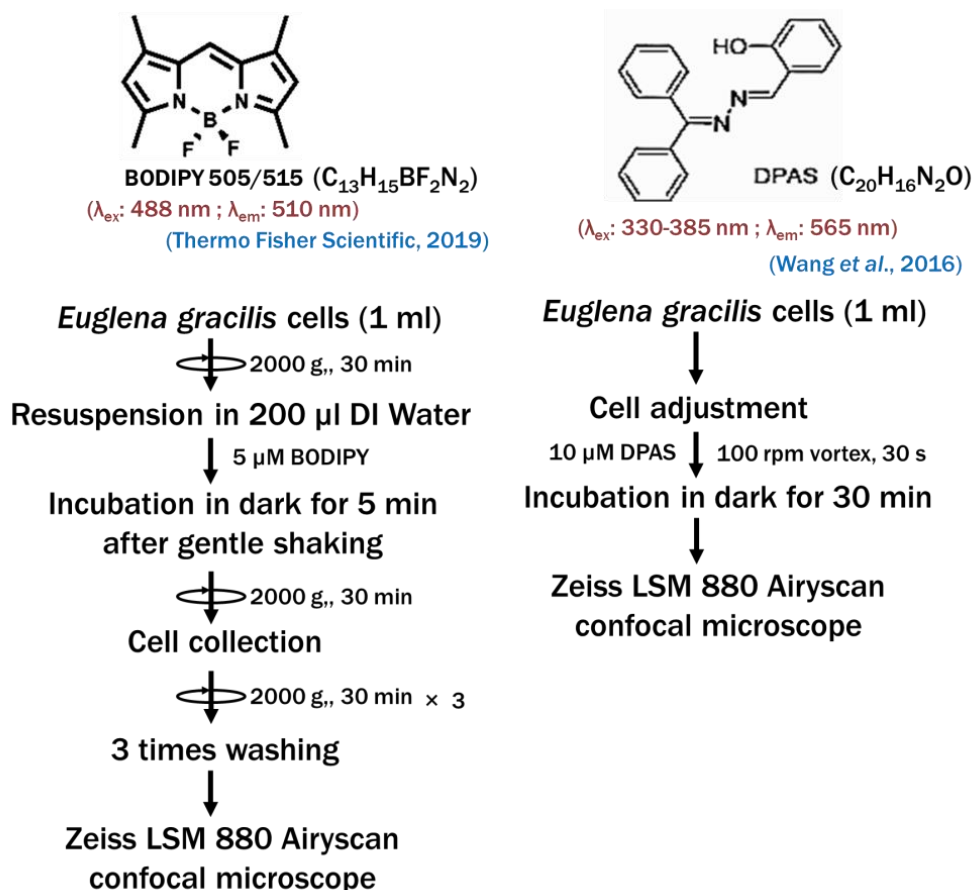


Fig. 2.2 Flow-diagram of sample preparation steps with BODIPY 505/515 and DPAS

2.3.7 Imaging of *Euglena gracilis* with confocal microscope

The *E. gracilis* cells were imaged under a Zeiss LSM 880 Airyscan confocal microscope. The excitation wavelength for BODIPY and DPAS was 488 nm, and the emission wavelengths for BODIPY™ 505/515 and DPAS were 490-561 nm and 570-650 nm, respectively.

Autofluorescence of the chlorophyll was detected with the excitation wavelength at 488 nm and emission wavelength of 685-758 nm.

2.3.8 Flow cytometric analysis of lipid content

Cytometric analysis was done using a flow cytometer (model CytoFLEX Flow Cytometer, Beckman Coulter, Inc. USA). According to the previously described methods, *Euglena* cells from different treatments were taken in three replicates and stained with 5.0 μM BODIPYTM 505/515 and 10 μM DPAS. FITC channel (488 nm laser) was used to detect the fluorescence from BODIPYTM 505/515 and chlorophyll, and Violet 610 (405 nm laser) was used to detect the fluorescence from DPAS. Mean fluorescence intensity from a minimum of 10,000 cells per sample was acquired. Relative fluorescence was determined using the population cell percentile, whereas Treatment 1 served as the control.

2.3.9 Data analysis

Data from the confocal microscopy were analyzed with ImageJ 1.52a (Schneider et al., 2012). The raw image was exported as "tiff" format in ImageJ, and the background of the image from the fluorescence channel was calculated and subtracted using "Sliding paraboloid". Consequently, "Area", "Mean gray value", "Integrated density" and "Area fraction" was measured, highlighting the image. Fluorescence intensity per cell from the total cells was then determined by subtracting the background IntDen value from IntDen value of samples.

The flow cytometry data were analyzed using CytExpert v2.4 software and presented as histogram overlays. To detect BODIPYTM 505/515 labelled cells and chlorophyll, samples were gated on FITC-A vs SSC-A and for DPAS, samples were gated on Violet610-A vs SSC-A. The data of confocal microscopy and flow cytometry were exported to prepare graphs using Excel 2010. The mean and median of different treatments were compared by the

relative fluorescence intensity of the gated population, where Treatment 1 was set as the control group. Data were analyzed by one-way analysis of variance (ANOVA) with SPSS statistics software (version 23). Specific differences in treatment means, and multiple comparisons were tested at $P < 0.05$ level through Waller-Duncan post hoc test and least significant difference (LSD) test, respectively.

2.4 Results

2.4.1 Screening algal growth conditions in different treatments

It is clearly appeared that the N and calcium availability regulated the growth of *E. gracilis*. A slower growth rate in all the treatments was observed except in the CM medium (Fig. 2.3). After 10 days of the initial culture, cells in the CM medium grew rapidly but showed slow growth in all stressed conditions from Treatment 2 to Treatment 5, with the slowest growth in Treatment 2, where nitrogen was deficient (Fig. 2.3a). Therefore, because the nitrogen could be completely utilized by the growing cells after 7 days (Tossavainen et al., 2019), cells were cultured in the CM medium and transferred to the different treatment groups from the exponential phase, where almost similar growth pattern has been observed (Fig. 2.3b). Except for the CM medium, after 7 days, algal growth in all the treatments showed a negative trend, while the dark condition in Treatment 5 showed the lowest value of OD_{780} : 0.317 of algal growth after 10 days of continuous culture compared to other treatments. In the dark condition of Treatment 5, the oxygen concentration was lowest (5.07 ± 0.5 mg/L), while it was highest at 8.19 ± 0.12 mg/L in Treatment 1 after 10 days of consecutive culture. Over the cultural period, the oxygen concentration in the treatments with light conditions remained almost the same (Fig. 2.4), which was due to the photosynthetic activities of algae.

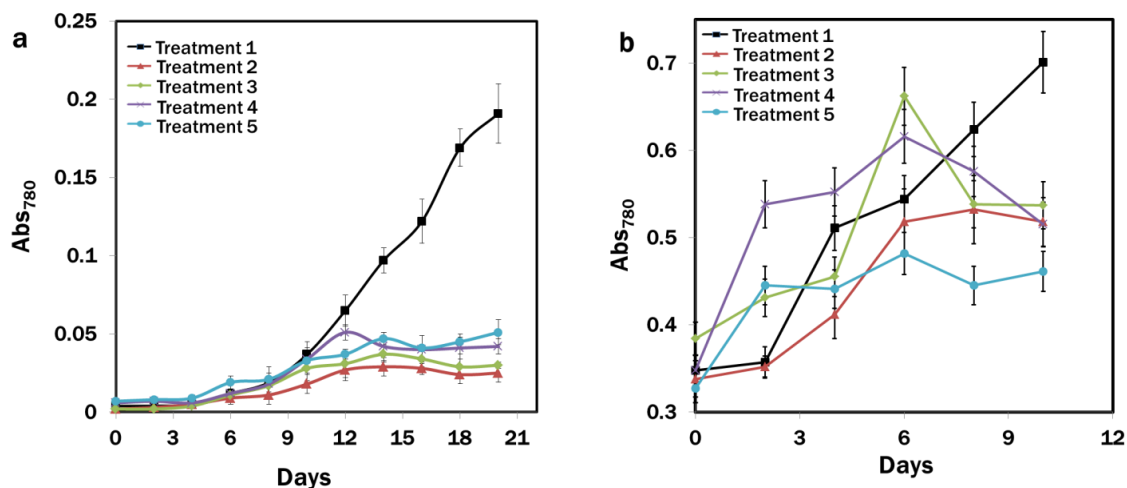


Fig. 2.3 Growth of *Euglena gracilis* in different time intervals. (a) initial culture started at the Abs₇₈₀ measure of 0.004 ± 0.002 ; (b) culture for lipid induction started at the Abs₇₈₀ measure of 0.349 ± 0.021 . Treatment 1: modified Cramer-Myers medium (MCM); Treatment 2: MCM, (-) N₂; Treatment 3: MCM, (-) N₂, (-) Ca²⁺; Treatment 4: MCM, (-) N₂, (-) Ca²⁺, (+) Glucose (24 h light); Treatment 5: MCM, (-) N₂, (-) Ca²⁺, (+) Glucose (24 h Dark) conditions.

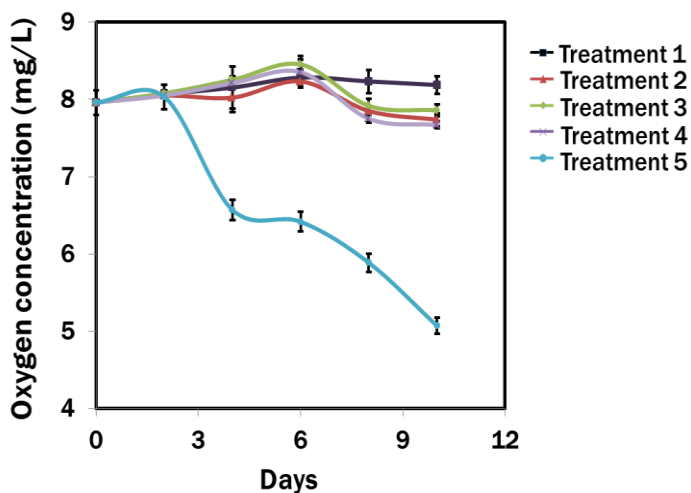


Fig. 2.4 Changes of oxygen concentration in medium over time. Treatment 1: modified Cramer-Myers medium (MCM); Treatment 2: MCM, (-) N₂; Treatment 3: MCM, (-) N₂, (-) Ca²⁺; Treatment 4: MCM, (-) N₂, (-) Ca²⁺, (+) Glucose (24 h light); Treatment 5: MCM, (-) N₂, (-) Ca²⁺, (+) Glucose (24 h Dark) conditions.

2.4.2 Autofluorescence properties of *Euglena gracilis*

Due to different intracellular pigments, microalgae often show strong autofluorescence that hinders the proper utilization of fluorophores for studying target molecules. To select the appropriate dyes for the study in spectrophotometry and confocal microscopy and minimize the background noise, the spectral profile of the autofluorescence from live *E. gracilis* cells was determined. The algal cells excited at 350 nm emitted weak fluorescence at around 460 nm (Fig. 2.5a), whereas cells excited at 405 nm showed two emission peaks at around 460 nm and 700 nm (Fig. 2.5b). Exciting the cells at 488 nm and 560 nm resulted in a single emission peak at 700 nm (Figs. 2.5c and 2.5d). The emission of around 460 nm was assumed due to the redox ratios ((NAD(P)H/FAD)), which are directly related to the cellular metabolic activity (Wu and Qu, 2006). The emission at 700 nm was due to the autofluorescence from chlorophyll since no fluorescence was detected from the heat-treated dead cells with excitation at 488 nm (Fig. 2.5e). Images from the confocal microscopy also showed that exciting the cells with laser light at 405 nm resulted in emission at 450-500 nm (Fig. 2.6b), while no fluorescence was detected at 450-500 nm, when the cells were excited at 488 nm (Fig. 2.7b). At both excitation wavelengths, autofluorescence from chlorophyll was detected at 680-760 nm (Figs. 2.6c and 2.7c). In spectrophotometry results, the maximum autofluorescence for chlorophyll occurred while the cells were excited at 488 nm. Therefore, the chlorophyll fluorescence from different treatments was measured at 488 nm excitation. As shown in Fig. 2.5e, Treatment 1 with CM medium under light conditions contained maximum chlorophyll, whereas N deficiency and dark conditions resulted in the lowest chlorophyll.

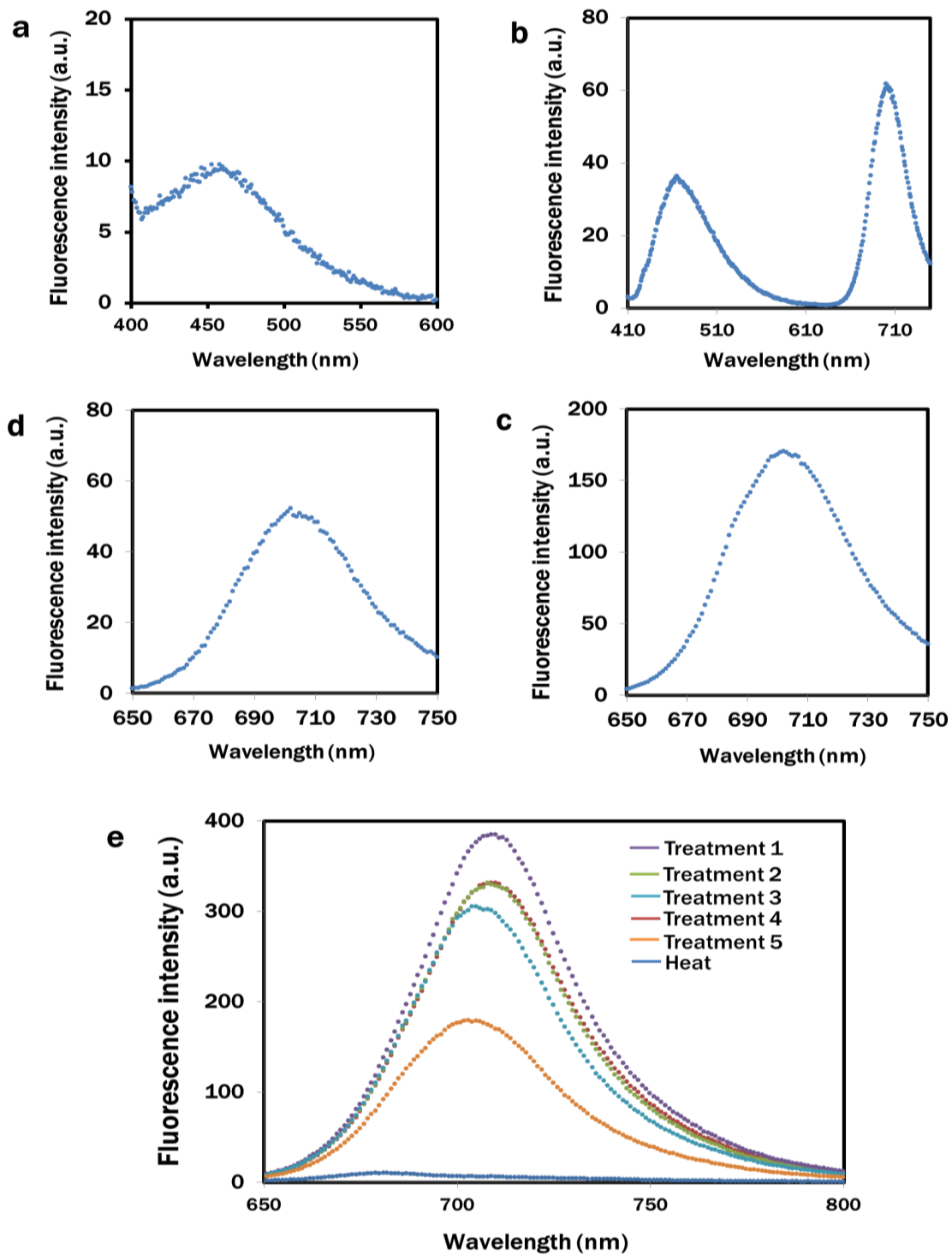


Fig. 2.5 Autofluorescence of *Euglena gracilis* excited at different excitation wavelengths (a) excitation at 350 nm; (b) excitation at 405 nm; (c) excitation at 488 nm; (d) excitation at 560 nm; (e) autofluorescence of chlorophyll from different treatments excited at 488 nm.

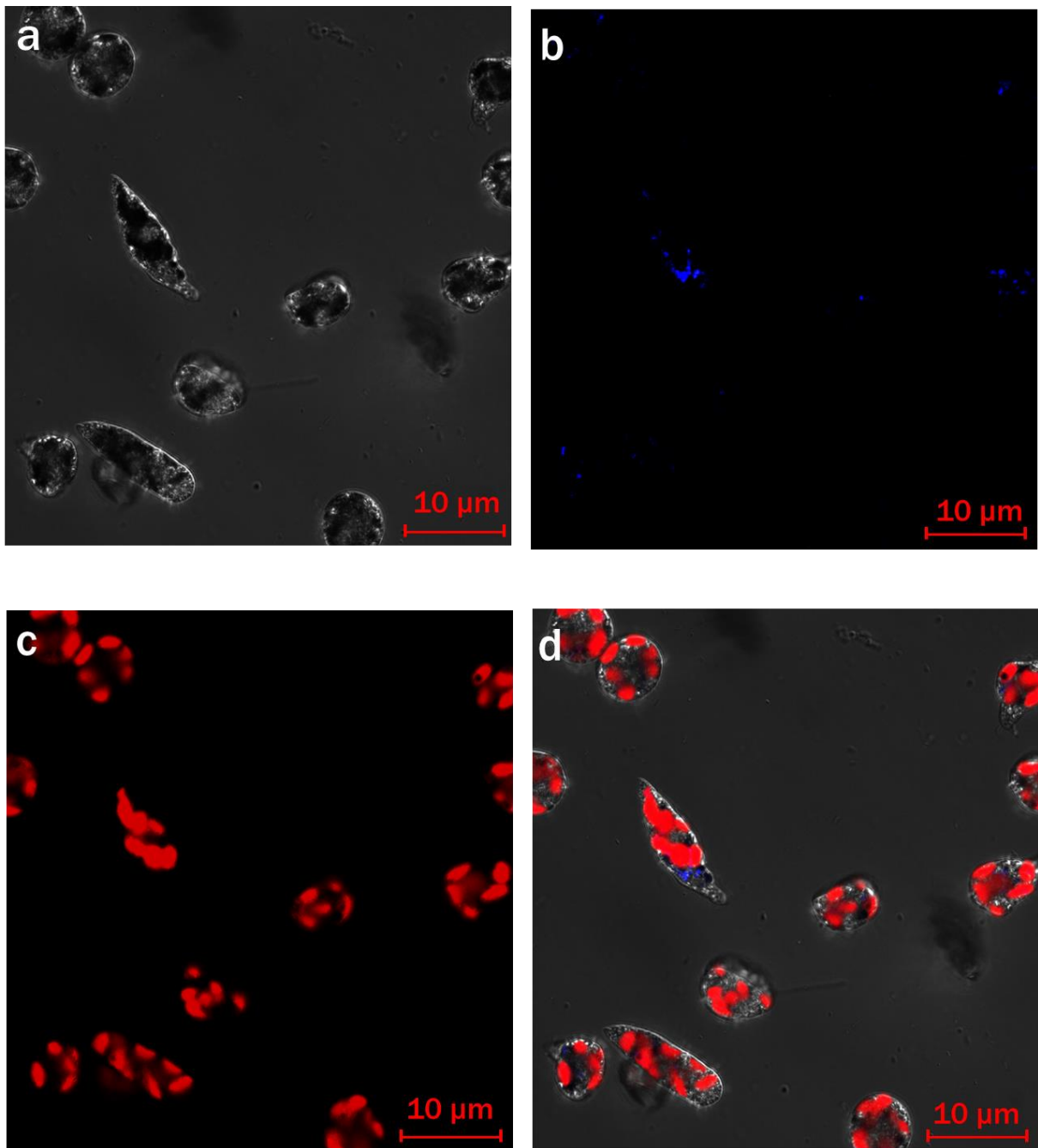


Fig. 2.6 Autofluorescence of *Euglena gracilis* under Zeiss LSM 880 Airyscan confocal microscopy at $\lambda_{\text{ex}} = 405 \text{ nm}$ (a-d). Brightfield (a); $\lambda_{\text{em}} = 450\text{-}500 \text{ nm}$ (b); Chlorophyll ($\lambda_{\text{em}} = 680\text{-}760 \text{ nm}$) (c); Merge (d)

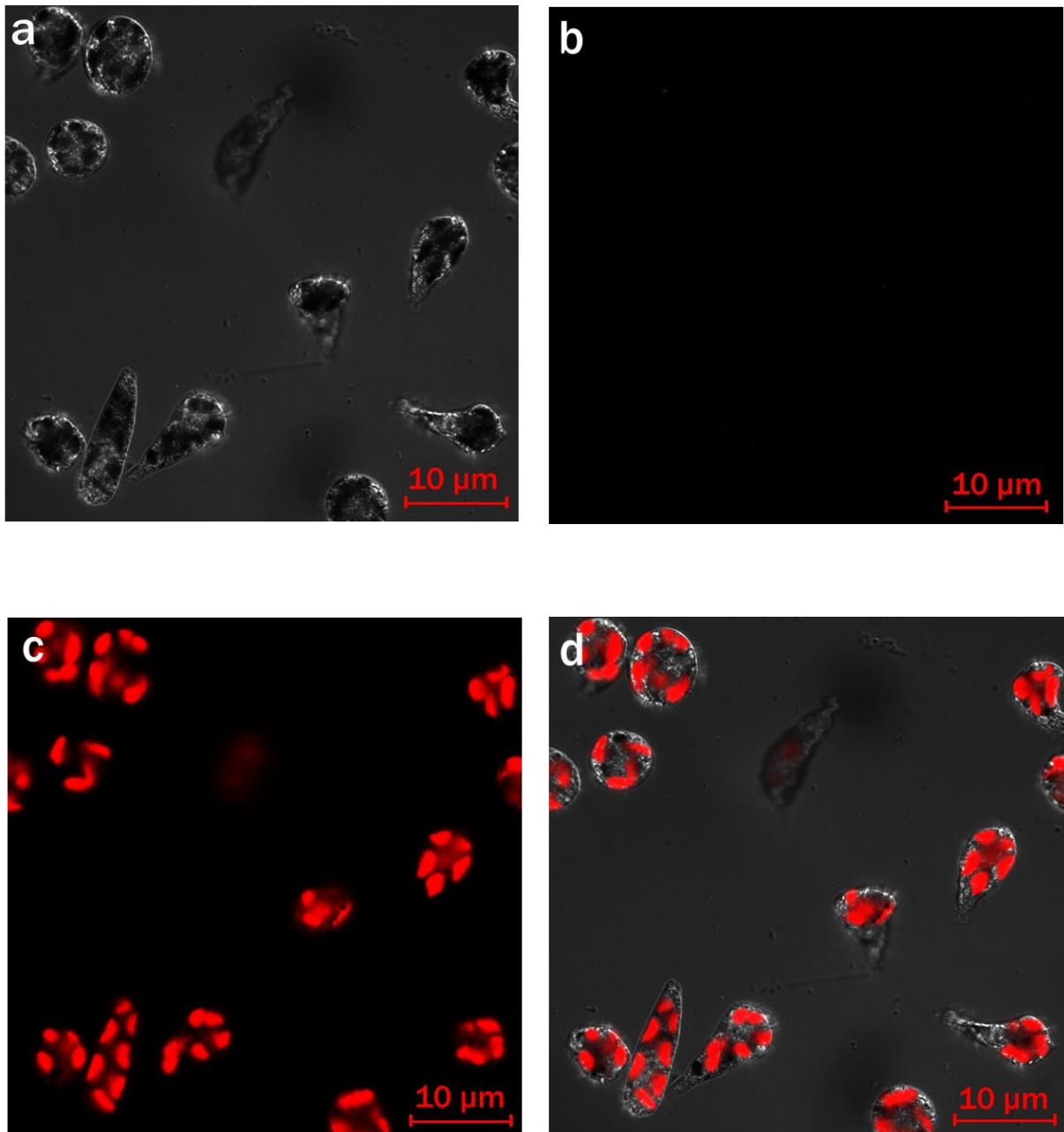


Fig. 2.7 Autofluorescence of *Euglena gracilis* under Zeiss LSM 880 Airyscan confocal microscopy at $\lambda_{\text{ex}} = 488 \text{ nm}$ (a-d). Brightfield (a); $\lambda_{\text{em}} = 450\text{-}500 \text{ nm}$ (b); Chlorophyll ($\lambda_{\text{em}} = 680\text{-}760 \text{ nm}$) (c); Merge (d)

2.4.3 Effects of DPAS on *Euglena gracilis* growth

We used lipid-specific DPAS to check its efficacy in algae with different cell membrane structures from the animal cell model used by Wang et al. (2016). Before the cells were introduced for lipid analysis, the effects of DPAS on growth were monitored. The conditions of the cells were also confirmed under a light microscope immediate after exposure to DPAS. In comparison to the control group, no difference was observed in the growth pattern of algae even after exposure to a significantly higher concentration of 100 μ M DPAS (Fig. 2.8a). Images from the light microscope (Figs 2.8b-2.8d) revealed that immediate after exposure, the movement of the cells was reduced, and the size decreased by 45% (Fig. 2.8b), while within 30 min the cells were completely recuperated (Fig. 2.8d), and were fully functional. The movement of *E. gracilis* after incorporating DPAS molecules in the lipid drops also confirmed that cells were alive and functional, suggesting that DPAS was not toxic for the algal cells.

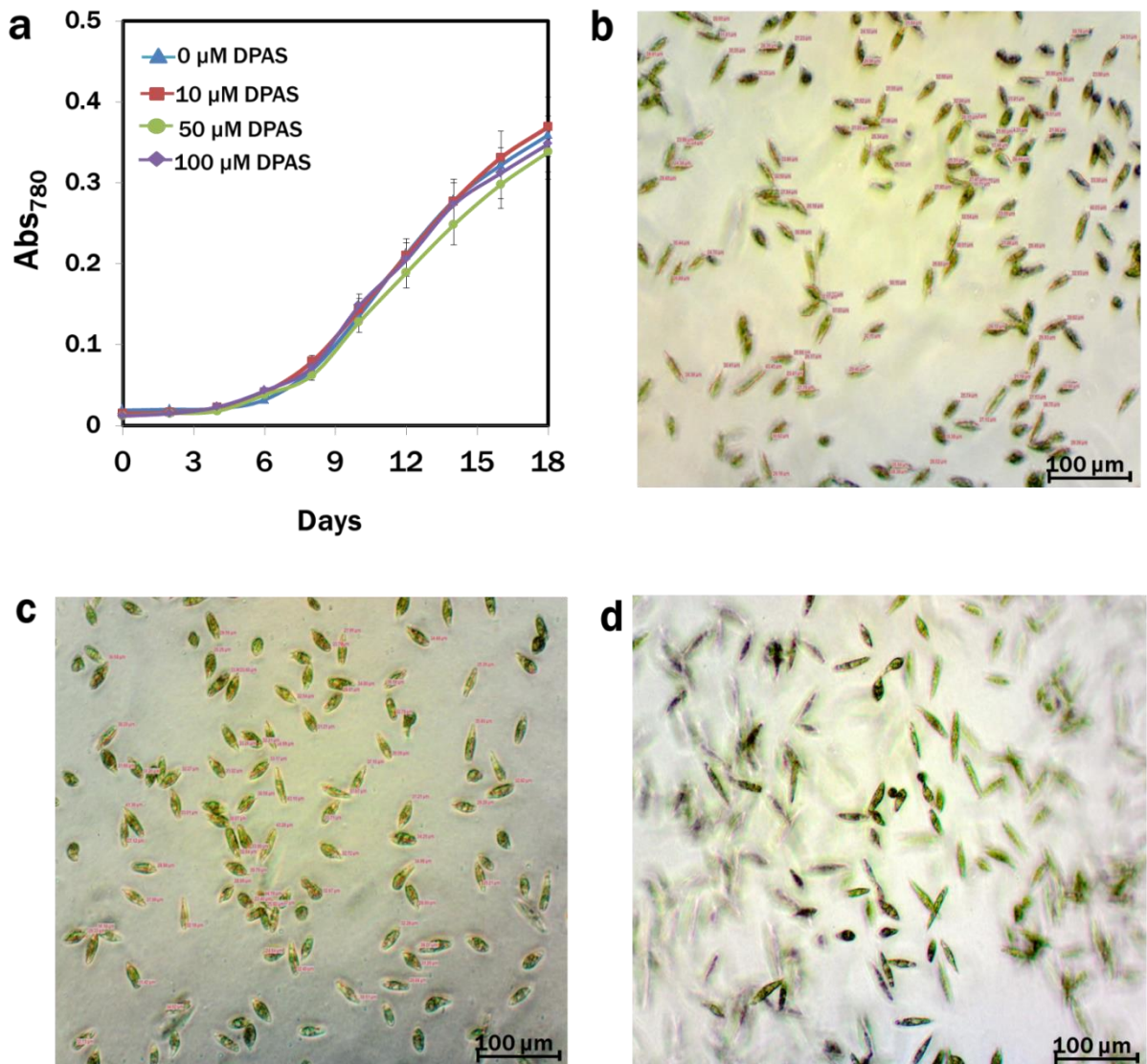


Fig. 2.8 Effects of DPAS on *Euglena gracilis*. Growth of *E. gracilis* exposed to different concentrations (0-100 μM) of DPAS (a). Changes in *E. gracilis* size and movement at different time intervals due to the exposure to 100 μM DPAS (b-d); (b) $26.32 \pm 4.74 \mu\text{m}$ (0 min after incubation); (c) $31.13 \pm 4.60 \mu\text{m}$ (10 min after incubation); (d) fully recovered and motile, $48.1 \pm 6.27 \mu\text{m}$ (30 min after incubation)

2.4.4 Fluorescent properties of DPAS

The absorption and photoluminescence (PL) spectra of DPAS (10 μM) in DMSO under the excitation of 405 nm were determined. DPAS showed weak emissions in DMSO solution, but the PL intensity started to increase with the addition of water in DMSO. The emission increased rapidly, while the water percentage increased from 80% to 90%, which signified the AIE attributes of DPAS (Figs. 2.9a and 2.9b). Images from the confocal microscope also suggested the aggregation of DPAS in the 2% sunflower oil (Figs. 2.9c- 2.9e).

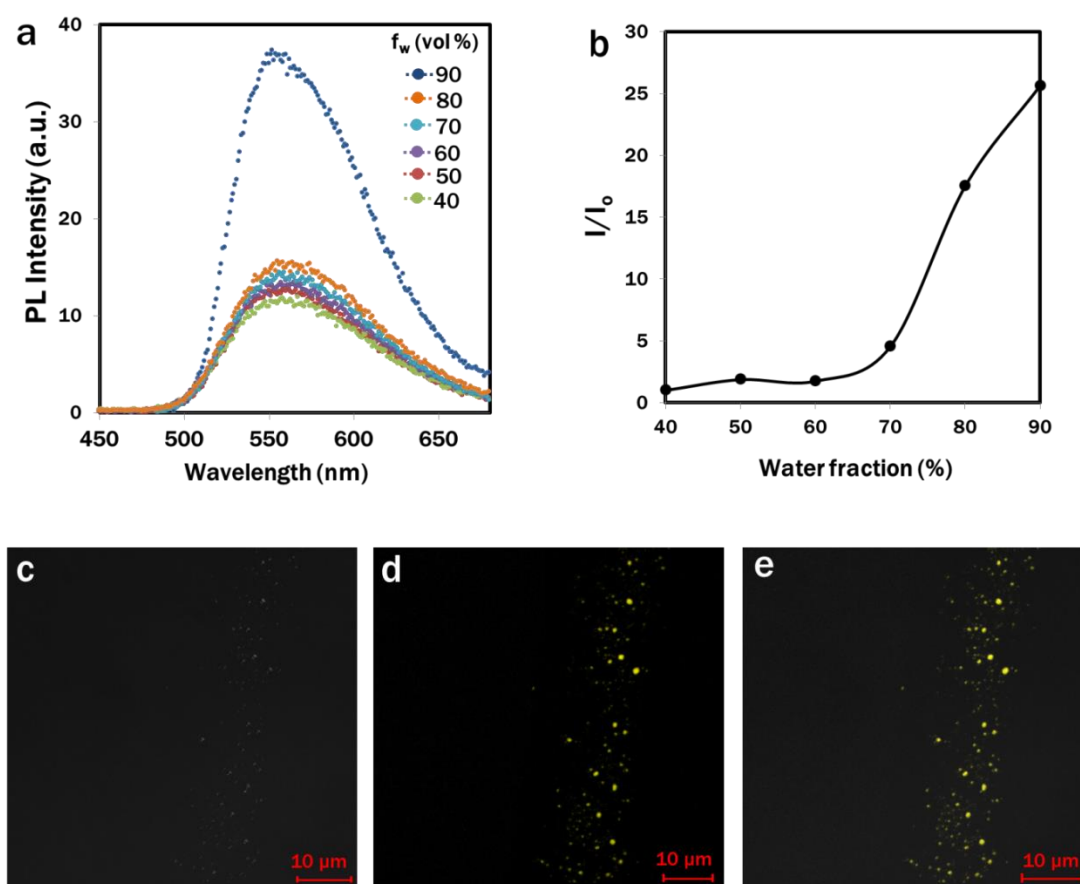


Fig. 2.9 Fluorescence properties of DPAS. Fluorescence spectra of DPAS (10 μM) in DMSO-water mixtures (a-b); Fluorescence of DPAS in 2% sunflower oil under Zeiss LSM 880 Airyscan confocal microscope (c-e). Brightfield (c); aggregation of DPAS in sunflower oil (λ_{ex} : 405 nm, λ_{em} : 560 nm) (d); Merge (e).

2.4.5 Optimization of DPAS concentration and incubation periods

While checking with different DPAS concentrations, no significant difference has been observed in the fluorescence intensity from the *E. gracilis* cells incubated with 10 μM and 20 μM DPAS (Fig. 2.10a). Furthermore, although the fluorescence intensity of DPAS in the presence of *E. gracilis* cells at 10 min was slightly lower than that of the incubation after 30 min, 60 min, and 120 min, the result was not significantly different (Fig. 2.10b). Therefore, it was assumed that 10 μM DPAS could completely label lipid drops in cells within 30 min.

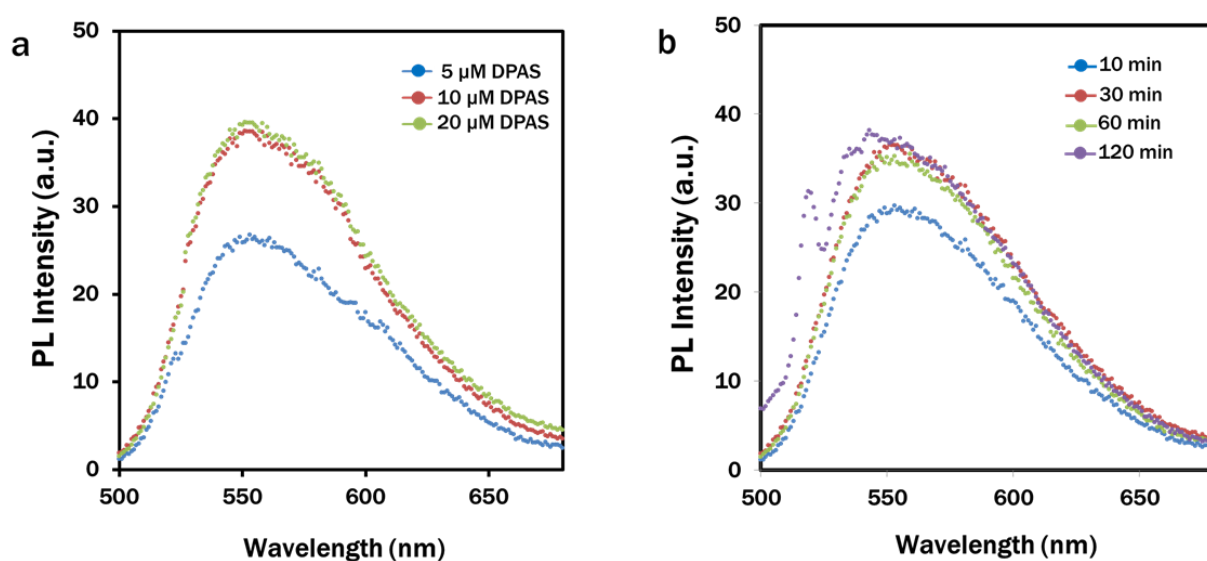


Fig. 2.10 Optimization of AIE probe, DPAS conditions in *Euglena gracilis* cells. Fluorescence spectra of different concentrations of DPAS in *E. gracilis* cells (a); Fluorescence spectra of DPAS (10 μM) in *E. gracilis* cells at different time intervals (b).

2.4.6 Labeling of stress-induced lipid droplets by DPAS in *Euglena gracilis*

Nutrient starvation is a well-known condition for lipid induction in microalgae (Sun et al., 2018; Alishah Aratboni et al., 2019). This experiment studied the effects of nitrogen and calcium starvation on lipid accumulation in *E. gracilis* cells. In addition to nitrogen and

calcium starvation, glucose supplemented light and dark conditions were also analyzed. As an approach to quick scanning for lipid accumulation, a simple staining procedure with minimal sample preparation was implemented on *E. gracilis* cells with DPAS, directly added to the growing media in different nutrient treatment groups. As the control, the lipophilic green fluorescent dye, BODIPY™ 505/515 was used to co-stain the cells for lipid detection in microalgae (Wu et al., 2014; Rumin et al., 2015). The images of different treatments showed lipid accumulation in the nutrient-starved conditions (Figs 2.11-2.15). However, cells from the Treatment 5 (MCM, (-) N₂, (-) Ca²⁺, (+) Glucose (24 h Dark) conditions) showed the highest lipid accumulation (Fig. 2.15), followed by the Treatment 4 (MCM, -N₂, -Ca²⁺, +Glucose, Fig. 14) and Treatment 2 (MCM, -N₂, Fig. 2.12). The control group detected the lowest fluorescence (Treatment 1: MCM medium in 24 h light condition) (Fig. 2.11). Autofluorescence from the chlorophyll detected was the lowest in Treatment 5 (Fig. 2.15). The merged image indicated that the yellow and green fluorescence channels assigned for DPAS and BODIPY, respectively, overlap each other (Fig. 2.15e). The arrow position in the merged image (Figs. 2.15e and 2.15v) demonstrated almost synchronized intensity changes of DPAS and BODIPY in *E. gracilis* cells with a higher intensity for DPAS (Fig. 2.15f). The intensity scatter plot was drafted, and the Pearson correlation coefficient and Mander's overlap coefficient were calculated as 0.90 and 0.92, respectively (Fig. 2.15g). ImageJ analysis of relative fluorescence per cell showed an almost similar pattern with DPAS and BODIPY™ 505/515 for lipid labelling (Fig. 2.16).

The present study results showed that DPAS had reasonable lipid specificity and penetration abilities to *E. gracilis* with higher sensitivity, which was very similar to the commercially available BODIPY™ 505/515 dye. Additionally, due to the photostable properties of AIE molecules and easy sample preparation techniques (Fig. 2.2), DPAS had good potential for rapid visualization and quick screening of lipid content in the cells from different treatments.

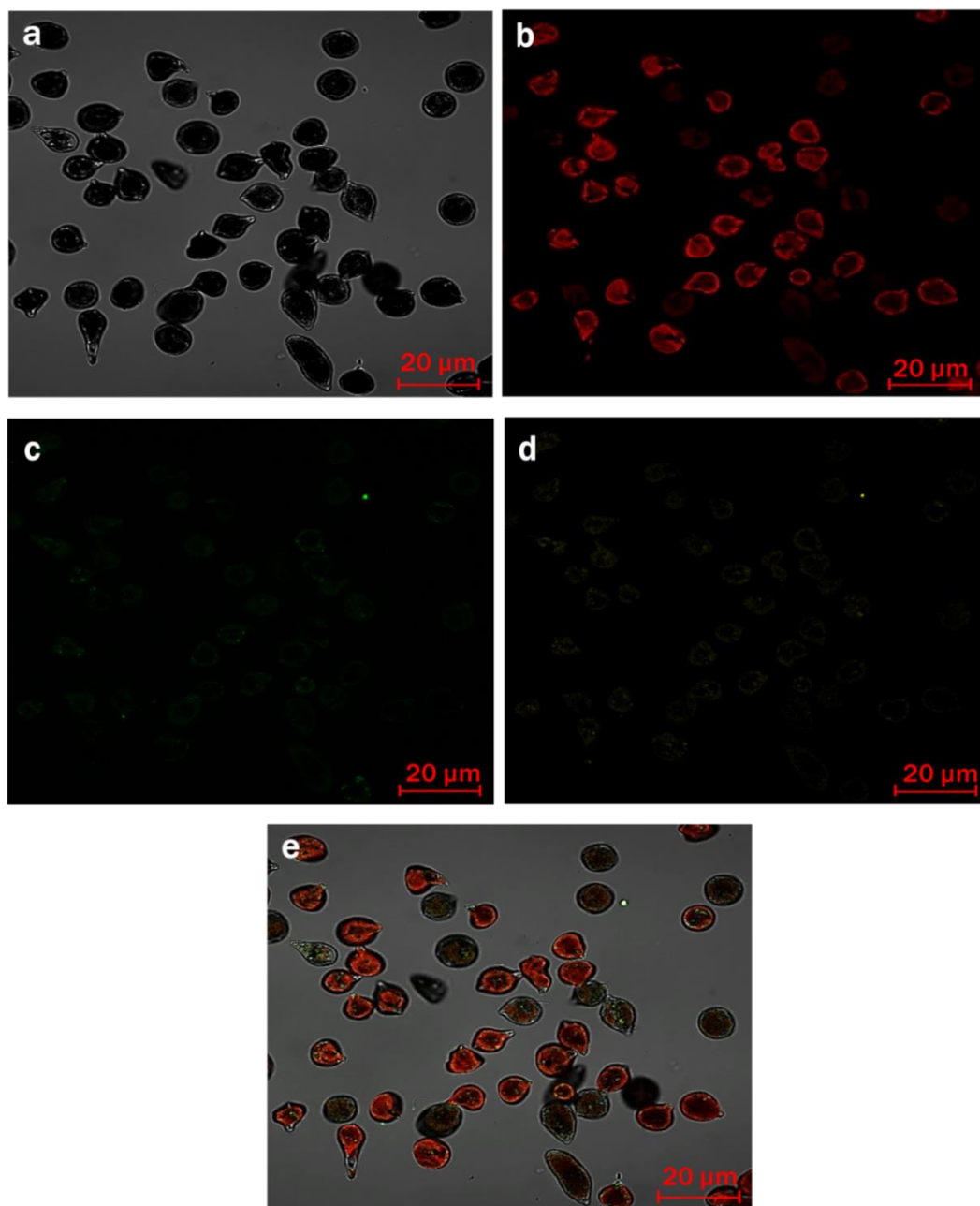


Fig. 2.11 Images of *E. gracilis* cells incubated with lipid specific aggregation-induced emission (AIE) nanoprobe, DPAS ($C_{20}H_{16}N_2O$) and commercial lipid-specific fluorescent probe, BODIPY. Cells were cultured in Treatment 1: modified Cramer-Myers medium (MCM). Bright-field image: a; Fluorescence images - Chlorophyll: b, BODIPY: c, and DPAS: d; Merged images: e. Images were taken with Zeiss LSM 880 Airyscan confocal microscope.

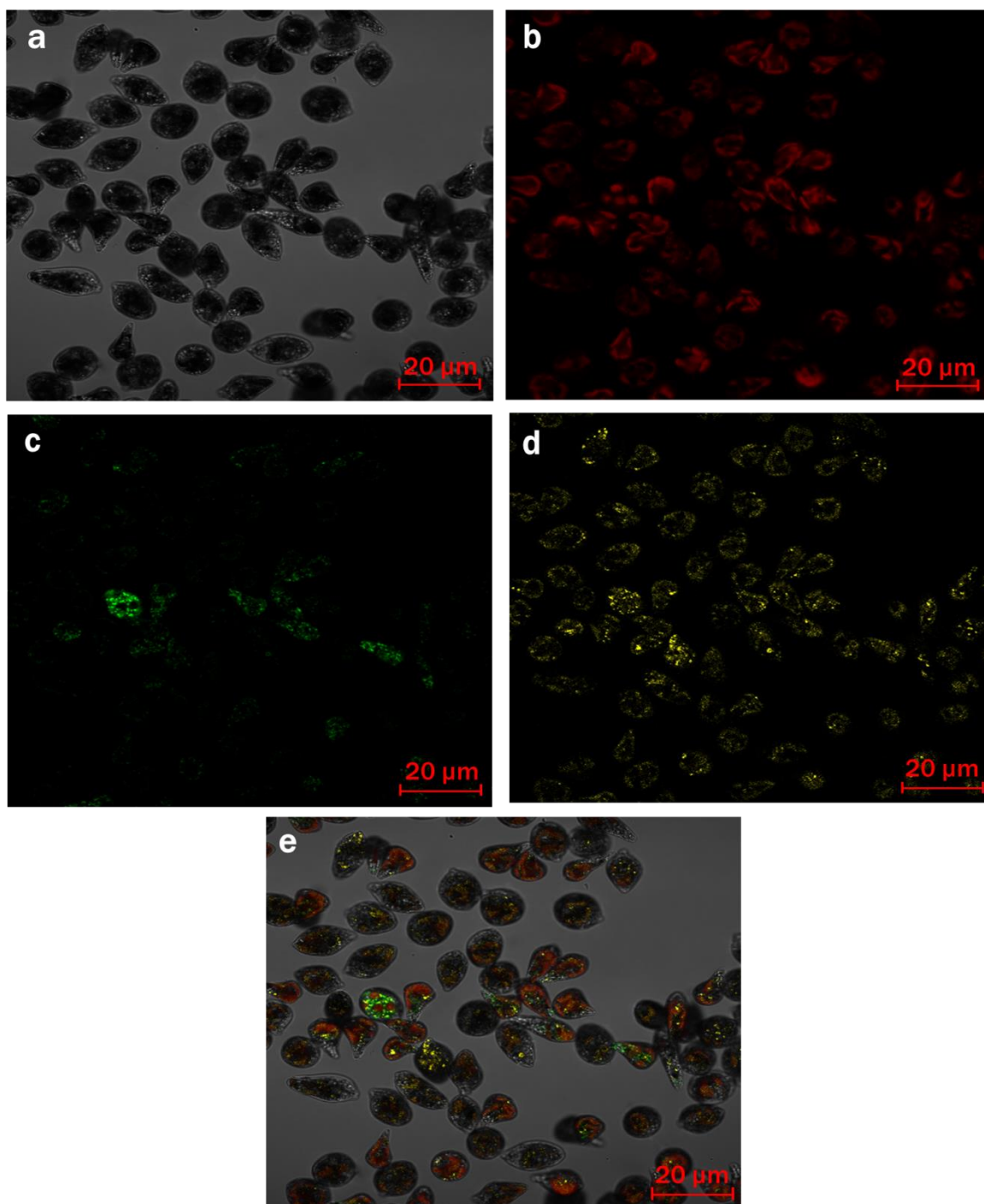


Fig. 2.12 Images of *E. gracilis* cells incubated with lipid specific aggregation-induced emission (AIE) nanoprobe, DPAS ($C_{20}H_{16}N_2O$) and commercial lipid-specific fluorescent probe, BODIPY. Cells were cultured in Treatment 2: MCM, (-) N_2 ; Bright-field image: a; Fluorescence images - Chlorophyll: b, BODIPY: c, and DPAS: d; Merged images: Images were taken with Zeiss LSM 880 Airyscan confocal microscope.

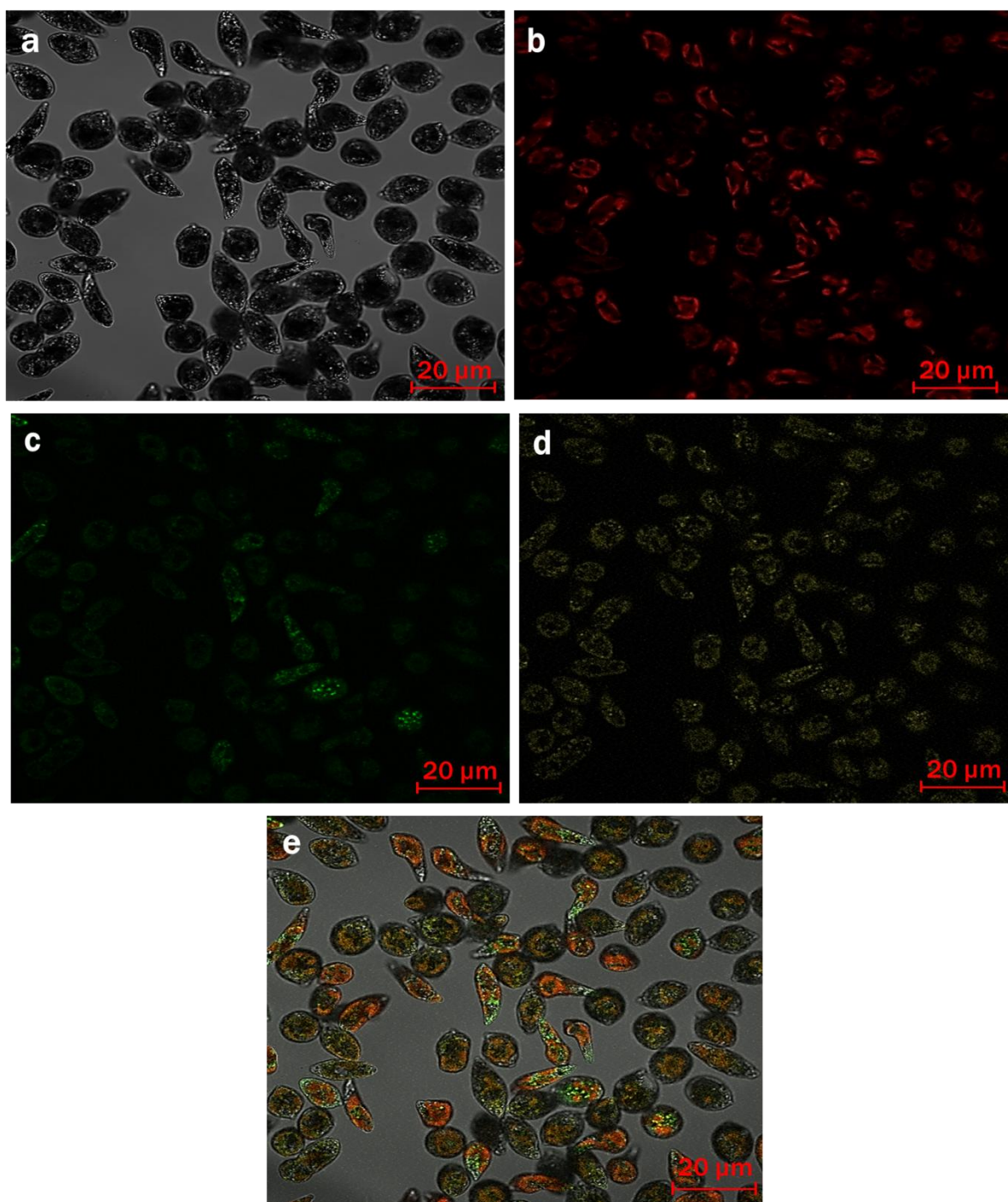


Fig. 2.13 Images of *E. gracilis* cells incubated with lipid-specific aggregation-induced emission (AIE) nanoprobe, DPAS ($C_{20}H_{16}N_2O$) and commercial lipid-specific fluorescent probe, BODIPY. Cells were cultured in Treatment 3: MCM, (-) N_2 , (-) Ca^{2+} ; Bright-field image: a; Fluorescence images - Chlorophyll: b, BODIPY: c, and DPAS: d; Merged images: e. Images were taken with Zeiss LSM 880 Airyscan confocal microscope.

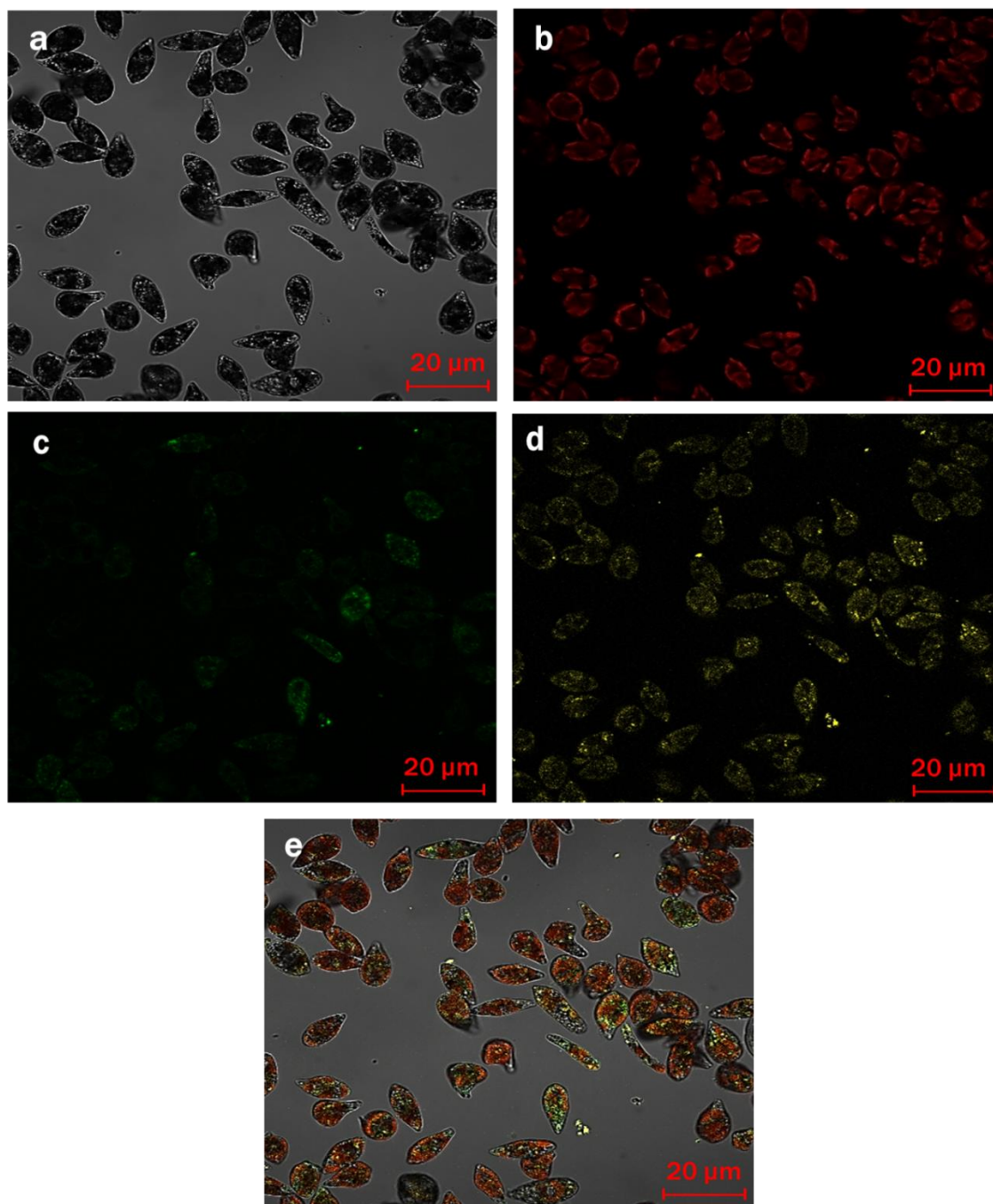


Fig. 2.14 Images of *E. gracilis* cells incubated with lipid-specific aggregation-induced emission (AIE) nanoprobe, DPAS ($C_{20}H_{16}N_2O$) and commercial lipid-specific fluorescent probe, BODIPY. Cells were cultured in Treatment 4: MCM, (-) N_2 , (-) Ca^{2+} , (+) Glucose (24 h light). Bright-field image: a; Fluorescence images - Chlorophyll: b, BODIPY: c, and DPAS: d; Merged images: e. Images were taken with Zeiss LSM 880 Airyscan confocal microscope.

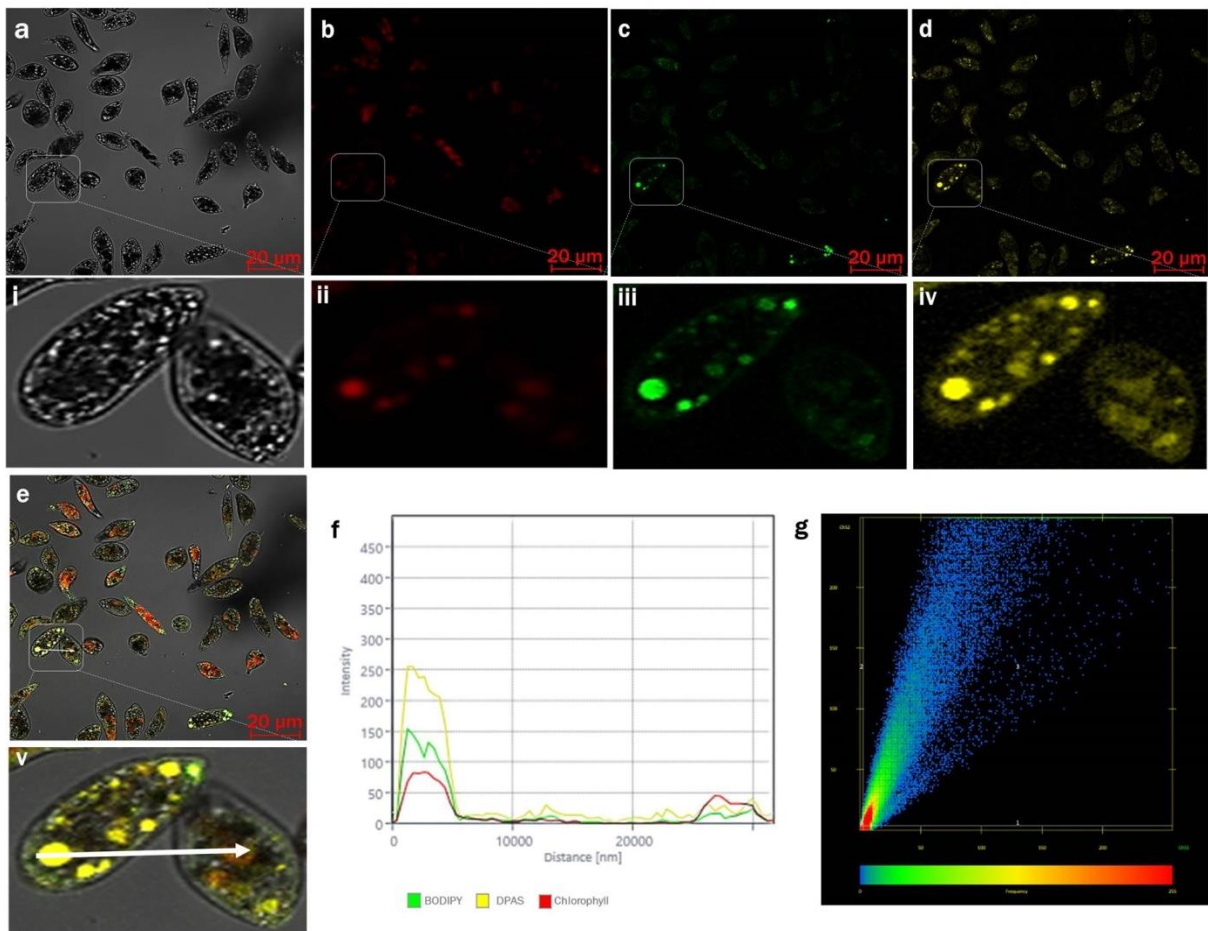


Fig. 2.15 Images of *E. gracilis* cells incubated with lipid specific aggregation-induced emission (AIE) nanoprobe, DPAS ($C_{20}H_{16}N_2O$) and commercial lipid-specific fluorescent probe, BODIPY. Cells were cultured in Treatment 5: MCM, (-) N_2 , (-) Ca^{2+} , (+) Glucose (24 h Dark) conditions. Bright-field image: a; Fluorescence images - Chlorophyll: b, BODIPY: c, and DPAS: d; Merged images: e, and the enlarged regions (i, ii, iii, iv, and v for bright-field, reduced chlorophyll, BODIPY™ 505/515, DPAS stained cells and merged image, respectively). (f) intensity profile of BODIPY and DPAS in green and yellow channels, respectively; (l) intensity scatter plot for the colocalized channels; Pearson correlation coefficient and Mander's overlap coefficient were calculated as 0.90 and 0.92, respectively Images were taken with Zeiss LSM 880 Airyscan confocal microscope.

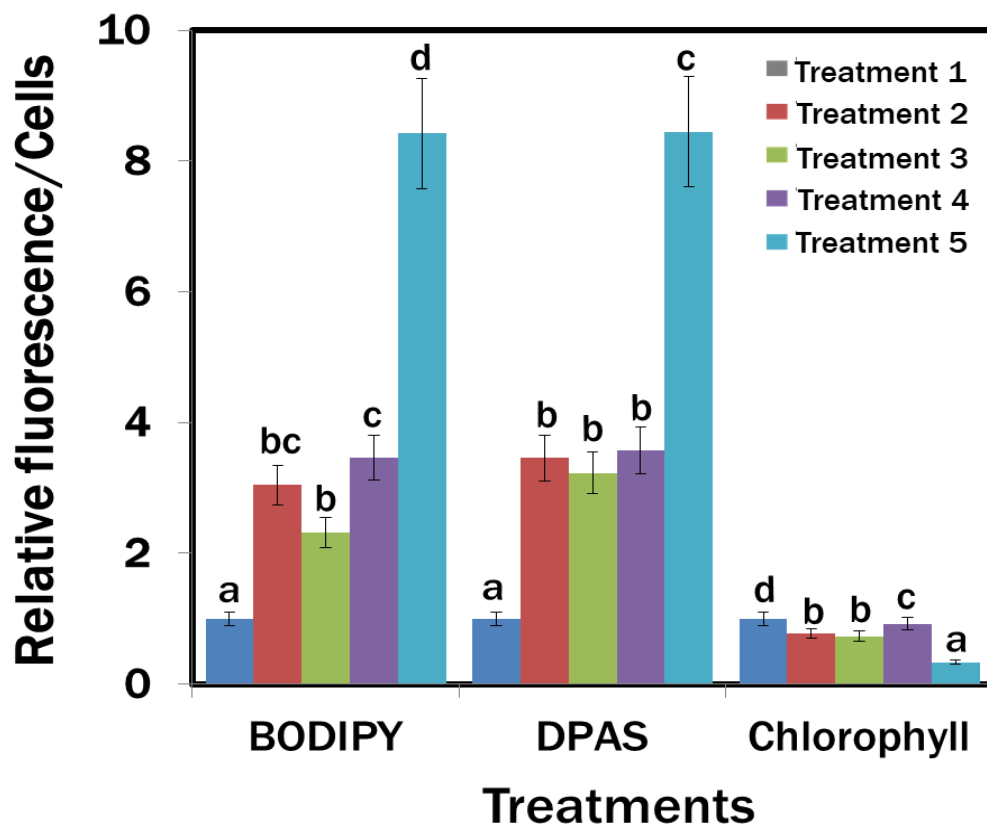


Fig. 2.16 Confocal analysis of relative fluorescence intensity / *E. gracilis* cell for different treatments. Cells were incubated with lipid-specific aggregation-induced emission (AIE) nanoprobes, DPAS (C₂₀H₁₆N₂O) and a commercial lipid-specific fluorescent probe, BODIPY. Cells were cultured in Treatment 1: modified Cramer-Myers medium (MCM); Treatment 2: MCM, (-) N₂; Treatment 3: MCM, (-) N₂, (-) Ca²⁺; Treatment 4: MCM, (-) N₂, (-) Ca²⁺, (+) Glucose (24 h light); Treatment 5: MCM, (-) N₂, (-) Ca²⁺, (+) Glucose (24 h Dark) conditions. Values are relative to the control condition (Treatment 1: modified Cramer-Myers medium (MCM)). Averages are shown as mean ± SE. Images were taken with Zeiss LSM 880 Airyscan confocal microscope.

2.4.7 Flow cytometric analysis of lipid content

The plots of the flow cytometry experiments revealed that BODIPY™ 505/515 (Fig. 2.17) and DPAS (Fig. 2.18) could successfully label the lipid in *E. gracilis* cells. In comparison to the MCM medium under 24 h light condition (Treatment 1) (Figs. 2.17a and 2.18a), cytograms of BODIPY fluorescence vs side scatter (Figs. 2.17b-2.17e) and DPAS fluorescence vs side scatter (Figs. 2.18b-2.18e) showed more lipid accumulation in cells cultured in the nutrient-starved cells. Maximum lipid accumulation has been observed in Treatment 5 (MCM, (-) N₂, (-) Ca²⁺, (+) Glucose (24 h Dark) conditions) (Figs. 2.17e and 2.18e), followed by Treatment 4 (MCM, (-) N₂, (-) Ca²⁺, (+) Glucose) (Figs. 2.17d and 2.18d).

Moreover, as the lipid accumulation in algae has been reported to produce obese phenotypes (Goodenough et al., 2014; Goncalves et al., 2016), cellular events in nutrient-starved populations with greater side scatter in this experiment were proportional to the cellular obesity and accumulation of probes inside the LDs. Therefore, histograms with increased fluorescence from BODIPY™ 505/515 and DPAS were consistent with obese cell types having higher relative lipid fluorescence per cell (Figs 2.17f, 2.18f and 2.19).

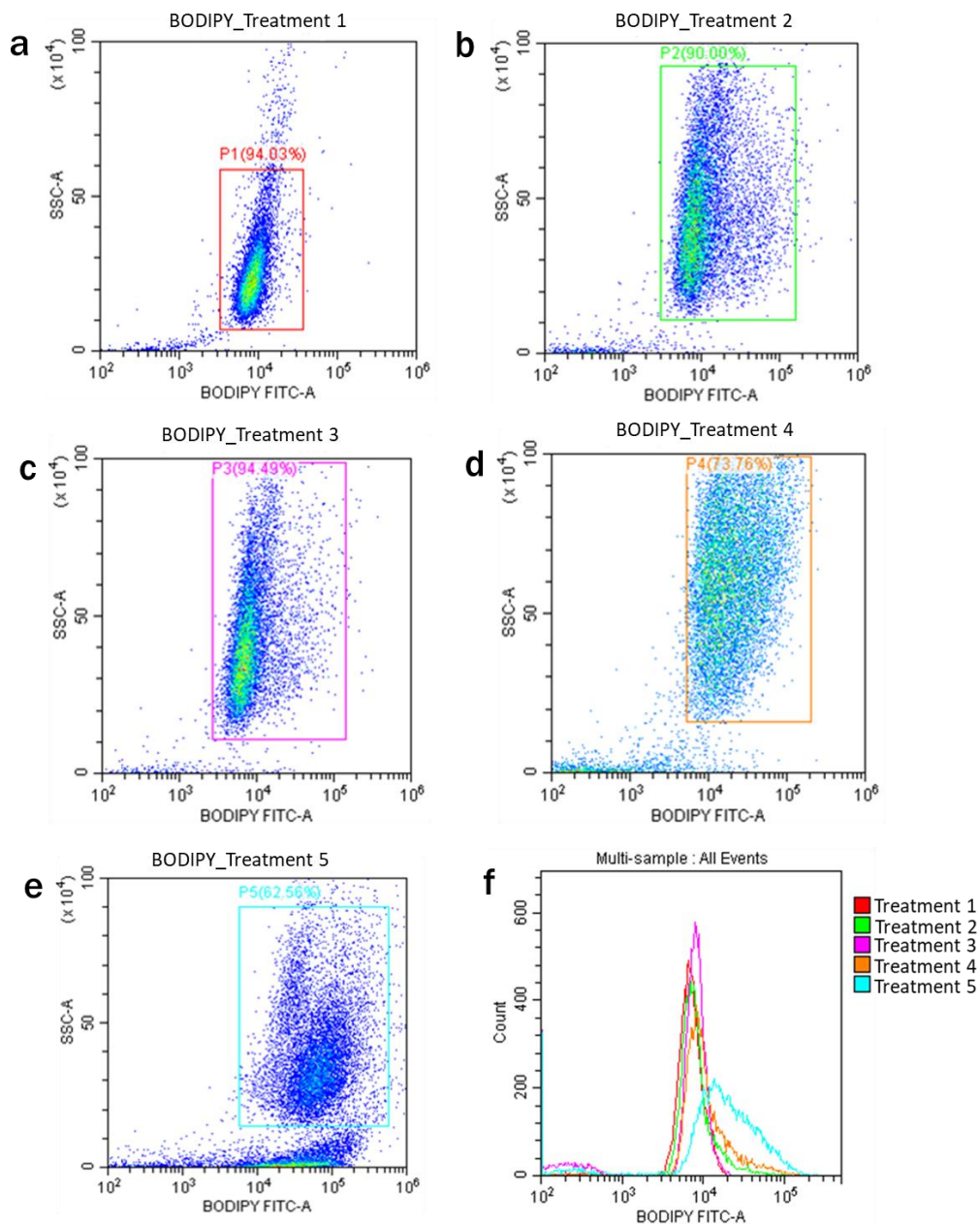


Fig. 2.17 Flow cytometry measurements for lipid in *Euglena gracilis* cells in different treatments labelled with BODIPY™ 505/515. (a-e) Flow cytogram of FITC-A vs SSC-A for BODIPY fluorescence in different treatments. Cells were cultured in Treatment 1: modified Cramer-Myers medium (MCM); Treatment 2: MCM, (-) N₂; Treatment 3: MCM, (-) N₂, (-) Ca²⁺; Treatment 4: MCM, (-) N₂, (-) Ca²⁺, (+) Glucose (24 h light); and Treatment 5: MCM, (-) N₂, (-) Ca²⁺, (+) Glucose (24 h Dark) conditions. (k) Histogram of BODIPY fluorescence for cells. All plots are on a logarithmic scale for both axes.

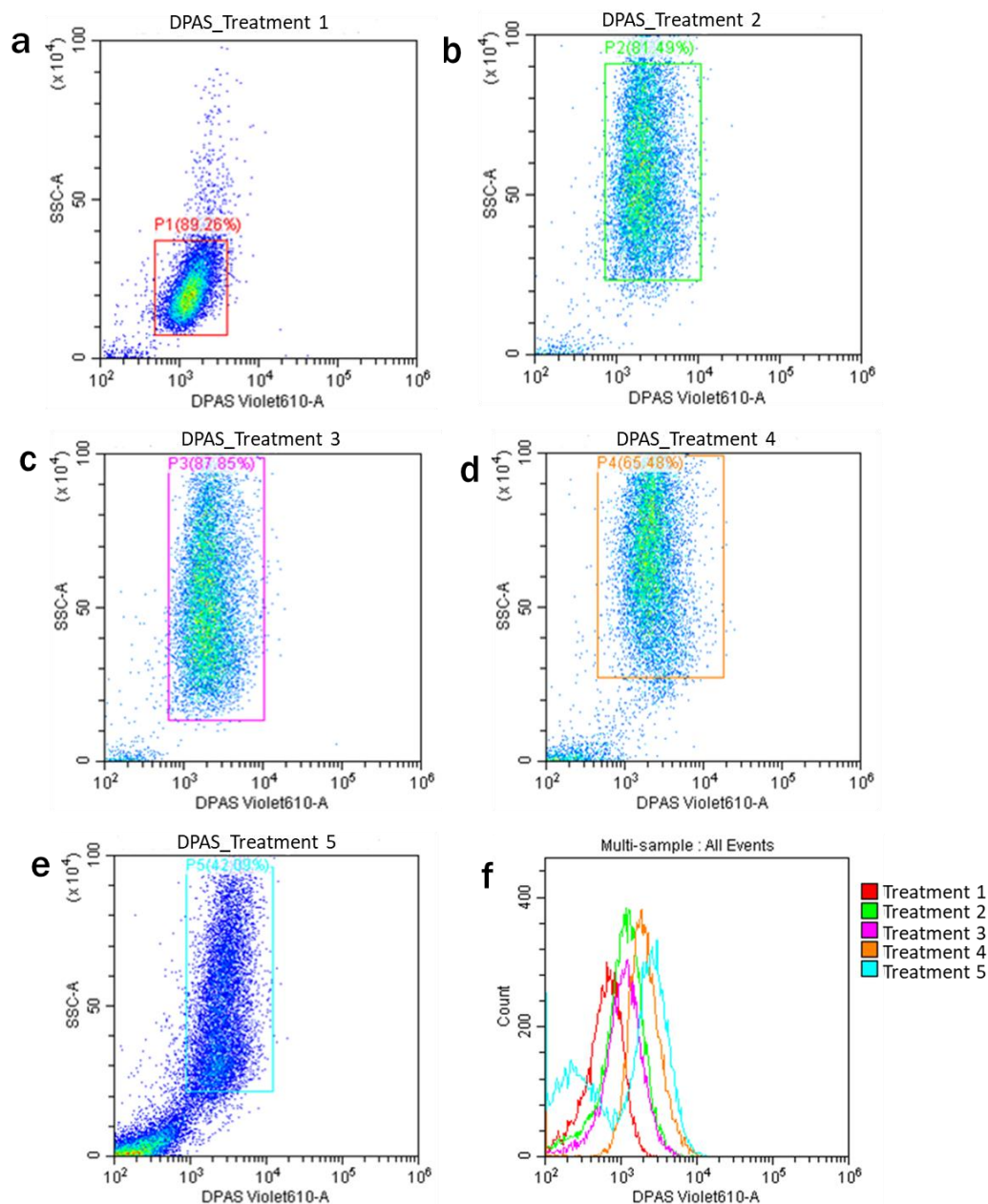


Fig. 2.18 Flow cytometry measurements for lipid in *Euglena gracilis* cells in different treatments labelled with AIE probe, DPAS. (a-e) Flow cytogram of FITC-A vs SSC-A for BODIPY fluorescence in different treatments. Cells were cultured in Treatment 1: modified Cramer-Myers medium (MCM); Treatment 2: MCM, (-) N_2 ; Treatment 3: MCM, (-) N_2 , (-) Ca^{2+} ; Treatment 4: MCM, (-) N_2 , (-) Ca^{2+} , (+) Glucose (24 h light); and Treatment 5: MCM, (-) N_2 , (-) Ca^{2+} , (+) Glucose (24 h Dark) conditions. (k) Histogram of DPAS fluorescence for cells. All plots are on a logarithmic scale for both axes.

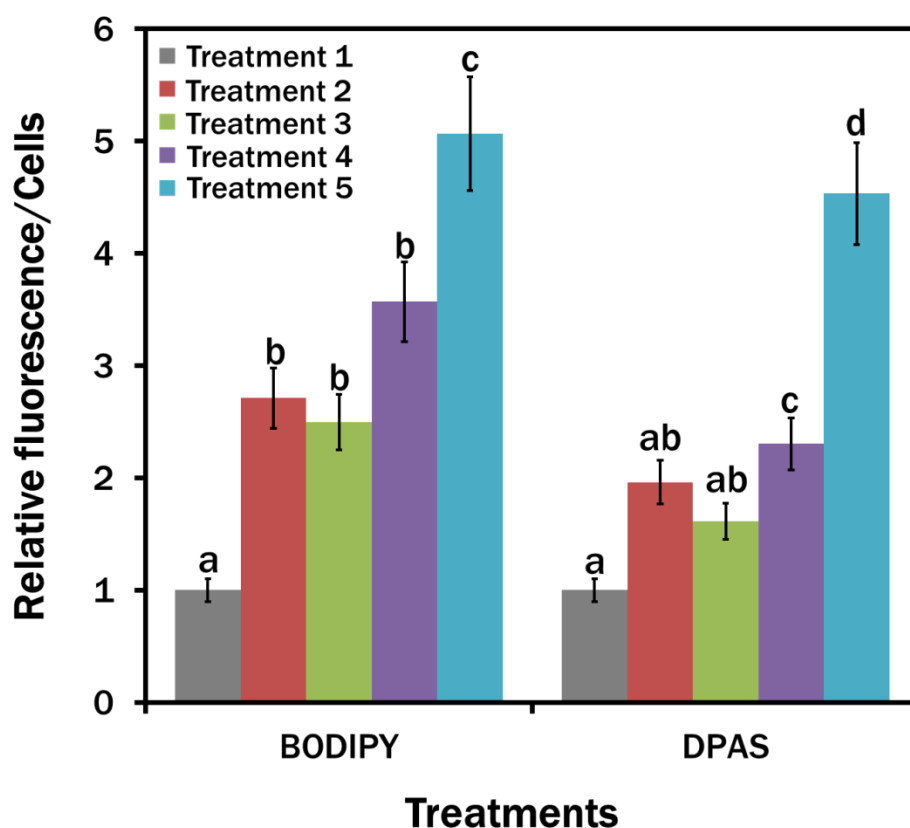


Fig. 2.19 Flow cytometry analysis for the relative fluorescence of BODIPY™ 505/515 and DPAS / cell for different treatments. Cells were cultured in Treatment 1: modified Cramer-Myers medium (MCM); Treatment 2: MCM, (-) N₂; Treatment 3: MCM, (-) N₂, (-) Ca²⁺; Treatment 4: MCM, (-) N₂, (-) Ca²⁺, (+) Glucose (24 h light); and Treatment 5: MCM, (-) N₂, (-) Ca²⁺, (+) Glucose (24 h Dark) conditions. Values are relative to the control condition (Treatment 1: modified Cramer-Myers medium (MCM)). Averages shown as mean ± SE.

2.4.8 Fatty acid analysis

The maximum amount of TFA (~19.03% of DW) content was found from *E. gracilis* cells cultured in Treatment 5 (MCM, (-) N₂, (-) Ca²⁺, (+) Glucose (24 h Dark) conditions). TFA contents in Treatment 2 (MCM, (-) N₂) and Treatment 4 (MCM, (-) N₂, (-) Ca²⁺, (+) Glucose)

were almost similar; ~14.06% and ~14.5% of DW, respectively, which was also significantly ($P < 0.05$) higher compared to the control group (Treatment 1: MCM medium) that contained ~7.1% TFA of DW. However, the difference between Treatment 3 (MCM, (-) N_2 , (-) Ca^{2+}) and Treatment 1 was not significant (Fig. 2.20). The percentage FA of FAMES (Table 2.1) revealed a high content of saturated fatty acids (SAFAs: C14:0-C20:0) of ~27.98%, and long-chain polyunsaturated fatty acids (LC-PUFAs: C20-C22) of ~30.66% in Treatment 5, which was followed by the Treatment 4 with ~22.22% and ~23.22% of SAFAs and LC-PUFAs, respectively. The lowest amount of SAFAs and LC-PUFAs of ~14.88% and ~16.30%, respectively, was found in Treatment 1. Monounsaturated fatty acids (MUFAs: C14:1-C20:1) content was found almost similar in all the treatments. Among the polyunsaturated fatty acids (PUFAs), α -linolenic acid (ALA) and linoleic acid (LA) were the most abundant in Treatment 1, Treatment 2, Treatment 3 and Treatment 4, whereas supplementation of glucose in a dark condition reduced their biosynthesis compared to other treatments. Among the MUFAs and SAFAs, the most abundant in all the treatments were palmitoleic acid (16:1n-7) and palmitic acid (C16:0), the precursor to longer fatty acids. The maximum amount of omega-3 fatty acids eicosapentaenoic acid (EPA) and docosahexaenoic acid (DHA) occurred in Treatment 5.

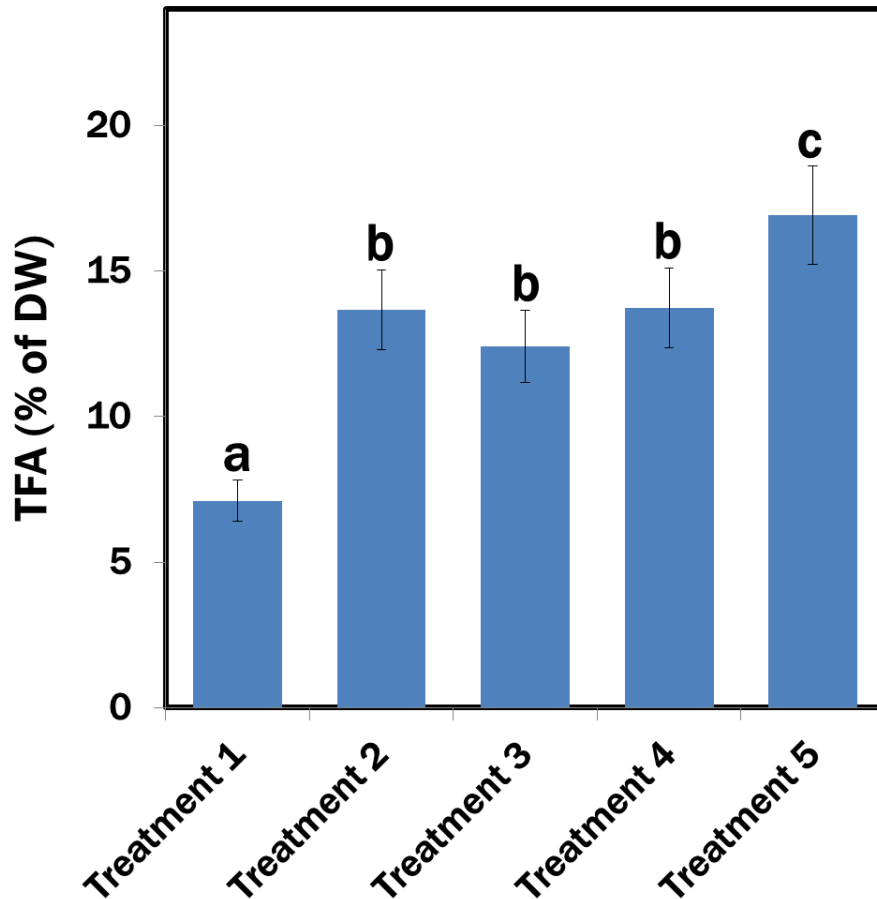


Fig. 2.20 TFA contents in different treatments. Treatment 1: modified Cramer-Myers medium (MCM); Treatment 2: MCM, (-) N₂; Treatment 3: MCM, (-) N₂, (-) Ca²⁺; Treatment 4: MCM, (-) N₂, (-) Ca²⁺, (+) Glucose (24 h light); and Treatment 5: MCM, (-) N₂, (-) Ca²⁺, (+) Glucose (24 h Dark) conditions. Data represented as mean ± SE, n = 3, Statistically significant (P < 0.05).

Table 2.1 Percentage of FAMES in *Euglena gracilis* cell cultured in different conditions.

Percentage of FAMES	Treatments				
	Treatment 1	Treatment 2	Treatment 3	Treatment 4	Treatment 5
C12:0	0.19±0.05	0.27±0.01	0.24±0.01	0.59±0.39	1.28±1.15
C13:0	0.28±0.01	0.37±0.03	0.36±0.08	1.36±1.19	3.63±2.78
C14:0	1.85±0.12	2.41±0.18	2.31±0.14	5.10±3.30	4.93±2.95
C15:0	0.44±0.26	0.64±0.41	0.63±0.31	1.07±0.97	1.27±0.93
C16:0	10.87±0.64	9.80±0.14	10.15±0.66	12.28±4.13	13.51±1.76
C16:1 N-7	15.18±2.33	13.94±0.54	13.87±1.06	11.19±0.82	12.85±0.38
C17:0	0.105±0.05	0.22±0.09	0.23±0.07	0.28±0.12	0.82±0.35
C17:1 N-7	4.38±0.24	4.03±0.58	4.01±0.60	3.33±1.11	4.15±3.06
C18:0	1.12±0.44	1.08±0.03	1.09±0.01	1.53±0.12	2.52±.09
C18:1T N-9	1.71±0.15	1.83±0.01	1.82±0.07	2.46±0.66	3.14±0.25
C18:2 TT N-6,9	22.48±1.55	23.18±4.06	22.52±3.97	20.63±7.51	13.68±7.59
C18:3 N-3,6,9 (ALA)	25.06±3.53	23.54±0.81	23.14±0.07	16.91±7.39	10.99±7.16
C20:2 N-6,9	1.92±1.20	2.76±0.56	2.89±0.55	3.92±1.80	4.26±1.92
C20:3 N-6,9,12	0.62±0.88	ND	1.08±0.01	0.93±0.14	0.45±0.18
C20:4 N-6,9,12,15	3.0±0.76	3.31±0.17	3.37±0.23	3.85±0.37	4.71±0.45
C20:3 N-3,6,9 (ETE)	1.38±0.10	1.92±0.02	1.9±0.08	2.23±0.21	3.59±2.93
C20:5 N-3,6,9,12,15 (EPA)	5.95±0.73	5.85±1.52	5.81±1.52	6.94±2.54	10.18±5.67
C22:1 N-9	0.65±0.30	1.58±0.66	0.91±0.15	1.41±0.25	2.01±0.71
C22:5 N-6, 9,12,15,18	0.99±0.81	0.99±0.71	1.36±0.29	1.49±0.18	2.18±0.34
C22:6 N-3,6,9,12,15,18 (DHA)	1.77±0.23	2.25±0.95	2.22±0.84	2.45±1.12	3.26±1.83
SAFAs	14.88±3.91	14.80±3.47	15.02±3.60	22.22±4.32	27.98±4.44
MUFAs	21.27±7.13	19.80±6.45	19.70±6.42	16.98±4.81	20.14±5.34
PUFAs	47.54±1.82	46.72±0.25	45.66±0.43	37.55±2.63	24.67±1.89

LC-PUFAs	16.30±1.76	18.68±1.75	19.56±1.61	23.22±1.96	30.66±2.90
----------	------------	------------	------------	------------	------------

*ND: Not detected

2.5 Discussion

Different nutrients, notably nitrogen, phosphorus, sulphur, potassium, and iron stressed conditions, have been studied for lipid production in different microalgal species (Zhu et al., 2016; Wang et al., 2018; Praveenkumar et al., 2012). The present study has checked the impact of the combination of nitrogen and calcium deprivation on lipid production alongside nitrogen stress. In addition, glucose was used in 24 h light and 24 h dark conditions as a supplementary carbon source. Interestingly, maximum lipid production was observed in the nitrogen and calcium-deprived, and glucose supplemented dark conditions.

During nitrogen starvation, biosynthesis of LDs occurs due to the increased TAG formation from acyl-CoA, recycling of acyl moieties from degraded membrane lipids products, and increased carbon flux towards the source compounds (e.g. glycerol-3-phosphate and acyl-CoA) for fatty acid synthesis (Miller et al., 2010; Goncalves et al. 2016; Fan et al., 2013; Fan et al., 2012). Supplementation of organic carbon like glucose to the nitrogen-starved growing media could alter the carbon fluxes towards the biosynthesis of necessary precursors of LDs, which are generally synthesized during photosynthesis using atmospheric carbon sources (CO₂) (Deng et al., 2013). The block of starch biosynthesis could effectively enhance TAG synthesis by diverting carbon flux (Work et al., 2010; Li et al., 2010). In the present study, the reduction of chlorophyll in dark conditions might reduce the starch biosynthesis in the chloroplast, and supplemented glucose supported the biosynthesis of glycerate 3-phosphate and glyceraldehyde 3-phosphate as the precursor molecules of pyruvate and acetyl-CoA through altered carbon flux and resulted in the increase of lipid production. In the nutrient-

starved light conditions, the blockage of the starch biosynthesis in the chlorophyll might not possibly happen, and in the glucose supplemented light condition, the availability of additional organic carbon might favour redirecting the carbon flux. However, starch biosynthesis still happens in the chloroplasts. Therefore, despite the accumulation of lipids, it did not reach the level at the dark condition.

Furthermore, a recent report on the model of photosynthetic organisms suggests that in the presence of light, chloroplasts take up Ca^{2+} from the cytosol and store it, while transitioning to dark conditions induces the chlorophyll to release the stored Ca^{2+} back into the cytosol (Sello et al., 2018). Additionally, during nitrogen starvation, carbon from the photosynthesis system channel into storage molecules, such as starch or lipids (Scott et al., 2010), which is supposed to require excess energy and adequate signalling functions. Generally, two photosystems, photosystem-I (PS-I) and photosystem-II (PS-II) are involved in achieving a linear electron flow (LEF) and cyclic electron flow (CEF) that create transmembrane proton (H^+) gradient and reduce power (NADPH), and consequently generate ATP (Takahashi et al., 2013; Alric et al., 2010). These ATPs are utilized in the Krebs cycle, glyoxylate cycle, and mitochondrion for respiratory oxidative phosphorylation. Furthermore, during the process of lipid biosynthesis under N deficiency, excess ATPs are also required by the system, whereby ATP production through CEF has been reported to be elevated to compensate for the reduction of ATP from PS II through LEF due to the limited CO_2 fixation activities (Zhang et al., 2014; Shikanai, 2007; Schmollinger et al., 2014). However, CEF is a Ca^{2+} -dependent process, responding appropriately through the combined acts of Ca^{2+} sensor calmodulin (CaM) and chloroplast-localized Ca^{2+} sensor (CAS) protein (Terashima et al., 2012; Chen et al., 2018; Chen et al., 2014).

The observed chlorophyll reduction in the present study in a dark condition could have resulted from the phosphorylation of the photosynthetic and thylakoid protein complexes that

could alter the proton (H^+) gradient and Ca^{2+} -buffering mechanism in the chloroplast (Stael et al., 2012; Fristedt et al., 2010; Fristedt et al., 2009), and subsequently increase Ca^{2+} concentration in the cytosol of *E. gracilis*. As a result, conceivably, the generated Ca^{2+} level in the dark condition was adequate to successfully run the cellular signalling for ATP production through CEF, which was definitely not the case for the calcium starved and light condition. As per the discussion above, a possible mechanistic pathway for the lipid accumulation in the nitrogen and calcium starved treatment or the glucose supplemented dark condition in *E. gracilis* cells has been proposed in Fig. 2.21.

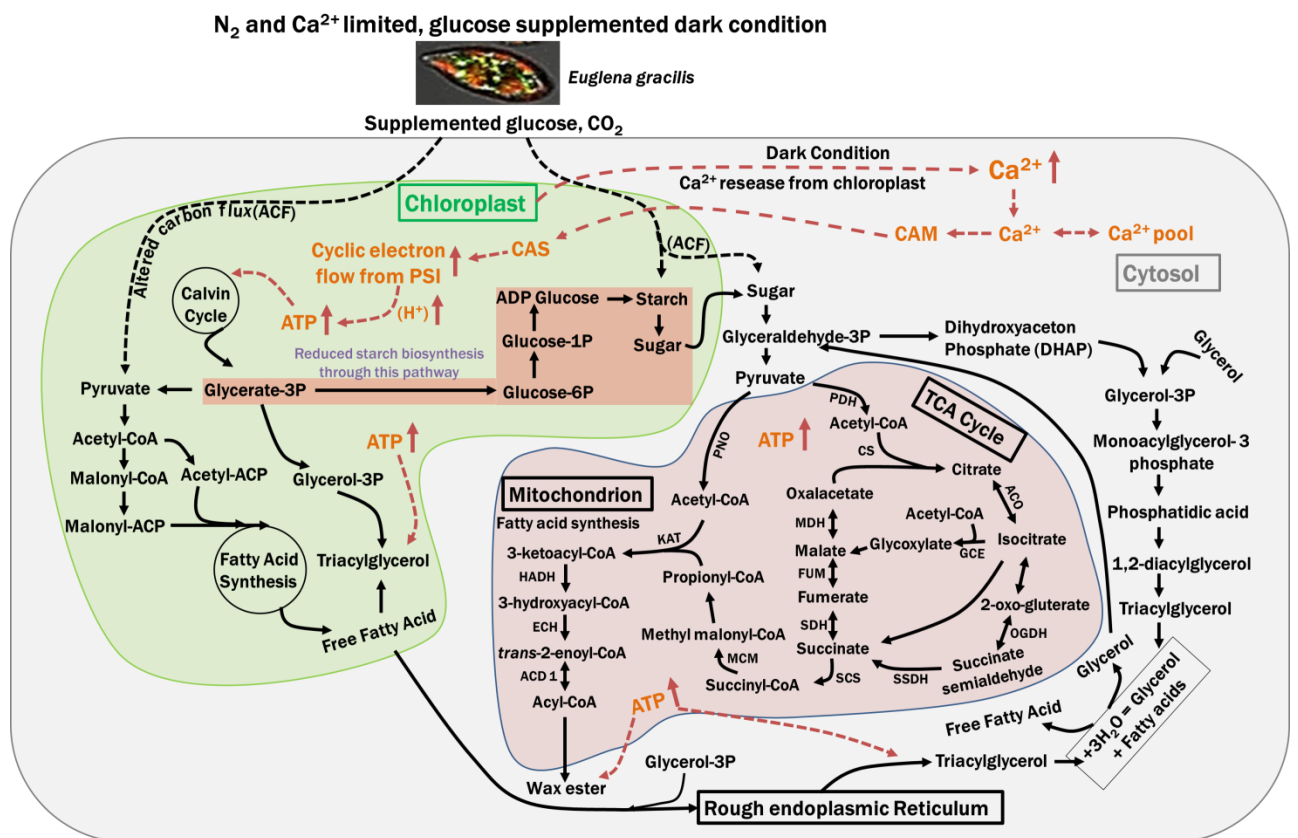


Fig. 2.21 Modified biochemical pathways (Tamaki et al., 2019; Alishah Aratboni et al., 2019) for LDs formation in the nitrogen and calcium deprived, glucose supplemented dark condition in the *Euglena gracilis* cells. PDH, pyruvate dehydrogenase; CS, citrate synthase;

ACO, aconitate hydratase; IDH, isocitrate dehydrogenase; OGDC, 2-oxoglutarate decarboxylase; SSDH, succinate-semialdehyde dehydrogenase; SDH, succinate dehydrogenase; FUM, fumarate hydratase; MDH, malate dehydrogenase; GCE, glyoxylate cycle enzyme; SCS, succinyl-CoA synthetase; MCM, methylmalonyl-CoA mutase; PCC, propionyl-CoA carboxylase; PNO, pyruvate: NADP⁺ oxidoreductase; KAT, 3-ketoacyl-CoA thiolase; HADH, 3-hydroxyacyl-CoA dehydrogenase; ECH, enoyl-CoA hydratase; TER, *trans*-2-enoyl-CoA reductase; ACD, acyl-CoA dehydrogenase. Broken black arrows indicate the altered carbon flux. Broken brown arrows indicate the Ca²⁺ dependent processes in dark condition. Upward brown arrows indicate the increasing amount of the respective components.

However, despite the reported facts of a positive correlation between carbon flux redirection and lipid biosynthesis, substantial differences have been found in lipid accumulation in the same condition, even for the same species, suggesting the complexities of controlling lipid biosynthesis mechanism (Siaut et al., 2011; Blaby et al., 2013). Therefore, a reliable and convenient tool is critical for easily detecting and visualizing LDs in algal culture.

This study used a novel and easy strategy to visualize LDs in *E. gracilis* by adopting a lipid-specific AIE fluorophore, DPAS. The emission of DPAS increased rapidly with the addition of water from 80% to 90% in DMSO due to the insoluble properties of AIE molecules and the formation of nanoaggregates in the aqueous media (Hong et al., 2009). However, fluorescent intensity was almost identical and stable for the samples after 2 h of staining, which is supported by the results of the previous study where DPAS is stable in continuous scanning with 2% laser power energy (Wang et al., 2016).

The results of the confocal microscopy and flow cytometry in the present study suggest well working condition of DPAS for lipid labelling in the *Euglena* cells that are similar to the

commercially available BODIPY™ 505/515 dye. However, given the priority of BODIPY in the visualization of LDs over other traditional lipid-specific probes (Govender et al., 2012; Fam et al., 2018), some studies suggest that inappropriate outcomes might result from disproportionate binding, unselective labelling of the mitochondrial, and background signals in plasma and nuclear membranes (Siegler et al., 2012; Daemen et al., 2015; Collot et al., 2018).

The hydrophobic nature of LDs and the absence of strong interactions with other organelles allow hydrophobic probes to accumulate in LDs. The specific structure with the partially negatively charged oxygen atoms attached to the electron acceptor in the carbonyl group can possibly make the lipid-specific AIE probes hydrophobic (Wang et al., 2014). Additionally, the cheap raw materials of DPAS synthesis fluorenone, benzophenone and salicylaldehyde are also hydrophobic to cause the hydrophobicity of DPAS. In addition, these materials allow this nanofluorophore to strongly target and interact with intercellular hydrophobic LDs (Wang et al., 2016).

The *E. gracilis* has a unique complex cell membrane structure composed of glucose, galactose, mannose, fucose, xylose, and rhamnose. Therefore, it appears that penetration of the AIE fluorophore, DPAS is not hindered by the cellular structure of this algal species. Once DPAS has been internalized by the cells, the restriction of the intramolecular motions and activation of the excited state intramolecular proton transfer (ESIPT) process can probably make the fluorescence turn on this AIE probe and let the LDs become visible (Peng et al., 2017). Furthermore, it is subtle that DPAS did not interfere with the red channel of chlorophyll autofluorescence or the green channel of BODIPY dye. Therefore, this lipid-specific AIE fluorophore might be an appropriate multicolour visualizing tool for microalgae.

This study also suggests a relatively easy application of DPAS compared to the BODIPY dye, since an extremely higher concentration of 100 μM DPAS did not negatively impact the growth, behaviour of *Euglena* cells and fluorescence intensity. The sample preparation was also relatively easy with fewer steps involved, which is time-efficient and less stressful for the living organism. This might allow studying other physiological factors within the cell in a natural condition. On the contrary, using commercial lipid-specific probes regardless of BODIPY and Nile Red requires extreme caution for dye adjustment since lower concentration can cause photobleaching problems and a slightly higher concentration or lower-level competencies during washing steps might result in severe background signals and ineffective lipid studies. Due to the AIE properties of DPAS, this dye is free from these limitations, and upon aggregation, the strong fluorescence of this probe clearly distinguishes LDs from the background. Moreover, a previous study by Wang et al. (2016) has already been approved that within 5 min of irradiation with 2% laser power energy under a confocal microscope, BODIPY could lose 90% of the fluorescence signals due to self-decomposition. In contrast, DPAS had almost no change in fluorescence intensity even after 60 min of continuous scanning with 2% laser power energy. This result is far better than any other commercially available lipid-specific fluorophores. Additionally, DPAS could label the lipid within 10 min in the organism, which suggests that this probe's flexible molecular structure might enable it to quickly adjust its conformation as per the penetration requirement of the *Euglena* cell membrane or transport receptor structures.

The fatty acid content and composition in algae depend on the species and cultivation conditions. In addition to being a great source of wax ester (C14:0), which is mainly a converted form of paramylon under hypoxic conditions, PUFAs obtained from *E. gracilis* also have good potential for biofuel production (Tomiya et al., 2017; Iwasaki et al., 2019, Alishah Aratboni et al., 2019). *E. gracilis* is also a producer of different biofunctional

components having several health benefits (Takaichi, 2011; Schwarzhans et al., 2015; Santek et al., 2009; Becker, 2007). However, since the composition of FAMES in microalgae could be affected by many factors, time point and cultural condition analysis is crucial to get desired biofunctional compounds from this organism (Liang et al., 2009; Heredia-Arroyo et al., 2010). Currently, most of the oils used for biodiesel mainly consist of C16 and C18 (Lin & Lin, 2012; Folayan et al., 2019; Durrett et al., 2008). In this study, the profile of fatty acids revealed a high content of SAFAs, and LC-PUFAs in Treatment 5 and Treatment 4 compared to Treatment 1. On the other hand, MUFAs content was almost similar in all the treatments. A higher amount of palmitoleic acid (16:1n-7) in all treatments and palmitic acid (C16:0) in Treatment 5 could be utilized as the biofuel stock, while the myristic acid (C14:0) from Treatment 4 and Treatment 5 could have the potential as drop-in jet fuel (Tomiyama et al., 2017). The extent of the unsaturation of PUFAs with more than four double bonds in all the treatments could be reduced by partial catalytic hydrogenation of the oil (Jang et al., 2005, Dijkstra, 2006; Chisti, 2007), and the fuel properties could further be improved by modifying the fatty ester composition for direct combustion in sensitive engines (Knothe, 2009).

In addition to biofuel production, microalgae are great sources of bioactive pharmaceutical and healthcare compounds with high commercial value (Gangl et al., 2015). In this study, all the conditions revealed a higher amount of α -linolenic acid, linoleic acid, palmitoleic acid, and palmitic acid. Much higher amount of LC-PUFAs, specifically DHA and EPA have been detected in treatment 5. These biofunctional components could have significant physiological and therapeutic functions for human well-being. Inverse correlations with obesity, diabetes and hepatosteatosis and consumption of palmitoleic acid have been reported in some studies (Tricò et al., 2020; Frigolet & Gutiérrez-Aguilar, 2017), while dietary supplementation of polyunsaturated omega-6 fatty acid, linoleic acid can also prevent hair loss and assist with wound healing properties (Silva et al., 2018; Guo and Katta, 2017). Moreover, the necessity

of α -linolenic acid as a dietary supplementation is crucial since it could improve the biosynthesis of beneficiary long-chain PUFAs as humans are unable to *de novo* synthesize α -linolenic acid from stearic acid due to the absence of the 12- and 15-desaturase enzymes (Burdge and Calder, 2005; Anderson and Ma, 2009). DHA can support multiplexed cell membrane and cell signalling, particularly in the brain and retina (Sun et al., 2018; Guesnet and Alessandri, 2011), while the EPA has an effective role in inflammation reduction (Koto et al., 2007). Both of these FAs also reduce bad cholesterol levels and improve cardiovascular functions (Asztalos et al., 2016). Since all these FAs were available in a larger proportion in all the treatments and DHA and EPA in Treatment 5, the present study results also suggest promising biofunctional compounds might be available from culturing *E. gracilis* in the applied conditions.

2.6 Conclusion

In this chapter, *E. gracilis* cultural condition has been reported, where the maximum total amount of SAFAs and MUFAs for biofuel production is available. At the same condition, the LC-PUFAs content was also found at the highest levels with many health beneficiary effects. An AIE bioprobe for rapid and easy detection of lipid drops in *E. gracilis* has also been introduced, which is cheap and convenient for high contrast visualization *in situ* conditions. The probe was biocompatible and easily penetrated the *Euglena* cells. The results enable the AIE probe DPAS to localize LDs accurately, similar to the traditional lipid-specific dye BODIPY. Additionally, due to the AIE attributes, DPAS is free of aggregation caused by quenching problems and background noises during imaging in confocal microscopy. Therefore, using this probe in lipid research of microalgae could ease the LDs-related studies and screen algae with high lipid content.

2.7 References

- Abramczyk, H., Surmacki, J., Kopeć, M., Olejnik, A. K., Lubecka-Pietruszewska, K. & Fabianowska-Majewska, K. (2015). The role of lipid droplets and adipocytes in cancer. Raman imaging of cell cultures: MCF10A, MCF7, and MDA-MB-231 compared to adipocytes in cancerous human breast tissue. *Analyst*, *140*(7), 2224-2235. <https://doi.org/10.1039/c4an01875c>
- Alishah Aratboni, H., Rafiei, N., Garcia-Granados, R., Alemzadeh, A., & Morones-Ramírez, J. R. (2019). Biomass and lipid induction strategies in microalgae for biofuel production and other applications. *Microbial Cell Factories*, *18*(1), 178. <https://doi.org/10.1186/s12934-019-1228-4>
- Alric, J., Lavergne, J., & Rappaport, F. (2010). Redox and ATP control of photosynthetic cyclic electron flow in *Chlamydomonas reinhardtii* (I) aerobic conditions. *Biochimica et Biophysica Acta*, *1797*(1), 44-51. <https://doi.org/10.1016/j.bbabi.2009.07.009>
- Asztalos, I. B., Gleason, J. A., Sever, S., Gedik, R., Asztalos, B. F., Horvath, K. V., Dansinger, M. L., Lamon-Fava, S., & Schaefer, E. J. (2016). Effects of eicosapentaenoic acid and docosahexaenoic acid on cardiovascular disease risk factors: a randomized clinical trial. *Metabolism: Clinical and Experimental*, *65*(11), 1636-1645. <https://doi.org/10.1016/j.metabol.2016.07.010>
- Anderson, B. M., & Ma, D. W. (2009). Are all n-3 polyunsaturated fatty acids created equal?. *Lipids in health and disease*, *8*, 33. <https://doi.org/10.1186/1476-511X-8-33>
- Bailey, R. (2019). "Euglena Cells." ThoughtCo, retrieved on 22 Jun, 2019, from <https://www.thoughtco.com/about-euglena-cells-4099133>.

Becker, E.W. (2007). Micro-algae as a source of protein. *Biotechnology Advances*, 25(2), 207-210. <https://doi.org/10.1016/j.biotechadv.2006.11.002>

Blaby, I. K., Glaesener, A. G., Mettler, T., Fitz-Gibbon, S. T., Gallaher, S. D., Liu, B., Boyle, N. R., Kropat, J., Stitt, M., Johnson, S., Benning, C., Pellegrini, M., Casero, D., & Merchant, S. S. (2013). Systems-level analysis of nitrogen starvation-induced modifications of carbon metabolism in a *Chlamydomonas reinhardtii* starchless mutant. *The Plant cell*, 25(11), 4305-4323. <https://doi.org/10.1105/tpc.113.117580>

Bligh, E. G., and Dyer, W. J. (1959). A rapid method of total lipid extraction and purification. *Canadian Journal of Biochemistry and Physiology*, 37, 911-917. <https://doi.org/10.1139/o59-099>

Brown, M. B., Miller, J. N. & Seare, N. J. (1995). An investigation of the use of Nile red as a long-wavelength fluorescent probe for the study of alpha 1-acid glycoprotein-drug interactions. *Journal of Pharmaceutical and Biomedical Analysis*, 13(8), 1011-7. [https://doi.org/10.1016/0731-7085\(95\)01524-O](https://doi.org/10.1016/0731-7085(95)01524-O)

Brown, W. J., Sullivan, T. R. & Greenspan, P. (1992). Nile red staining of lysosomal phospholipid inclusions. *Histochemistry*, 97(4), 349. <https://doi.org/10.1007/BF00270037>

Burdge, G. C., & Calder, P. C. (2005). Conversion of alpha-linolenic acid to longer-chain polyunsaturated fatty acids in human adults. *Reproduction, Nutrition, Development*, 45(5), 581-597. <https://doi.org/10.1051/rnd:2005047>

Chen, Z., Wang, L., Qiu, S., & Ge, S. (2018). Determination of Microalgal Lipid Content and Fatty Acid for Biofuel Production. *BioMed Research International*, Article ID 1503126, 17. <https://doi.org/10.1155/2018/1503126>

- Chen, H., Zhang, Y., He, C., & Wang, Q. (2014). Ca²⁺ signal transduction related to neutral lipid synthesis in an oil-producing green alga *Chlorella* sp. C2. *Plant and Cell Physiology*, 55(3), 634-44. <https://doi.org/10.1093/pcp/pcu015>
- Chen, W., Sommerfeld, M., & Hu, Q. (2011). Microwave-assisted Nile red method for in vivo quantification of neutral lipids in microalgae. *Bioresource Technology*, 102(1), 135-141. <https://doi.org/10.1016/j.biortech.2010.06.076>
- Chisti, Y. (2007). Biodiesel from microalgae. *Biotechnology Advances*, 25(3), 294-306. <https://doi.org/10.1016/j.biotechadv.2007.02.001>
- Collot, M., Fam, T. K., Ashokkumar, P., Faklaris, O., Galli, T., Danglot, L., & Klymchenko, A. S. (2018). Ultrabright and Fluorogenic Probes for Multicolor Imaging and Tracking of Lipid Droplets in Cells and Tissues. *Journal of the American Chemical Society*, 140(16), 5401-5411. <https://doi.org/10.1021/jacs.7b12817>
- Cooper, M. S., Hardin, W. R., Petersen, T. W., & Cattolico, R. A. (2010). Visualizing "green oil" in live algal cells. *Journal of Bioscience and Bioengineering*, 109(2), 198-201. <https://doi.org/10.1016/j.jbiosc.2009.08.004>
- Christie, W. W. (1993). "Preparation of ester derivatives of fatty acids for chromatographic analysis." *Advances in Lipid Methodology*, 2, 69, e111.
- Daemen, S., van Zandvoort, M. A. M. J., Parekh, S. H., & Hesselink, M. K. C. (2015). Microscopy tools for the investigation of intracellular lipid storage and dynamics. *Molecular Metabolism*, 5, 153-163. <https://doi.org/10.1016/j.molmet.2015.12.005>
- Deng, X., Cai, J., & Fei, X. (2013). Effect of the expression and knockdown of citrate synthase gene on carbon flux during triacylglycerol biosynthesis by green algae

Chlamydomonas reinhardtii. *BMC biochemistry*, 14, 38. <https://doi.org/10.1186/1471-2091-14-38>

Dijkstra, A.J. (2006). Revisiting the formation of trans isomers during partial hydrogenation of triacylglycerol oils. *European Journal of Lipid Science and Technology*, 108 (3), 249-264. <https://doi.org/10.1002/ejlt.200500335>

Domozych, D. S., Ciancia, M., Fangel, J. U., Mikkelsen, M. D., Ulvskov, P., & Willats, W. G. T. (2012). The cell walls of green algae: a journey through evolution and diversity. *Frontiers in Plant Science*, 3, 82. <https://doi.org/10.3389/fpls.2012.00082>

Durrett, T. P., Benning, C., & Ohlrogge, J. (2008). Plant triacylglycerols as feedstocks for the production of biofuels. *The Plant Journal: for Cell and Molecular Biology*, 54(4), 593-607. <https://doi.org/10.1111/j.1365-313X.2008.03442.x>

Elsay, D., Jameson, D., Raleigh, B., & Cooney, M. J. (2007). Fluorescent measurement of microalgal neutral lipids. *Journal of Microbiological Methods*, 68(3), 639-642. <https://doi.org/10.1016/j.mimet.2006.11.008>

Fam, T. K., Klymchenko, A. S., & Collot, M. (2018). Recent Advances in Fluorescent Probes for Lipid Droplets. *Materials (Basel)*, 11(9), pii: E1768. <https://doi.org/10.3390/ma11091768>

Fan, J., Yan, C., & Xu, C. (2013). Phospholipid:diacylglycerol acyltransferase-mediated triacylglycerol biosynthesis is crucial for protection against fatty acid-induced cell death in growing tissues of Arabidopsis. *The Plant Journal : for Cell and Molecular Biology*, 76(6), 930-942. <https://doi.org/10.1111/tpj.12343>

Fan, J., Yan, C., Andre, C., Shanklin, J., Schwender, J., & Xu, C. (2012). Oil accumulation is controlled by carbon precursor supply for fatty acid synthesis in *Chlamydomonas reinhardtii*. *Plant & Cell Physiology*, 53(8), 1380-1390. <https://doi.org/10.1093/pcp/pcs082>

- Fan, J., Andre, C., & Xu C. (2011). A chloroplast pathway for the de novo biosynthesis of triacylglycerol in *Chlamydomonas reinhardtii*. *FEBS Letters*, 585(12), 1985-1991. <https://doi.org/10.1016/j.febslet.2011.05.018>
- Folayan, A. J., Anawe, P. A. L., Aladejare, A. E., & Ayeni, A. O. (2019). Experimental investigation of the effect of fatty acids configuration, chain length, branching and degree of unsaturation on biodiesel fuel properties obtained from lauric oils, high-oleic and high-linoleic vegetable oil biomass. *Energy Reports*, 5, 793-806. <https://doi.org/10.1016/j.egy.2019.06.013>.
- Friegolet, M. E., & Gutiérrez-Aguilar, R. (2017). The role of the novel lipokine palmitoleic acid in health and disease. *Advances in Nutrition (Bethesda, Md.)*, 8(1), 173S-181S. <https://doi.org/10.3945/an.115.011130>
- Fristedt, R., Granath, P., & Vener, A. V. (2010). A protein phosphorylation threshold for functional stacking of plant photosynthetic membranes. *PloS One*, 5(6), e10963. <https://doi.org/10.1371/journal.pone.0010963>
- Fristedt, R., Willig, A., Granath, P., Crèvecoeur, M., Rochaix, J. D., & Vener, A. V. (2009). Phosphorylation of photosystem II controls functional macroscopic folding of photosynthetic membranes in *Arabidopsis*. *The Plant Cell*, 21(12), 3950-3964. <https://doi.org/10.1105/tpc.109.069435>
- Fuchs, B., Süß, R., Teubera, K., Eibisch, M. & Schiller, J. (2011). Lipid analysis by thin-layer chromatography—A review of the current state. *Journal of Chromatography A*, 1218(19), 2754-2774. <https://doi.org/10.1016/j.chroma.2010.11.066>

Fujita, A., Cheng, J. & Fujimoto, T. (2010). Quantitative electron microscopy for the nanoscale analysis of membrane lipid distribution. *Nature Protocols*, 5(4), 661-9. <https://doi.org/10.1038/nprot.2010.20>

Galasso, C., Gentile, A., Orefice, I., Ianora, A., Bruno, A., Noonan, D. M., Sansone, C., Albini, A., & Brunet, C. (2019). Microalgal derivatives as potential nutraceutical and food supplements for human health: A focus on cancer prevention and interception. *Nutrients*, 11(6), 1226. <https://doi.org/10.3390/nu11061226>

Gangl, D., Zedler, J. A., Rajakumar, P. D., Martinez, E. M., Riseley, A., Włodarczyk, A., Purton, S., Sakuragi, Y., Howe, C. J., Jensen, P. E., & Robinson, C. (2015). Biotechnological exploitation of microalgae. *Journal of Experimental Botany*, 66(22), 6975-6990. <https://doi.org/10.1093/jxb/erv426>

Gissibl, A., Sun, A., Care, A., Nevalainen, H., & Sunna, A. (2019). Bioproducts From *Euglena gracilis*: Synthesis and Applications. *Frontiers in Bioengineering and Biotechnology*, 7, 108. <https://doi.org/10.3389/fbioe.2019.00108>

Goncalves, E. C., Wilkie, A. C., Kirst, M., & Rathinasabapathi, B. (2016). Metabolic regulation of triacylglycerol accumulation in the green algae: identification of potential targets for engineering to improve oil yield. *Plant Biotechnology Journal*, 14(8), 1649-60. <https://doi.org/10.1111/pbi.12523>

Goodenough, U., Blaby, I., Casero, D., Gallaher, S. D., Goodson, C., Johnson, S., Lee, J. H., Merchant, S. S., Pellegrini, M., Roth, R., Rusch, J., Singh, M., Umen, J. G., Weiss, T. L., & Wulan, T. (2014). The path to triacylglyceride obesity in the sta6 strain of *Chlamydomonas reinhardtii*. *Eukaryotic Cell*, 13(5), 591-613. <https://doi.org/10.1128/EC.00013-14>

- Govender, T., Ramanna, L., Rawat, I., & Bux, F. (2012). BODIPY staining, an alternative to the Nile Red fluorescence method for the evaluation of intracellular lipids in microalgae. *Bioresource Technology*, *114*, 507-511. <https://doi.org/10.1016/j.biortech.2012.03.024>
- Greenspan, P., Mayer, E. P. & Fowler, S. D. (1985). Nile Red: A Selective Fluorescent Stain for Intracellular Lipid Droplets. *The Journal of Cell Biology*, *100*(3), 965-973. <https://doi.org/10.1083/jcb.100.3.965>
- Grimm, P., Risse, J.M., Cholewa, D., Müller, J.M., Beshay, U., Friehs K, Flaschel, E. (2015). Applicability of *Euglena gracilis* for biorefineries demonstrated by the production of α -tocopherol and paramylon followed by anaerobic digestion. *Journal of Biotechnology*, *215*, 72-79. <https://doi.org/10.1016/j.jbiotec.2015.04.004>
- Guesnet, P., & Alessandri, J. M. (2011). Docosahexaenoic acid (DHA) and the developing central nervous system (CNS) - Implications for dietary recommendations. *Biochimie*, *93*(1), 7-12. <https://doi.org/10.1016/j.biochi.2010.05.005>
- Guo, E. L., & Katta, R. (2017). Diet and hair loss: effects of nutrient deficiency and supplement use. *Dermatology Practical & Conceptual*, *7*(1), 1-10. <https://doi.org/10.5826/dpc.0701a01>
- Heredia-Arroyo, T., Wei, W., & Hu, B. (2010). Oil accumulation via heterotrophic/mixotrophic *Chlorella protothecoides*. *Applied Biochemistry and Biotechnology*, *162*(7), 1978-1995. <https://doi.org/10.1007/s12010-010-8974-4>
- Horn, P. J., Ledbetter, N. R., James, C. N., Hoffman, W. D., Case, C. R., Verbeck, G. F. & Chapman, K. D. (2011). Visualization of lipid droplet composition by direct organelle mass

spectrometry. *Journal of Biological Chemistry*, 286(5), 3298-3306.
<https://doi.org/10.1074/jbc.M110.186353>

Hu, Q., Sommerfeld, M., Jarvis, E., Ghirardi, M., Posewitz, M., Seibert, M., & Darzins, A. (2008). Microalgal triacylglycerols as feedstocks for biofuel production: perspectives and advances. *The Plant Journal*, 54(4), 621-639. <https://doi.org/10.1111/j.1365-313X.2008.03492.x>

Ishihara, M., Kujiraoka, T., Iwasaki, T., Nagano, M., Takano, M., Ishii, J., Tsuji, M., Ide, H., Miller, I. P., Miller, N. E. & Hattori, H. (2005). A sandwich enzyme-linked immunosorbent assay for human plasma apolipoprotein A-V concentration. *The Journal of Lipid Research*, 46(9), 2015-22. <https://doi.org/10.1194/jlr.D500018-JLR200>

Iwasaki, K., Kaneko, A., Tanaka, Y., Ishikawa, T., Noothalapati, H., & Yamamoto, T. (2019). Visualizing wax ester fermentation in single *Euglena gracilis* cells by Raman microspectroscopy and multivariate curve resolution analysis. *Biotechnology for Biofuels*, 12, 128. <https://doi.org/10.1186/s13068-019-1471-2>

Jaeger, D., Pilger, C., Hachmeister, H., Oberländer, E., Wördenweber, R., Wichmann, J., Mussnug, J. H., Huser, T. & Kruse, O. (2016). Label-free in vivo analysis of intracellular lipid droplets in the oleaginous microalga *Monoraphidium neglectum* by coherent Raman scattering microscopy. *Scientific Reports*, 6, 35340. <https://doi.org/10.1038/srep35340>

Jang, E. S., Jung, M. Y., & Min, D. B. (2005). Hydrogenation for Low Trans and High Conjugated Fatty Acids. *Comprehensive Reviews in Food Science and Food Safety*, 4, 22-30. <https://doi.org/10.1111/j.1541-4337.2005.tb00069.x>

- Janssen, J. H., Wijffels, R. H., & Barbosa, M. J. (2019). Lipid production in *Nannochloropsis gaditana* during nitrogen starvation. *Biology (Basel)*, 8(1), pii: E5. <https://doi.org/10.3390/biology8010005>
- Jones, C. S., & Mayfield, S. P. (2012). Algae biofuels: versatility for the future of bioenergy. *Current Opinion in Biotechnology*, 23(3), 346-351. <https://doi.org/10.1016/j.copbio.2011.10.013>
- Khozin-Goldberg, I., Iskandarov, U., & Cohen, Z. (2011). LC-PUFA from photosynthetic microalgae: occurrence, biosynthesis, and prospects in biotechnology. *Applied Microbiology and Biotechnology*, 91(4), 905-915. <https://doi.org/10.1007/s00253-011-3441-x>
- Knothe, G. (2009). Improving biodiesel fuel properties by modifying fatty ester composition. *Energy & Environmental Science*, 2(7), 759-766. <https://doi.org/10.1039/B903941D>
- Koreivienė, J. (2017). Microalgae lipid staining with fluorescent BODIPY dye. SpringerLink, Humana Press; New York City, NY, USA, *Methods in Molecular Biology*, 1-7.
- Koto, T., Nagai, N., Mochimaru, H., Kurihara, T., Izumi-Nagai, K., Satofuka, S., Shinoda, H., Noda, K., Ozawa, Y., Inoue, M., Tsubota, K., Oike, Y., & Ishida, S. (2007). Eicosapentaenoic acid is anti-inflammatory in preventing choroidal neovascularization in mice. *Investigative Ophthalmology & Visual Science*, 48(9), 4328-4334. <https://doi.org/10.1167/iovs.06-1148>
- Li, J., Vosegaard, T. & Guo, Z. (2017). Applications of nuclear magnetic resonance in lipid analyses: An emerging powerful tool for lipidomics studies. *Progress in Lipid Research*, 68, 37-56. <https://doi.org/10.1016/j.plipres.2017.09.003>

- Li, L., Han, J., Wang, Z., Liu, J., Wei, J., Xiong, S. & Zhao, Z. (2014). Mass spectrometry methodology in lipid analysis. *International Journal of Molecular Sciences*, *15*(6), 10492-507. <https://doi.org/10.3390/ijms150610492>
- Li, H. Y., Lu, Y., Zheng, J. W., Yang, W. D., & Liu, J. S. (2014). Biochemical and genetic engineering of diatoms for polyunsaturated fatty acid biosynthesis. *Marine Drugs*, *12*(1), 153-166. <https://doi.org/10.3390/md12010153>
- Li, Y., Han, D., Hu, G., Dauvillee, D., Sommerfeld, M., Ball, S., & Hu, Q. (2010). *Chlamydomonas* starchless mutant defective in ADP-glucose pyrophosphorylase hyperaccumulates triacylglycerol. *Metabolic Engineering*, *12*(4), 387-391. <https://doi.org/10.1016/j.ymben.2010.02.002>
- Liang, Y., Sarkany, N., & Cui, Y. (2009). Biomass and lipid productivities of *Chlorella vulgaris* under autotrophic, heterotrophic and mixotrophic growth conditions. *Biotechnology Letters*, *31*(7), 1043-1049. <https://doi.org/10.1007/s10529-009-9975-7>
- Lin, C.Y., & Lin, Y.W. (2012). Fuel characteristics of biodiesel produced from a high-acid oil from soybean soapstock by supercritical-methanol transesterification. *Energies*, *5*, 2370-2380. <https://doi.org/10.3390/en5072370>
- Luo, X., Su, P., Zhang, W. (2015). Advances in microalgae-derived phytosterols for functional food and pharmaceutical applications. *Marine Drugs*, *13*, 4231-4254. <https://doi.org/10.3390/md13074231>
- Miller, R., Wu, G., Deshpande, R. R., Vieler, A., Gartner, K., Li, X., Moellering, E. R., Zäuner, S., Cornish, A.J., Liu, B., Bullard, B., Sears, B. B., Kuo, M. H., Hegg, E. L., Shachar-Hill, Y., Shiu, S. H., & Benning, C. (2010). Changes in transcript abundance

in *Chlamydomonas reinhardtii* following nitrogen deprivation predict diversion of metabolism. *Plant Physiology*, 154(4), 1737-1752. [https://doi.org/ 10.1104/pp.110.165159](https://doi.org/10.1104/pp.110.165159)

Mutanda, T., Ramesh, D., Karthikeyan, S., Kumari, S., Anandraj, A., & Bux, F. (2011). Bioprospecting for hyper-lipid producing microalgal strains for sustainable biofuel production. *Bioresource technology*, 102(1), 57-70. [https://doi.org/ 10.1016/j.biortech.2010.06.077](https://doi.org/10.1016/j.biortech.2010.06.077)

Nygren, H., Seppänen-Laakso, T. & Rischer, H. (2017). Liquid chromatography-mass spectrometry (LC-MS)-based analysis of molecular lipids in algae samples. *In: Methods in Molecular Biology. Humana Press*, 1-8. [https://doi.org/ 10.1007/7651_2017_108](https://doi.org/10.1007/7651_2017_108)

O'Neill, E. C., Kuhadomlarp, S., Rejzek, M., Fangel, J. U., Alagesan, K., Kolarich, D., Willats, W. G. T., & Field, R. A. (2017). Exploring the glycans of *Euglena gracilis*. *Biology (Basel)*, 6(4), pii: E45. [https://doi.org/ 10.3390/biology6040045](https://doi.org/10.3390/biology6040045)

O'Neill, E. C., Trick, M., Hill, L., Rejzek, M., Dusi, R. G., Hamilton, C. J., Zimba, P. V., Henrissat, B., & Field, R. A. (2015). The transcriptome of *Euglena gracilis* reveals unexpected metabolic capabilities for carbohydrate and natural product biochemistry. *Molecular BioSystems*, 11(10), 2808-2820. [https://doi.org/ 10.1039/c5mb00319a](https://doi.org/10.1039/c5mb00319a)

Peng, H., He, L. & Haritos, V.S. (2019). Flow-cytometry-based physiological characterisation and transcriptome analyses reveal a mechanism for reduced cell viability in yeast engineered for increased lipid content. *Biotechnol Biofuels*, 12, 98. [https://doi.org/ 10.1186/s13068-019-1435-6](https://doi.org/10.1186/s13068-019-1435-6)

Peng, L., Xu, S., Zheng, X., Cheng, X., Zhang, R., Liu, J., Liu, B., & Tong, A. (2017). Author information rational design of a red-emissive fluorophore with AIE and ESIPT

characteristics and its application in light-up sensing of esterase. *Analytical Chemistry*, 89(5), 3162-3168. [https://doi.org/ 10.1021/acs.analchem.6b04974](https://doi.org/10.1021/acs.analchem.6b04974).

Pick, U. & Rachutin-Zalagin, T. (2012). Kinetic anomalies in the interactions of Nile red with microalgae. *Journal of Microbiological Methods*, 88(2), 189-96. [https://doi.org/ 10.1016/j.mimet.2011.10.008](https://doi.org/10.1016/j.mimet.2011.10.008)

Praveenkumar, R., Shameera, K., Mahalakshmi, G., Akbarsha, M.A., & Thajuddin, N. (2012). Influence of nutrient deprivations on lipid accumulation in a dominant indigenous microalga *Chlorella* sp. *Biomass and Bioenergy*, 37, 60-66. <https://doi.org/10.1016/j.biombioe.2011.12.035>

Reza, A.H.M.M., Tavakoli, J., Zhou, Y., Qin, J., & Tang, Y. (2020). Synthetic fluorescent probes to apprehend calcium signalling in lipid droplet accumulation in microalgae—an updated review. *SCIENCE CHINA Chemistry*, 63. [https://doi.org/ 10.1007/s11426-019-9664-7](https://doi.org/10.1007/s11426-019-9664-7)

Rimm, E. B., Appel, L. J., Chiuve, S. E., Djoussé, L., Engler, M. B., Kris-Etherton, P. M., Mozaffarian, D., Siscovick, D. S., Lichtenstein, A. H. and American Heart Association Nutrition Committee of the Council on Lifestyle and Cardiometabolic Health, Council on Epidemiology and Prevention, Council on Cardiovascular Disease in the Young, Council on Cardiovascular and Stroke Nursing; and Council on Clinical Cardiology (2018). Seafood long-chain n-3 polyunsaturated fatty acids and cardiovascular disease: A science advisory from the American Heart Association, *Circulation*, 138, e35-e47. <https://doi.org/10.1161/CIR.0000000000000574>

Rodríguez-Zavala, J. S., Ortiz-Cruz, M. A., Mendoza-Hernández, G., Moreno-Sánchez, R. (2010). Increased synthesis of α -tocopherol, paramylon and tyrosine by *Euglena gracilis*

under conditions of high biomass production. *Journal of Applied Microbiology*, 109(6):2160-2172. <https://doi.org/10.1111/j.1365-2672.2010.04848.x>

Rumin, J., Bonnefond, H., Saint-Jean, B., Rouxel, C., Sciandra, A., Bernard, O., Cadoret, J. P., & Bougaran, G. (2015). The use of fluorescent Nile red and BODIPY for lipid measurement in microalgae. *Biotechnology for Biofuels*, 8, 42. <https://doi.org/10.1186/s13068-015-0220-4>

Santek, B., Felski, M., Friehs, K., Lotz, M., & Flaschel, E. (2009). Production of paramylon, a β -1,3-glucan, by heterotrophic cultivation of *Euglena gracilis* on a synthetic medium. *Engineering in Life Sciences*, 9(1):23-28. <https://doi.org/10.1002/elsc.200700032>

Schmollinger, S., Mühlhaus, T., Boyle, N. R., Blaby, I. K., Casero, D., Mettler, T., Moseley, J. L., Kropat, J., Sommer, F., Strenkert, D., Hemme, D., Pellegrini, M., Grossman, A. R., Stitt, M., Schroda, M., & Merchant, S. S. (2014). Nitrogen-sparing mechanisms in *Chlamydomonas* affect the transcriptome, the proteome, and photosynthetic metabolism. *The Plant cell*, 26(4), 1410-1435. <https://doi.org/10.1105/tpc.113.122523>

Schwarzahns, J.P., Cholewa, D., Grimm, P., Beshay, U., Risse, J.M., Friehs, K., & Flaschel, E. (2015). Dependency of the fatty acid composition of *Euglena gracilis* on growth phase and culture conditions. *Journal of Applied Phycology*, 27(4):1389-1399. <https://doi.org/10.1007/s10811-014-0458-4>

Scott, S. A., Davey, M. P., Dennis, J. S., Horst, I., Howe, C. J., Lea-Smith, D. J., & Smith, A. G. (2010). Biodiesel from algae: challenges and prospects. *Current Opinion in Biotechnology*. 21(3), 277-86. <https://doi.org/10.1016/j.copbio.2010.03.005>

- Shibata, S., Arimura, S. I., Ishikawa, T., & Awai, K. (2018). Alterations of membrane lipid content correlated with chloroplast and mitochondria development in *Euglena gracilis*. *Frontiers in Plant Science*, *9*, 370. <https://doi.org/10.3389/fpls.2018.00370>
- Shikanai, T. (2007). Cyclic electron transport around photosystem I: genetic approaches. *Annual Review of Plant Biology*, *58*, 199-217. <https://doi.org/10.1146/annurev.arplant.58.091406.110525>
- Sello, S., Moscatiello, R., Mehlmer, N., Leonardelli, M., Carraretto, L., Cortese, E., Zanella, F. G., Baldan, B., Szabò, I., Vothknecht, U. C., & Navazio, L. (2018). Chloroplast Ca²⁺ fluxes into and across thylakoids revealed by thylakoid-targeted aequorin Probes. *Plant Physiology*, *177*(1), 38-51. <https://doi.org/10.1104/pp.18.00027>
- Siaut, M., Cuiné, S., Cagnon, C., Fessler, B., Nguyen, M., Carrier, P., Beyly, A., Beisson, F., Triantaphylidès, C., Li-Beisson, Y., & Peltier, G. (2011). Oil accumulation in the model green alga *Chlamydomonas reinhardtii*: characterization, variability between common laboratory strains and relationship with starch reserves. *BMC Biotechnology*, *11*, 7. <https://doi.org/10.1186/1472-6750-11-7>
- Siegler, H.D., Ayidzoe, W., Ben-Zvi, A., Burrell, R.E., & McCaffrey, W.C. (2012). Improving the reliability of fluorescence-based neutral lipid content measurements in microalgal cultures. *Algal Research*, *1*(2), 176-184. <https://doi.org/10.1016/j.algal.2012.07.004>
- Silva, J. R., Burger, B., Kühn, C., Candreva, T., Dos Anjos, M., & Rodrigues, H. G. (2018). Wound healing and omega-6 fatty acids: From inflammation to repair. *Mediators of Inflammation*, *2018*, 2503950. <https://doi.org/10.1155/2018/2503950>

Singh, A. P., & Olsen, S. I. (2011). A critical review of biochemical conversion, sustainability and life cycle assessment of algal biofuels, *Applied Energy*, 88, 3548-3555. <https://doi.org/10.1016/j.apenergy.2010.12.012>

Spandl, J., White, D. J., Peychl, J. & Thiele, C. (2009). Live cell multicolor imaging of lipid droplets with a new dye, LD540. *Traffic*, 10(11), 1579-1584. <https://doi.org/10.1111/j.1600-0854.2009.00980.x>

Spangenburg, E. E., Pratt, S. J., Wohlers, L. M. & Lovering, R. M. (2011). Use of BODIPY (493/503) to visualize intramuscular lipid droplets in skeletal muscle. *Journal of Biomedicine and Biotechnology*, Article ID 598358, 8. <https://doi.org/10.1155/2011/598358>

Stael, S., Wurzinger, B., Mair, A., Mehlmer, N., Vothknecht, U. C., & Teige, M. (2012). Plant organellar calcium signalling: an emerging field. *Journal of Experimental Botany*, 63(4), 1525-1542. <https://doi.org/10.1093/jxb/err394>

Sun, G. Y., Simonyi, A., Fritsche, K. L., Chuang, D. Y., Hannink, M., Gu, Z., Greenlief, C. M., Yao, J. K., Lee, J. C., & Beversdorf, D. Q. (2018). Docosahexaenoic acid (DHA): An essential nutrient and a nutraceutical for brain health and diseases. *Prostaglandins, Leukotrienes, and Essential Fatty Acids*, 136, 3-13. <https://doi.org/10.1016/j.plefa.2017.03.006>

Sun, X. M., Ren, L. J., Zhao, Q. Y., Ji, X. J., & Huang, H. (2018). Microalgae for the production of lipid and carotenoids: a review with focus on stress regulation and adaptation. *Biotechnology for Biofuels*, 11, 272. <https://doi.org/10.1186/s13068-018-1275-9>

Takahashi, H., Clowez, S., Wollman, F. A., Vallon, O., & Rappaport, F. (2013). Cyclic electron flow is redox-controlled but independent of state transition. *Nature Communications*, 4, 1954. <https://doi.org/10.1038/ncomms2954>

Takaichi, S. (2011). Carotenoids in algae: Distributions, biosyntheses and functions. *Marine Drugs*, *9*, 1101-1118. <https://doi.org/10.3390/md9061101>

Tamaki, S., Nishino, K., Ogawa, T., Maruta, T., Sawa, Y., Arakawa, K., & Ishikawa, T. (2019). Comparative proteomic analysis of mitochondria isolated from *Euglena gracilis* under aerobic and hypoxic conditions. *PLoS One*, *14*(12), e0227226. <https://doi.org/10.1371/journal.pone.0227226>

Thermo Fisher Scientific BODIPY 505/515. (accessed on 08 July 2019), Available from: <https://www.thermofisher.com/order/catalog/product/D3921>.

Thermo Fisher Scientific BODIPY 493/503. (accessed on 08 July 2019), Available from: <https://www.thermofisher.com/order/catalog/product/D3922>.

Terashima, M., Petroustos, D., Hüdig, M., Tolstygina, I., Trompelt, K., Gäbelein, P., Fufezan, C., Kudla, J., Weinl, S., Finazzi, G., & Hippler, M. (2012). Calcium-dependent regulation of cyclic photosynthetic electron transfer by a CAS, ANR1, and PGRL1 complex. *Proceedings of the National Academy of Sciences of the United States of America*, *109*(43), 17717-17722. <https://doi.org/10.1073/pnas.1207118109>

Tomiyama, T., Goto, K., Tanaka, Y., Maruta, T., Ogawa, T., Sawa, Y., Ito, T., & Ishikawa, T. (2019). A major isoform of mitochondrial trans-2-enoyl-CoA reductase is dispensable for wax ester production in *Euglena gracilis* under anaerobic conditions. *PLoS One*, *14*(1), e0210755. <https://doi.org/10.1371/journal.pone.0210755>

Tomiyama, T., Kurihara, K., Ogawa, T., Maruta, T., Ogawa, T., Ohta, D., Sawa, Y., & Ishikawa, T. (2017). Wax ester synthase/diacylglycerol acyltransferase isoenzymes play a pivotal role in wax ester biosynthesis in *Euglena gracilis*. *Scientific Reports*, *7*, 13504. <https://doi.org/10.1038/s41598-017-14077-6>

Tossavainen, M., Ilyass, U., Ollilainen, V., Valkonen, K., Ojala, A., & Romantschuk, M. (2019). Influence of long term nitrogen limitation on lipid, protein and pigment production of *Euglena gracilis* in photoheterotrophic cultures. *PeerJ*, 7, e6624. <https://doi.org/10.7717/peerj.6624>

Tricò, D., Mengozzi, A., Nesti, L., Hatunic, M., Gabriel Sanchez, R., Konrad, T., Lalić, K., Lalić, N. M., Mari, A., Natali, A., & EGIR-RISC Study Group (2020). Circulating palmitoleic acid is an independent determinant of insulin sensitivity, beta cell function and glucose tolerance in non-diabetic individuals: a longitudinal analysis. *Diabetologia*, 63(1), 206-218. <https://doi.org/10.1007/s00125-019-05013-6>

Venegas-Calcrón, M., Sayanova, O., Napier, J. A. (2010). An alternative to fish oils: Metabolic engineering of oil-seed crops to produce omega-3 long chain polyunsaturated fatty acids, *Progress in Lipid Research*, 49, 108-119. <https://doi.org/10.1016/j.plipres.2009.10.001>

Volin, P. (2001). Analysis of steroidal lipids by gas and liquid chromatography. *Journal of Chromatography A*, 935(1-2), 125-140. [https://doi.org/10.1016/s0021-9673\(01\)01089-5](https://doi.org/10.1016/s0021-9673(01)01089-5)

Wang, Z., Yang, L., Liu, Y., Huang, X., Qiao, F., Qin, W., Hu, Q., & Tang, B. Z. (2017). Ultra long-term cellular tracing by a fluorescent AIE bioconjugate with good water solubility over a wide pH range. *Journal of Materials Chemistry B*, 5(25), 4981-4987. <https://doi.org/10.1039/C7TB00861A>

Wang, Z., Gui, C., Zhao, E., Wang, J., Li, X., Qin, A., Zhao, Z., Yu, Z., & Tang, B. Z. (2016). Specific fluorescence probes for lipid droplets based on simple AIEgens. *ACS Applied Materials & Interfaces*, 8(16), 10193-10200. <https://doi.org/10.1021/acsami.6b01282>

Wang, E., Zhao, E., Hong, Y., Lam, J. W. Y., & Tang, B. Z. (2014). A highly selective AIE fluorogen for lipid droplet imaging in live cells and green algae. *Journal of Materials Chemistry B*, 2, 2013-2019. <https://doi.org/10.1039/C3TB21675F>

Wang, Z. T., Ullrich, N., Joo, S., Waffenschmidt, S., & Goodenough, U. (2009). Algal lipid bodies: stress induction, purification, and biochemical characterization in wild-type and starchless *Chlamydomonas reinhardtii*. *Eukaryotic Cell*, 8(12), 1856-1868. <https://doi.org/10.1128/EC.00272-09>

Woloski, K. (2002). "Phylum Euglenophyta". In John, David M.; Whitton, Brian A.; Brook, Alan J. (eds.). *The freshwater algal flora of the British Isles: an identification guide to freshwater and terrestrial algae*. p. 144.

Work, V. H., Radakovits, R., Jinkerson, R. E., Meuser, J. E., Elliott, L. G., Vinyard, D. J., Laurens, L. M., Dismukes, G. C., & Posewitz, M. C. (2010). Increased lipid accumulation in the *Chlamydomonas reinhardtii* sta7-10 starchless isoamylase mutant and increased carbohydrate synthesis in complemented strains. *Eukaryotic Cell*, 9(8), 1251-1261. <https://doi.org/10.1128/EC.00075-10>

World Population Prospects 2019, <https://population.un.org/wpp/Graphs/Probabilistic/POP/TOT/900>, (accessed August 2020).

Wu, S., Zhang, B., Huang, A., Huan, L., He, L., Lin, A., Niu, J., & Wang, G. (2014). Detection of intracellular neutral lipid content in the marine microalgae *Prorocentrum micans* and *Phaeodactylum tricornutum* using Nile red and BODIPY 505/515. *Journal of Applied Psychology*, 26, 1659-1668. <https://doi.org/10.1007/s10811-013-0223-0>

- Wu, Y., & Qu, J. Y. (2006). Autofluorescence spectroscopy of epithelial tissues. *Journal of Biomedical Optics*, *11*(5), 054023. <https://doi.org/10.1117/1.2362741>
- Yanowitz, J., Ratcliff, M. A., McCormick, R. L., Taylor, J. D., & Murphy, M. J. (2014). Compendium of experimental cetane numbers. In: Technical Repot. *National Renewable Energy Laboratory*. Available from: <http://www.nrel.gov/docs/fy14osti/61693.pdf>
- Yu, S. J., Kang, M. W., Chang, H. C., Chen, K. M., Yu, Y. C. (2005). Bright fluorescent nanodiamonds: No photobleaching and low cytotoxicity. *Journal of the American Chemical Society*, *127*, 17604–17605. <https://doi.org/10.1021/ja0567081>
- Zhang, X. Rong, J., Chen, H., He, C., & Wang, Q. (2014). Current status and outlook in the application of microalgae in biodiesel production and environmental protection. *Frontiers in Energy Research*, <https://doi.org/10.3389/fenrg.2014.00032>.
- Zhu, J. K. (2016). Abiotic stress signaling and responses in plants. *Cell*, *167*(2), 313-324. <https://doi.org/10.1016/j.cell.2016.08.029>

**Chapter 3: Stress-Induced Lipid Droplet Conditions with
Aggregation Induced Emission Fluorophores in a
Flagellate Microalga *Chlamydomonas reinhardtii* with
Carbohydrate Cell Walls**

3.1 Abstract

Under stress conditions, microalgae can bioaccumulate intracellular lipid droplets (LDs). However, the composition and extent of lipid production are highly species-specific and depend on the surrounding environment. Precise localization of the LDs and biochemical changes are crucial for portraying the lipid production strategy in algae, but it requires an *in vivo* tool to rapidly visualize LD distribution. As a novel strategy, this study focuses on detecting lipid bioaccumulation in a green microalga, *Chlamydomonas reinhardtii* using the aggregation-induced emission (AIE)-based probes, 2-DPAN (C₂₄H₁₈N₂O). The performance of this new AIE-probe was compared with lipid-specific AIE- probe, DPAS (C₂₀H₁₆N₂O) and commercial lipid-specific probe, BODIPY. Five treatments included (1) modified Woods Hole (MBL) medium, (2) MBL without nitrogen (-), (3) MBL without nitrogen (-) and calcium (-), (4) MCM without nitrogen (-) and calcium (-), but with sodium acetate (2.0 g/L) (+), and (5) MCM without nitrogen (-) and calcium (-), but with sodium acetate (2.0 g/L) (+) in dark. Except for no light in treatment 5, all treatments provided continual illumination at 70 mmol photons per m⁻² s⁻¹. Distinctive LDs labelled with 2-DPAN have elucidated the lipid inducing conditions, where more health beneficiary α -linolenic acid was produced. Increased levels of H₂O₂ content in the lipid-induced cells clarified the involvement of H₂O₂ during lipid biogenesis. Co-staining with traditional green BODIPY dye and red chlorophyll indicates that DPAS and 2-DPAN are suitable for multicolour imaging. This study demonstrates a biocompatible AIEgen as a rapid and easy *in vivo* tool to detect lipid production and H₂O₂ involvement in a microalga with carbohydrate cell walls to advance the research of lipid production in microalgae.

Keywords: *Chlamydomonas reinhardtii*, 2-DPAN, DPAS, hydrogen peroxide, lipid drops, TPEBO

3.2 Introduction

Lipid droplets (LDs) are well-connected subcellular organelles synthesized through complex pathways in various organisms. These droplets are involved in vital biological functions, such as cell membrane protection, signalling molecules, cell division, insulation, and energy storage. The majority of the lipid compounds have fatty acids (FA) structures, and the source of lipid compounds is either *de novo* synthesis or exogenous sources (de Carvalho & Caramujo, 2018). Deregulation in the lipid homeostasis can lead to different pathophysiological conditions in organisms, while specific FAs, such as polyunsaturated fatty acids (PUFAs) are health beneficiaries for higher vertebrates (Shahidi & Ambigaipalan, 2018). Therefore, expanding knowledge on lipidomics is a major target for revolution in medical research and system biology (Oresic et al., 2008). In humans, PUFAs are the precursors of eicosanoids that play pivotal roles in preventing chronic diseases, such as cancers (Fasano et al., 2017) and diabetes (Coelho et al., 2017) through modulating the pro- and anti-inflammatory activities (Lee et al., 2016). Long-chain, omega-3 fatty acids such as eicosapentaenoic acid (EPA) and docosahexaenoic acid (DHA) have been linked to the recovery of asthma, cognition, inflammatory bowel disease, and brain development (Calder, 2013; Brenna & Diau, 2007, 2007). Due to the lack of desaturase enzymes, humans cannot synthesize omega-3 fatty acids and depend on external sources (Lee et al., 2016). Plants can *de novo* synthesize up to 18 carbon PUFAs (Leonard et al., 2004), whereas some fish can convert long-chain PUFA from C18 PUFA (Castro et al., 2016). A large portion of the human ω -3 PUFAs is sourced from fish, and a continuous supply of which is currently under threat because of pollution and climate changes (Khozin-Goldberg et al., 2011). Photosynthetic microalgae possess the key desaturases necessary for synthesizing long-chain PUFAs (Harwood & Guschina, 2009). Additionally, with more efficient CO₂ fixation, these miniature sunlight-driven cell factories can use chlorophyll and various pigments to convert

photons into energy to grow in a harsh environment (Demirbas, & Demirbas, 2011, Dong et al., 2013). Therefore, microalgae have been more focused on producing health beneficiary biofunctional components over the last decade.

Among green microalgae, *Chlamydomonas* is a genus of unicellular flagellates that includes ~325 species of about 10 micrometres in diameter (Smith, 1955). These microorganisms can grow photoautotrophically (Wikipedia contributors, *Chlamydomonas reinhardtii*, 2019) and are widely distributed in various environmental conditions, including stagnant water, soil, freshwater, seawater, and even snow (Hoham et al., 2002). As a model organism, *Chlamydomonas reinhardtii* is often used in molecular biology to study recombinant proteins, oils, and chemicals with broad industrial applications (Rasala and Mayfield, 2015; Almaraz-Delgado et al., 2014). The cell wall of these biflagellates is deficient in cellulose and is mainly composed of a multilayered extracellular matrix of carbohydrates and 20-25 polypeptides (Imam et al., 1985).

In addition to the complete genome sequence of *C. reinhardtii*, fast growth and little cultivation costs have made this green alga an ideal contender for lipidomics and genetic manipulation studies. It has been revealed that the wild type and the mutant *C. reinhardtii*, blocked by the starch biosynthetic ADP-glucose pyrophosphorylase gene, *sta6*, can increase lipid synthesis by 15-fold and 30-fold, respectively, in 48 h nitrogen starved, acetate supplemented conditions. Moreover, this species is rich in triacylglycerol (TAG) (~90%), ~50% of which is saturated (C16 and C18) fatty acids, and ~50% is unsaturated fatty acids. Half of the TAG is in oleic acid (C18:1). However, only 10% of the lipid bodies have originated as free fatty acids (FFA), of which ~50% is C16, and ~50% is C18 (Wang et al., 2009). Interestingly, co-culturing of *C. reinhardtii* with *Azotobacter chroococcum*, a bacterium responsible for tobacco mosaic disease, was able to increase the production of lipid by 65.85% and 387.76 mg/L, which were 2.3 and 5.9 times higher than the control's levels of

29.11% and 65.99 mg/L, respectively (Xu et al., 2018). Lipid biosynthesis in microalgae also varies intermittently. During exponential growth, microalgae generally synthesize more protein, while in the later phases, the algae start to produce lipid. Lipids can also be changed from saturated fat to more unsaturation at later phases, falling in the post-maximal lipid accumulation stages (Morales et al., 2021). Therefore, tight temporal and spatial controls on harvesting cells during maximal lipid biogenesis are essential for optimal lipid extraction.

Recently, the intertwined relation between stress response and LD formation in photosynthetic organisms has become apparent (You et al., 2019; 2 Z. Y. Du). Under stress conditions, most microalgae show elevated reactive oxygen species (ROS) activities (Sivaramakrishnan & Incharoensakdi, 2017; Yilancioglu et al., 2014). It is well established that ROS, such as superoxide (O_2^-), hydroxyl radical (OH^\bullet) and hydrogen peroxide (H_2O_2) that are formed by the partial reduction of oxygen, can react with specific biomolecules. A high level of oxidative stress can alter or impair photosynthesis and damage DNA and proteins, leading to autophagy. However, over the last few years, increasing evidence suggests the role of ROS as a mediator of lipid accumulation by acting as the second messenger in various signal transduction mechanisms associated with the changes in the transcriptome, proteome, and metabolome (Schieber & Chandel, 2014; Zhang et al., 2016). Compared to other ROS, H_2O_2 is much more stable and can cross the phospholipid bilayer to link many complex biological systems (Reczek & Chandel, 2015; Niethammer et al., 2009). Therefore, it is necessary to understand the H_2O_2 activity in the stress response during lipid induction in microalgae (Haskew-Layton et al., 2010; Miller et al., 2007).

Bioimaging the LDs can provide valuable information on lipid metabolism and associated biophysical properties during lipid formation in microalgae. Currently, one of the major challenges of using the traditional fluorophores *in vivo* to visualize the biological molecules is developing dye acquisition and penetration techniques. Besides, commercial fluorescent

dyes often suffer from reduced photostability and aggregation-caused quenching (ACQ) phenomena that limit the purposes of the studies (Yu et al., 2005; Collot et al., 2018). Nanotechnology advancements have introduced several probes in molecular and biological studies with unique aggregation-induced emission (AIE) properties, which is an opposite phenomenon of ACQ. These probes show increased emission due to the restrictions of the intramolecular motion through binding with the target biomolecules or during exposure to certain environments (Zhang et al., 2015; Leung et al., 2014). Recently, AIEgens, DPAS (C₂₀H₁₆N₂O) (Wang et al., 2016), and 2-DPAN (C₂₄H₁₈N₂O) (Li et al., 2019) have been utilized to detect LDs in animal cells. The incorporation of AIE-based nanoparticles has improved these AIE probes' photostability, making these molecules suitable as long-term high contrast imaging tools (Qian & Tang, 2017). However, since these probes have been only studied in animal cells, their efficiency needs to be tested in other biological environments with different cellular compositions. Microalgae need to thrive in adverse conditions and have developed evolutionary conserved complex structures, such as cell walls. Besides providing a stable osmotic environment for the cellular machinery, the algal cell wall offers defence against microbial attack and limits the entry of foreign particles. In some cases, these extracellular structures can act as the barrier for the molecular probes that must be overcome to effectively label the intracellular target components. Therefore, efficacies of DPAS, and 2-DPAN need to be determined across multiple cell types for advance in lipid research.

In this study, as a model species of microalgae containing carbohydrate cell walls, *C. reinhardtii* was used to identify the lipid inducing conditions with lipid-specific AIEgens, DPAS and 2-DPAN. Furthermore, the effects of light, nutrient starvation, and supplemented carbon sources on lipid biosynthesis in this microalga have been evaluated. As a messenger molecule and stress biomarker, H₂O₂ activity has also been detected in different cultural

conditions. More importantly, a novel method was developed to visualize the LDs in a complex carbohydrates-based cell wall containing microalga using the lipid-specific AIEgens, and the H₂O₂ contents were determined in the cells cultured in different conditions to understand the LDs enriching mechanism in the specified conditions.

3.3 Materials and Methods

3.3.1 Microalga cultivation and lipid induction

The green microalga, *C. reinhardtii* (diameter: $8.0 \pm 2.0 \mu\text{m}$), was collected from the College of Science and Engineering, Flinders University, Australia. A pure culture of *C. reinhardtii* was established in 500 mL Erlenmeyer flasks containing 250 mL of Woods Hole (MBL) medium after autoclaving at 121 °C for 5 min, then cooling at room temperature. The culture medium in 1-L distilled water contained CaCl₂·2H₂O (0.04 g), MgSO₄·7H₂O (0.04 g), NaHCO₃ (0.01 g), K₂HPO₄ (0.008 g), NaNO₃ (0.08 g), EDTA-Na₂ (0.004 g), FeCl₃·6H₂O (0.004 g), CuSO₄·5H₂O (0.01 mg), ZnSO₄·7H₂O (0.02 g), CoCl₂·6H₂O (0.01 mg), MnCl₂·4H₂O (0.02 mg), Na₂MoO₄·2H₂O (0.006 mg), C₆₃H₈₈CoN₁₄O₁₄P (Vitamin B₁₂) (0.0005 mg), C₁₂H₁₇ClN₄OS·HCl (Vitamin B₁) (0.1 mg), C₁₀H₁₆N₂O₃S (Biotin) (0.0005 mg), and C₄H₁₁NO₃, (Tris(hydroxymethyl)aminomethane) (0.25 g). The pH was adjusted to 7.2 (Nichols, 1973). The culture was then maintained at 25 °C in a temperature-controlled room under continuous light and rotation (70 μmol photons per m⁻² s⁻¹; 100 rpm). All the reagents for growth media preparation were obtained from Thermo Fisher Scientific, Australia. For growth determination, the cells of *C. reinhardtii* were counted on a haemocytometer (Improved Marienfeld Neubauer, Germany).

To find the effects of nutrient and light manipulation on lipid biosynthesis, we used *C. reinhardtii* cells (0.3×10^6 cells/ml) from the exponential growth phase and subsequently cultured them for 8 days in a nutrient-starved stress phase. Five treatments included (1)

modified Woods Hole (MBL) medium, (2) MBL without nitrogen (-), (3) MBL without nitrogen (-) and calcium (-), (4) MCM without nitrogen (-) and calcium (-), but with sodium acetate (2.0 g/L) (+), and (5) MCM without nitrogen (-) and calcium (-), but with sodium acetate (2.0 g/L) (+) in dark. To determine the effects of exogenous H₂O₂ application on the growth and lipid accumulation in *C. reinhardtii*, cells were cultured in different H₂O₂ concentrations (0, 0.4, 0.6, 0.8 and 1.0 mM) supplemented with an MBL medium. Unless specified otherwise, all the experiments were performed in triplicate (n = 3).

3.3.2 The fluorescence properties of *Chlamydomonas reinhardtii* and AIEgens

Different natural biomolecules in photosynthetic organisms (e.g. different chlorophyll and accessory pigments) exhibit autofluorescence properties that must be determined to avoid interference during fluorescent staining. The autofluorescence properties of *C. reinhardtii* were detected at different excitation-emission wavelengths using a fluorescence spectrophotometer (Cary Eclipse, MY17180002, Agilent Technologies, CA, USA). AIEgens DPAS and 2-DPAN were obtained from Hong Kong University of Science and Technology, China and South China University of Technology, China, respectively (Wang et al., 2016, Li et al., 2019). Fluorescence properties of DPAS have been previously determined for a microalga *Euglena gracilis* in chapter 3 (Reza et al., 2021). The absorption and photoluminescence (PL) spectra of 2-DPAN in DMSO/water mixtures were determined using the fluorescence spectrophotometer with quartz cuvettes of 1 cm path length. Fluorescence spectra of 10 µM 2-DPAN in DMSO (Sigma-Aldrich, Australia) and 50-90% water fractions (fw) were measured at room temperature.

3.3.3 Determination of algal growth in different concentrations of AIEgens

To determine the effects of AIEgens on *C. reinhardtii* growth, cells at the density of $1.0 \pm 0.015 (\times 10^4)$ cells / mL were introduced to different concentrations (10, 50, and 100 μ M) of DPAS and 2-DPAN. The experiment was conducted in the MBL medium and cultured under the previously described condition. The growth rate was determined by counting the cells with a haemocytometer (Improved Marienfeld Neubauer, Germany) at regular intervals for up to 6 days.

3.3.4 Determination of H_2O_2 content

For the colorimetric measurement of H_2O_2 content in *C. reinhardtii*, cells cultured in different nutrient altered conditions were harvested by centrifugation for 10 min at $10,000 \times g$. The weight of 0.5 g of fresh algae was then homogenized in 5 ml of 0.1% w/v TCA solution. The supernatant was then collected by centrifugation at $15,880 \times g$ for 10 min. An aliquot of 0.5 ml of the supernatant was then mixed with 0.5 ml phosphate buffer (10 mM, pH 7.0) and 1 ml potassium iodide (1 M). The absorbance of the solution was measured at 390 nm. The H_2O_2 concentration (μ mol H_2O_2 /g FW) in the sample was then determined using a calibration curve prepared with the known concentrations of H_2O_2 (Chokshi et al., 2017).

3.3.5 Sample preparation for fluorescent staining of lipid and H_2O_2

In the dark, a stock solution of 1.0 mM BODIPY™ 505/515 in DMSO (Thermo Fisher Scientific Inc.) was prepared and stored at $-20^\circ C$ in the dark. The stock solution was diluted to 10 μ M in DI water, and the final concentration of DMSO was adjusted to 0.1% in each sample. Fluorometric quantification of the lipids was done according to the modified method of Cooper *et al.* (2010). Briefly, the cultured algae were adjusted to 10^6 cells/ml, and the cells were collected by centrifugation at $2000 \times g$ for 60 sec. Subsequently, the cells were re-suspended in 200 μ L DI water, gently mixed with 200 μ L of the prepared 10 μ M BODIPY™

505/515 solution and incubated in the dark for 5 min. The cells were washed three times with DI, centrifuged at $2,000 \times g$ for 60 sec, and re-suspended in water. The stained cells were then protected from light for further analysis.

To determine the fluorescence intensities of different concentration of DPAS and 2-DPAN (5 μM , 10 μM , 20 μM , and 30 μM), *C. reinhardtii* cells (10^6) of Treatment 4 was used. A 1.0 mM stock solution of each AIEgen was prepared and was stored at 4 °C in the dark. Fluorescence intensities were determined using the fluorescence spectrophotometer with quartz cuvettes of 1 cm path length. Fluorometric quantification of lipids in *C. reinhardtii* cells with confocal microscopy was done by adjusting the cells at 10^6 cells/ml. Twenty μM DPAS and 2-DPAN were added, and the samples were vortexed at 100 rpm for 30 sec and then stored in the dark for 30 min. The final concentration of the DMSO was adjusted to 0.1% for all the studies. The wash-free performance of BODIPY, DPAS, 2-DPAN was determined by analyzing the samples before and after the washing process (wash with DI three times).

3.3.6 Imaging of Chlamydomonas reinhardtii with a confocal microscope

The *C. reinhardtii* cells were imaged under a Zeiss LSM 880 Airyscan confocal microscope using ZEN 2.6 software (Carl Zeiss, Australia). The excitation wavelength for BODIPY™ 505/515, DPAS and 2-DPAN was 488 nm, and the emission wavelengths for BODIPY™ 505/515, DPAS and 2-DPAN were 490-561 nm, 570-650 nm, and 526-570 nm, respectively. Autofluorescence of the chlorophyll was detected with the excitation wavelength at 488 nm and emission wavelength of 685-758 nm.

3.3.7 Flow cytometric analysis of lipid content

Cytometric analysis was done using a flow cytometer (model CytoFLEX Flow Cytometer, Beckman Coulter, Inc. USA). Microalgae from different treatments were taken in three

replicates and were stained with BODIPY™ 505/515 (5.0 μM) and 2-DPAN (20 μM) according to the previously described methods. FITC (488 nm laser) and KO525-A (405 nm laser) channels were used to detect the fluorescence from BODIPY™ 505/515 and 2-DPAN, respectively. The mean fluorescence intensity from a minimum of 10,000 cells per sample was acquired. Relative fluorescence was determined using the population cell percentile, with cells cultured in an MBL medium serving as the control.

3.3.8 Lipid extraction and analysis of fatty acids

The total lipid was extracted according to the adapted method of Bligh and Dyer (1959). Briefly, a sample volume was taken from each growing *C. reinhardtii* culture to provide approximately 500 mg of dry algal biomass. The supernatant was discarded after centrifugation at $10000 \times g$ and 4 °C for 10 min. The collected pellet was then washed three times with an equal volume of potassium phosphate buffer (pH: 7.2). After that, the pellet was resuspended in DI water and subsequently transferred and weighed in a weighing dish. The samples were dried for 48 h at 60 °C, and stored at -20 °C for further analysis. Approximately 50 mg of dried algal biomass was then taken into a pre-washed (hexane) mortar. Using a Pasteur pipette, the weighing dish was washed with 1 ml of hexane to transfer the samples into the mortar. Using a pestle, the algal biomass was then grounded into a fine, smooth paste. During the grinding process, hexane was added to replenish the evaporated hexane, and the resulting slurry was mixed with the pestle until complete homogenization. All the process was done under the fume hood. After that, the homogenized hexane-cell mass mixture was centrifuged at $10,000 \times g$ (4 °C, 20 min), and the supernatant was collected in a pre-weighed vial. The pellet was then resuspended with hexane (3 ml) by vigorous vortexing for 1 min and centrifuged at $10,000 \times g$ (4 °C, 30 min) to ensure the removal of all the cell debris. After complete evaporation of the hexane, the extracted oil mass was then determined gravimetrically. All the lipid extracts were stored at -20 °C for

further analysis. Quantitative analysis of fatty acids was done with a Perkin Elmer GC-MS (Clarus 500 and 560S) using internal standards. Crude lipids were extracted from the sample using solvents. The lipids were transmethylated, and the profiles of different fatty acids were obtained with gas chromatography. Results were expressed as a percentage of fatty acid methyl esters (Christie, 1993).

3.3.9 Data analysis

Data from the confocal microscopy were analyzed with ImageJ 1.52a (Schneider et al., 2012). Briefly, the raw images were exported in "tiff" format in ImageJ. Using "Sliding paraboloid", the background was subtracted from each image, and the fluorescence channel was calculated. Subsequently, "Area", "Mean grey value", "Integrated density", and "Area fraction" were determined. Fluorescence intensity per cell was then calculated from the total cells by subtracting the background IntDen value from the IntDen value.

The flow cytometry data were analyzed using CytExpert v2.4 software and presented as histogram overlays. To detect BODIPY™ 505/515 labelled cells, samples were gated on FITC-A vs SSC-A. For 2-DPAN, samples were gated on KO525-A vs SSC-A. Confocal microscopy and flow cytometry data were exported to Excel 2010 to prepare the graphs. The means and medians of different treatments were compared by the relative fluorescence intensity of the gated population, with setting cells from the MBL medium as the control group. Data were analyzed by one-way analysis of variance (ANOVA) with SPSS statistics software (version 23) to compare the treatments. Specific differences in treatment means and multiple comparisons were tested at $P < 0.05$ level through Waller-Duncan post hoc and least significant difference (LSD) tests, respectively.

3.4 Results

3.4.1 Effects of nutrient and light manipulation on algal growth

Except for the MCM medium in continuous light, a slower growth rate was found in all the treatments (Fig. 3.1). After 8 days of continuous culture, maximum growth of 1.14 ± 0.38 (10^6) cells/ml was observed in Treatment 1. Nitrogen starvation decreased the algal growth by 16.4% in Treatment 2 than in Treatment 1. A maximum reduction of 57.1% in growth was observed in nitrogen and calcium starved, but sodium acetate supplemented dark condition of Treatment 5. Exposure to light under similar nutrient manipulation increased the algal growth by 26.5% in Treatment 4, while the presence of calcium in nitrogen starved but sodium acetate supplemented culture medium showed the same growth trend in Treatment 3.

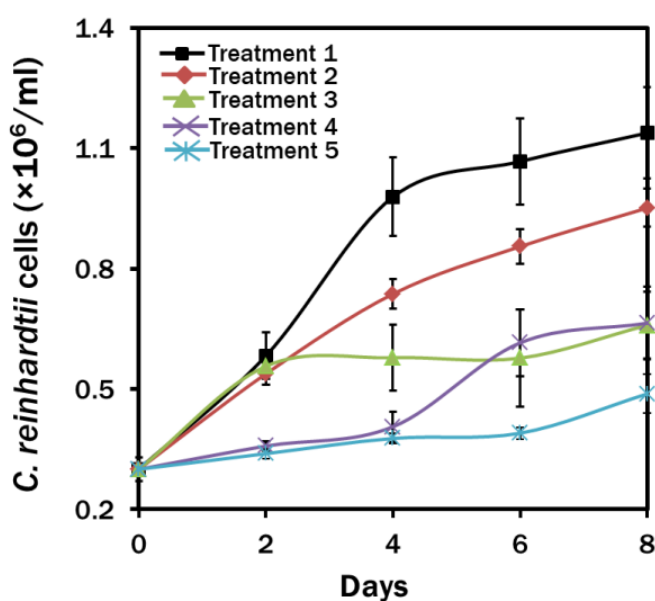


Fig. 3.1 Effects of nutrient and light manipulation on the growth of *Chlamydomonas reinhardtii* at different time intervals. Treatment 1: MBL medium; Treatment 2: MBL, (-) N₂; Treatment 3: MBL, (-) N₂, (-) Ca²⁺; Treatment 4: MBL, (-) N₂, (-) Ca²⁺, (+) Sodium acetate (2.0 g/L) (24 h light); and Treatment 5: MBL, (-) N₂, (-) Ca²⁺, (+) Sodium acetate (2.0 g/L) (24 h dark) conditions.

3.4.2 Autofluorescence properties of *Chlamydomonas reinhardtii*

The presence of chlorophyll and different natural pigments causes strong autofluorescence in microalgae that often interferes with the fluorescent staining of target molecules. To select the appropriate phosphorescent probes, spectrophotometric analysis of the autofluorescence spectral profile of live *C. reinhardtii* was done to minimize the background noise in this study. Algal cells excited at 350 nm emitted weak fluorescence at around 400 nm (Fig. 3.2a), whereas excitation at 405 nm resulted in two emission peaks at around 470 nm and 685 nm (Fig. 3.2b). A single emission peak at 685 nm was observed, while cells were excited at 488 nm. The cause of the fluorescence at around 400 nm was unclear, while that of around 470 nm was assumed due to the number of redox ratios (NAD(P)H/FAD) (Wu & Qu, 2006). The emission peak at 685 nm was due to the autofluorescence from chlorophyll. As shown in Fig. 3.2c, excitation at 488 nm resulted in a single peak with maximum fluorescence from chlorophyll.

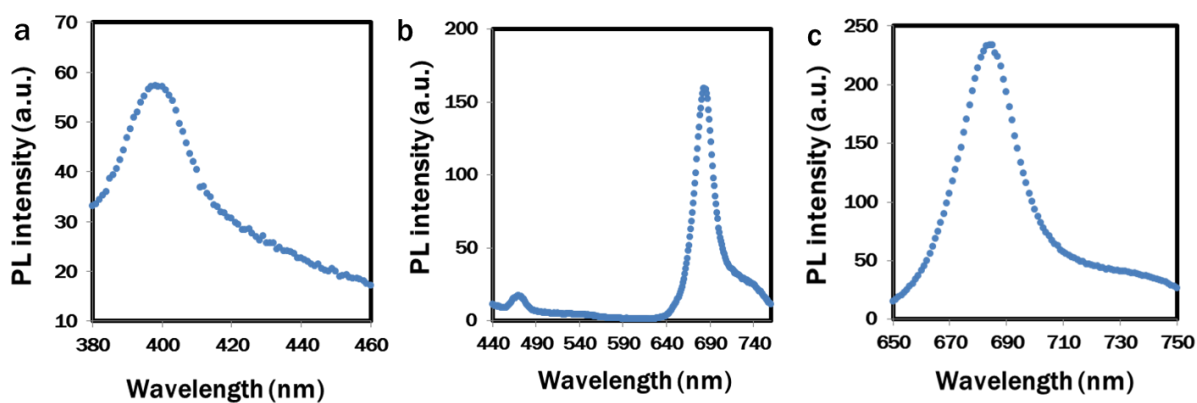


Fig. 3.2 Autofluorescence of *Chlamydomonas reinhardtii* excited at different wavelength (a) λ_{ex} : 350 nm; (b) λ_{ex} : 405 nm; (c) λ_{ex} : 488 nm

3.4.3 Fluorescent properties of 2-DPAN

The absorption and photoluminescence (PL) spectra of 2-DPAN (10 μM) in DMSO were analyzed under 405 nm excitation. An absorption peak was observed at 380 nm in a 90% water fraction (Fig. 3.3a). In the DMSO solution, 2-DPAN showed weak emissions. Increasing the water percentage from 50% to 90% also increased the PL intensity of 2-DPAN, which signified the AIE attributes of 2-DPAN (Figs. 3.2b and 3.2c).

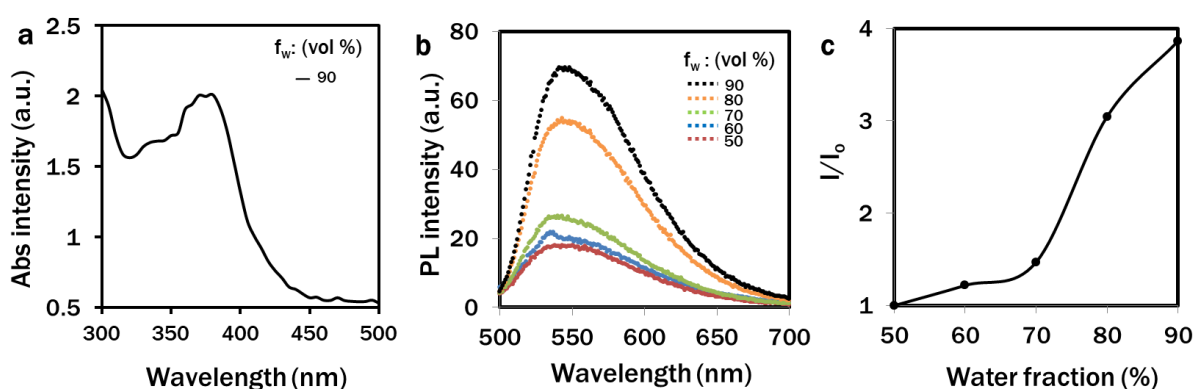


Fig. 3.3 Fluorescence properties of 2-DPAN. Absorption spectra (a) and fluorescence spectra (b, c) of 2-DPAN (10 μM) in 90% water fraction and DMSO-water mixtures, respectively.

3.4.4 Algal growth and acquisition of probe concentration

Prior to the lipid analysis, the effects of DPAS and 2-DPAN on the growth of *C. reinhardtii* were determined. The fluorescence intensity of these AIE probes at different concentrations and at different time intervals was also monitored. Compared with the control group, no significant difference was found in the algal growth pattern even at a very high concentration of 100 μM DPAS and 2-DPAN (Fig. 3.4) exposure.

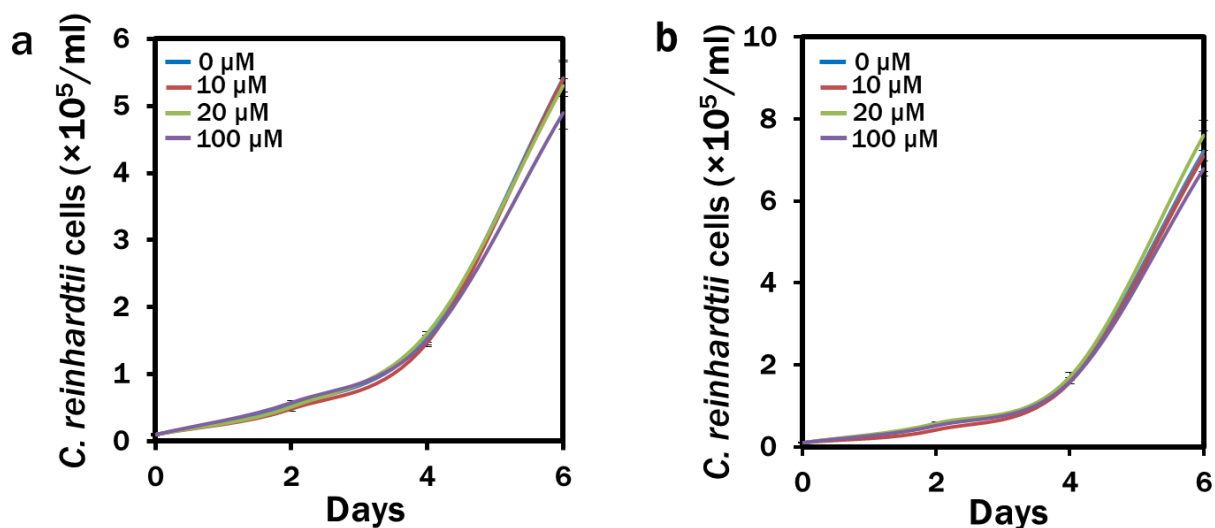


Fig. 3.4 Growth of *Chlamydomonas reinhardtii* in different AIEgen concentrations. (a) Algal growth at different concentrations of DPAS exposure; (b) Algal growth at different concentrations of 2-DPAN exposure. Growth determination cells were cultured in an MBL medium.

However, increased fluorescence intensity was observed when cells treated with 20 μM DPAS and 2-DPAN were compared to the 5 μM and 10 μM (Figs. 3.5a and 3.5c). Since the differences between the fluorescence intensity of 20 μM and 30 μM were very insignificant, 20 μM was used to label the LDs in this experiment. Furthermore, while incubating the cells at different time intervals, the fluorescence intensity was slightly lower in 10 min incubation than in 30 min (Figs. 3.5b and 3.5d). As no significant difference was observed between the 30 min and 60 min incubation, it was assumed that these AIEgens could thoroughly label lipid drops in *C. reinhardtii* cells within 30 min of the incubation period.

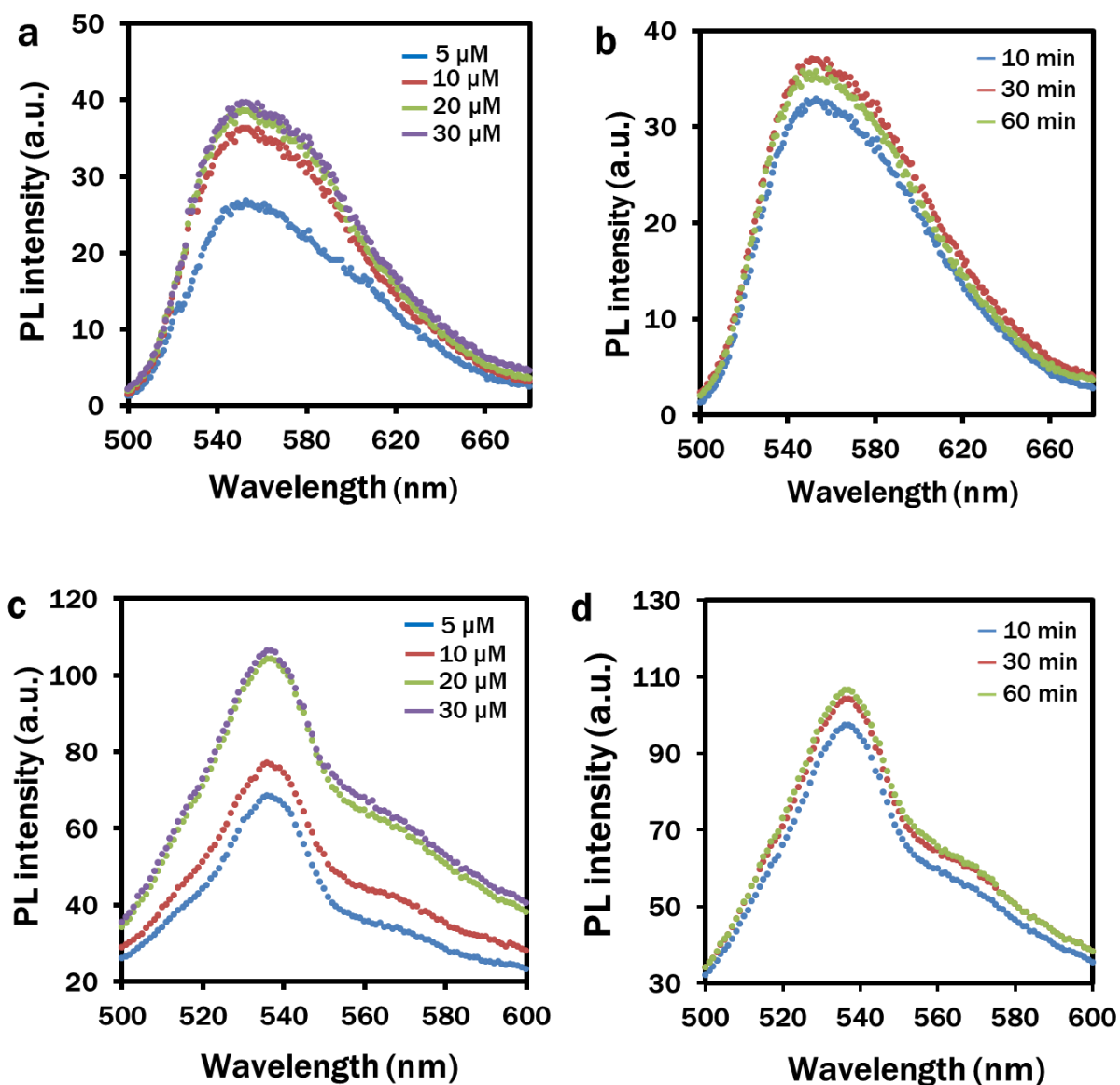


Fig. 3.5 Acquisition of AIEgen concentration in *Chlamydomonas reinhardtii*. (a) Fluorescence intensity at different concentrations of DPAS exposure; (b) Fluorescence spectra of DPAS (20 μM) in *C. reinhardtii* cells at different time intervals; (c) Fluorescence intensity at different concentrations of 2-DPAN exposure; (d) Fluorescence spectra of 2-DPAN (20 μM) in *C. reinhardtii* cells at different time intervals. For the fluorescence intensities, *C. reinhardtii* cells (10^6) of Treatment 4 (MCM, (-) nitrogen, (-) calcium, (+) sodium acetate (2.0 g/L)) were used.

3.4.5 Wash free imaging technique with DPAS and 2-DPAN

The sample preparation techniques among the AIE probes, DPAS and 2-DPAN and the traditional probe BODIPY™ 505/515 were compared (Fig. 3.6), and the wash-free samples' fluorescence intensity was analyzed spectrophotometrically (Fig. 3.7). Compared to the BODIPY dye, sample preparation with DPAS and 2-DPAN required fewer steps that excluded the centrifugation and washing.

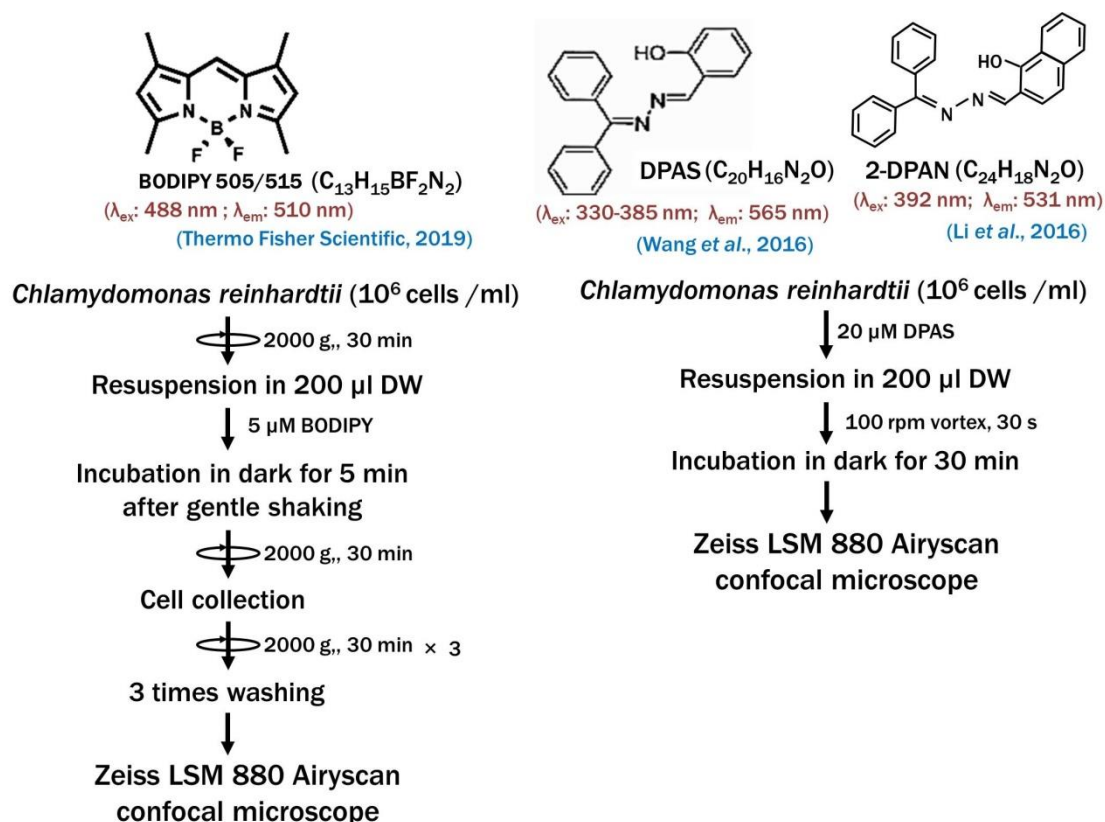


Fig. 3.6 Flow-diagram of sample preparation steps with BODIPY 505/515, DPAS and 2-DPAN

Spectrophotometric results suggested that without washing, the fluorescence intensity of the BODIPY dye reached outside the meaningful range of the spectrometer (Fig. 3.7a). In contrast, there was almost no difference in the PL intensities between the wash and wash-free samples with DPAS and 2-DPAN (Figs. 3.7b and 3.7c).

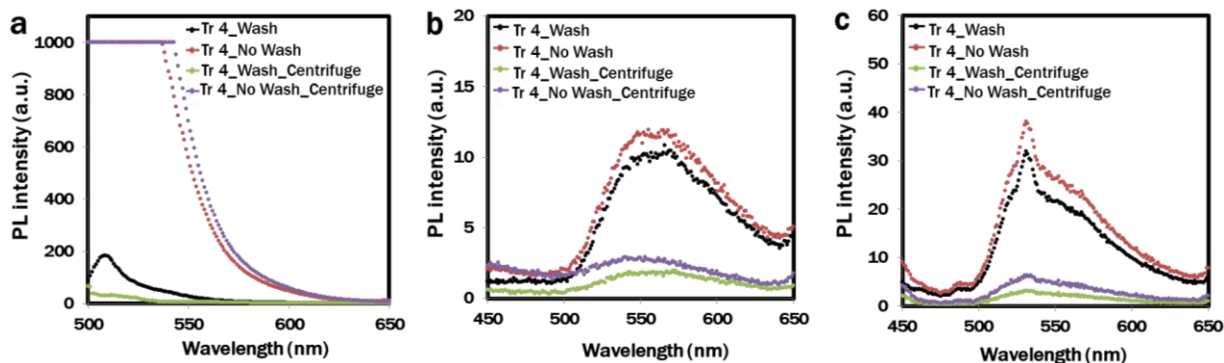


Fig. 3.7 Spectrophotometric analysis of the *Chlamydomonas reinhardtii* cells prepared with and without washing steps. Samples prepared with (a) BODIPY™ 505/515 (5 μM); (b) DPAS (20 μM), and (c) 2-DPAN (20 μM). Lipid induced *C. reinhardtii* cells from Treatment 4 (MBL medium, (-) N_2 , (+) Sodium Acetate (2.0 g/L), (-) Ca^{2+}) (24 h light condition) were analyzed. Images were taken with Zeiss LSM 880 Airyscan confocal microscope.

Furthermore, confocal images of the wash-free BODIPY samples could not distinguish the chlorophyll from the lipid as no autofluorescence could be detected in the red channel, which was due to the photobleaching of the samples (Figs. 3.8a-3.8d).

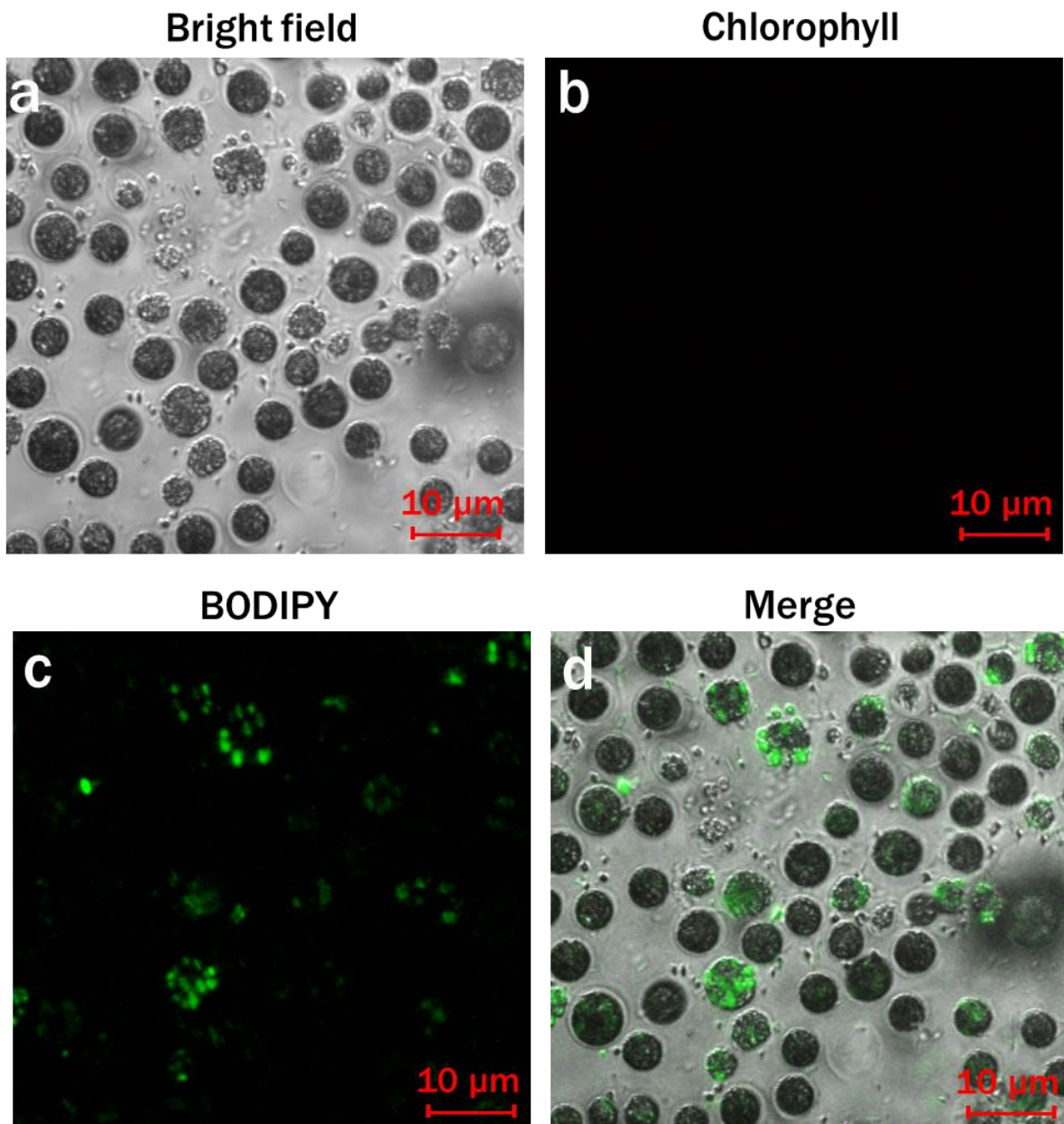


Fig. 3.8 Confocal analysis of the BODIPY-labelled *Chlamydomonas reinhardtii* cells prepared with and without washing steps. (Bright-field images: a; Fluorescence images - Chlorophyll: b; BODIPY: c; Merged image: d. Lipid induced *C. reinhardtii* cells from Treatment 4 (MBL medium, (-) N₂, (+) Sodium Acetate (2.0 g/L), (-) Ca²⁺) (24 h light condition) were analyzed. Images were taken with Zeiss LSM 880 Airyscan confocal microscope.

3.4.6 Comparison of the lipid-specific probes

Confocal images of *C. reinhardtii* cells of Treatment 4 (MCM, (-) N₂, (-) Ca²⁺, (+) sodium acetate (2.0 g/L) (24 h Light) conditions) were used to distinguish the performances of the lipid-specific probes (Figs. 3.9-3.11). The lipophilic traditional fluorescent dye, BODIPYTM 505/515 was used as a control to co-stain the cells (Rumin et al., 2015). Green (Figs. 3.9c and 3.10c) fluorescence channel was assigned to the BODIPY dye, whereas yellow fluorescence channels were exclusively assigned to the DPAS (Fig. 3.9d) and 2-DPAN (Fig. 3.10d). The images show that the AIE probes, DPAS (Fig. 3.9d), and 2-DPAN (Fig. 3.10d) could successfully label the LDs. The merged images indicated that the yellow and green fluorescence channels overlap (Figs. 3.9e and 3.10e). Arrow positions in the merged images demonstrated almost synchronized intensity changes of DPAS (Fig. 3.9f), 2-DPAN (Fig. 3.10f) and BODIPY in *C. reinhardtii* cells. The intensity scatter plots were drafted, and the Pearson correlation coefficient and Mander's overlap coefficient for DPAS were calculated as 0.90 and 0.92 (Fig. 3.9g), respectively, and for 2-DPAN were calculated as 0.91 and 0.92, respectively (Fig. 3.10g). Since relative fluorescence per cell (Fig. 3.11) indicated the superior performance of 2-DPAN ($P < 0.05$) to the BODIPY and DPAS, in the rest of the experiment, the AIE probe, 2-DPAN was utilized for the confocal analysis of LDs in *C. reinhardtii* cells.

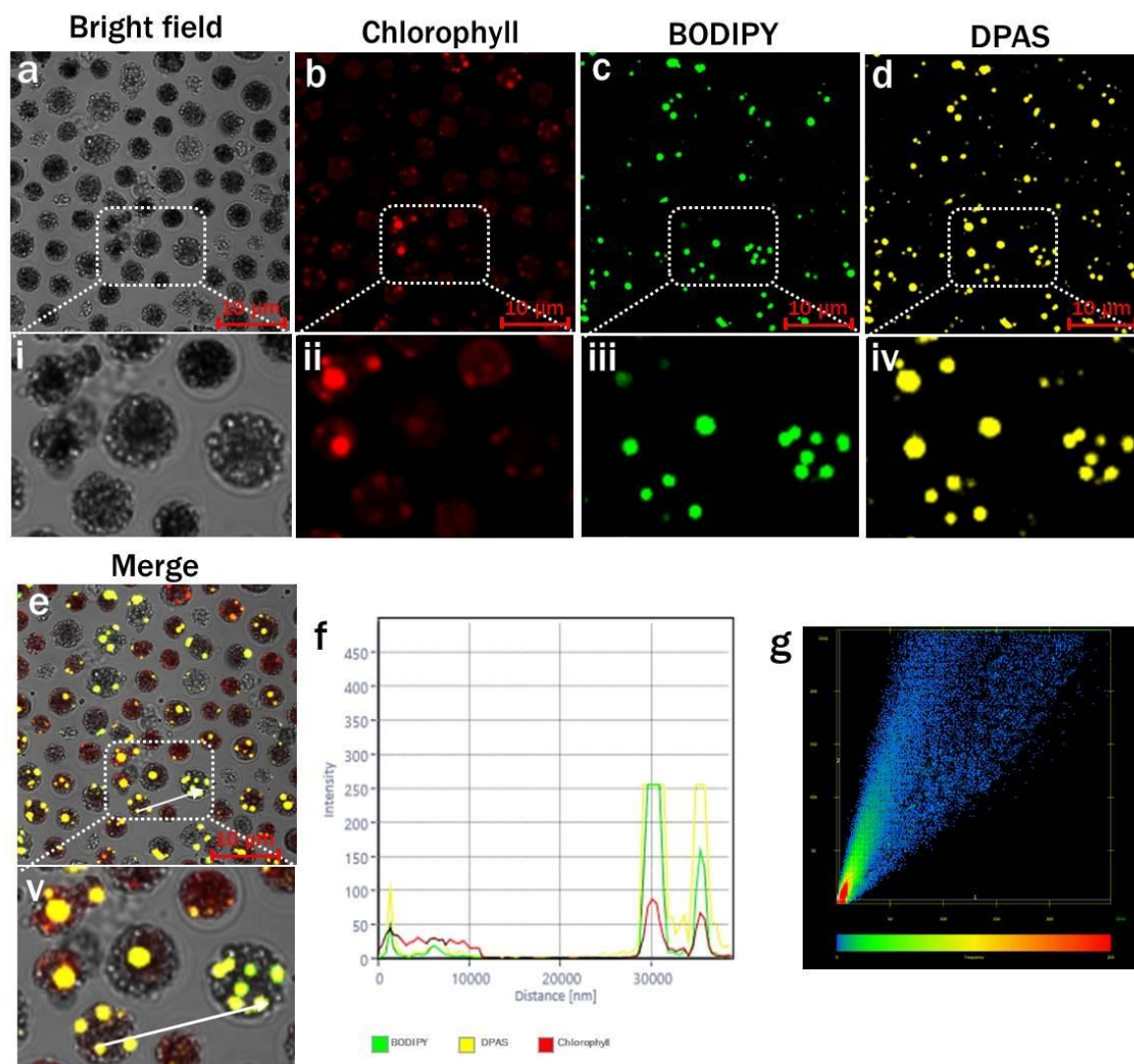


Fig. 3.9 Comparison of the lipid-specific probes under confocal microscopy. Lipid drops in *Chlamydomonas reinhardtii* cells of Treatment 4 ((MBL medium, (-) N₂, (+) Sodium Acetate (2.0 g/L), (-) Ca²⁺, (24 h light condition)) were labeled with traditional BODIPY™ 505/515 (c) and AIE probes, DPAS (d). (Bright-field images: a; Fluorescence images - Chlorophyll: b; BODIPY: c; DPAS: d; Merged images: e; i, ii, iii, iv, and v are the enlarged regions of a, b, c, d and e, respectively. (f) intensity profile of BODIPY and DPAS in green and yellow channels, respectively; (g) intensity scatter plot for the colocalized channels; Pearson correlation coefficient and Mander's overlap coefficient were calculated as 0.90 and 0.92, respectively. Images were taken with a Zeiss LSM 880 Airyscan confocal microscope.

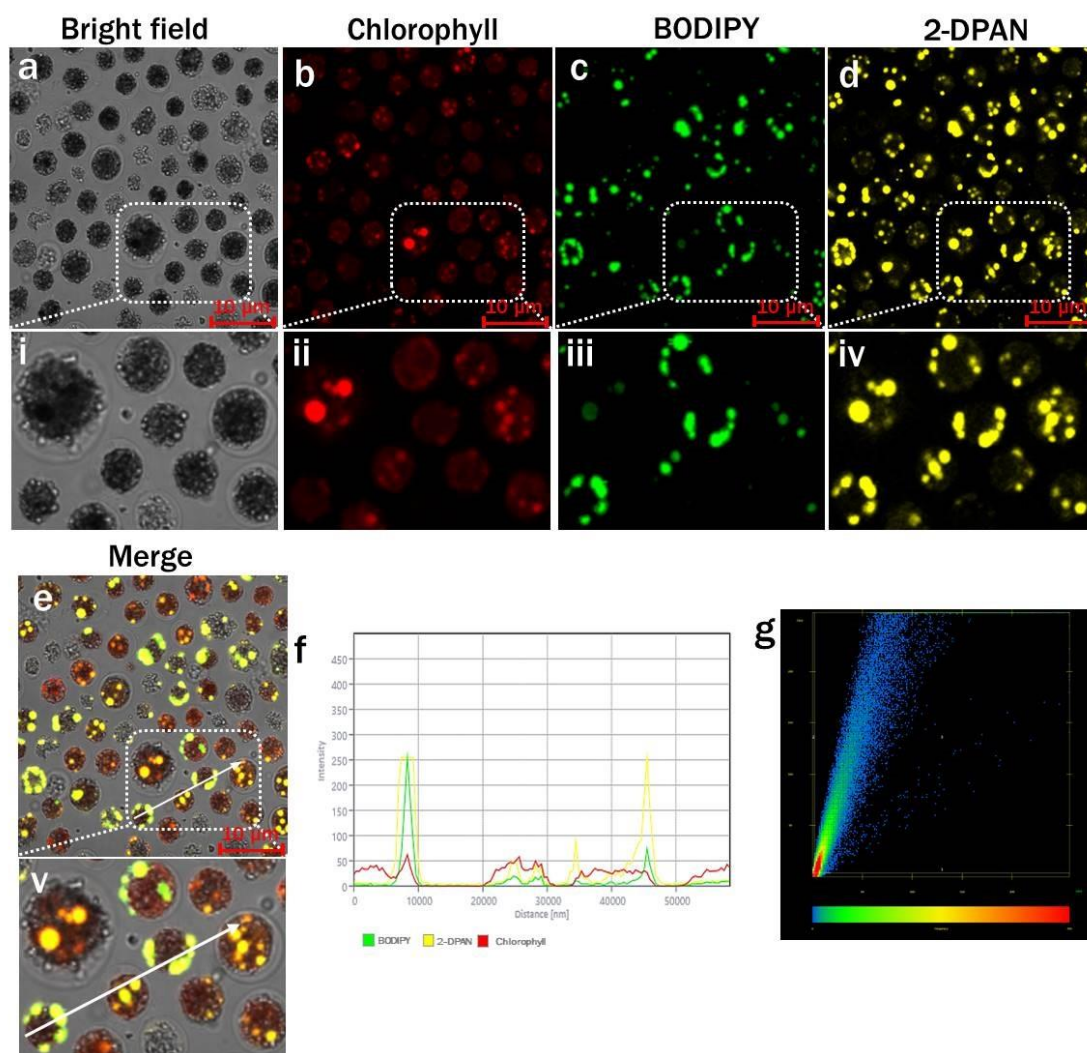


Fig. 3.10 Comparison of the lipid-specific probes under confocal microscopy. Lipid drops in *Chlamydomonas reinhardtii* cells of Treatment 4 ((MBL medium, (-) N₂, (+) Sodium Acetate (2.0 g/L), (-) Ca²⁺, (24 h light condition)) were labeled with traditional BODIPY™ 505/515 (c) and AIE probes, 2-DPAN (d). (Bright-field images: a; Fluorescence images - Chlorophyll: b; BODIPY: c; DPAS: d; Merged images: e; i, ii, iii, iv, and v are the enlarged regions of a, b, c, d and e, respectively. (f) intensity profile of BODIPY and 2-DPAN in green and yellow channels, respectively; (g) intensity scatter plot for the colocalized channels; Pearson correlation coefficient and Mander's overlap coefficient were calculated as 0.91 and 0.92, respectively. Images were taken with a Zeiss LSM 880 Airyscan confocal microscope.

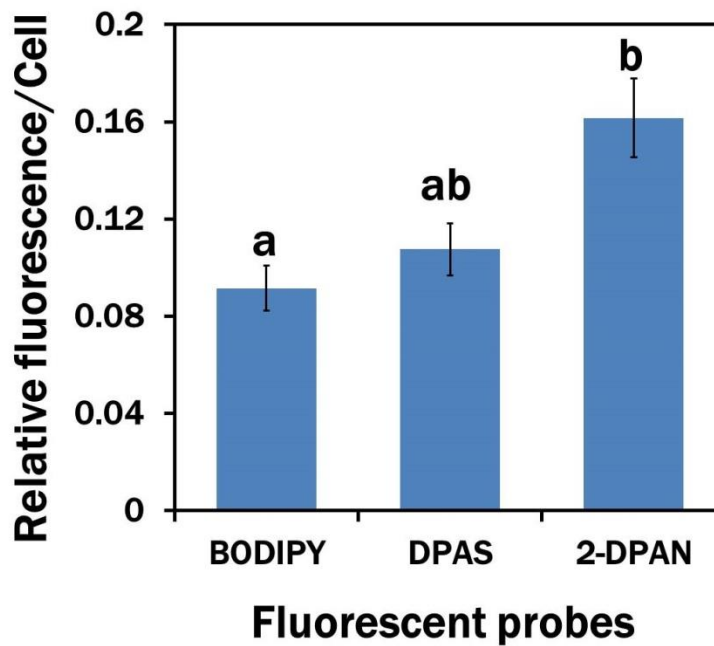


Fig. 3.11 Confocal analysis of the relative fluorescence intensity/cell for different lipid-specific probes in *Chlamydomonas reinhardtii*. Cells were cultured in Treatment 4 ((MBL medium, (-) N₂, (+) Sodium Acetate (2.0 g/L), (-) Ca²⁺, (24 h light condition)) Values are relative to the control BODIPY dye. Averages are shown as mean ± SE.

3.4.7 Flow cytometric analysis of lipid content

The plots from the flow cytometry indicated the efficient labelling of lipid drops in *C. reinhardtii* with BODIPY™ 505/515 (Fig. 3.12) and 2-DPAN (Fig. 3.13). Except Treatment 5 ((MCM, (-) N₂, (-) Ca²⁺, (+) sodium acetate (2.0 g/L) (24 h Dark) conditions)), cytograms of BODIPY fluorescence vs side scatter (Figs. 3.12a-3.12e), and 2-DPAN fluorescence vs side scatter (Figs. 3.13a-3.13e) showed more lipid accumulation in the nutrient-starved cells than that of the nutrient-enriched cells of Treatment 1 (MCM medium under 24 h light condition) (Figs. 3.12a and 3.13a). Maximum fluorescence was observed in N₂ and Ca²⁺ deprived, but sodium acetate (2.0 g/L) supplemented the light condition of Treatment 4 (Figs.

3.12d and 3.13d), which was followed by the Treatment 3 (N₂ deprived, but sodium acetate (2.0 g/L) supplemented light condition) (Figs. 3.12c and 3.13c). Moreover, greater side scatters in the nutrient-starved population indicated the obese phenotypes (Goodenough et al., 2014; Goncalves et al., 2016) caused by the lipid production and accumulation of probes within the LDs (Figs. 3.12c, 3.12d, 3.13c, and 3.13d) that was consistent with the higher relative lipid fluorescence per cell (Fig. 3.14). Since it was evident that nutrient-starved dark conditions of Treatment 5 (Figs. 3.12f, 3.13f, and 3.14) could not induce lipid production in *C. reinhardtii* cells, this treatment has been deduced from the later confocal analysis.

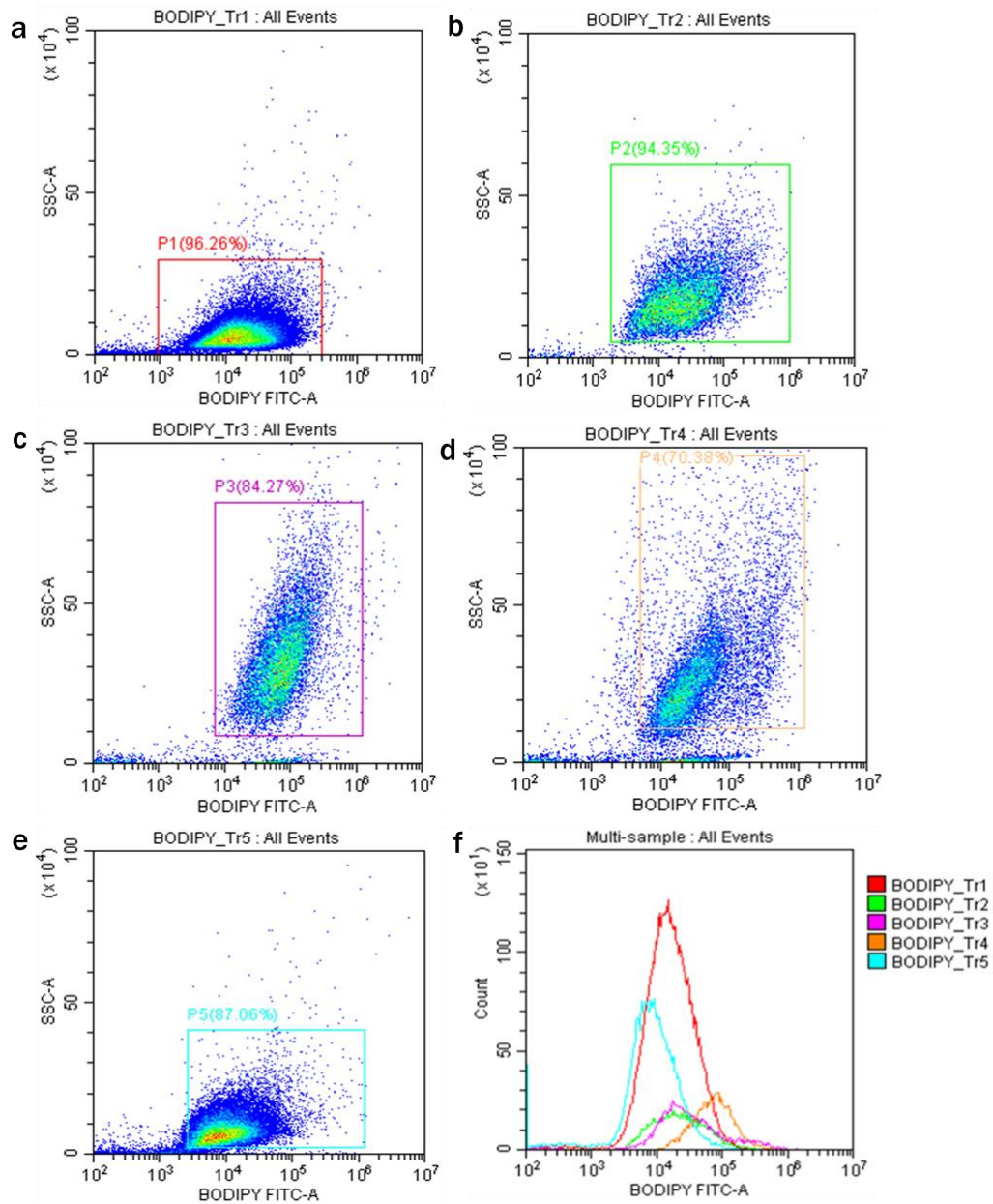


Fig. 3.12 Flow cytometry measurements for lipid in *Chlamydomonas reinhardtii* cells in different treatments labelled with BODIPY™ 505/515. (a-e) Flow cytogram of FITC-A vs SSC-A for BODIPY fluorescence in different treatments. Cells were cultured in Treatment 1: modified Woods Hole (MBL) medium; Treatment 2: MBL, (-) N₂; Treatment 3: MBL, (-) N₂, (-) Ca²⁺; Treatment 4: MBL, (-) N₂, (-) Ca²⁺, (+) sodium acetate (2.0 g/L) (24 h light); and Treatment 5: MCM, (-) N₂, (-) Ca²⁺, (+) sodium acetate (2.0 g/L) (24 h Dark) conditions. (f) Histogram of BODIPY™ 505/515 fluorescence for cells.

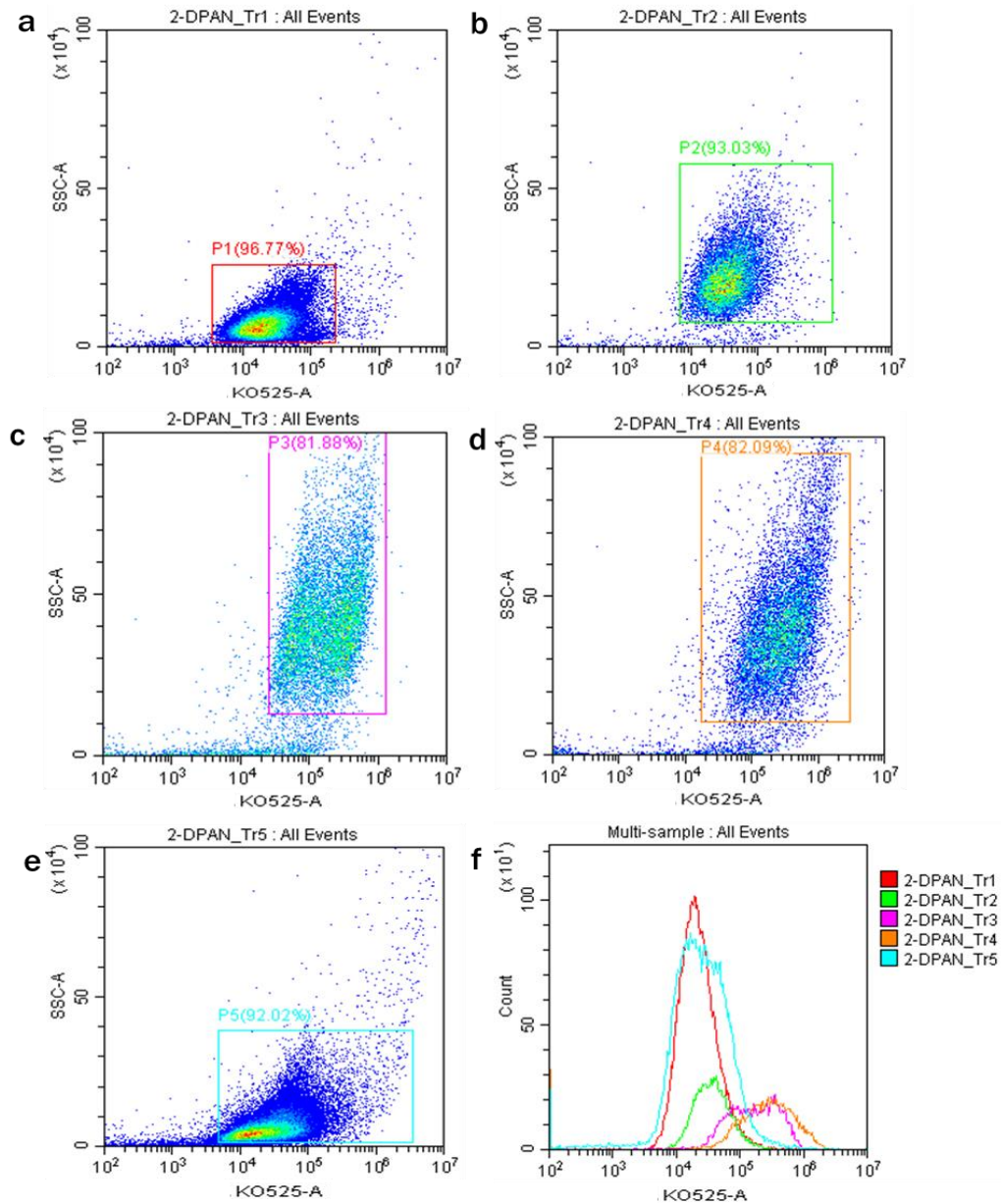


Fig. 3.13 Flow cytometry measurements for lipid in *Chlamydomonas reinhardtii* cells in different treatments labelled with AIE probe, 2-DPAN. (a-e) Flow cytogram of KO525-A vs SSC-A for 2-DPAN fluorescence. Cells were cultured in Treatment 1: modified Woods Hole (MBL) medium; Treatment 2: MBL, (-) N_2 ; Treatment 3: MBL, (-) N_2 , (-) Ca^{2+} ; Treatment 4: MBL, (-) N_2 , (-) Ca^{2+} , (+) sodium acetate (2.0 g/L) (24 h light); and Treatment 5: MCM, (-) N_2 , (-) Ca^{2+} , (+) sodium acetate (2.0 g/L) (24 h Dark) conditions. (f) Histogram of 2-DPAN fluorescence for cells.

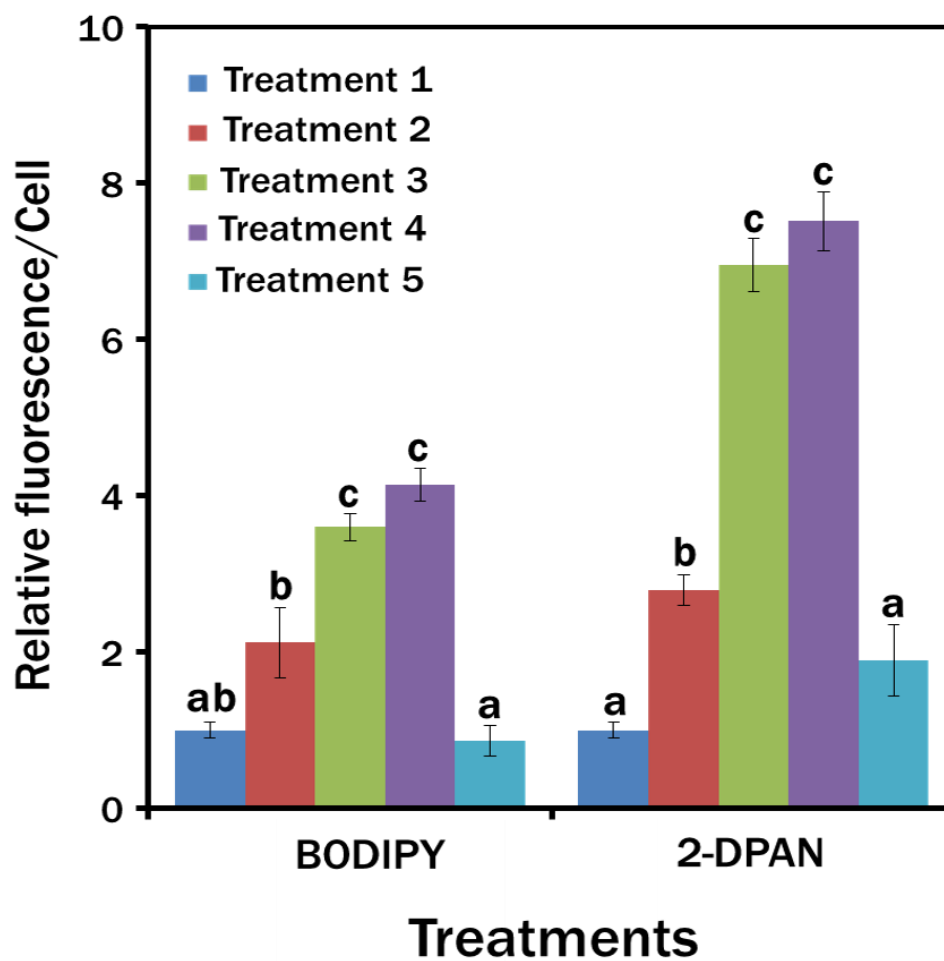


Fig. 3.14 Flow cytometry analysis of relative fluorescence of lipid/cell in *Chlamydomonas reinhardtii* cells in different treatments labelled with BODIPY™ 505/515 and AIE probe, 2-DPAN. Values are relative to the control condition of Treatment 1. Cells were cultured in Treatment 1: modified Woods Hole (MBL) medium; Treatment 2: MBL, (-) N₂; Treatment 3: MBL, (-) N₂, (-) Ca²⁺; Treatment 4: MBL, (-) N₂, (-) Ca²⁺, (+) sodium acetate (2.0 g/L) (24 h light); and Treatment 5: MCM, (-) N₂, (-) Ca²⁺, (+) sodium acetate (2.0 g/L) (24 h Dark) conditions. Averages are shown as mean ± SE.

3.4.8 Confocal analysis of the stress-induced lipid droplets in *Chlamydomonas reinhardtii*

Altering the physical and chemical parameters are well-known strategies for lipid induction in microalgae (Alishah Aratboni et al., 2019; Sun et al., 2018a). This experiment studied the effects of nitrogen and calcium deprivation, sodium acetate supplementation, and light on lipid biosynthesis in *C. reinhardtii*. As the rapid and efficient scanning approach for identifying lipid inducing conditions, the lipid-specific AIE probe, 2-DPAN was directly introduced to the growing media of different treatment groups (Fig. 3.6). Distinguished LDs from different treatments were clearly visible in the 2-DPAN labelled confocal images (Figs. 3.15-3.18). It was evident that Treatment 4 (MBL, (-) N₂, (-) Ca²⁺, (+) sodium acetate (2.0 g/L)) showed the highest lipid accumulation (Figs. 3.18 and 3.19), followed by those in Treatment 3 (MBL, (-) N₂, (+) sodium acetate (2.0 g/L), (Figs. 3.17 and 3.19) and Treatment 2 (MBL, (-) N₂, (Figs. 3.16 and 3.19). The lowest amount of lipid was produced in the nutrient-enriched condition of Treatment 1 (MBL medium). Autofluorescence from the chlorophyll was lowest in Treatment 4 (Figs. 3.18 and 3.19), where maximum lipid was produced.

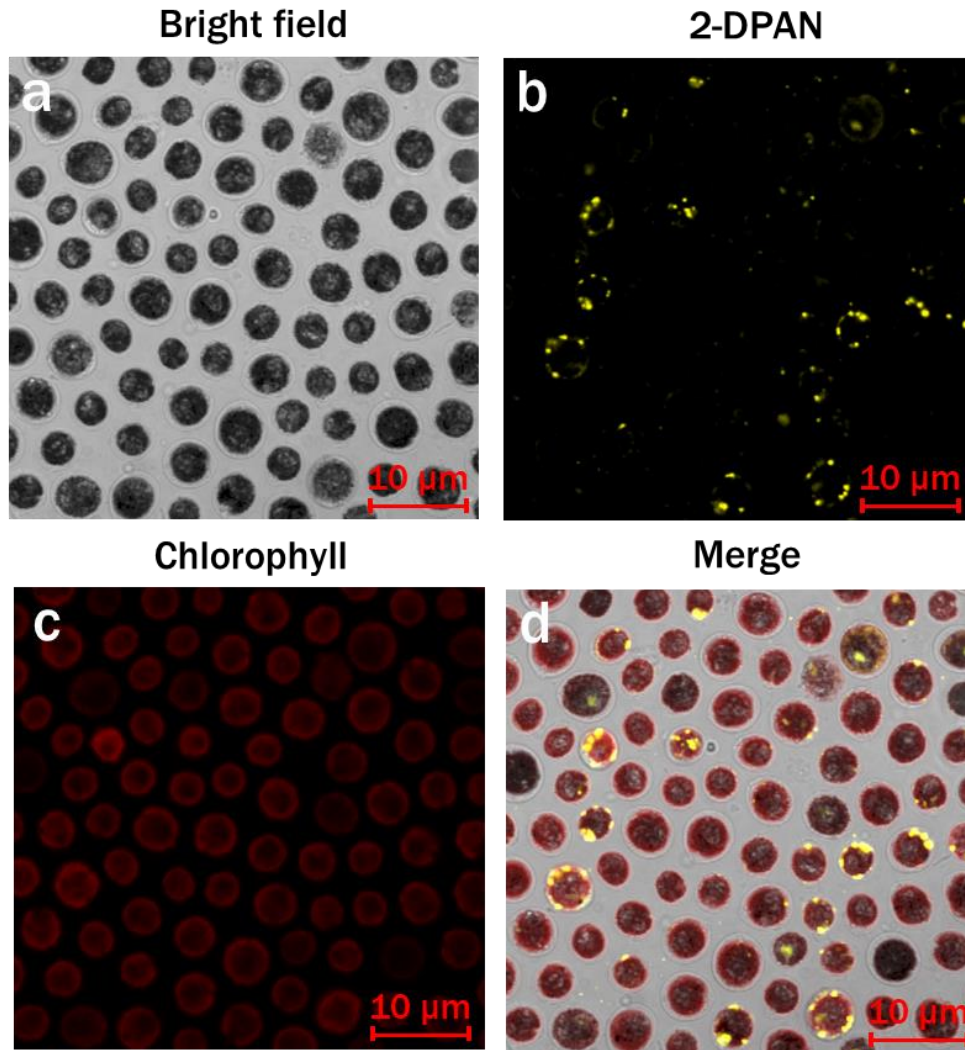


Fig. 3.15 Labeled lipid drops with lipid-specific AIE nanoprobe, 2-DPAN ($C_{24}H_{18}N_2O$) in *Chlamydomonas reinhardtii*. Cells were cultured in Treatment 1: modified Woods Hole (MBL) medium (24 h light condition). Bright-field image: a; Fluorescence images - 2-DPAN: b, Chlorophyll: c; Merged image: d. Images were taken with a Zeiss LSM 880 Airyscan confocal microscope.

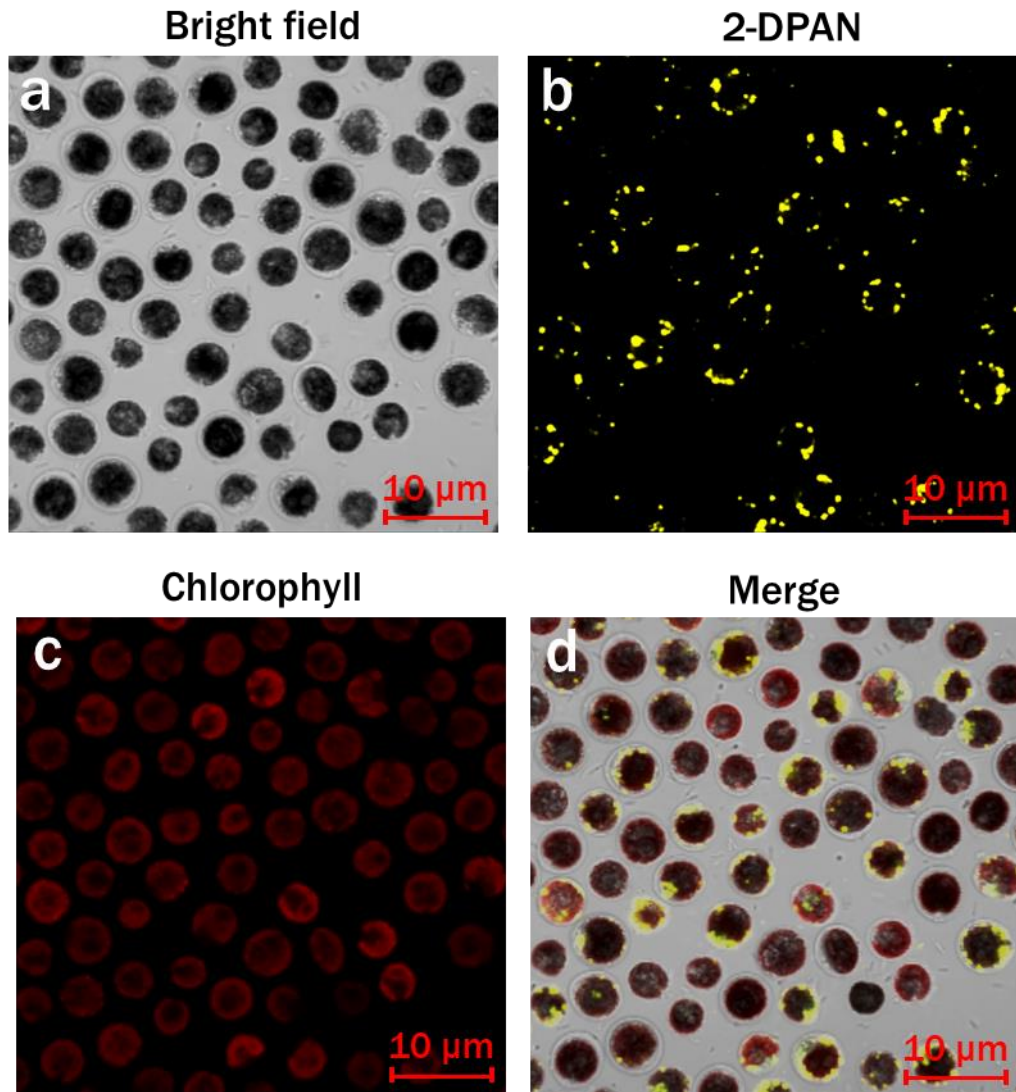


Fig. 3.16 Labelling lipid drops with lipid-specific AIE nanoprobe, 2-DPAN ($C_{24}H_{18}N_2O$) in *Chlamydomonas reinhardtii*. Cells were cultured in Treatment 2: MBL, (-) N_2 (24 h light condition). Bright-field images: a; Fluorescence images - 2-DPAN: b, Chlorophyll: c; Merged image: d. Images were taken with a Zeiss LSM 880 Airyscan confocal microscope.

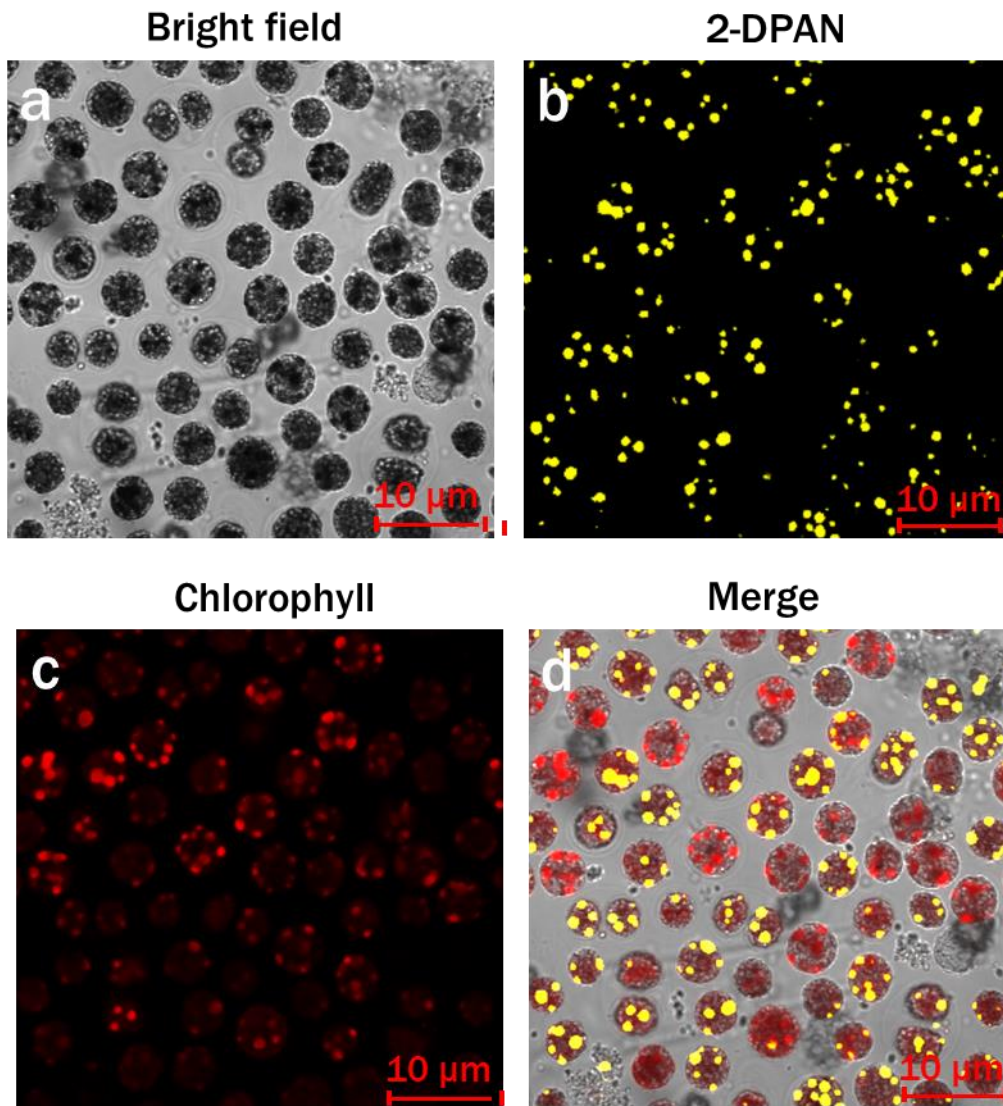


Fig. 3.17 Labeled lipid drops with lipid-specific AIE nanoprobe, 2-DPAN ($C_{24}H_{18}N_2O$) in *Chlamydomonas reinhardtii*. Cells were cultured in Treatment 3: MBL, (-) N_2 , (-) Ca^{2+} (24 h light condition). Bright-field image: a; Fluorescence images - 2-DPAN: b, Chlorophyll: c; Merged image: d. Images were taken with a Zeiss LSM 880 Airyscan confocal microscope.

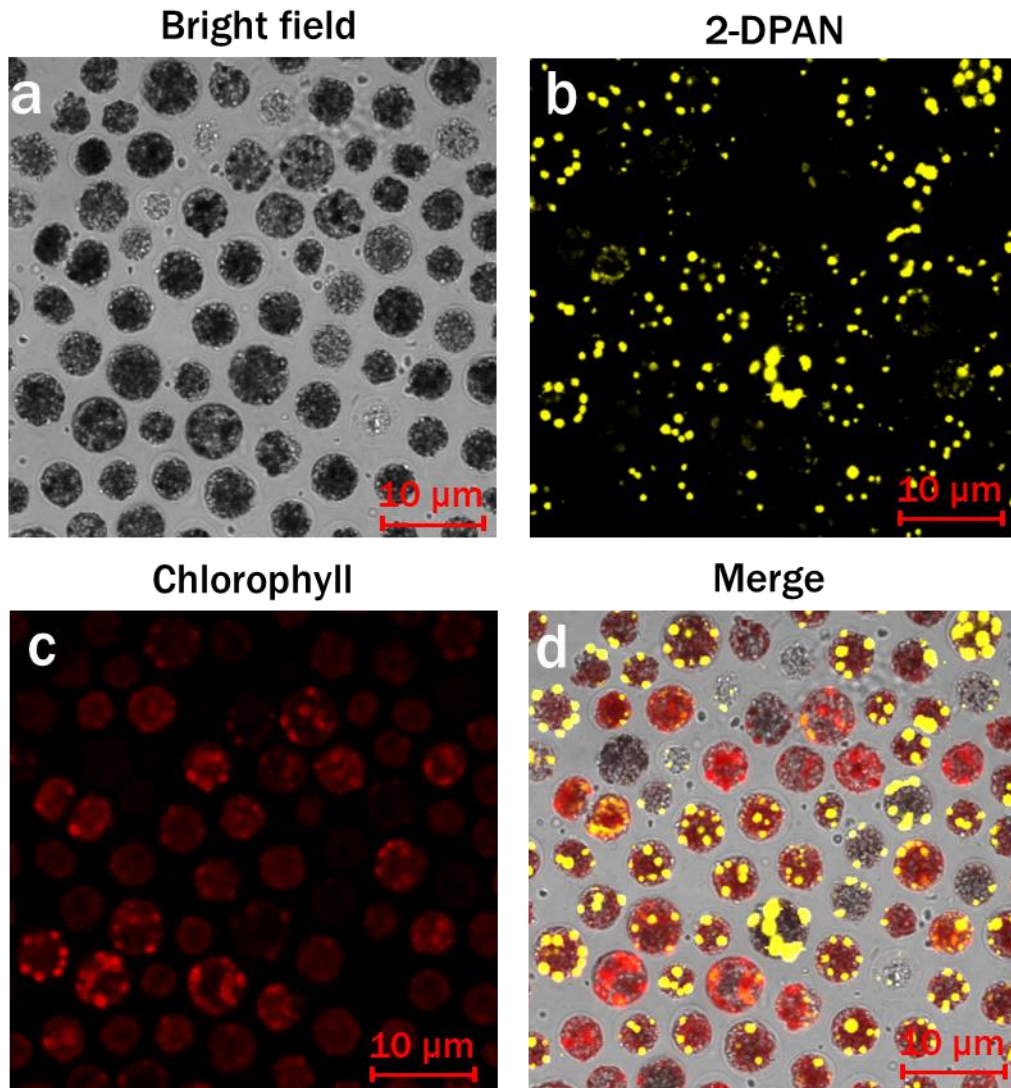


Fig. 3.18 Labelling lipid drops with lipid-specific AIE nanoprobe, 2-DPAN ($C_{24}H_{18}N_2O$) in *Chlamydomonas reinhardtii*. Cells were cultured in Treatment 4: MBL, (-) N_2 , (-) Ca^{2+} , (+) sodium acetate (2.0 g/L) (24 h light condition). Bright-field image: a; Fluorescence images - 2-DPAN: b, Chlorophyll: c; Merged image: d. Images were taken with Zeiss LSM 880 Airyscan confocal microscope.

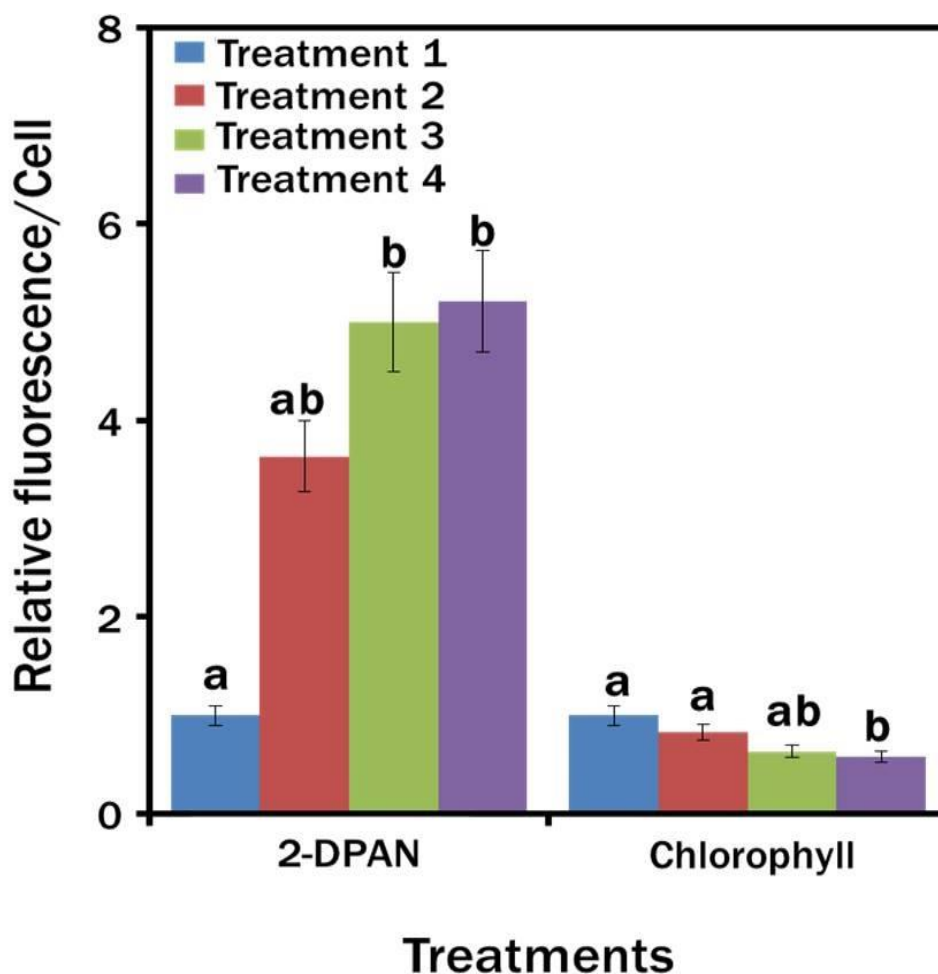


Fig. 3.19 Confocal analysis of *Chlamydomonas reinhardtii* for relative fluorescence intensity/cell for different treatments. Cells were cultured in Treatment 1: modified Woods Hole (MBL) medium; Treatment 2: MBL, (-) N₂; Treatment 3: MBL, (-) N₂, (-) Ca²⁺; and Treatment 4: MBL, (-) N₂, (-) Ca²⁺, (+) sodium acetate (2.0 g/L) (all the treatments were in 24 h light condition). Values are relative to the control condition (Treatment 1: modified Cramer-Myers medium (MCM)). Averages are shown as mean ± SE.

The present study results suggested that 2-DPAN had reasonable lipid specificity and higher sensitivity and penetration abilities to complex carbohydrate cell walls containing microalgae, *C. reinhardtii*. It was also evident that without washing, the fluorescence intensity of the BODIPY dye reached outside the meaningful range of the spectrometer (Fig. 3.7), whereas almost no difference in the PL intensities was observed between the wash and

wash-free samples with AIE probes, DPAS and 2-DPAN (Figs. 3.7b and 3.7c). Furthermore, confocal images of the wash-free BODIPY samples also showed photobleaching of the samples (Fig. 3.8). Therefore, the photostable properties of AIE molecules, wash free and easy sample preparation techniques could make these AIE probes superior to traditional BODIPY™ 505/515 dye for rapid visualization and quick screening of lipid inducing conditions in microalgae.

3.4.9 H_2O_2 content in the *Chlamydomonas reinhardtii* cells

ROS has been associated with increased metabolite production in microalgae, and high levels of H_2O_2 inside the microalgal cells have been observed in stress conditions (Anand et al., 2021). In this experiment, we have determined the amount of H_2O_2 in lipid-induced *C. reinhardtii* cells. It was apparent that a maximum amount of 38.57 μM H_2O_2 was produced in 1 g of fresh microalgal cells of Treatment 4, where the maximum lipid was produced. Compared to the 6.38 μM H_2O_2/g of fresh microalgal cells of Treatment 1, about 3.2 and 3.8 fold rise in H_2O_2 production was found in the cells of Treatment 2 and Treatment 3, respectively (Fig. 3.20).

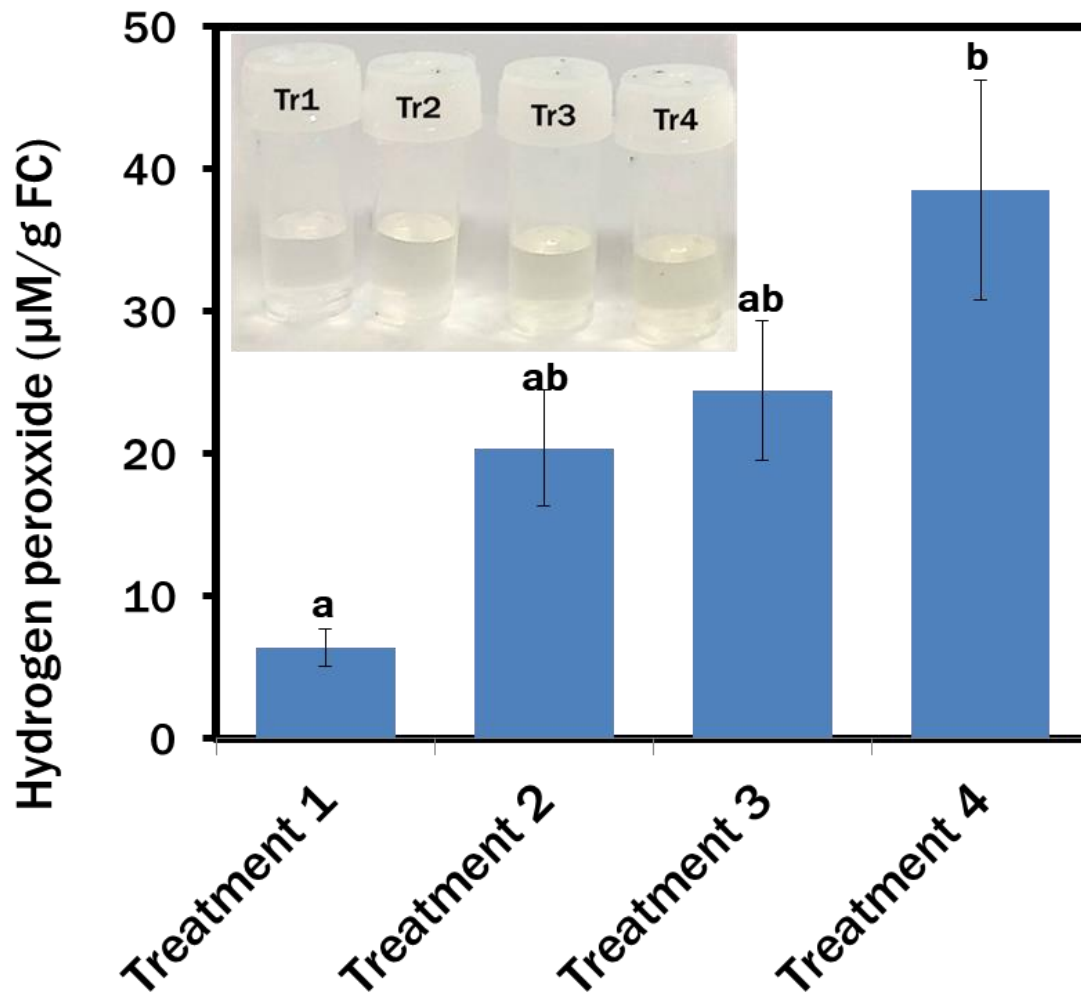


Fig. 3.20 Hydrogen peroxide content in the *Chlamydomonas reinhardtii* cells of different treatments. Treatment 1: modified Woods Hole (MBL) medium; Treatment 2: MBL, (-) N₂; Treatment 3: MBL, (-) N₂, (-) Ca²⁺; Treatment 4: MBL, (-) N₂, (-) Ca²⁺, (+) sodium acetate (2.0 g/L) (all the treatments were in 24 h light condition). Inset showing the colorimetric change in the reaction products due to the presence of H₂O₂ in the *C. reinhardtii* cells of different treatments. Data are represented as mean ± SE, n = 3.

3.4.10 Fatty acid analysis

Altering the cultural conditions significantly increased the total fatty acid (TFA) content in the *C. reinhardtii* cells. Among the nutrient altered conditions, the maximum amount of TFA (~11% of DW) was found in the cells of Treatment 3 (MBL, (-) N₂, (-) Ca²⁺) and Treatment 4 (MBL, (-) N₂, (-) Ca²⁺, (+) sodium acetate (2.0 g/L)) that was followed by the 8.4% TFA content of Treatment 2 (MBL, (-) N₂). Conversely, the lowest TFA content of 6.7% was observed in the cells cultured in the controlled condition of Treatment 1 (MBL medium) (Fig. 3.21).

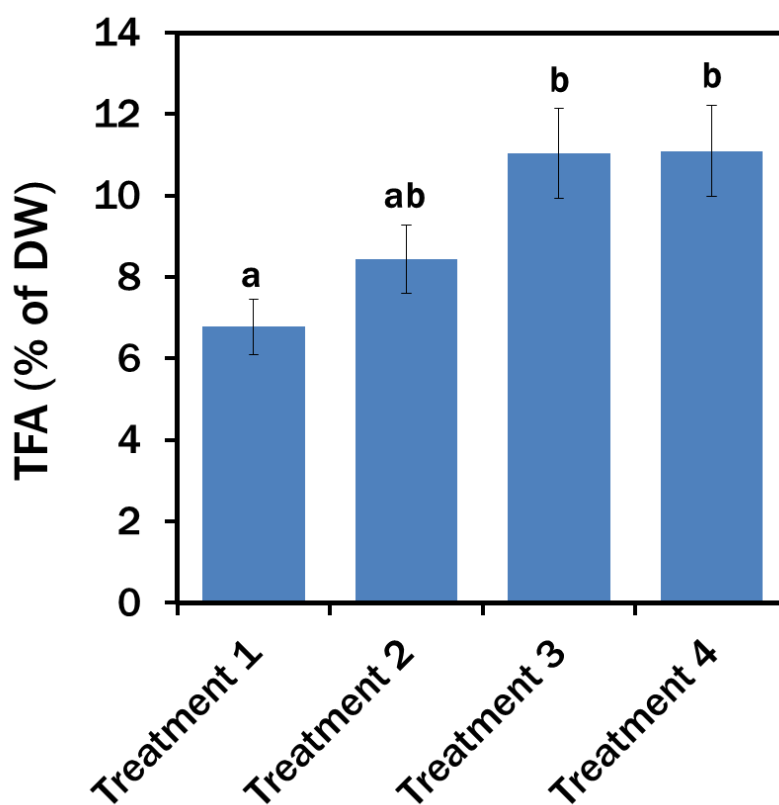


Fig. 3.21 Total fatty acid contents in different treatments. Cells were cultured in Treatment 1: modified Woods Hole (MBL) medium; Treatment 2: MBL, (-) N₂; Treatment 3: MBL, (-) N₂, (-) Ca²⁺; Treatment 4: MBL, (-) N₂, (-) Ca²⁺, (+) sodium acetate (2.0 g/L) (all the treatments were in 24 h light condition). Data are represented as mean ± SE, n = 3.

Almost the same trend in the rise of PUFAs was observed in the lipid-induced *C. reinhardtii* cells (Table 3.1). The PUFAs content was found maximum 55.2% in Treatment 4 (MBL, (-) N₂, (-) Ca²⁺, (+) sodium acetate (2.0 g/L)), which was 17.8% higher than Treatment 1 (MBL medium). Production of PUFAs also increased to 48.9% in the cells of Treatment 3 (MBL, (-) N₂, (-) Ca²⁺). Cells, cultured in the nutrient-enriched condition of Treatment 1 produced the maximum amount of SAFAs (~51.6%). Among the PUFAs, α -linolenic acid (ALA) was the most abundant in the lipid-induced conditions of Treatment 3 and Treatment 4, while the nutrient-enriched control condition of Treatment 1 showed the lowest production of ALA. The amount of linoleic acid found was almost similar in all the treatments. In all the treatments, the most abundant SAFA was palmitic acid (C16:0), with a maximum production of ~43.7% in Treatment 1.

Table 3.1 Percentage of FAMES in *Chlamydomonas reinhardtii* cells under different cultural conditions.

Percentage of FAMES	Treatments			
	Treatment 1	Treatment 2	Treatment 3	Treatment 4
C4:0	1.29 ±0.18	1.25±0.17	1.01±0.01	0.91±0.15
C12:0	0.22 ±0.02	0.21±0.03	0.17±0.01	0.15±0.03
C13:0	0.16 ±0.042	--*	--*	--*
C14:0	0.87 ±0.07	0.96±0.05	0.53±0.01	0.25±0.35
C14:1 N-5	0.12±0.01	0.12±0.01	0.15±0.01	0.11±.01
C15:0	0.42±0.03	0.45±0.06	0.26±0.01	0.32±0.03
C16:0	43.66±1.05	41.10±0.70	37.0±1.28	33.60±0.22
C16:1 N-7	0.98±0.03	2.01±0.03	1.27±0.22	0.71±0.03
C17:0	0.95±0.13	0.92±0.13	0.75±0.01	0.71±0.08
C17:1 N-7	1.79±0.03	2.37±0.08	2.22±0.05	2.19±0.26
C18:0	2.30±0.03	2.47±0.01	1.70±0.17	1.32±0.19
C18:1 N-9	5.70±0.78	6.45±1.68	3.06±0.11	1.77±0.23
C18:2 N-6,9	18.91±0.09	14.13±1.97	12.84±0.60	8.84±0.18
C18:3 N-3,6,9	17.75±1.53	23.79±2.47	35.19±2.50	46.05±2.31
C20:0	0.89±0.10	0.87±0.11	0.63±0.01	0.57±0.10
C20:1 N-9	0.41±0.03	0.39±0.04	0.31±0.01	0.15±0.22

C20:2 N-6,9	0.42±0.08	--*	0.16±0.23	--*
C20:3 N-6,9,12	--*	--*	--*	0.17±0.240
C21:0	0.33±0.04	0.32±0.05	0.12±0.18	0.10±0.14
C20:4 N-6,9,12,15	0.48±0.10	--*	--*	--*
C20:3 N-3,6,9	--*	--*	0.35±0.01	--*
C20:5 N-3,6,9,12,15	0.21±0.30	0.15±0.21	0.15±0.21	--*
C22:0	0.42±0.35	0.41±0.03	0.33±0.01	0.29±0.05
C22:1 N-9	1.39±0.17	1.43±0.02	1.55±0.25	1.53±0.69
C22:2 N-6,9	0.12±0.14	0.05±0.07	0.10±0.01	0.05±0.08
C22:4 N-6,9,12,15	--*	--*	--*	0.06±0.08
C24:0	0.08±0.01	0.09±0.01	0.03±0.01	0.03±0.01
C22:6 N-3,6,9,12,15,18	0.06±0.01	--*	0.06±0.08	0.04±0.06
C24:1 N-9	0.04±0.01	0.01±0.01	--*	0.01±0.01
SAFAs	51.61±12.41	49.07±11.68	42.55±10.55	38.27±9.59
MUFAs	10.44±1.97	12.80±2.24	8.58±1.15	6.49±0.89
PUFAs	37.42±8.04	38.13±8.69	48.86±11.92	55.22±11.25

***Not detected.**

3.5 Discussion

Although the current levels of lipid research are extremely promising, many research questions are still pending (Chen & Wang, 2021). Many aspects of lipid biosynthesis in microalgae differ among species due to evolutionary diversity and complex regulatory pathways of lipid metabolism (Liu & Benning, 2013). Significant differences in lipid accumulation have been observed in the same species under the same assay conditions (Siaut et al., 2011). Therefore, deliberate identification of the lipid-inducing conditions, screening, and selecting suitable candidates are the keys to progress in microalgal lipid research. In this study, using AIE-based techniques, the lipid-inducing conditions have been identified in a carbohydrates-based cell wall containing microalga, *C. reinhardtii*. With a lipid-specific AIE probe, 2-DPAN, the impact of different nutrient starvation, carbon source and light on lipid bioaccumulation and fatty acid composition in this algal species have been determined. As a

messenger molecule and stress marker, the H₂O₂ content in the cells under different conditions have also been determined.

The results showed the importance of the light, nitrogen and supplemented carbon sources for the growth and lipid biosynthesis in *C. reinhardtii*. Regarding the nutrient-enriched condition, lipid production in the nutrient-starved cells significantly increased, whereas cell growth decreased. The dark condition could not induce lipid synthesis in the nutrient-starved cells. Nitrogen starvation increased lipid production, but supplementation of sodium acetate as the primary carbon source in nitrogen starved cells showed a marked increase in lipid biosynthesis. This possibly happened due to the redirection of the metabolic pathway of acetate towards fatty acid biosynthesis instead of acting as the cellular building block precursors through the glyoxylate cycle and gluconeogenesis (Miller et al., 2010). All the nitrogen starved conditions showed decreased chlorophyll content. To adjust the altered cellular metabolism and changed energy content of the cells during nutrient limitation, downregulation of the protein synthesis and photosynthetic apparatus might occur (Miller et al., 2010, López García de Lomana et al., 2015). Simultaneously, chlorophyll can be served as the internal nitrogen reserve during nutrient starvation, while their reduction can decrease the light uptake to minimize the accumulation of excessive ROS (Miller et al., 2010).

While excessive ROS could be lethal for the cells, a certain level can act as the secondary messengers in various signal transduction mechanisms, including lipid biosynthesis (Shi et al., 2017, Reza et al., 2021). Among all ROS components, H₂O₂ can easily pass across the phospholipid bilayer via the aquaporins (Reczek & Chandel, 2015), and as a key signalling molecule interact with receptor proteins and redox-sensitive transcriptional factors (Mittler, 2002; Smirnov & Arnaud, 2019). Correlation among H₂O₂-induced lipid accumulation, enhanced calcium (Ca²⁺)-ATPase and glutathione activity has been evident in microalgae from previous studies (Sun et al., 2018a; Qiao et al., 2021; Zhang et al., 2017). Higher lipid

production in *C. reinhardtii* cells during N₂ and Ca²⁺ starvation in this study is possibly due to the modulation of H₂O₂ and Ca²⁺ pathways, which is also evident from the increased H₂O₂ levels in the lipid-induced cells. H₂O₂ perhaps triggered Ca²⁺ signals and transferred the extracellular stimuli to the algal cells to regulate the response mechanisms further. At the point of Ca²⁺ deficiency in the culture media, intracellular Ca²⁺ stores maintained the cytosolic Ca²⁺ levels (Chen et al., 2014). During nutrient starvation, photosynthesis continues while the membrane component synthesis is reduced. Therefore, biosynthesis of the fatty acids occurs (Sharma et al., 2012). Generally, photosynthesis generates ATP and NADPH for cell growth and proliferation. While the *C. reinhardtii* cells are starved by the nutrients, growth decreases, and NADPH is utilized for FA synthesis (Hu et al., 2018; Gorain et al., 2013).

This study has found novel, rapid and wash-free strategies *in vivo* to visualize LDs and H₂O₂ in *C. reinhardtii* using AIE-based fluorophores. With the increase in water fraction from 50% to 90% in DMSO, the PL intensity of 2-DPAN significantly increased due to the AIE properties and the formation of the insoluble nanoaggregates 2-DPAN in the aqueous media (Hong et al., 2009). Successful labelling of LDs with AIEgens, DPAS and 2-DPAN in *C. reinhardtii* cells has been visualized from the confocal images, whereas complete co-localization with the traditional BODIPY dye has been observed in this study. Therefore, it appears that penetration of the AIE fluorophore, DPAS and 2-DPAN is not hindered by the complex carbohydrate-based cell wall structure of this algal species. The structure of the lipid-specific AIE probes with negatively charged oxygen atoms attached to the electron acceptor carbonyl group perhaps makes lipid-specific AIE probes hydrophobic (Wang et al., 2014). Additionally, the cheap raw material benzophenone to synthesize the keto-salicylaldehyde hydrazine (KSA) derivatives, DPAS, and 2-DPAN are also hydrophobic to increase the hydrophobicity of these AIE probes (Wang et al., 2016, Li et al., 2019). Being

uniquely constituted hydrophobic structures among different organelles, LDs allow these nanofluorophores to strongly target and accumulate inside these organelles. Upon aggregation, KSA forms six-membered ring structures that subsequently restrict the intramolecular motion and increase the fluorescence. Additionally, the presence of KSA retains some hydrophilic ability and enhances the probe efficiency to enter the cells and successfully label the target molecules (Li et al., 2019; Hu et al., 2018; Wang et al., 2016). Furthermore, confocal images of the *C. reinhardtii* cells in this study revealed the superior performance of 2-DPAN to the BODIPY and DPAS, which is possibly due to the presence of 2-naphthalene group in 2-DPAN that can enhance the luminous efficiency of this AIE probe (Li et al., 2019).

This study also demonstrated a relatively easy and rapid application method of AIEgens compared to the traditional dye, BODIPY. Using DPAS and 2-DPAN required fewer steps than the BODIPY, whereas no significant differences in the PL intensities were observed between the wash and wash-free samples with the AIE probes. Conversely, BODIPY dye showed unacceptable results and photobleaching in the wash-free samples. The dye acquisition techniques with the traditional probes, regardless of BODIPY and Nile Red, require utmost care. Using lower concentrations of these commercial probes can cause self-decomposition, while slightly higher concentration or lower-level competencies during washing steps might result in marked background signals. Having the AIE properties, DPAS and 2-DPAN are free from these limitations. Furthermore, both AIEgens were biocompatible at much higher concentrations since no negative impact on the growth of *C. reinhardtii* was observed even after exposure to 100 μ M of DPAS and 2-DPAN. Moreover, a previous study suggests that BODIPY can lose 90% of the signals at 2% laser power energy under confocal microscopy within 5 min of irradiation, whereas no change in the fluorescence intensity of DPAS is observed even after 60 min of continuous scanning (Wang et al., 2016). BODIPY

can also unselectively label the mitochondria and nuclear membranes (Daemen et al., 2015). Additionally, the non-fluorogenic nature of BODIPY can produce more background signals, while limited photostability with a slight Stokes shift can cause self-absorption of this traditional dye (Collot et al., 2018). Another study also demonstrates that under 99% laser density, Nile Red can lose more than 95% signal after 20 min and 60 min scans, while the fluorescent intensity of 2-DPAN remains unaffected (Li et al., 2019). Therefore, these studies indicate stronger photostability of DPAS and 2-DPAN than the traditional fluorophores, BODIPY and Nile Red. It also appears that DPAS and 2-DPAN do not interfere with the red channel of chlorophyll autofluorescence or the green channel of BODIPY dye. In addition, a wash-free, rapid and easy experimental procedure allows *in vivo* detection of LDs and H₂O₂ under the same assay condition. The current study signifies the effectiveness of these AIEgens as a multicolour visualizing tool for the target molecules in microalgae.

FAs can affect human health and well-being by directly and indirectly associating cellular functions like tissue metabolism, bioactive lipid mediators production, membrane structure regulation, function, transcription factor activity, intracellular signalling pathways, and gene expression. The effects of saturated fatty acids (SAFAs), monounsaturated fatty acids (MUFAs), and PUFAs are distinct. Thus, the FAs classes influence a range of diseases, including cardiovascular disease, metabolic disorder, type 2 diabetes, inflammatory diseases, and cancer (Calder, 2013, Sokoła-Wysoczańska et al., 2018). As desaturases and elongases enzymes in humans are scarce, *de novo* synthesis of essential ω -3 and ω -6 PUFA families could be declined over time and in certain diseases (Khozin-Goldberg et al., 2011; Molfino et al., 2014; Lukiw & Bazan, 2008). Hence, dietary supplementation of essential PUFAs is crucial to reducing the risk factors for different diseases (Freitas & Campos, 2019; Avallone et al., 2019). In this experiment, the FA profile of *C. reinhardtii* consisted of a range of SAFAs, MUFAs and PUFAs, whereas palmitic acid, linoleic acid, and α -linolenic acids were

predominant. As *Chlamydomonas* and higher plants retain the same ancestry (Merchant et al., 2007), the FA composition of *Chlamydomonas* is almost similar to that of higher plants like *Arabidopsis thaliana* (Li-Beisson et al., 2015). However, cultural conditions can significantly affect FAs content and composition in microalgae (Castilla Casadiego et al., 2016), which is also evident in this experiment as lipid-induced conditions of Treatment 3 (MBL, (-) N₂, (-) Ca²⁺) and Treatment 4 (MBL, (-) N₂, (-) Ca²⁺, (+) sodium acetate (2.0 g/L)) produced more α -linolenic acid (ALA) than the control group (MBL medium).

As an essential fatty acid, the beneficiary effects of ALA have been suggested by previous studies since it could have anti-inflammatory (Stark et al., 2008; Zhao et al., 2004), anti-arrhythmic (Albert et al., 2005), anti-thrombotic (Albert et al., 2005; Campos et al., 2008), and neuroprotective effects (Nguemeni et al., 2010) in humans. Other prospective studies suggest the positive effects of ALA intake on fatal coronary heart disease (CHD) and gene programming to prevent metabolic diseases and promote health in offspring (Hu et al., 1999; Leikin-Frenkel, 2016; de Lorgeril, 2004). ALA is easier to burn by the body than palmitic, stearic, oleic, or linoleic acid. Therefore, ALA is expected to induce fat utilization as energy and reduce obesity (Saito et al., 2016). In a study on adult males and females, ingestion of 2.6 g/day ALA reduces systolic and diastolic blood pressure without any negative impact on oxidation or blood coagulation (Takeuchi et al., 2007). Moreover, ALA can also be converted into eicosapentaenoic acid (EPA) and docosahexaenoic acid (DHA). EPA can be utilized to improve conditions like asthma and atopic diseases. Additionally, as the building block precursors of prostaglandins, leukotrienes, tromboxanes, and lipoxines, EPA also plays important roles in different bio-physiological processes (Koto et al., 2007; Fussbroich et al., 2020). DHA can support cell membrane and signalling, specifically in the brain and retina, allowing improved visual activities, immunity, and cognitive functions in humans (Sun et al., 2018b; Guesnet & Alessandri, 2011). However, the conversion occurs to a limited extent,

lower for DHA than EPA, and found to be higher in women than men (Brenna & D'haeseleer, 2007; Burdge & Calder, 2005). As the lipid-inducing conditions in this study produced more ALA, the results showed more promises to increase the availability of this biofunctional component from a green microalga, *C. reinhardtii*.

3.6 Conclusion

This study identified the lipid-inducing conditions in *C. reinhardtii* as the source of health beneficiary metabolites. H₂O₂ in the cells of this microalga has also been detected as the messenger molecules and stress biomarker. A rapid, wash-free and multicolor imaging technique to visualize LDs in *C. reinhardtii* with AIE-based bioprobes has also been established in this study. These AIE probes are cheap, biocompatible and convenient for high contrast visualization of LDs in an *in situ* condition. Due to the AIE properties, these probes surpassed the performances of the traditional fluorophores through increased photostability, reduced background noise and aggregation-caused quenching problems. The AIE probes were able to efficiently localize the LDs and H₂O₂ by penetrating the complex carbohydrate-based cell wall of *C. reinhardtii*. As reliable and easy bioimaging tools, these probes are more auspicious to identify the optimum lipid production conditions at early cultural stages in microalgae, which would be more cost-effective, time-saving, and labour-efficient. This study has discovered cultural conditions that could produce more health beneficiary α -linolenic acid, which is important for preventing life-threatening heart diseases in humans. This new technique would significantly ease microalgal lipid research. However, more studies focusing on other cell types, such as diatoms with silica cell walls, are recommended for further assurance of the reliability of this probe for other microalgae species further to broaden the horizon of these probes for biological research.

3.7 References

- Albert, C. M., Oh, K., Whang, W., Manson, J. E., Chae, C. U., Stampfer, M. J., Willett, W. C., & Hu, F. B. (2005). Dietary alpha-linolenic acid intake and risk of sudden cardiac death and coronary heart disease. *Circulation*, *112*(21), 3232-3238. <https://doi.org/10.1161/CIRCULATIONAHA.105.572008>
- Alishah Aratboni, H., Rafiei, N., Garcia-Granados, R., Alemzadeh, A., & Morones-Ramírez, J. R. (2019). Biomass and lipid induction strategies in microalgae for biofuel production and other applications. *Microbial Cell Factories*, *18*(1), 178. <https://doi.org/10.1186/s12934-019-1228-4>
- Almaraz-Delgado, A. L., Flores-Uribe, J., Pérez-España, V. H., Salgado-Manjarrez, E., & Badillo-Corona, J. A. (2014). Production of therapeutic proteins in the chloroplast of *Chlamydomonas reinhardtii*. *AMB Express*, *4*, 57. <https://doi.org/10.1186/s13568-014-0057-4>
- Anand, V., Kashyap, M., Ghosh, A., Samadhiya, K., & Kiran, B. (2021). A strategy for lipid production in *Scenedesmus* sp. by multiple stresses induction. *Biomass Conversion and Biorefinery*, 1-11. <https://doi.org/10.1007/s13399-021-01392-2>.
- Avallone, R., Vitale, G., & Bertolotti, M. (2019). Omega-3 fatty acids and neurodegenerative diseases: New evidence in clinical trials. *International Journal of Molecular Sciences*, *20*(17), 4256. <https://doi.org/10.3390/ijms20174256>
- Brenna, J. T., & Diau, G. Y. (2007). The influence of dietary docosahexaenoic acid and arachidonic acid on central nervous system polyunsaturated fatty acid composition. *Prostaglandins, Leukotrienes, and Essential Fatty Acids*, *77*(5-6), 247-250. <https://doi.org/10.1016/j.plefa.2007.10.016>

Bligh, E. G., & Dyer W. J. (1959). A rapid method of total lipid extraction and purification. *Canadian Journal of Biochemistry and Physiology*, 37(8), 911-917. <https://doi.org/10.1139/o59-099>

Burdge, G. C., & Calder, P. C. (2005). Conversion of alpha-linolenic acid to longer-chain polyunsaturated fatty acids in human adults. *Reproduction, Nutrition, Development*, 45(5), 581-597. <https://doi.org/10.1051/rnd:2005047>

Calder P. C. (2013). Omega-3 polyunsaturated fatty acids and inflammatory processes: nutrition or pharmacology?. *British Journal of Clinical Pharmacology*, 75(3), 645-662. <https://doi.org/10.1111/j.1365-2125.2012.04374.x>

Campos, H., Baylin, A., & Willett, W. C. (2008). Alpha-linolenic acid and risk of nonfatal acute myocardial infarction. *Circulation*, 118(4), 339-345. <https://doi.org/10.1161/CIRCULATIONAHA.107.762419>

Castilla Casadiego, D. A., Albis Arrieta, A. R., Angulo Mercado, E. R., Cervera Cahuana, S. J., Baquero Noriega, K. S., Suárez Escobar, A. F., & Morales Avendaño, E. D. (2016). Evaluation of culture conditions to obtain fatty acids from saline microalgae species: *Dunaliella salina*, *Sinecosyfis* sp., and *Chroomonas* sp. *BioMed Research International*, 5081653. <https://doi.org/10.1155/2016/5081653>

Castro, L. F., Tocher, D. R., & Monroig, O. (2016). Long-chain polyunsaturated fatty acid biosynthesis in chordates: Insights into the evolution of Fads and Elovl gene repertoire. *Progress in Lipid Research*, 62, 25-40. <https://doi.org/10.1016/j.plipres.2016.01.001>

Chen, H., & Wang, Q. (2021). Regulatory mechanisms of lipid biosynthesis in microalgae. *Biological reviews of the Cambridge Philosophical Society*, 96(5), 2373-2391. <https://doi.org/10.1111/brv.12759>

Chen, H., Zhang, Y., He, C., & Wang, Q. (2014). Ca²⁺ signal transduction related to neutral lipid synthesis in an oil-producing green alga *Chlorella* sp. C2. *Plant & Cell Physiology*, 55(3), 634-644. <https://doi.org/10.1093/pcp/pcu015>

Chokshi, K., Pancha, I., Ghosh, A., & Mishra, S. (2017). Nitrogen starvation-induced cellular crosstalk of ROS-scavenging antioxidants and phytohormone enhanced the biofuel potential of green microalga *Acutodesmus dimorphus*. *Biotechnology for Biofuels*, 10, 60. <https://doi.org/10.1186/s13068-017-0747-7>

Christie, W. W. (1993). "Preparation of ester derivatives of fatty acids for chromatographic analysis." *Advances in Lipid Methodology*, 2, 69, e111.

Coelho, O., da Silva, B. P., Rocha, D., Lopes, L. L., & Alfenas, R. (2017). Polyunsaturated fatty acids and type 2 diabetes: Impact on the glycemic control mechanism. *Critical Reviews in Food Science and Nutrition*, 57(17), 3614-3619. <https://doi.org/10.1080/10408398.2015.1130016>

Collot, M., Fam, T. K., Ashokkumar, P., Faklaris, O., Galli, T., Danglot, L., & Klymchenko, A. S. (2018). Ultrabright and fluorogenic probes for multicolor imaging and tracking of lipid droplets in cells and tissues. *Journal of the American Chemical Society*, 140(16), 5401-5411. <https://doi.org/10.1021/jacs.7b12817>

Cooper, M. S., Hardin, W. R., Petersen, T. W., & Cattolico, R. A. (2010). Visualizing "green oil" in live algal cells. *Journal of Bioscience and Bioengineering*, 109(2), 198-201. <https://doi.org/10.1016/j.jbiosc.2009.08.004>

- Daemen, S., van Zandvoort, M., Parekh, S. H., & Hesselink, M. (2015). Microscopy tools for the investigation of intracellular lipid storage and dynamics. *Molecular Metabolism*, 5(3), 153-163. <https://doi.org/10.1016/j.molmet.2015.12.005>
- de Carvalho, C., & Caramujo, M. J. (2018). The various roles of fatty acids. *Molecules (Basel, Switzerland)*, 23(10), 2583. <https://doi.org/10.3390/molecules23102583>
- de Lorgeril, M., & Salen, P. (2004). Alpha-linolenic acid and coronary heart disease. *Nutrition, Metabolism, and Cardiovascular Diseases: NMCD*, 14(3), 162-169. [https://doi.org/10.1016/s0939-4753\(04\)80037-1](https://doi.org/10.1016/s0939-4753(04)80037-1)
- Demirbas, A., & Demirbas, M. (2011). Importance of algae oil as a source of biodiesel. *Energy Conversion and Management*, 52, 163-170. <https://doi.org/10.1016/j.enconman.2010.06.0555>
- Dong, H. P., Williams, E., Wang, D. Z., Xie, Z. X., Hsia, R. C., Jenck, A., Halden, R., Li, J., Chen, F., & Place, A. R. (2013). Responses of *Nannochloropsis oceanica* IMET1 to long-term nitrogen starvation and recovery. *Plant Physiology*, 162(2), 1110-1126. <https://doi.org/10.1104/pp.113.214320>
- Du, Z. Y., Hoffmann-Benning, S., Wang, S., Yin, L., Zienkiewicz, A., & Zienkiewicz, K. (2021). Editorial: Lipid metabolism in development and environmental stress tolerance for engineering agronomic traits. *Frontiers in Plant Science*, 12, 739786. <https://doi.org/10.3389/fpls.2021.739786>
- Fasano, E., Serini, S., Cittadini, A., & Calviello, G. (2017). Long-chain n-3 PUFA against breast and prostate cancer: Which are the appropriate doses for intervention studies in animals and humans?. *Critical Reviews in Food Science and Nutrition*, 57(11), 2245-2262. <https://doi.org/10.1080/10408398.2013.850060>

- Freitas, R., & Campos, M. M. (2019). Protective Effects of Omega-3 Fatty Acids in Cancer-Related Complications. *Nutrients*, *11*(5), 945. <https://doi.org/10.3390/nu11050945>
- Fussbroich, D., Colas, R. A., Eickmeier, O., Trischler, J., Jerkic, S. P., Zimmermann, K., Göpel, A., Schwenger, T., Schaible, A., Henrich, D., Baer, P., Zielen, S., Dalli, J., Beermann, C., & Schubert, R. (2020). A combination of LCPUFA ameliorates airway inflammation in asthmatic mice by promoting pro-resolving effects and reducing adverse effects of EPA. *Mucosal Immunology*, *13*(3), 481-492. <https://doi.org/10.1038/s41385-019-0245-2>
- Goodenough, U., Blaby, I., Casero, D., Gallaher, S. D., Goodson, C., Johnson, S., Lee, J. H., Merchant, S. S., Pellegrini, M., Roth, R., Rusch, J., Singh, M., Umen, J. G., Weiss, T. L., & Wulan, T. (2014). The path to triacylglyceride obesity in the sta6 strain of *Chlamydomonas reinhardtii*. *Eukaryotic Cell*, *13*(5), 591-613. <https://doi.org/10.1128/EC.00013-14>
- Goncalves, E. C., Wilkie, A. C., Kirst, M., & Rathinasabapathi, B. (2016). Metabolic regulation of triacylglycerol accumulation in the green algae: identification of potential targets for engineering to improve oil yield. *Plant Biotechnology Journal*, *14*(8), 1649-1660. <https://doi.org/10.1111/pbi.12523>
- Gorain, P. C., Bagchi, S. K., & Mallick, N. (2013). Effects of calcium, magnesium and sodium chloride in enhancing lipid accumulation in two green microalgae. *Environmental Technology*, *34*(13-16), 1887-1894. <https://doi.org/10.1080/09593330.2013.812668>
- Guesnet, P., & Alessandri, J. M. (2011). Docosahexaenoic acid (DHA) and the developing central nervous system (CNS) - Implications for dietary recommendations. *Biochimie*, *93*(1), 7-12. <https://doi.org/10.1016/j.biochi.2010.05.005>
- Harwood, J. L., & Guschina, I. A. (2009). The versatility of algae and their lipid metabolism. *Biochimie*, *91*(6), 679-684. <https://doi.org/10.1016/j.biochi.2008.11.004>

Haskew-Layton, R. E., Payappilly, J. B., Smirnova, N. A., Ma, T. C., Chan, K. K., Murphy, T. H., Guo, H., Langley, B., Sultana, R., Butterfield, D. A., Santagata, S., Alldred, M. J., Gazaryan, I. G., Bell, G. W., Ginsberg, S. D., & Ratan, R. R. (2010). Controlled enzymatic production of astrocytic hydrogen peroxide protects neurons from oxidative stress via an Nrf2-independent pathway. *Proceedings of the National Academy of Sciences of the United States of America*, *107*(40), 17385-17390. <https://doi.org/10.1073/pnas.1003996107>

Hoham, R. W., Bonome, T. A., Martin, C. W. & Leebens-mack, J. H. (2002). A combined 18S rDNA and rbcL phylogenetic analysis of *Chloromonas* and *Chlamydomonas* (Chlorophyceae, Volvocales) emphasizing snow and other cold-temperature habitats. *Journal of Phycology*, *38*(5), 1051-1064. <https://doi.org/10.1046/j.1529-8817.2002.t01-1-01227.x>

Hong, Y., Lam, J. W., & Tang, B. Z. (2009). Aggregation-induced emission: phenomenon, mechanism and applications. *Chemical Communications (Cambridge, England)*, *29*, 4332-4353. <https://doi.org/10.1039/b904665h>

Hu, R., Zhou, F., Zhou, T., Shen, J., Wang, Z., Zhao, Z., Qin, A., & Tang, B. Z. (2018). Specific discrimination of gram-positive bacteria and direct visualization of its infection towards mammalian cells by a DPAN-based AIEgen. *Biomaterials*, *187*, 47-54. <https://doi.org/10.1016/j.biomaterials.2018.09.019>

Hu, Q., Sommerfeld, M., Jarvis, E., Ghirardi, M., Posewitz, M., Seibert, M., & Darzins, A. (2008). Microalgal triacylglycerols as feedstocks for biofuel production: perspectives and advances. *The Plant Journal : for Cell and Molecular Biology*, *54*(4), 621-639. <https://doi.org/10.1111/j.1365-313X.2008.03492.x>

Hu, F. B., Stampfer, M. J., Manson, J. E., Rimm, E. B., Wolk, A., Colditz, G. A., Hennekens, C. H., & Willett, W. C. (1999). Dietary intake of alpha-linolenic acid and risk of fatal

ischemic heart disease among women. *The American Journal of Clinical Nutrition*, 69(5), 890-897. <https://doi.org/10.1093/ajcn/69.5.890>

Imam, S. H., Buchanan, M. J., Shin, H. C., & Snell, W. J. (1985). The *Chlamydomonas* cell wall: characterization of the wall framework. *The Journal of Cell Biology*, 101(4), 1599-1607. <https://doi.org/10.1083/jcb.101.4.1599>

Khozin-Goldberg, I., Iskandarov, U., & Cohen, Z. (2011). LC-PUFA from photosynthetic microalgae: occurrence, biosynthesis, and prospects in biotechnology. *Applied Microbiology and Biotechnology*, 91(4), 905-915. <https://doi.org/10.1007/s00253-011-3441-x>

Koto, T., Nagai, N., Mochimaru, H., Kurihara, T., Izumi-Nagai, K., Satofuka, S., Shinoda, H., Noda, K., Ozawa, Y., Inoue, M., Tsubota, K., Oike, Y., & Ishida, S. (2007). Eicosapentaenoic acid is anti-inflammatory in preventing choroidal neovascularization in mice. *Investigative Ophthalmology & Visual Science*, 48(9), 4328-4334. <https://doi.org/10.1167/iovs.06-1148>

Lee, J. M., Lee, H., Kang, S., & Park, W. J. (2016). Fatty acid desaturases, polyunsaturated fatty acid regulation, and biotechnological advances. *Nutrients*, 8(1), 23. <https://doi.org/10.3390/nu8010023>

Leikin-Frenkel A. I. (2016). Is there a role for alpha-linolenic acid in the fetal programming of health?. *Journal of Clinical Medicine*, 5(4), 40. <https://doi.org/10.3390/jcm5040040>

Leonard, A. E., Pereira, S. L., Sprecher, H., & Huang, Y. S. (2004). Elongation of long-chain fatty acids. *Progress in Lipid Research*, 43(1), 36-54. [https://doi.org/10.1016/s0163-7827\(03\)00040-7](https://doi.org/10.1016/s0163-7827(03)00040-7)

- Leung, N.L., Xie, N., Yuan, W., Liu, Y., Wu, Q., Peng, Q., Miao, Q., Lam, J. W., & Tang, B. Z. (2014). Restriction of intramolecular motions: the general mechanism behind aggregation-induced emission. *Chemistry*, *20*, 15349-15353. <https://doi.org/10.1002/chem.201403811>.
- Li, L., Zhou, F., Gao, Q., Lu, Y., Xu, X., Hu, R., Wang, Z., Peng, M., Yang, Z., & Tang, B. Z. (2019). Visualizing dynamic performance of lipid droplets in a Parkinson's disease model via a smart photostable aggregation-induced emission probe. *iScience*, *21*, 261-272. <https://doi.org/10.1016/j.isci.2019.10.027>
- Li-Beisson, Y., Beisson, F., & Riekhof, W. (2015). Metabolism of acyl-lipids in *Chlamydomonas reinhardtii*. *The Plant Journal : for Cell and Molecular Biology*, *82*(3), 504-522. <https://doi.org/10.1111/tpj.12787>
- Liu, B., & Benning, C. (2013). Lipid metabolism in microalgae distinguishes itself. *Current Opinion in Biotechnology*, *24*(2), 300-309. <https://doi.org/10.1016/j.copbio.2012.08.008>
- López García de Lomana, A., Schäuble, S., Valenzuela, J., Imam, S., Carter, W., Bilgin, D. D., Yohn, C. B., Turkarslan, S., Reiss, D. J., Orellana, M. V., Price, N. D., & Baliga, N. S. (2015). Transcriptional program for nitrogen starvation-induced lipid accumulation in *Chlamydomonas reinhardtii*. *Biotechnology for Biofuels*, *8*, 207. <https://doi.org/10.1186/s13068-015-0391-z>
- Lukiw, W. J., & Bazan, N. G. (2008). Docosahexaenoic acid and the aging brain. *The Journal of Nutrition*, *138*(12), 2510-2514. <https://doi.org/10.3945/jn.108.096016>
- Merchant, S. S., Prochnik, S. E., Vallon, O., Harris, E. H., Karpowicz, S. J., Witman, G. B., Terry, A., Salamov, A., Fritz-Laylin, L. K., Maréchal-Drouard, L., Marshall, W. F., Qu, L. H., Nelson, D. R., Sanderfoot, A. A., Spalding, M. H., Kapitonov, V. V., Ren, Q., Ferris, P., Lindquist, E., Shapiro, H., ... Grossman, A. R. (2007). The *Chlamydomonas* genome reveals

the evolution of key animal and plant functions. *Science (New York, N.Y.)*, 318(5848), 245-250. <https://doi.org/10.1126/science.1143609>

Miller, R., Wu, G., Deshpande, R. R., Vieler, A., Gärtner, K., Li, X., Moellering, E. R., Zäuner, S., Cornish, A. J., Liu, B., Bullard, B., Sears, B. B., Kuo, M. H., Hegg, E. L., Shachar-Hill, Y., Shiu, S. H., & Benning, C. (2010). Changes in transcript abundance in *Chlamydomonas reinhardtii* following nitrogen deprivation predict diversion of metabolism. *Plant Physiology*, 154(4), 1737-1752. <https://doi.org/10.1104/pp.110.165159>

Miller, E. W., Tulyathan, O., Isacoff, E. Y., & Chang, C. J. (2007). Molecular imaging of hydrogen peroxide produced for cell signaling. *Nature Chemical Biology*, 3(5), 263-267. <https://doi.org/10.1038/nchembio871>

Mittler R. (2002). Oxidative stress, antioxidants and stress tolerance. *Trends in Plant Science*, 7(9), 405-410. [https://doi.org/10.1016/s1360-1385\(02\)02312-9](https://doi.org/10.1016/s1360-1385(02)02312-9)

Molfino, A., Gioia, G., Rossi Fanelli, F., & Muscaritoli, M. (2014). The role for dietary omega-3 fatty acids supplementation in older adults. *Nutrients*, 6(10), 4058-4073. <https://doi.org/10.3390/nu6104058>

Morales, M., Aflalo, C., & Bernard, O. (2021). Microalgal lipids: A review of lipids potential and quantification for 95 phytoplankton species. *Biomass and Bioenergy*, 150, 106108. <https://doi.org/10.1016/j.biombioe.2021.106108>

Nguemeni, C., Delplanque, B., Rovère, C., Simon-Rousseau, N., Gandin, C., Agnani, G., Nahon, J. L., Heurteaux, C., & Blondeau, N. (2010). Dietary supplementation of alpha-linolenic acid in an enriched rapeseed oil diet protects from stroke. *Pharmacological Research*, 61(3), 226-233. <https://doi.org/10.1016/j.phrs.2009.12.007>

Nichols, H. W. (1973) in *Handbook of Phycological Methods*, Ed. J. R. Stein, pp. 16-17. Camb. Univ. Press. (R. R. L. Guillard, personal communication).

Niethammer, P., Grabher, C., Look, A. T., & Mitchison, T. J. (2009). A tissue-scale gradient of hydrogen peroxide mediates rapid wound detection in zebrafish. *Nature*, *459*(7249), 996-999. <https://doi.org/10.1038/nature08119>

Oresic, M., Hänninen, V. A., & Vidal-Puig, A. (2008). Lipidomics: a new window to biomedical frontiers. *Trends in Biotechnology*, *26*(12), 647-652. <https://doi.org/10.1016/j.tibtech.2008.09.001>

Qiao, T., Zhao, Y., Zhao, Y., Zhong, D., & Yu., X. (2021). Hydrogen peroxide and salinity stress act synergistically to enhance lipids production in microalga by regulating reactive oxygen species and calcium. *Algal Research*, *53*, 102017. <https://doi.org/10.1016/j.algal.2020.102017>.

Qian, J., & Tang B. Z. (2017). AIE luminogens for bioimaging and theranostics: from organelles to animals. *Chem*, *3*(1), 56-91 <https://doi.org/10.1016/j.chempr.2017.05.010>

Rasala, B. A., & Mayfield, S. P. (2015). Photosynthetic biomanufacturing in green algae; production of recombinant proteins for industrial, nutritional, and medical uses. *Photosynthesis Research*, *123*(3), 227-239. <https://doi.org/10.1007/s11120-014-9994-7>

Reczek, C. R., & Chandel, N. S. (2015). ROS-dependent signal transduction. *Current opinion in cell biology*, *33*, 8-13. <https://doi.org/10.1016/j.ceb.2014.09.010>

Reza, A. H. M. M., Zhu, X., Qin, J., & Tang, Y. (2021). Microalgae-derived health supplements to therapeutic shifts: Redox-based study opportunities with AIE-based technologies. *Advanced Healthcare Materials*, *10*(24), e2101223. <https://doi.org/10.1002/adhm.202101223>

- Reza, A. H. M. M., Zhou, Y., Tavakoli, J., Tang, Y., & Qin, J. (2021). Understanding the lipid production mechanism in *Euglena gracilis* with a fast-response AIEgen bioprobe, DPAS. *Materials Chemistry Frontiers*, 5, 268. <https://doi.org/10.1039/D0QM00621A>
- Rumin, J., Bonnefond, H., Saint-Jean, B., Rouxel, C., Sciandra, A., Bernard, O., Cadoret, J. P., & Bougaran, G. (2015). The use of fluorescent Nile red and BODIPY for lipid measurement in microalgae. *Biotechnology for Biofuels*, 8, 42. <https://doi.org/10.1186/s13068-015-0220-4>
- Saito, S., Fukuhara, I., Osaki, N., Nakamura, H., & Katsuragi, Y. (2016). Consumption of alpha-linolenic acid-enriched diacylglycerol reduces visceral fat area in overweight and obese subjects: a randomized, double-blind controlled, parallel-group designed trial. *Journal of Oleo Science*, 65(7), 603-611. <https://doi.org/10.5650/jos.ess16059>
- Schieber, M., & Chandel, N. S. (2014). ROS function in redox signaling and oxidative stress. *Current Biology : CB*, 24(10), R453-R462. <https://doi.org/10.1016/j.cub.2014.03.034>
- Schneider, C. A., Rasband, W. S., & Eliceiri, K. W. (2012). NIH Image to ImageJ: 25 years of image analysis. *Nature Methods*, 9(7), 671-675. <https://doi.org/10.1038/nmeth.2089>
- Shahidi, F., & Ambigaipalan, P. (2018). Omega-3 Polyunsaturated Fatty Acids and Their Health Benefits. *Annual Review of Food Science and Tchnology*, 9, 345-381. <https://doi.org/10.1146/annurev-food-111317-095850>
- Sharma, K. K., Schuhmann, H., & Schenk, P. M. (2012). High lipid induction in microalgae for biodiesel production, *Energies*, 5, 1532-1553. <https://doi.org/10.3390/en5051532>.
- Shi, K., Gao, Z., Shi, T. Q., Song, P., Ren, L. J., Huang, H., & Ji, X. J. (2017). Reactive Oxygen Species-mediated cellular stress response and lipid accumulation in oleaginous

microorganisms: The state of the art and future perspectives. *Frontiers in Microbiology*, 8, 793. <https://doi.org/10.3389/fmicb.2017.00793>

Siaut, M., Cuiné, S., Cagnon, C., Fessler, B., Nguyen, M., Carrier, P., Beyly, A., Beisson, F., Triantaphylidès, C., Li-Beisson, Y., & Peltier, G. (2011). Oil accumulation in the model green alga *Chlamydomonas reinhardtii*: characterization, variability between common laboratory strains and relationship with starch reserves. *BMC Biotechnology*, 11, 7. <https://doi.org/10.1186/1472-6750-11-7>

Sivaramakrishnan, R., & Incharoensakdi, A. (2017). Enhancement of lipid production in *Scenedesmus* sp. by UV mutagenesis and hydrogen peroxide treatment. *Bioresource Technology*, 235, 366-370. <https://doi.org/10.1016/j.biortech.2017.03.102>

Smirnoff, N., & Arnaud, D. (2019). Hydrogen peroxide metabolism and functions in plants. *The New Phytologist*, 221(3), 1197-1214. <https://doi.org/10.1111/nph.15488>

Smith, G. M. (1955). *Cryptogamic Botany Volume 1. Algae and Fungi* McGraw-Hill Book Company Inc.

Sokoła-Wysoczańska, E., Wysoczański, T., Wagner, J., Czyż, K., Bodkowski, R., Lochyński, S., & Patkowska-Sokoła, B. (2018). Polyunsaturated fatty acids and their potential therapeutic role in cardiovascular system disorders-A review. *Nutrients*, 10(10), 1561. <https://doi.org/10.3390/nu10101561>

Stark, A. H., Crawford, M. A., & Reifen, R. (2008). Update on alpha-linolenic acid. *Nutrition Reviews*, 66(6), 326-332. <https://doi.org/10.1111/j.1753-4887.2008.00040.x>

Sun, X. M., Ren, L. J., Zhao, Q. Y., Ji, X. J., & Huang, H. (2018a). Microalgae for the production of lipid and carotenoids: a review with focus on stress regulation and adaptation. *Biotechnology for Biofuels*, 11, 272. <https://doi.org/10.1186/s13068-018-1275-9>

Sun, G. Y., Simonyi, A., Fritsche, K. L., Chuang, D. Y., Hannink, M., Gu, Z., Greenlief, C. M., Yao, J. K., Lee, J. C., & Beversdorf, D. Q. (2018b). Docosahexaenoic acid (DHA): An essential nutrient and a nutraceutical for brain health and diseases. *Prostaglandins, Leukotrienes, and Essential Fatty Acids*, *136*, 3-13. <https://doi.org/10.1016/j.plefa.2017.03.006>

Takeuchi, H., Sakurai, C., Noda, R., Sekine, S., Murano, Y., Wanaka, K., Kasai, M., Watanabe, S., Aoyama, T., & Kondo, K. (2007). Antihypertensive effect and safety of dietary alpha-linolenic acid in subjects with high-normal blood pressure and mild hypertension. *Journal of Oleo Science*, *56*(7), 347-360. <https://doi.org/10.5650/jos.56.347>

Wang, Z., Gui, C., Zhao, E., Wang, J., Li, X., Qin, A., Zhao, Z., Yu, Z., & Tang, B. Z. (2016). Specific fluorescence probes for lipid droplets based on simple. *ACS Applied Materials & Interfaces*, *8*(16), 10193-10200. <https://doi.org/10.1021/acsami.6b01282>

Wang, E., Zhao, E., , Hong, Y., , Lam, J., , & Tang, B. Z. (2014). A highly selective AIE fluorogen for lipid droplet imaging in live cells and green algae. *Journal of Materials Chemistry. B*, *2*(14), 2013-2019. <https://doi.org/10.1039/c3tb21675f>

Wang, Z. T., Ullrich, N., Joo, S., Waffenschmidt, S., & Goodenough, U. (2009). Algal lipid bodies: stress induction, purification, and biochemical characterization in wild-type and starchless *Chlamydomonas reinhardtii*. *Eukaryotic Cell*, *8*(12), 1856-1868. <https://doi.org/10.1128/EC.00272-09>

Wu, Y., & Qu, J. Y. (2006). Autofluorescence spectroscopy of epithelial tissues. *Journal of Biomedical Optics*, *11*(5), 054023. <https://doi.org/10.1117/1.2362741>

- Xu, L., Cheng, X., & Wang, Q. (2018). Enhanced lipid production in *Chlamydomonas reinhardtii* by co-culturing with *Azotobacter chroococcum*. *Frontiers in Plant Science*, 9, 741. <https://doi.org/10.3389/fpls.2018.00741>
- Yilancioglu, K., Cokol, M., Pastirmaci, I., Erman, B., & Cetiner, S. (2014). Oxidative stress is a mediator for increased lipid accumulation in a newly isolated *Dunaliella salina* strain. *PloS one*, 9(3), e91957. <https://doi.org/10.1371/journal.pone.0091957>
- You, Z., Zhang, Q., Peng, Z., & Miao, X. (2019). Lipid Droplets Mediate Salt Stress Tolerance in *Parachlorella kessleri*. *Plant Physiology*, 181(2), 510-526. <https://doi.org/10.1104/pp.19.00666>
- Yu, S. J., Kang, M. W., Chang, H. C., Chen, K. M., & Yu, Y. C. (2005). Bright fluorescent nanodiamonds: no photobleaching and low cytotoxicity. *Journal of the American Chemical Society*, 127(50), 17604-17605. <https://doi.org/10.1021/ja0567081>
- Zhang, X., Tang, X., Wang, M., Zhang, W., Zhou, B., & Wang, Y. (2017). ROS and calcium signaling mediated pathways involved in stress responses of the marine microalgae *Dunaliella salina* to enhanced UV-B radiation. *Journal of Photochemistry and Photobiology. B, Biology*, 173, 360-367. <https://doi.org/10.1016/j.jphotobiol.2017.05.038>
- Zhang, J., Wang, X., Vikash, V., Ye, Q., Wu, D., Liu, Y., & Dong, W. (2016). ROS and ROS-mediated cellular signaling. *Oxidative Medicine and Cellular Longevity*, 2016, 4350965. <https://doi.org/10.1155/2016/4350965>
- Zhang, T., Ma, H., Niu, Y., Li, W., Wang, D., Peng, Q., Shuai, Z., & Liang, W. (2015). Spectroscopic signature of the aggregation-induced emission phenomena caused by restricted nonradiative decay: A theoretical proposal. *The Journal of Physical Chemistry C*, 119(9), 5040-5047 <https://doi.org/10.1021/acs.jpcc.5b01323>.

Zhao, G., Etherton, T. D., Martin, K. R., West, S. G., Gillies, P. J., & Kris-Etherton, P. M. (2004). Dietary alpha-linolenic acid reduces inflammatory and lipid cardiovascular risk factors in hypercholesterolemic men and women. *The Journal of Nutrition*, *134*(11), 2991-2997. <https://doi.org/10.1093/jn/134.11.2991>

**Chapter 4: Supplementation of H₂O₂ to the Medium
Enhanced Lipid Accumulation in Microalgae: Visualizing
Lipid Drops with a Novel Fluorescent Probe**

4.1 Abstract

Stress-based strategies are a common practice to induce the production of lipid drops (LDs) in microalgae. However, due to the impacts of stressors on biomass accumulation, these techniques have not reached their full potential. Apprehending the causes and effects of lipid induction strategies can increase the effectiveness of microalgal lipid production. As a messenger molecule and stress marker, this study determined the H₂O₂ activity during lipid induction in a green alga *Chlamydomonas reinhardtii*. As a new technique for rapid *in vivo* detection of H₂O₂ activity, a new H₂O₂-specific AIEgen, TPE-BO (C₃₈H₄₂B₂O₄) was used. The effects of different concentrations of H₂O₂ supplementation on lipid accumulation in *C. reinhardtii* cells in the MBL medium were analyzed with a lipid specific AIE probe, 2-DPAN. The growth of the *C. reinhardtii* was not affected by the supplementation of 0.4 mM and 0.6 mM H₂O₂ compared to the control. Lipid production and health beneficiary α -linolenic acid were induced in H₂O₂ supplemented cells. In the confocal images, more H₂O₂ activities were visualized in lipid-induced cells during cell division, autophagic cells, and cell death. This study reports a novel strategy of a wash free, biocompatible, photostable, multicolour imaging technique to detect H₂O₂ activities during lipid biosynthesis in *C. reinhardtii*.

Keywords

α -linolenic acid; *Chlamydomonas reinhardtii*; Hydrogen peroxide; Lipid drops; TPE-BO

4.2 Introduction

Over the last few decades, microalgae have been considered promising for the biosynthesis of valuable metabolites (Henley, 2019). The stress-based strategies are widely used to induce the production of biofunctional components. However, due to the adverse effects of stressors on biomass accumulation, their commercial exploitation has not reached its full potential (Mutanda et al., 2020). Therefore, optimization of the algal biomass during the production of the biofunctional components is a challenge in algal research (Ruiz et al., 2016). Among different stress strategies, starvation by the essential nutrients, alteration of light, temperature, salinity, and chemical treatments are commonly practised (Shi et al., 2020). Knowing the stressors that trigger principal metabolic steps for the synthesis of value-added molecules would allow novel research to enhance the accumulation of those molecules. During stress, increased intracellular reactive oxygen species (ROS) activities change the metabolic flux from glycolysis to the oxidative pentose phosphate pathway and produce reducing powers, such as NADPH (Shi et al., 2017). Microalgae would produce more lipids than protein or carbohydrates to counter the stress effects on cells (Shi et al., 2020). Increasing evidence also suggests that ROS, as the secondary messenger, is associated with the change in transcriptome, proteome, and metabolome during lipid accumulation (Shi et al., 2017). H_2O_2 is relatively more stable among ROS molecules and can cross through the phospholipid bilayer to intervene in many complex biological systems (Reczek and Chandel, 2015; Niethammer et al., 2009). A controlled surge in H_2O_2 production can improve cell functioning. Therefore, it is a concurrent focus to determine the cellular signal transduction mechanisms (Haskew-Layton et al., 2010; Miller et al., 2007).

An insight into the ROS mediated mechanisms during the biosynthesis of valuable metabolites can guide choosing the appropriate stress conditions in microalgae. However, a proper tool is a prerequisite for pursuing this study. Among different techniques, such as

spectrophotometry (Hayashi et al., 2007), chemiluminescent techniques (Kim et al., 2019), chromatography (Vaneev et al., 2020), electron spin resonance (D'Errico et al., 2018), and fluorescent-dependent methods, *in vivo* fluorescence-based imaging is relatively non-invasive and time-saving and allows temporal and spatial analysis of ROS molecules. Among commercially available ROS-specific probes (Reza et al., 2021), H₂DCFDA (2',7'-dichlorodihydrofluorescein diacetate) (Wang and Joseph, 1999) and its derivatives, dihydroethidium (DHE) (Wang and Zou, 2018) and Amplex Red (Karakuzu et al., 2019) are generally used to measure the intracellular redox states. However, the short lifetime, the ROS species' high reactivity, and the slow responsiveness of the ROS-specific traditional fluorophores make their efficient utilization challenging in the biological environment (Prasad et al., 2019).

Amplex Red is relatively stable among the ROS targeting dyes and shows specificity to the H₂O₂ in horseradish peroxidase (HRP). However, cellular reduced glutathione and NADPH can react with HRP and generate additional H₂O₂. The presence of ONOO⁻ could also induce the catalysis of HRP and lead to a false impression about H₂O₂ content in the cell (Dębski et al., 2016). The lower cell membrane affinity could also impede the precision of H₂O₂ measurement (Dikalov et al., 2007) and decrease fluorescence due to reducing resorufin by NADPH-CYP450 reductases (Votyakova and Reynolds, 2004). Additionally, the aggregation-caused quenching (ACQ) phenomenon makes the dye acquisition techniques challenging for the traditional fluorophores (Yu et al., 2005; Collot et al., 2018). Recent nanotechnologies advancements have introduced some AIE-based phosphorescent probes for *in vivo* bioimaging of H₂O₂ (Reza et al., 2021). Among these dyes, TPE-BO (C₃₈H₄₂B₂O₄) is a well-designed probe with the increased polarity of C-B bonds to be selective for H₂O₂. TPE-BO has been reported suitable for long-term, high contrast imaging of H₂O₂ in animal cells. Furthermore, the incorporation of AIE-based nanoparticles has improved the

photostability of this probe (Zhang et al., 2015). However, the labelling efficiency of this probe needs to be established in all types of cell walls in microalgae.

In Chapter 3, the increased levels of H₂O₂ have been detected in the lipid-induced *C. reinhardtii* cells during nutrient starvation. This chapter aims to adopt a new technique for an in-depth investigation to understand the H₂O₂-activities as the messenger molecule and stress marker in nutrient-starved cells with H₂O₂-specific AIEgen, TPE-BO. Furthermore, the effects of direct H₂O₂ supplementation on the lipid production in *C. reinhardtii* was investigated. This study has reported an AIE-based technique for *in vivo* analysis of H₂O₂ activities during lipid enrichment in microalgal cells containing a carbohydrate-based cell wall.

4.3 Materials and methods

4.3.1 Microalga cultivation and lipid induction

The culture of the *C. reinhardtii* was established in 500 mL Erlenmeyer flasks containing 250 mL (autoclaved at 121 °C for 5 min) of Woods Hole (MBL). The nutrient content of the culture medium was (1 L distilled water): CaCl₂·2H₂O (0.04 g), MgSO₄·7H₂O (0.04 g), NaHCO₃ (0.01 g), K₂HPO₄ (0.008 g), NaNO₃ (0.08 g), EDTA-Na₂ (0.004 g), FeCl₃·6H₂O (0.004 g), CuSO₄·5H₂O (0.01 mg), ZnSO₄·7H₂O (0.02 g), CoCl₂·6H₂O (0.01 mg), MnCl₂·4H₂O (0.02 mg), Na₂MoO₄·2H₂O (0.006 mg), C₆₃H₈₈CoN₁₄O₁₄P (vitamin B₁₂) (0.0005 mg), C₁₂H₁₇ClN₄OS·HCl (vitamin B₁) (0.1 mg), C₁₀H₁₆N₂O₃S (biotin) (0.0005 mg), C₄H₁₁NO₃, (tris(hydroxymethyl)aminomethane) (0.25 g) (pH: 7.2) (Nichols, 1973). The culture was then maintained at 25 °C in a temperature-controlled room under continuous light and rotation (70 μmol photons per m⁻² s⁻¹; 100 rpm). All the reagents were obtained from Thermo Fisher Scientific, Australia.

For lipid induction, *C. reinhardtii* cells (0.3×10^6 cell/ml) were taken from the exponential growth phase and subsequently cultured for 8 days in nutrient-starved stress phases. Four treatments investigated were: (1) modified Woods Hole (MBL) medium, (2) MBL without nitrogen (-), (3) MBL without nitrogen (-) and calcium (-), (4) MCM without nitrogen (-) and calcium (-), but with sodium acetate (2.0 g/L) (+). To determine the effects of exogenous H_2O_2 application on growth and lipid accumulation in *C. reinhardtii*, cells were cultured in different H_2O_2 concentrations (0, 0.4, 0.6, 0.8 and 1.0 mM) supplemented with an MBL medium. Unless specified otherwise, all the experiments were performed in triplicate ($n = 3$).

4.3.2 Determination of algal growth in different concentrations of TPE-BO and H_2O_2

To determine the effects of AIEgens on *C. reinhardtii* growth, cells at the density of $1.0 \pm 0.015 (\times 10^4)$ cells / mL were introduced to different concentrations (10, 50, and 100 μ M) of TPEBO in the MBL medium under the previously described condition. Prior to studying the effects of H_2O_2 supplementation on lipid biosynthesis in *C. reinhardtii*, the algal growth at different concentrations of H_2O_2 was determined. $1.0 \pm 0.015 (\times 10^4)$ cells / mL were introduced to different concentrations (0 mM, 0.4 mM, 0.6 mM, 0.8 mM and 1.0 mM) of H_2O_2 . The experiment was conducted in the MBL medium and cultured under the previously described condition. To determine the H_2O_2 utilization by algal cells, $1.0 \pm 0.05 (\times 10^5)$ cells/ml were cultured in 0.4 and 0.6 mM H_2O_2 supplemented with the MBL medium up to 40 h. H_2O_2 concentration in the culture medium was determined colorimetrically as previously described. A control group without algal cells was set against each H_2O_2 concentration treatment, and the reduction rate of H_2O_2 content at each time point in the presence of algae was normalized against the values of the control groups. Cell growth was determined with a haemocytometer (Improved Marienfeld Neubauer, Germany) at regular intervals for up to 6 days.

4.3.3 Sample preparation for fluorescent staining of lipid and H₂O₂

To determine the lipid content in the algal cells of different treatments, a 1.0 mM stock solution of 2-DPAN was prepared and was stored in the dark at 4 °C. Fluorescence intensities were determined using the fluorescence spectrophotometer (Cary Eclipse, MY17180002, Agilent Technologies, CA, USA) with 1 cm path length quartz cuvettes. After adding 2-DPAN (20 µM), the samples were vortexed at 100 rpm for 30 sec and then stored in the dark for 30 min. The final concentration of the DMSO was adjusted to 0.1% for all the studies. For BODIPY™ 505/515 staining of LDs in flow cytometry, a stock solution of 1.0 mM BODIPY™ 505/515 in DMSO (Thermo Fisher Scientific Inc., Australia) was prepared and stored at -20 °C in the dark. Prior to use, the stock solution was diluted to 10 µM in DI water, and the final DMSO concentration was adjusted at 0.1% for each sample. Fluorometric quantification of the lipids was done according to the modified method of Cooper *et al.* (2010). Briefly, the cultured algae were adjusted at 10⁶ cells/ml, and the cells were collected by centrifugation at 2000 × g for 60 sec. Subsequently, the cells were resuspended in 200 µL DI water, gently mixed with 200 µL of the prepared 10 µM BODIPY™ 505/515 solution and incubated in the dark for 5 min. The cells were then washed three times with DI, followed by centrifugation at 2,000 × g for 60 sec to re-suspended in water. The stained cells were then protected from light for further analysis.

TPE-BO was synthesized at La Trobe University, Australia. The fluorescence intensity and H₂O₂ specificity of TPE-BO have been previously characterized by Zhang *et al.* (2015). To determine the H₂O₂ activity in *C. reinhardtii*, 1 mM stock solution of probe TPE-BO was prepared in DMSO and was stored at 4 °C in the dark. Consequently, cells were incubated with 100 µM TPE-BO for 15 min to determine the H₂O₂ activities. The final concentration of DMSO was adjusted to 0.1%. For fluorometric quantification of lipids and H₂O₂, algal cells were adjusted to 10⁶ cells/ml.

4.3.4 Imaging of *Chlamydomonas reinhardtii* with confocal microscope

The *C. reinhardtii* cells were imaged under a Zeiss LSM 880 Airyscan confocal microscope using ZEN 2.6 software (Carl Zeiss, Australia). The excitation and emission wavelength of 2-DPAN was 488 nm, and 526-570 nm, respectively. Excitation and emission wavelength for TPEBO were set at 405 nm, and 428-499 nm, respectively. Autofluorescence of the chlorophyll was detected with the excitation wavelength at 488 nm and emission wavelength of 685-758 nm.

4.3.5 Flow cytometric analysis of lipid content

Cytometric analysis was done using a flow cytometer (model CytoFLEX Flow Cytometer, Beckman Coulter, Inc. USA). Microalgae from different treatments were taken in three replicates and were stained with BODIPY™ 505/515 (5.0 µM) and 2-DPAN (20 µM) according to the previously described methods. FITC (488 nm laser) and KO525-A (405 nm laser) channels were used to detect the fluorescence from BODIPY™ 505/515 and 2-DPAN, respectively. The mean fluorescence intensity from a minimum of 10,000 cells per sample was acquired. Relative fluorescence was determined using the population cell percentile, with cells cultured in the MBL medium serving as the control.

4.3.6 Lipid extraction and analysis of fatty acids

The total lipid was extracted according to the adapted method of Bligh and Dyer (1959). Briefly, a sample volume was taken to provide approximately 500 mg of dry algal biomass from each growing *C. reinhardtii* culture. The supernatant was discarded after centrifugation at $10000 \times g$ and 4 °C for 10 min. The collected pellet was then washed three times with an equal volume of potassium phosphate buffer (pH: 7.2). Subsequently, the pellet was re-suspended in deionized water, transferred and weighed. Following that, the samples were

dried for 48 h at 60 °C, and were stored at -20 °C for further analysis. An approximate 50 mg of dried algal biomass was then taken into a pre-washed (with hexane) mortar. Using a Pasteur pipette, the weighing dish was washed with 1 ml of hexane to transfer the samples completely into the mortar. The algal biomass was then grounded into a fine, smooth paste using a pestle. During the grinding process, hexane was added to replenish the evaporated hexane, and the resulting slurry was mixed with the pestle until complete homogenization. All the process was done under the fume hood. After that, the homogenized hexane-cell mass mixture was centrifuged at $10,000 \times g$ (4 °C, 20 min), and the supernatant was collected in a pre-weighed vial. Following that, the pellet was resuspended with hexane (3 ml) by vigorous vortexing for 1 min and centrifuged at $10,000 \times g$ (4 °C, 30 min) to ensure the removal of all the cell debris. After complete evaporation of the hexane, the extracted oil mass was then determined gravimetrically. All the lipid extracts were stored at -20 °C for further analysis. Quantitative analysis of fatty acids was done with a Perkin Elmer GC-MS (Clarus 500 and 560S) using internal standards. Crude lipids were extracted from the sample using solvents. The lipids were transmethylated, and the profiles of different fatty acids were obtained with gas chromatography. Results were expressed as % of fatty acid methyl esters (Christie, 1998).

4.3.7 Data analysis

Data from the confocal microscopy were analyzed with ImageJ 1.52a (Schneider et al., 2012). Briefly, the raw images were exported in "tiff" format in ImageJ. Using "Sliding paraboloid", the background was subtracted from each image, and the fluorescence channel was calculated. Subsequently, "Area", "Mean grey value", "Integrated density", and "Area fraction" were determined. Fluorescence intensity per cell was then calculated to form the total cells by subtracting the background IntDen value from the IntDen value.

The flow cytometry data were analyzed using CytExpert v2.4 software and presented as histogram overlays. To detect BODIPY™ 505/515 labelled cells, samples were gated on FITC-A vs SSC-A. For DPAS and 2-DPAN, samples were gated on Violet610-A vs SSC-A, and KO525-A vs SSC-A, respectively. Confocal microscopy and flow cytometry data were exported to Excel 2010 to prepare the graphs. The means and medians of different treatments were compared by the relative fluorescence intensity of the gated population, with setting cells from the MBL medium as the control group. Data were analyzed by one-way analysis of variance (ANOVA) with SPSS statistics software (version 23). Specific differences in treatment means and multiple comparisons were tested at $P < 0.05$ level through Waller-Duncan post hoc and least significant difference (LSD) tests, respectively.

4.4 Results

4.4.1 Growth of Chlamydomonas reinhardtii in different concentrations of TPE-BO

The effects of different concentrations of H₂O₂-specific AIE probe, TPE-BO, on *C. reinhardtii* growth were monitored. In comparison with the control group, no significant difference was found in the growth pattern of algae even at a very high concentration of 100 µM of TPE-BO exposure, indicating the biocompatibility of this AIEgen (Fig. 4.1).

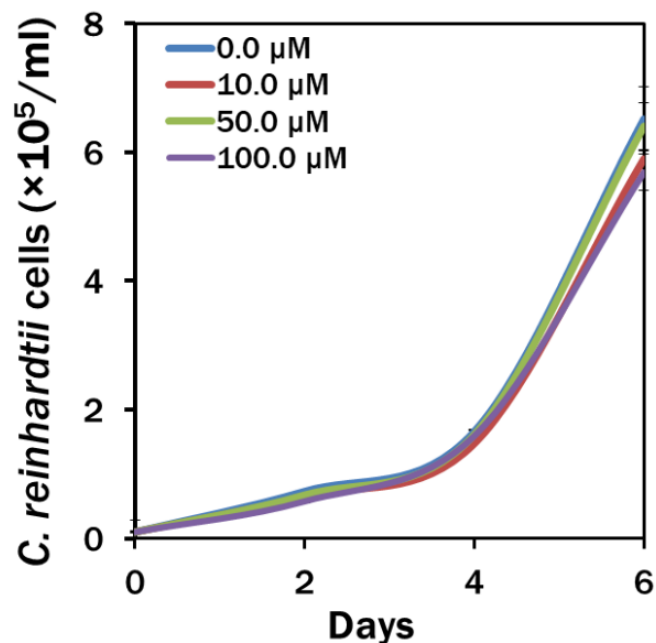


Fig. 4.1 Growth of *Chlamydomonas reinhardtii* in different concentrations of TPE-BO

4.4.2 Confocal analysis of H₂O₂ activity in nutrient-starved *Chlamydomonas reinhardtii* cells

H₂O₂-specific AIE probe, TPE-BO was used to check H₂O₂ in a microalga, *C. reinhardtii*, with a different cell membrane structure from that of the animal cell model (Zhang et al., 2015). In addition to the H₂O₂-specific AIE probe, TPE-BO AIE probe, 2-DPAN was used to label the LDs under the same assay condition that enabled the visualization of the H₂O₂ activities in the cells during lipid induction. From the confocal images, H₂O₂ activities were detected in all microalgae cells, whereas more activities were evident in the lipid accumulated (orange arrow) and autophagic cells (white arrow) (Figs. 4.2-4.5). It was apparent that with the increase of lipid production in the cells, H₂O₂ activities were increased. A 2.5 and 3.5 fold rise in H₂O₂ production was observed in Treatment 2 (Figs. 4.3 and 4.6) and Treatment 3 (Figs. 4.4 and 4.6), respectively, than that of Treatment 1 (Figs. 4.2 and 4.6). Compared to Treatment 1, a maximum of a 3.8 fold increase of H₂O₂ was found in Treatment 4, where the maximum lipid was biosynthesized (Figs. 4.5 and 4.6).

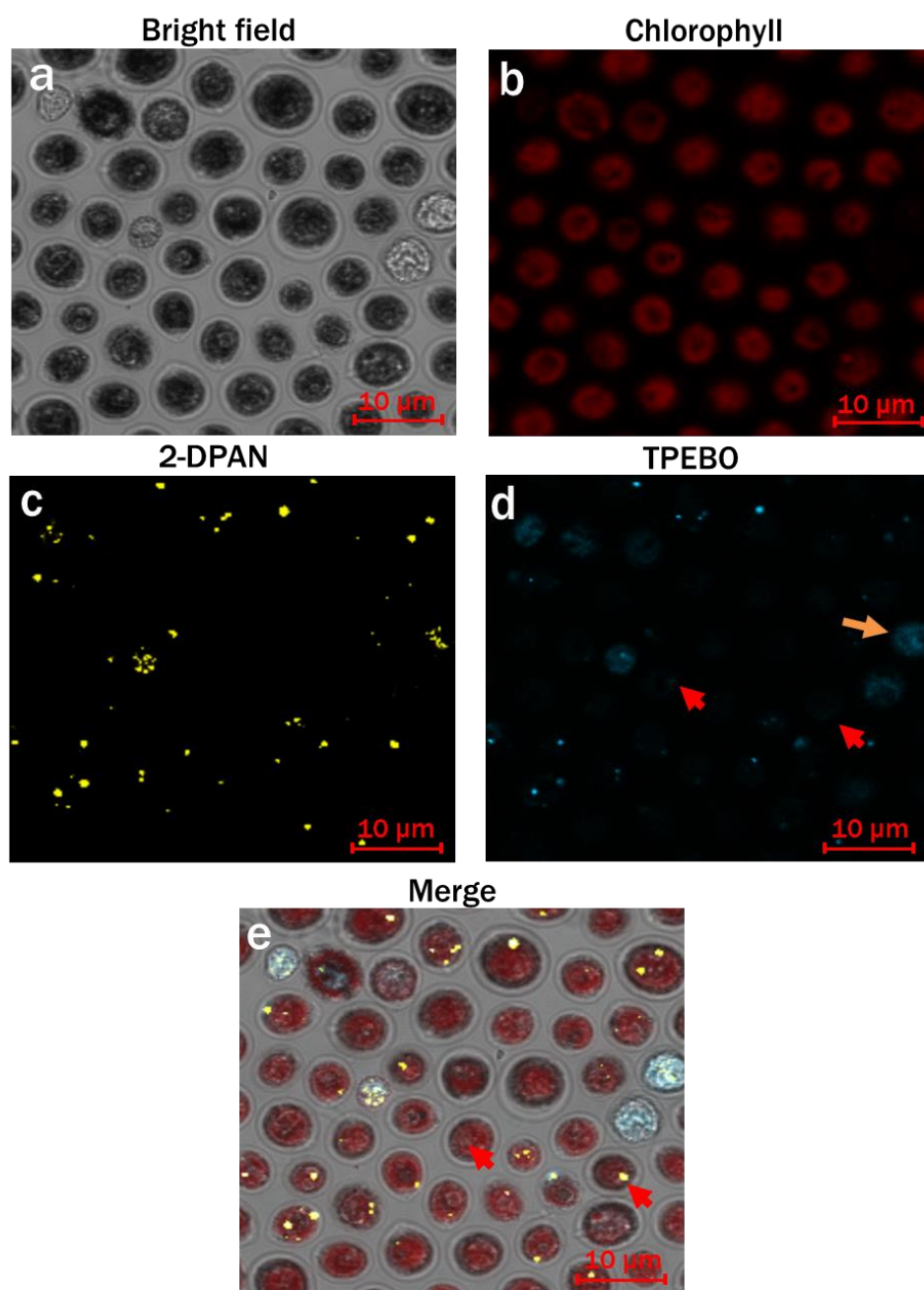


Fig. 4.2 Confocal images of H_2O_2 activities in *Chlamydomonas reinhardtii* cells during lipid induction. H_2O_2 and lipid drops were labelled with AIE-probes, TPE-BO and 2-DPAN, respectively. Cells were cultured in Treatment 1: modified Woods Hole (MBL) medium (24 h light condition). The red arrow indicates H_2O_2 activity in normal cells and during cell division. The orange arrow indicates H_2O_2 activity in lipid accumulated cells. Images were taken with a Zeiss LSM 880 Airyscan confocal microscope.

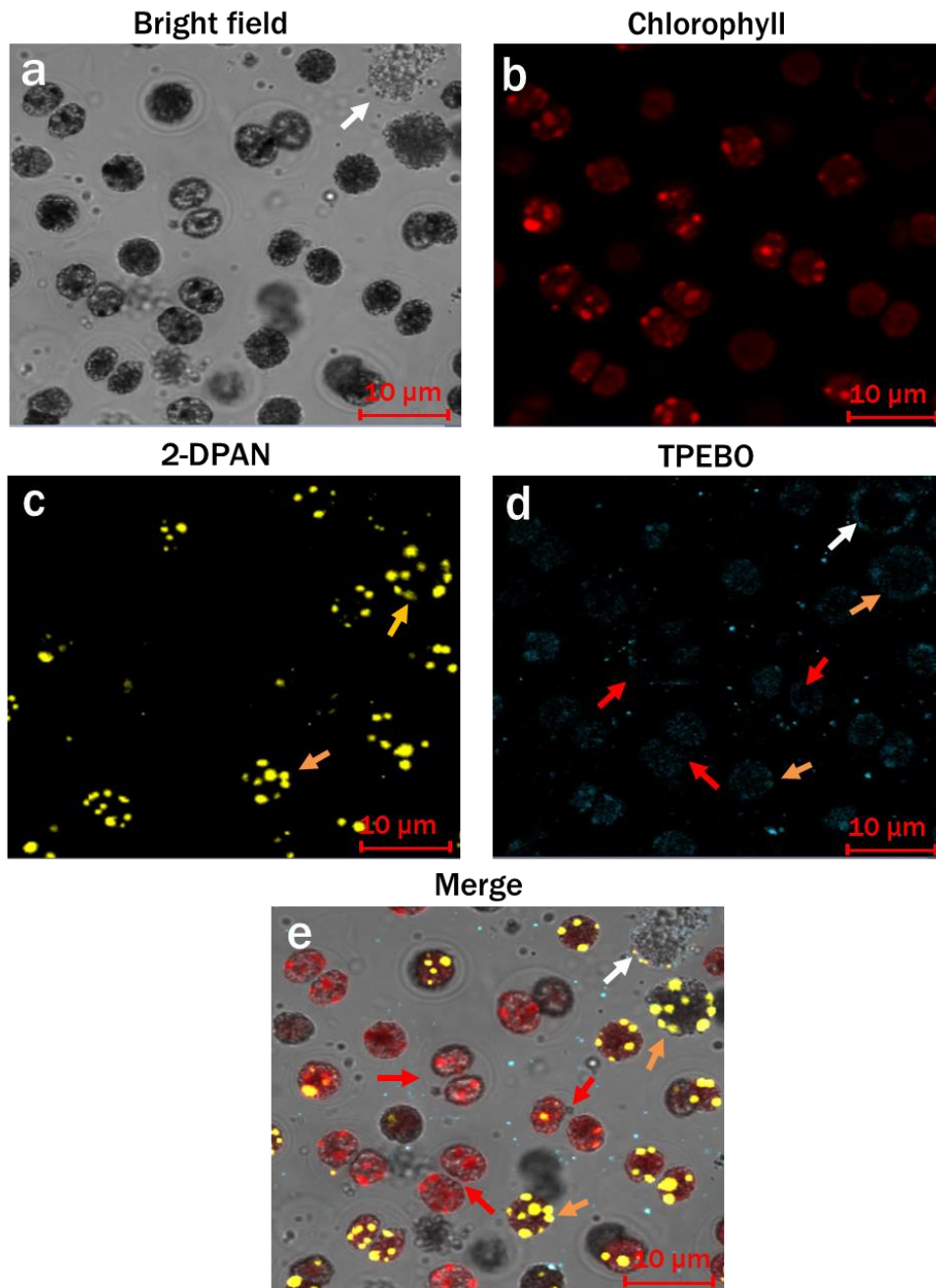


Fig. 4.3 Confocal images of H₂O₂ activities in *Chlamydomonas reinhardtii* cells during lipid induction. H₂O₂ and lipid drops were labelled with AIE-probes, TPE-BO and 2-DPAN, respectively. Cells were cultured in Treatment 2: MBL, (-) N₂ (24 h light condition. Red arrows indicate H₂O₂ activity in normal cells and during cell division. Orange arrows indicate H₂O₂ activity in lipid accumulated cells. White arrows indicate H₂O₂ activity in autophagic cells. Images were taken with a Zeiss LSM 880 Airyscan confocal microscope.

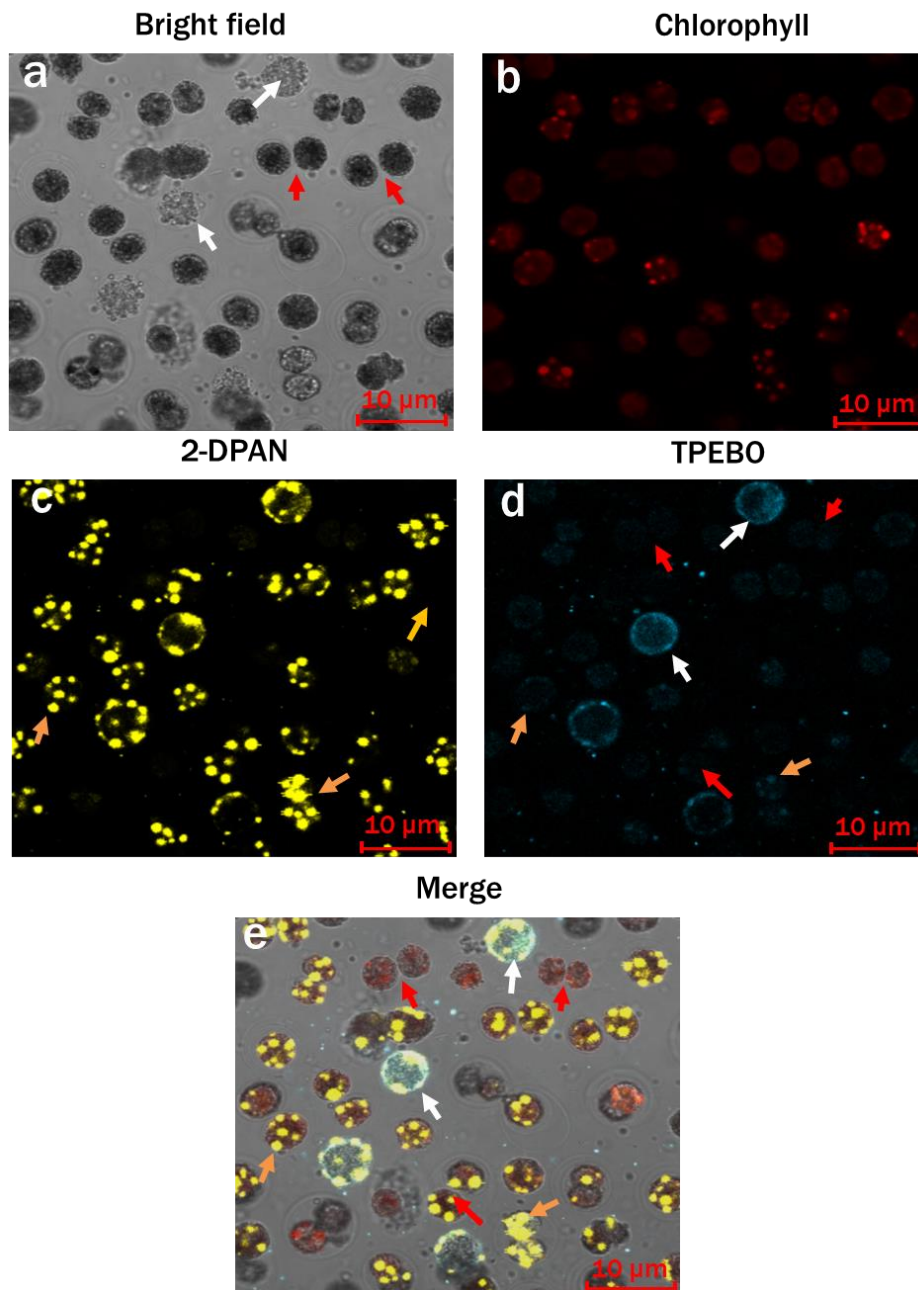


Fig. 4.4 Confocal images of H₂O₂ activities in *Chlamydomonas reinhardtii* cells during lipid induction. H₂O₂ and lipid drops were labelled with AIE-probes, TPE-BO and 2-DPAN, respectively. Cells were cultured in Treatment 3: MBL, (-) N₂, (-) Ca²⁺ (24 h light condition). Red arrows indicate H₂O₂ activity in normal cells and during cell division. Orange arrows indicate H₂O₂ activity in lipid accumulated cells. White arrows indicate H₂O₂ activity in autophagic cells. Images were taken with a Zeiss LSM 880 Airyscan confocal microscope.

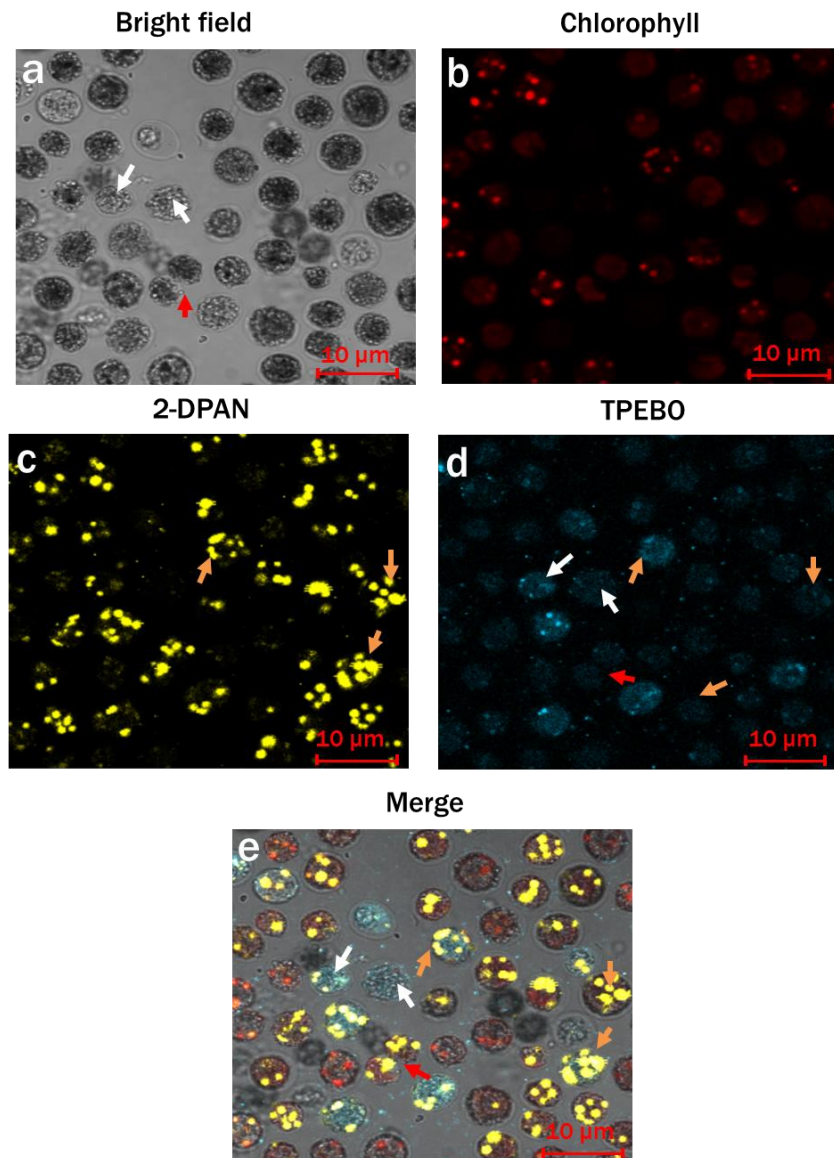


Fig. 4.5 Confocal images of H₂O₂ activities in *Chlamydomonas reinhardtii* cells during lipid induction. H₂O₂ and lipid drops were labelled with AIE-probes, TPE-BO and 2-DPAN, respectively. Cells were cultured in Treatment 4: MBL, (-) N₂, (-) Ca²⁺, (+) sodium acetate (2.0 g/L) (24 h light condition). Red arrows indicate H₂O₂ activity in normal cells and during cell division; Orange arrows indicate H₂O₂ activity in lipid accumulated cells; White arrow indicates H₂O₂ activity in autophagic cells. Images were taken with a Zeiss LSM 880 Airyscan confocal microscope.

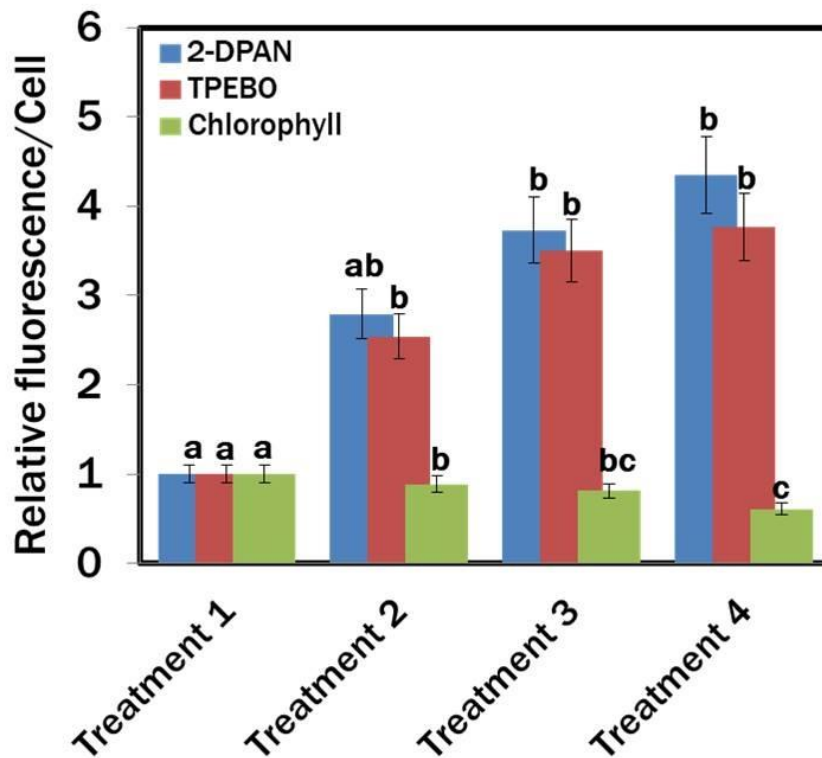


Fig. 4.6 Confocal analysis of *Chlamydomonas reinhardtii* for relative fluorescence intensity/cell during lipid induction in different treatments. H₂O₂ and lipid drops were labelled with AIE-probes, TPE-BO and 2-DPAN, respectively. Treatment 1: modified Woods Hole (MBL) medium; Treatment 2: MBL, (-) N₂; Treatment 3: MBL, (-) N₂, (-) Ca²⁺; Treatment 4: MBL, (-) N₂, (-) Ca²⁺, (+) sodium acetate (2.0 g/L) (all the treatments were in 24 h light condition). Values are relative to the control condition (Treatment 1: modified Woods Hole (MBL) medium). Averages are shown as mean ± SE.

4.4.3 Effects of H₂O₂ supplementation on *Chlamydomonas reinhardtii*

Data of this study showed clear relation to the lipid biosynthesis and intracellular H₂O₂ accumulation under a nutrient-depleted condition. As H₂O₂ can act as a messenger molecule (Miller et al., 2007), many complex biological systems have been linked to a controlled surge

of H₂O₂ (Niethammer et al., 2009; Haskew-Layton et al., 2010). In this study, the effects of direct supplementation of H₂O₂ on the growth and lipid accumulation in *C. reinhardtii* were studied. It was apparent that the concentration of H₂O₂ is very critical for cells as almost no change in algal growth was observed until 0.6 mM of H₂O₂ exposure, while a slight increase in H₂O₂ of 0.2 mM from 0.6 mM inhibited the cell growth by 60% (Fig. 4.7). Furthermore, cells did not survive above 1.0 mM H₂O₂ (data are not presented).

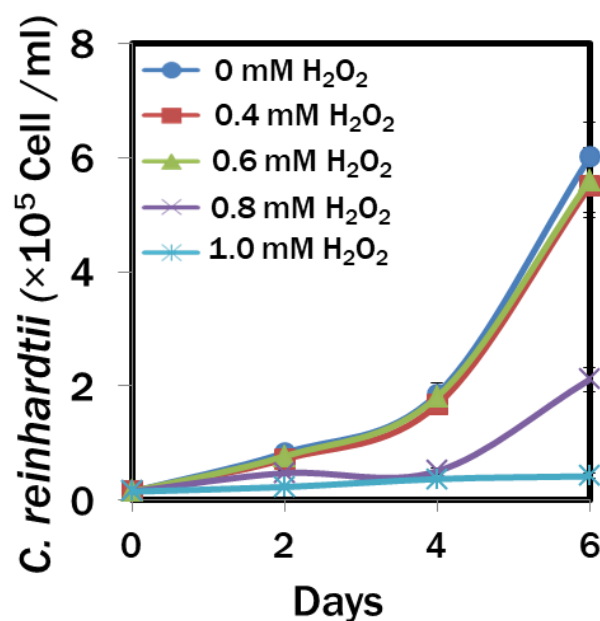


Fig. 4.7 Growth of *C. reinhardtii* in different concentrations of H₂O₂. Data are represented as mean \pm SE, n = 3.

During monitoring the cells exposed to 0.4 mM (Fig. 4.8a) and 0.6 mM (Fig. 4.8b) H₂O₂, it was obvious that utilization of the H₂O₂ increased with the growth of the *C. reinhardtii* cells. However, a declining trend in the H₂O₂ utilization was observed during the exponential growth period, possibly due to the reduction of the H₂O₂ concentration in later phases (Figs. 4.8a and 4.8b).

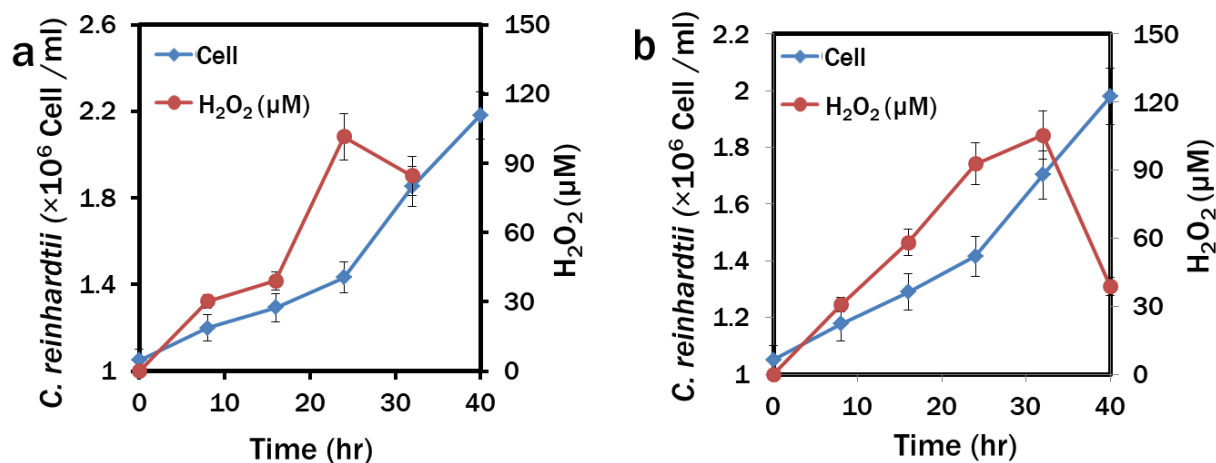


Fig. 4.8 Utilization of H₂O₂ by *C. reinhardtii* cultured in H₂O₂ supplemented MBL medium. Cells were exposed to 0.4 mM H₂O₂ (a) and 0.6 mM H₂O₂ (b). Data are represented as mean \pm SE, n = 3.

4.4.4 Effects of H₂O₂ supplementation on lipid bioaccumulation

The flow cytometric analysis and confocal microscopy suggested that H₂O₂ supplementation induced lipid accumulation in *C. reinhardtii*. In comparison to the control (0.0 mM H₂O₂) group (Figs. 4.9a, 4.10a, and 4.11), cytograms of BODIPY and 2-DPAN labelled cells showed maximum lipid accumulation in 0.6 mM H₂O₂ supplementation (Figs. 4.9c, 4.10c, and 4.11) that was followed by the 0.4 mM H₂O₂ (Figs. 4.9b, 4.10b, 4.11). Additionally, more obese cells due to the lipid accumulation were also apparent from the greater side scattering of the H₂O₂ supplemented cells (Figs. 4.9b, 4.9c, 4.10b, 4.10c). For further clarification, imaging of the 2-DPAN labelled *C. reinhardtii* cells was done with confocal microscopy.

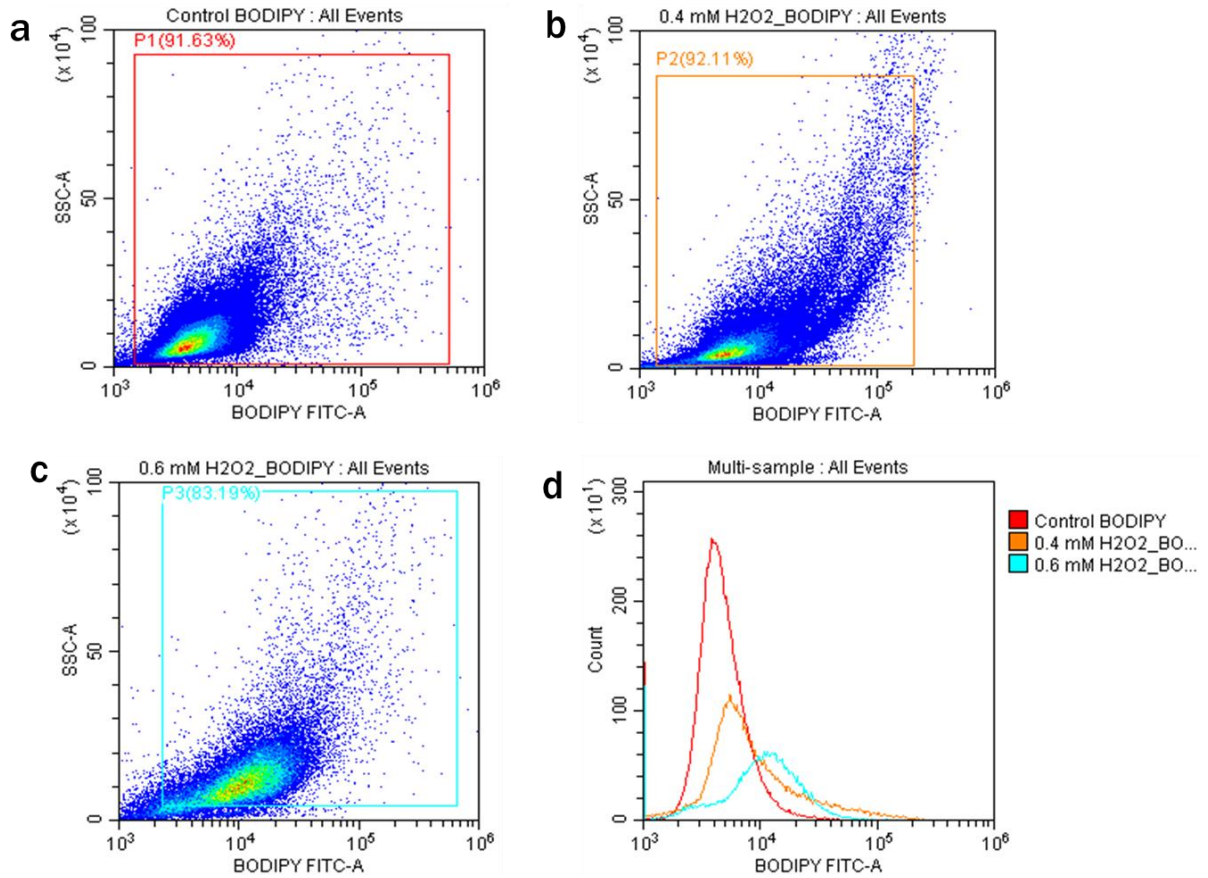


Fig. 4.9 Flow cytometric analysis of lipid accumulation in H₂O₂ treated *Chlamydomonas reinhardtii*. Lipids were labelled with BODIPY™ 505/515. (a-c) Flow cytogram of FITC-A vs SSC-A for BODIPY fluorescence in different treatments; (d) Histogram of BODIPY™ 505/515 fluorescence for cells. Cells were cultured in 0.0 mM (a), 0.4 mM (b) and 0.6 mM (c) H₂O₂ supplemented MBL medium (24 h light). All plots are on a logarithmic scale for both axes.

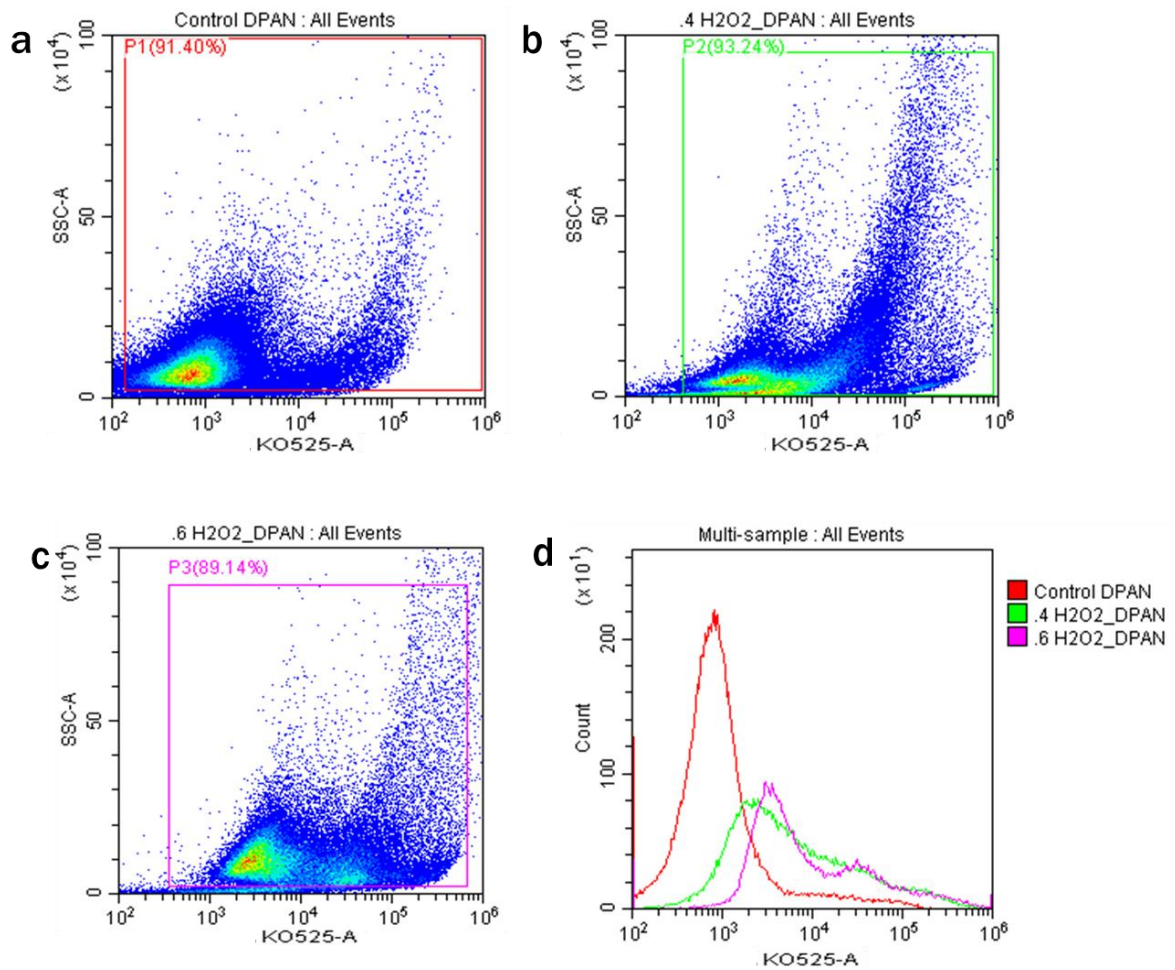


Fig. 4.10 Flow cytometric analysis of lipid accumulation in H₂O₂ treated *Chlamydomonas reinhardtii*. Lipids were labelled with AIE probe, 2-DPAN. (a-c) Flow cytogram of KO525-A vs SSC-A for 2-DPAN fluorescence. (d) Histogram of 2-DPAN fluorescence for cells. Cells were cultured in 0.0 mM (a), 0.4 mM (b) and 0.6 mM (c) H₂O₂ supplemented MBL medium (24 h light). All plots are on a logarithmic scale for both axes.

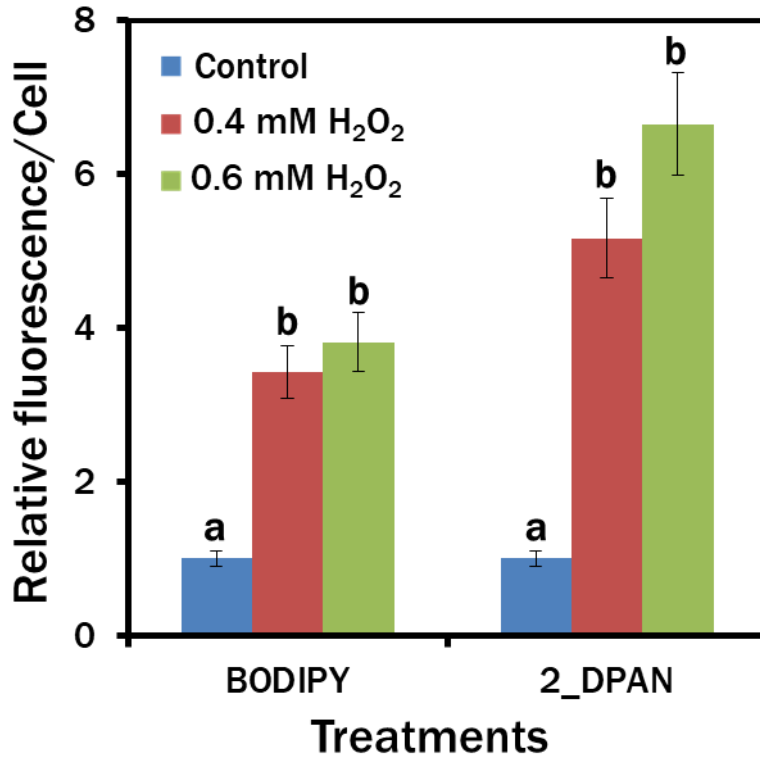


Fig. 4.11 Flow cytometry analysis of relative fluorescence of lipid/cell in H₂O₂ treated *Chlamydomonas reinhardtii* labelled with BODIPY™ 505/515 and AIE probe, 2-DPAN. Cells were cultured in 0.0 mM (control), 0.4 mM and 0.6 mM H₂O₂ supplemented MBL medium. Values are relative to the control condition (0.0 mM H₂O₂). Averages are shown as mean ± SE.

The confocal images (Figs. 4.12-4.15) also supported the flow cytometry results. More LDs were observed in the 2-DPAN labelled H₂O₂ supplemented cells (Figs. 4.13-4.15), which were almost 5 fold and 4.6 fold higher in 0.6 mM H₂O₂ and 0.4 mM H₂O₂, respectively, than the control (0.0 mM H₂O₂) group (Fig. 4.15). Interestingly, despite a significantly higher amount of lipid accumulation ($P < 0.05$), there was not any noticeable change in the chlorophyll autofluorescence among the groups (Fig. 4.15).

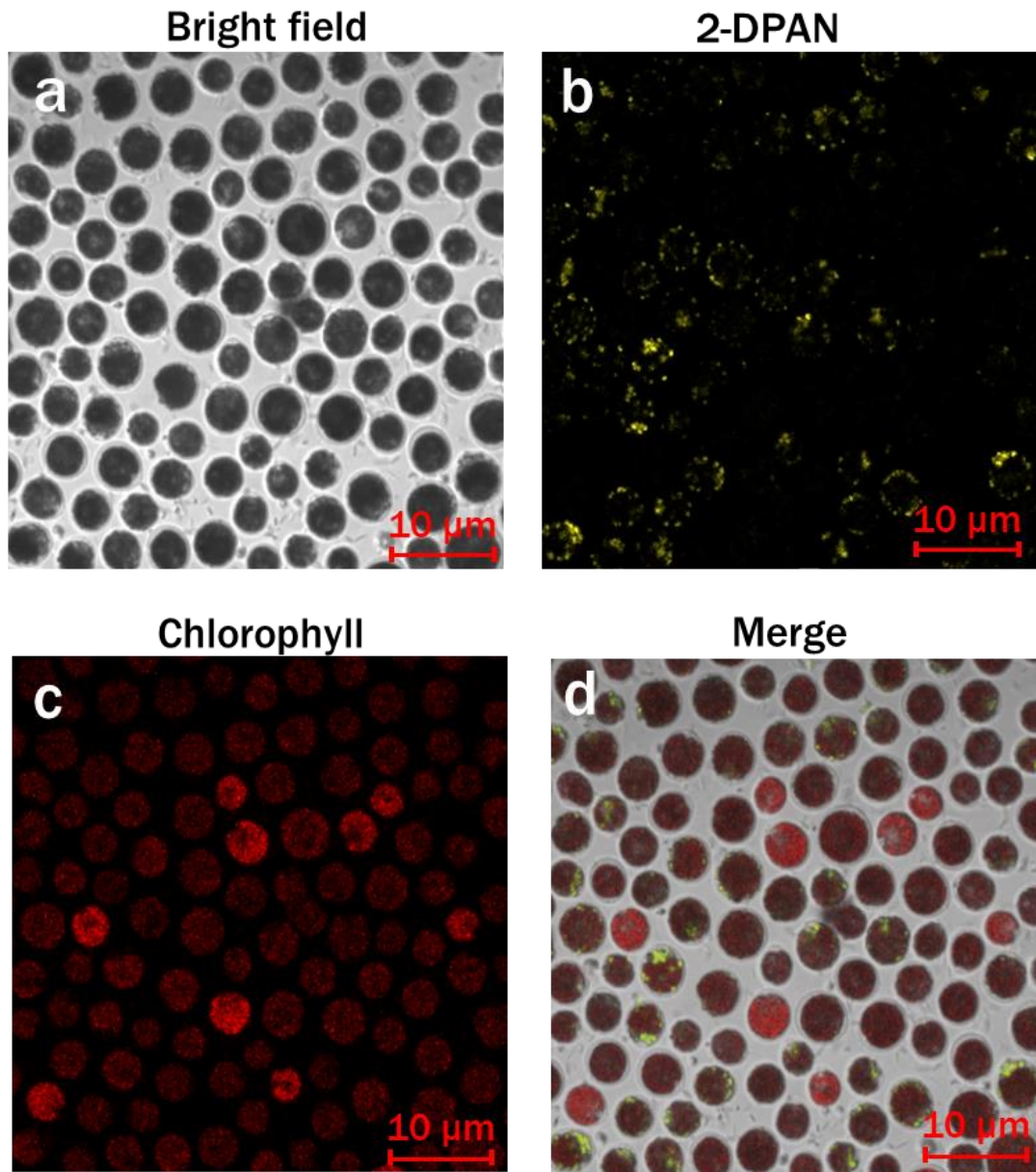


Fig. 4.12 Confocal imaging of lipid drops in H_2O_2 treated *Chlamydomonas reinhardtii*. Lipids were labeled with lipid-specific AIE nanoprobe, 2-DPAN ($\text{C}_{24}\text{H}_{18}\text{N}_2\text{O}$). Cells were cultured in an MBL medium without H_2O_2 supplementation. (Bright-field images: a; Fluorescence images - 2-DPAN: b and Chlorophyll: c); Merged image: d, Images were taken with Zeiss LSM 880 Airyscan confocal microscope.

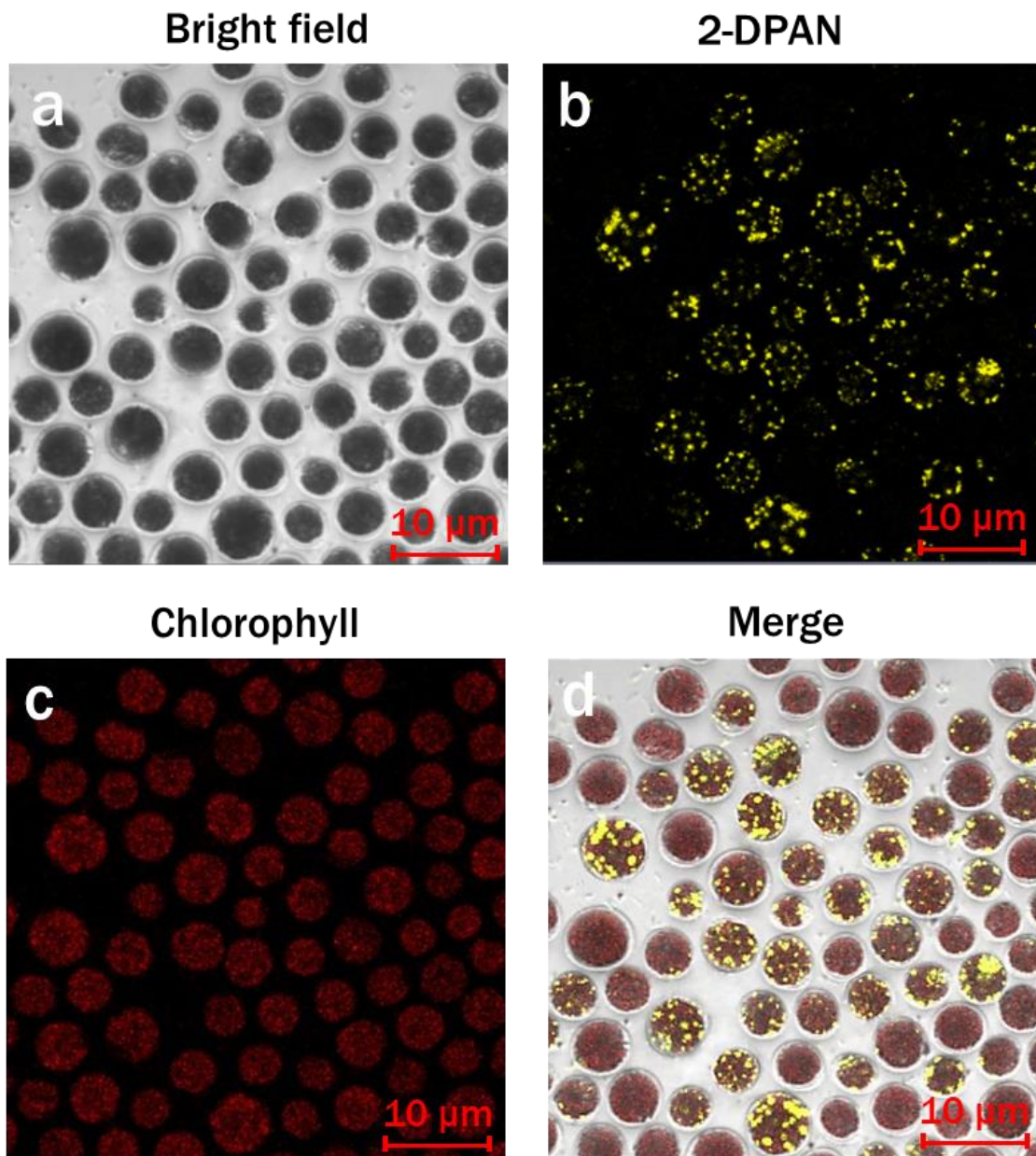


Fig. 4.13 Confocal imaging of lipid drops in H_2O_2 treated *Chlamydomonas reinhardtii*. Lipids were labeled with lipid-specific AIE nanoprobe, 2-DPAN ($\text{C}_{24}\text{H}_{18}\text{N}_2\text{O}$). Cells were cultured 0.4 mM H_2O_2 supplemented MBL medium. (Bright-field images: a; Fluorescence images - 2-DPAN: b and Chlorophyll: c); Merged image: d, Images were taken with Zeiss LSM 880 Airyscan confocal microscope.

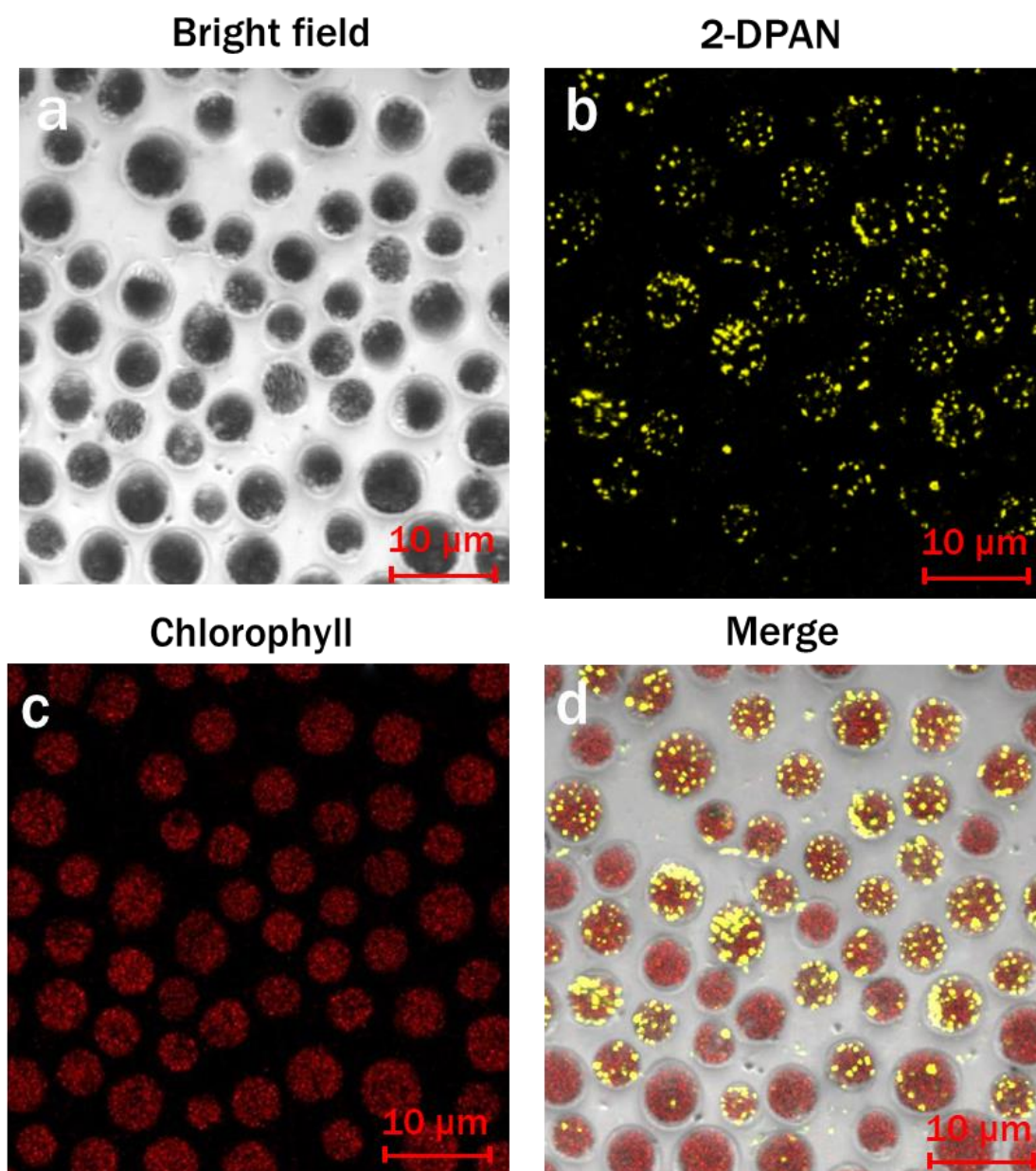


Fig. 4.14 Confocal imaging of lipid drops in H_2O_2 treated *Chlamydomonas reinhardtii*. Lipids were labeled with lipid-specific AIE nanoprobe, 2-DPAN ($\text{C}_{24}\text{H}_{18}\text{N}_2\text{O}$). Cells were cultured in $0.6 \text{ mM H}_2\text{O}_2$ supplemented MBL medium. (Bright-field images: a; Fluorescence images - 2-DPAN: b and Chlorophyll: c); Merged image: d, Images were taken with Zeiss LSM 880 Airyscan confocal microscope.

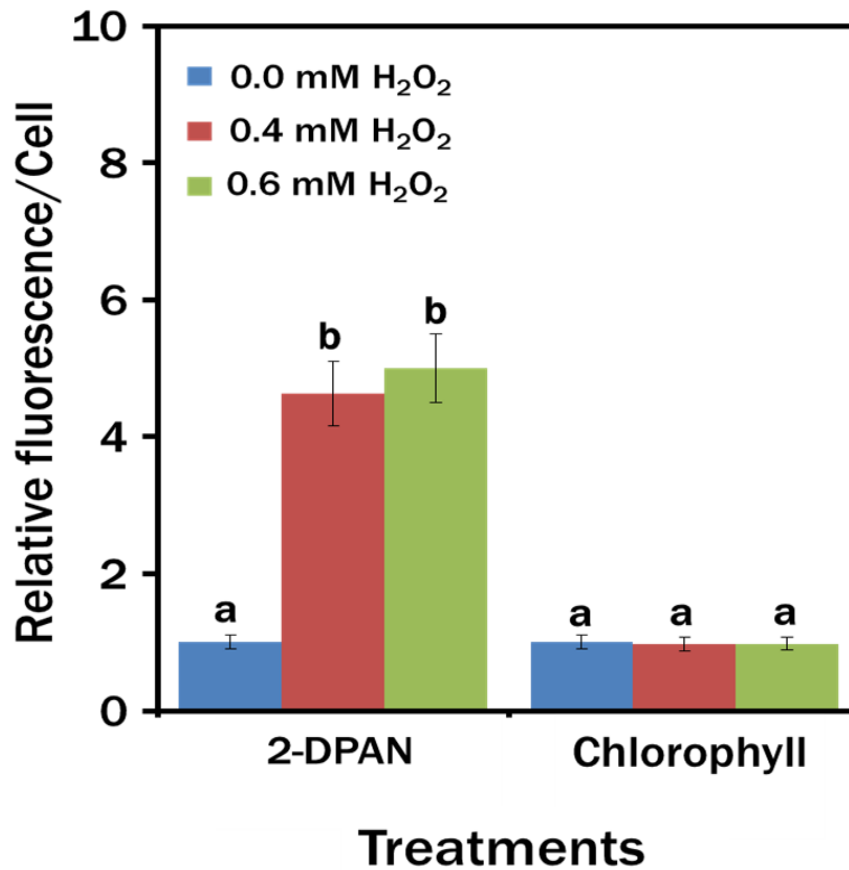


Fig. 4.15 Confocal analysis of *Chlamydomonas reinhardtii* for relative fluorescence intensity/cell in H₂O₂ treatments. Lipids were labeled with lipid-specific AIE nanoprobe, 2-DPAN (C₂₄H₁₈N₂O). Cells were cultured in 0.0 mM, 0.4 mM and 0.6 mM H₂O₂ supplemented MBL medium. Values are relative to the control condition (0.0 mM H₂O₂). Averages are shown as mean ± SE.

4.4.5 Effects of H₂O₂ supplementation on lipid composition in *Chlamydomonas reinhardtii*

Supplementation of H₂O₂ increased the PUFAs content up to ~54% in the *C. reinhardtii* cells, which was about ~17% higher than the control group (Table 4.1). Cells, cultured in the controlled condition produced the maximum amount of SAFAs (~51.6%), whereas SAFAs content was ~38% in the 0.4 mM and 0.6 mM H₂O₂ treatments. Among the PUFAs, the production of α -linolenic acid (ALA) was almost doubled in the H₂O₂ supplemented groups

compared to the control group (~17%). Most abundant SAFA in all the treatments were palmitic acid (C16:0), with a maximum production of ~43.7% in Treatment 1.

Table 4.1 Percentage of FAMES in *Chlamydomonas reinhardtii* cells under different cultural conditions.

Percentage of FAMES	Treatments		
	Control	0.4 mM H ₂ O ₂	0.6 mM H ₂ O ₂
C4:0	1.29 ±0.18	0.91±0.35	0.72±0.08
C12:0	0.22 ±0.02	0.15±0.05	0.12±0.03
C13:0	0.16 ±0.042	--*	--*
C14:0	0.87 ±0.07	0.50±0.06	0.48±0.03
C14:1 N-5	0.12±0.01	0.11±0.02	0.09±0.01
C15:0	0.42±0.03	0.26±0.07	0.23±0.04
C16:0	43.66±1.05	33.60±0.23	33.66±1.0
C16:1 N-7	0.98±0.03	0.56±0.03	0.61±0.16
C17:0	0.95±0.13	0.69±0.23	0.56±0.04
C17:1 N-7	1.79±0.03	1.93±0.23	1.85±0.07
C18:0	2.30±0.03	1.53±0.03	1.50±0.17
C18:1 N-9	5.70±0.78	2.98±0.03	3.19±0.21
C18:2 N-6,9	18.91±0.09	15.75±1.92	16.19±0.28
C18:3 N-3,6,9	17.75±1.53	38.29±2.91	37.38±1.88
C20:0	0.89±0.10	0.59±0.23	0.47±0.03
C20:1 N-9	0.41±0.03	0.27±0.09	0.23±0.02
C20:2 N-6,9	0.42±0.08	0.10±0.15	0.23±0.02

C20:3 N-6,9,12	--*	--*	--*
C21:0	0.33±0.04	0.24±0.10	0.18±0.02
C20:4 N-6,9,12,15	0.48±0.10	--*	--*
C20:3 N-3,6,9	--*	--*	--*
C20:5 N-3,6,9,12,15	0.21±0.30	0.10±0.14	0.10±0.15
C22:0	0.42±0.35	0.26±0.09	0.22±0.01
C22:1 N-9	1.39±0.17	1.03±0.04	1.79±0.50
C22:2 N-6,9	0.12±0.14	0.03±0.05	0.08±0.01
C22:4 N-6,9,12,15	--*	--*	--*
C24:0	0.08±.01	0.03±0.01	0.02±0.01
C22:6 N-3,6,9,12,15,18	0.06±.01	0.04±0.06	0.04±0.06
C24:1 N-9	0.04±.01	0.01±0.01	0.01±0.02
SAFAs	51.61±12.41	38.78±9.57	38.18±9.61
MUFAs	10.44±1.97	6.90±1.10	7.79±1.19
PUFAs	37.42±8.04	54.32±13.16	54.04±12.92

*none detectable. Indicate what the bold letters mean

4.5 Discussion

Nutrient accessibility has a major impact on the growth, dispersion and synthesis of the beneficiary biomolecules in microalgae. Altering the culturing constituents can extensively affect the lipid and fatty acid (FA) profile (Xin et al., 2010). The underlying mechanistic pathways for the biosynthesis of these molecules are critical to understanding for maximizing the production of desired components. To advance the research in algal biofunctional components, rapid and easy *in vivo* tools for studying the molecules associated with the

production of the essential biomolecules are much desired. In this study, using AIE-based techniques, H₂O₂ activities in the lipid inducing conditions in a carbohydrates-based cell wall containing microalga, *C. reinhardtii* was studied. Following the detection of the H₂O₂ activities with H₂O₂-specific AIE probe, TPE-BO in the nutrient-starved cells, the effects of direct supplementation of H₂O₂ on growth, lipid accumulation and fatty acid composition in this microalga were further investigated.

While stress-based strategies are widely used to produce biofunctional components in microalgae, these strategies can also increase oxidative damage. After a certain level of oxidative stress, it might lead to increased cell death, followed by biomass reduction. In this experiment, all the nutrient-starved conditions showed a marked increase in lipid biosynthesis compared to the nutrient-enriched condition. A similar trend in the surge of H₂O₂ activities has been observed in lipid-induced nutrient-starved cells, where chlorophyll was reduced. ROS homeostasis underlies mechanisms to preserve cellular integrity, development, defence processes, and controlled cell death in organisms to recycle cellular constituents (Bhattacharjee, 2012). During nutrient limitation, *C. reinhardtii* perhaps altered the cellular metabolism from glycolysis to the oxidative pentose phosphate pathway, downregulated carbohydrate and protein synthesis (Miller et al., 2010; López García de Lomana et al., 2015). To protect the cells from excessive reduction equivalents, such as NADPH, algal cells then synthesized more lipids (Hu et al., 2008; Shi et al., 2017). Subsequently, chlorophyll could be utilized as the internal nitrogen reserve and decrease the light uptake to minimize excess ROS accumulation (Miller et al., 2010; Shene et al., 2018). Increased H₂O₂ levels in the nutrient-starved *C. reinhardtii* cells may also trigger the Ca²⁺ signals and further regulate the stress response mechanisms towards FA biosynthesis (Gorain et al., 2013).

For further analyzing the effects of H₂O₂ on lipid accumulation and cell growth, we supplemented the nutrient-enriched culture medium with different concentrations of H₂O₂.

Although exposure to *C. reinhardtii* in a higher concentration of exogenous H₂O₂ (>0.6 mM) significantly decreased algal growth, supplementation of 0.4 and 0.6 mM H₂O₂ maximized the lipid bioaccumulation without affecting the algal growth and chlorophyll content. Therefore, the results of this study suggest that the H₂O₂ concentration is critical, and prior to the application, need to be studied carefully for different species. A certain concentration of H₂O₂ (0.4 and 0.6 mM for *C. reinhardtii*) supplementation perhaps induced the cytosolic Ca²⁺ level in algal cells that consequently alleviated the oxidative stress by triggering glutathione (GSH) activity; modulating the calmodulin and *MAPK* expression levels, and resulting in increased lipid production (Shi et al., 2017; Ikner & Shiozaki, 2005; Zhang et al., 2017). Simultaneously, improved cellular signalling promotes cytokinesis by persuading the signal transduction cascades without affecting the nucleic acids content, genes expression, cell size and photosynthetic activity that accelerated the growth of the algal cells (Pokora et al., 2018).

This chapter also reported a novel and rapid strategy *in vivo* to visualize LDs and H₂O₂ in *C. reinhardtii* using AIE-based fluorophores, 2-DPAN and TPE-BO, respectively. Distinguished labelling of LDs and H₂O₂ with 2-DPAN and TPE-BO in the presence of red chlorophyll indicated that both AIEgens are effective as multicolor *in vivo* imaging tools under the same assay condition. It also appeared that the carbohydrate-based cell wall structure of this microalga could not hinder the efficacy of these probes from the labelling of the respective molecules. The hydrophilic properties of keto-salicylaldehyde hydrazine in 2-DPAN perhaps efficiently allowed the probe to enter the cells (Li et al., 2019; Hu et al., 2018; Wang et al., 2016; Wang and Zou, 2018). Alongside, the cheap raw material benzophenone (Li et al., 2019; Wang et al., 2016) and the specific structure with oxygen atoms attached to the electron acceptor carbonyl group perhaps increased the hydrophobicity (Wang et al., 2014) that enabled this AIE probe to aggregate in the hydrophobic LDs. Inside the LDs, upon

aggregation of 2-DPAN, the intramolecular motion restricts and results in increased fluorescence. Moreover, the simple structure of TPE-BO with phenylboronic ester moiety enabled this probe to transform into the phenol group in the presence of H₂O₂. This restricted the intramolecular rotation and turned on the fluorescence that allowed TPE-BO to detect H₂O₂ rapidly in microalgae (Zhang et al., 2015). Results of this study were also supported by a former study, where TPE-BO detected H₂O₂ within seconds in living mice macrophage (RAW264.7) cells, and TPE-BO was established as a very low toxic, photostable, highly effective, and very first AIEgen for *in vivo* H₂O₂ research (Zhang et al., 2015).

In this experiment, supplementation of 0.4 and 0.6 mM H₂O₂ increased PUFA biosynthesis, where more than double the production of ALA was observed (Table 1). As an essential fatty acid in humans, many health beneficiary effects of ALA, such as anti-inflammatory (Stark et al., 2008; Zhao et al., 2004), anti-arrhythmic (Albert et al., 2005), anti-thrombotic (Albert et al., 2005; Campos et al., 2008), and neuroprotective effects (Nguemeni et al., 2010) have been suggested from previous studies. Increasing levels of dietary ALA have also been associated with the reduction of obesity, metabolism and coronary heart diseases (Leikin-Frenkel, 2016; de Lorgeril & Salen, 2004). Additionally, partial conversion of ALA into beneficiary PUFAs, eicosapentaenoic acid and docosahexaenoic acid to a certain level have further health implications in humans (Fussbroich et al., 2020; Sun et al., 2018; Guesnet & Alessandri, 2011). Generally, ALA is mostly found in plant-based oils and food sources, such as flaxseed, English walnut, chia, and hemp seed. However, the linoleic acid content is also very high in these sources. Therefore, increasing the dietary ALA content is difficult without increasing the LA content (Burns-Whitmore et al., 2019). Furthermore, increasing the production of the ALA content in microalgae could be more promising due to their high biomass ratio and non-requirement of the arable lands.

4.6 Conclusion

This study identified conditions for the production enhancement of lipids with a higher amount of healthy ALA in *C. reinhardtii* without compromising the growth. Furthermore, H₂O₂ activities in the cells were detected and it was revealed that up to a certain level, H₂O₂ supplementation could induce the production of biofunctional components in microalgae. A rapid, multi-color imaging technique for high contrast visualisation of LDs and H₂O₂ in *in situ* conditions with biocompatible and convenient AIE-based bioprobes, 2-DPAN and TPE-BO, respectively, have also been developed. These probes could be utilized industrially as reliable, labour-efficient, and cost-effective bioimaging tools and therefore are more auspicious to advance lipid research in microalgae as a sustainable bio-factory for lipid production.

4.7 Reference

Albert, C. M., Oh, K., Whang, W., Manson, J. E., Chae, C. U., Stampfer, M. J., Willett, W. C., & Hu, F. B. (2005). Dietary alpha-linolenic acid intake and risk of sudden cardiac death and coronary heart disease. *Circulation*, *112*(21), 3232-3238. <https://doi.org/10.1161/CIRCULATIONAHA.105.572008>

Bhattacharjee, S. (2012). The language of reactive oxygen species signaling in plants. *Journal of Botany*, 985298, 22. <https://doi.org/10.1155/2012/985298>

Bligh, E. G., & Dyer, W. J. (1959). A rapid method of total lipid extraction and purification. *Canadian Journal of Biochemistry and Physiology*, *37*(8), 911-917. <https://doi.org/10.1139/o59-099>

Burns-Whitmore, B., Froyen, E., Heskey, C., Parker, T., & San Pablo, G. (2019). Alpha-linolenic and linoleic fatty acids in the vegan diet: Do they require dietary reference intake/adequate intake special consideration?. *Nutrients*, *11*(10), 2365. <https://doi.org/10.3390/nu11102365>

Campos, H., Baylin, A., & Willett, W. C. (2008). Alpha-linolenic acid and risk of nonfatal acute myocardial infarction. *Circulation*, *118*(4), 339-345. <https://doi.org/10.1161/CIRCULATIONAHA.107.762419>

Christie W. W. (1998). Gas chromatography-mass spectrometry methods for structural analysis of fatty acids. *Lipids*, *33*(4), 343-353. <https://doi.org/10.1007/s11745-998-0214-x>

Collot, M., Fam, T. K., Ashokkumar, P., Faklaris, O., Galli, T., Danglot, L., & Klymchenko, A. S. (2018). Ultrabright and fluorogenic probes for multicolor imaging and tracking of lipid droplets in cells and tissues. *Journal of the American Chemical Society*, *140*(16), 5401-5411. <https://doi.org/10.1021/jacs.7b12817>

Cooper, M. S., Hardin, W. R., Petersen, T. W., & Cattolico, R. A. (2010). Visualizing "green oil" in live algal cells. *Journal of Bioscience and Bioengineering*, *109*(2), 198-201. <https://doi.org/10.1016/j.jbiosc.2009.08.004>

Dębski, D., Smulik, R., Zielonka, J., Michałowski, B., Jakubowska, M., Dębowska, K., Adamus, J., Marcinek, A., Kalyanaraman, B., & Sikora, A. (2016). Mechanism of oxidative conversion of Amplex® Red to resorufin: Pulse radiolysis and enzymatic studies. *Free Radical Biology & Medicine*, *95*, 323-332. <https://doi.org/10.1016/j.freeradbiomed.2016.03.027>

D'Errico, G., Vitiello, G., De Tommaso, G., Abdel-Gawad, F. K., Brundo, M. V., Ferrante, M., De Maio, A., Trocchia, S., Bianchi, A. R., Ciarcia, G., & Guerriero, G. (2018). Electron Spin Resonance (ESR) for the study of Reactive Oxygen Species (ROS) on the isolated frog skin (*Pelophylax bergeri*): A non-invasive method for environmental monitoring. *Environmental Research*, *165*, 11-18. <https://doi.org/10.1016/j.envres.2018.03.044>

de Lorgeril, M., & Salen, P. (2004). Alpha-linolenic acid and coronary heart disease. *Nutrition, Metabolism, and Cardiovascular Diseases: NMCD*, *14*(3), 162-169. [https://doi.org/10.1016/s0939-4753\(04\)80037-1](https://doi.org/10.1016/s0939-4753(04)80037-1)

Dikalov, S., Griendling, K. K., & Harrison, D. G. (2007). Measurement of reactive oxygen species in cardiovascular studies. *Hypertension (Dallas, Tex.: 1979)*, *49*(4), 717-727. <https://doi.org/10.1161/01.HYP.0000258594.87211.6b>

Fussbroich, D., Colas, R. A., Eickmeier, O., Trischler, J., Jerkic, S. P., Zimmermann, K., Göpel, A., Schwenger, T., Schaible, A., Henrich, D., Baer, P., Zielen, S., Dalli, J., Beermann, C., & Schubert, R. (2020). A combination of LCPUFA ameliorates airway inflammation in

asthmatic mice by promoting pro-resolving effects and reducing adverse effects of EPA. *Mucosal Immunology*, *13*(3), 481-492. <https://doi.org/10.1038/s41385-019-0245-2>

Gorain, P. C., Bagchi, S. K., & Mallick, N. (2013). Effects of calcium, magnesium and sodium chloride in enhancing lipid accumulation in two green microalgae. *Environmental Technology*, *34*(13-16), 1887-1894. <https://doi.org/10.1080/09593330.2013.812668>

Guesnet, P., & Alessandri, J. M. (2011). Docosahexaenoic acid (DHA) and the developing central nervous system (CNS) - Implications for dietary recommendations. *Biochimie*, *93*(1), 7-12. <https://doi.org/10.1016/j.biochi.2010.05.005>

Haskew-Layton, R. E., Payappilly, J. B., Smirnova, N. A., Ma, T. C., Chan, K. K., Murphy, T. H., Guo, H., Langley, B., Sultana, R., Butterfield, D. A., Santagata, S., Alldred, M. J., Gazaryan, I. G., Bell, G. W., Ginsberg, S. D., & Ratan, R. R. (2010). Controlled enzymatic production of astrocytic hydrogen peroxide protects neurons from oxidative stress via an Nrf2-independent pathway. *Proceedings of the National Academy of Sciences of the United States of America*, *107*(40), 17385-17390. <https://doi.org/10.1073/pnas.1003996107>

Hayashi, I., Morishita, Y., Imai, K., Nakamura, M., Nakachi, K., & Hayashi, T. (2007). High-throughput spectrophotometric assay of reactive oxygen species in serum. *Mutation Research*, *631*(1), 55-61. <https://doi.org/10.1016/j.mrgentox.2007.04.006>

Henley, W.J. (2019). The past, present and future of algal continuous cultures in basic research and commercial applications. *Algal Research*, *43*, 101636. <https://doi.org/10.1016/j.algal.2019.101636>

Hu, R., Zhou, F., Zhou, T., Shen, J., Wang, Z., Zhao, Z., Qin, A., & Tang, B. Z. (2018). Specific discrimination of gram-positive bacteria and direct visualization of its infection

towards mammalian cells by a DPAN-based AIEgen. *Biomaterials*, 187, 47-54.
<https://doi.org/10.1016/j.biomaterials.2018.09.019>

Hu, Q., Sommerfeld, M., Jarvis, E., Ghirardi, M., Posewitz, M., Seibert, M., & Darzins, A. (2008). Microalgal triacylglycerols as feedstocks for biofuel production: perspectives and advances. *The Plant Journal : for Cell and Molecular Biology*, 54(4), 621-639.
<https://doi.org/10.1111/j.1365-313X.2008.03492.x>

Ikner, A., & Shiozaki, K. (2005). Yeast signaling pathways in the oxidative stress response. *Mutation Research*, 569(1-2), 13-27.
<https://doi.org/10.1016/j.mrfmmm.2004.09.006>

Karakuzu, O., Cruz, M. R., Liu, Y., & Garsin, D. A. (2019). Amplex Red assay for measuring hydrogen peroxide production from *Caenorhabditis elegans*. *Bio-protocol*, 9(21), e3409.
<https://doi.org/10.21769/BioProtoc.3409>

Kim, J. S., Jeong, K., Murphy, J. M., Rodriguez, Y., & Lim, S. S. (2019). A quantitative method to measure low levels of ROS in nonphagocytic cells by using a chemiluminescent imaging system. *Oxidative Medicine and Cellular Longevity*, 2019, 1754593.
<https://doi.org/10.1155/2019/1754593>

Leikin-Frenkel A. I. (2016). Is there a role for alpha-linolenic acid in the fetal programming of health?. *Journal of Clinical Medicine*, 5(4), 40. <https://doi.org/10.3390/jcm5040040>

Li, L., Zhou, F., Gao, Q., Lu, Y., Xu, X., Hu, R., Wang, Z., Peng, M., Yang, Z., & Tang, B. Z. (2019). Visualizing dynamic performance of lipid droplets in a Parkinson's disease model via a smart photostable Aggregation-Induced Emission probe. *iScience*, 21, 261-272.
<https://doi.org/10.1016/j.isci.2019.10.027>

- López García de Lomana, A., Schäuble, S., Valenzuela, J., Imam, S., Carter, W., Bilgin, D. D., Yohn, C. B., Turkarslan, S., Reiss, D. J., Orellana, M. V., Price, N. D., & Baliga, N. S. (2015). Transcriptional program for nitrogen starvation-induced lipid accumulation in *Chlamydomonas reinhardtii*. *Biotechnology for Biofuels*, 8, 207. <https://doi.org/10.1186/s13068-015-0391-z>
- Miller, R., Wu, G., Deshpande, R. R., Vieler, A., Gärtner, K., Li, X., Moellering, E. R., Zäuner, S., Cornish, A. J., Liu, B., Bullard, B., Sears, B. B., Kuo, M. H., Hegg, E. L., Shachar-Hill, Y., Shiu, S. H., & Benning, C. (2010). Changes in transcript abundance in *Chlamydomonas reinhardtii* following nitrogen deprivation predict diversion of metabolism. *Plant Physiology*, 154(4), 1737-1752. <https://doi.org/10.1104/pp.110.165159>
- Miller, E. W., Tulyathan, O., Isacoff, E. Y., & Chang, C. J. (2007). Molecular imaging of hydrogen peroxide produced for cell signaling. *Nature Chemical Biology*, 3(5), 263-267. <https://doi.org/10.1038/nchembio871>
- Mutanda, T., Naidoo, D., Bwapwa, J.K. & Anandraj, A. (2020). Biotechnological applications of microalgal oleaginous compounds: current trends on microalgal bioprocessing of products. *Frontiers in Energy Research*, 8, 598803. <https://doi.org/10.3389/fenrg.2020.598803>
- Nguemni, C., Delplanque, B., Rovère, C., Simon-Rousseau, N., Gandin, C., Agnani, G., Nahon, J. L., Heurteaux, C., & Blondeau, N. (2010). Dietary supplementation of alpha-linolenic acid in an enriched rapeseed oil diet protects from stroke. *Pharmacological Research*, 61(3), 226-233. <https://doi.org/10.1016/j.phrs.2009.12.007>
- Nichols H. W. (1973). In *Handbook of Phycological Methods*, Ed. J. R. Stein, pp. 16-17. Camb. Univ. Press. (R. R. L. Guillard, personal communication).

- Niethammer, P., Grabher, C., Look, A. T., & Mitchison, T. J. (2009). A tissue-scale gradient of hydrogen peroxide mediates rapid wound detection in zebrafish. *Nature*, *459*(7249), 996-999. <https://doi.org/10.1038/nature08119>
- Prasad, A., Pospíšil, P., & Tada, M. (2019). Editorial: Reactive Oxygen Species (ROS) Detection Methods in Biological System. *Frontiers in Physiology*, *10*, 1316. <https://doi.org/10.3389/fphys.2019.01316>
- Pokora, W., Aksmann, A., Baścik-Remisiewicz, A., Dettlaff-Pokora, A., & Tukaj, Z. (2018). Exogenously applied hydrogen peroxide modifies the course of the *Chlamydomonas reinhardtii* cell cycle. *Journal of Plant Physiology*, *230*, 61-72. <https://doi.org/10.1016/j.jplph.2018.07.015>
- Reza, A.H.M.M., Zhu, X., Qin, J., & Tang, Y. (2021). Microalgae-derived health supplements to therapeutic shifts: Redox-based study opportunities with AIE-based technologies. *Advanced Healthcare Materials*, *10*(24), e2101223. <https://doi.org/10.1002/adhm.202101223>
- Reczek, C. R., & Chandel, N. S. (2015). ROS-dependent signal transduction. *Current Opinion in Cell Biology*, *33*, 8-13. <https://doi.org/10.1016/j.ceb.2014.09.010>
- Ruiz, J., Olivieri, G., de Vree, J., Bosma, R. & Willems, P., Reith, J.H., Eppink, M.H.M., Kleinegris, D.M.M., Wijffels, R.H., Barbosa, M.J. (2016). Towards industrial products from microalgae. *Energy & Environmental Science*, *9*, 3036-3043. <https://doi.org/10.1039/C6EE01493C>
- Schneider, C. A., Rasband, W. S., & Eliceiri, K. W. (2012). NIH Image to ImageJ: 25 years of image analysis. *Nature Methods*, *9*(7), 671-675. <https://doi.org/10.1038/nmeth.2089>

- Shene, C., Asenjo, J. A., & Chisti, Y. (2018). Metabolic modelling and simulation of the light and dark metabolism of *Chlamydomonas reinhardtii*. *The Plant Journal: for Cell and Molecular Biology*, 96(5), 1076-1088. <https://doi.org/10.1111/tpj.14078>
- Shi, T. Q., Wang, L. R., Zhang, Z. X., Sun, X. M., & Huang, H. (2020). Stresses as first-line tools for enhancing lipid and carotenoid production in microalgae. *Frontiers in Bioengineering and Biotechnology*, 8, 610. <https://doi.org/10.3389/fbioe.2020.00610>
- Shi, K., Gao, Z., Shi, T.Q., Song, P., Ren, L.J., Huang, H., & Ji, X.J. (2017). Reactive oxygen species-mediated cellular stress response and lipid accumulation in oleaginous microorganisms: The state of the art and future perspectives. *Frontiers in Microbiology*, 8, 793. <https://doi.org/10.3389/fmicb.2017.00793>
- Stark, A. H., Crawford, M. A., & Reifen, R. (2008). Update on alpha-linolenic acid. *Nutrition Reviews*, 66(6), 326-332. <https://doi.org/10.1111/j.1753-4887.2008.00040.x>
- Sun, G. Y., Simonyi, A., Fritsche, K. L., Chuang, D. Y., Hannink, M., Gu, Z., Greenlief, C. M., Yao, J. K., Lee, J. C., & Beversdorf, D. Q. (2018). Docosahexaenoic acid (DHA): An essential nutrient and a nutraceutical for brain health and diseases. *Prostaglandins, Leukotrienes, and Essential Fatty Acids*, 136, 3-13. <https://doi.org/10.1016/j.plefa.2017.03.006>
- Vaneev, A. N., Gorelkin, P. V., Garanina, A. S., Lopatukhina, H. V., Vodopyanov, S. S., Alova, A. V., Ryabaya, O. O., Akasov, R. A., Zhang, Y., Novak, P., Salikhov, S. V., Abakumov, M. A., Takahashi, Y., Edwards, C., Klyachko, N. L., Majouga, A. G., Korchev, Y. E., & Erofeev, A. S. (2020). *In vitro* and *in vivo* electrochemical measurement of reactive oxygen species after treatment with anticancer drugs. *Analytical Chemistry*, 92(12), 8010-8014. <https://doi.org/10.1021/acs.analchem.0c01256>

- Votyakova, T. V., & Reynolds, I. J. (2004). Detection of hydrogen peroxide with Amplex Red: interference by NADH and reduced glutathione auto-oxidation. *Archives of Biochemistry and Biophysics*, 431(1), 138-144. <https://doi.org/10.1016/j.abb.2004.07.025>
- Wang, Q., & Zou, M. H. (2018). Measurement of reactive oxygen species (ROS) and mitochondrial ROS in AMPK knockout mice blood vessels. *Methods in Molecular Biology (Clifton, N.J.)*, 1732, 507-517. https://doi.org/10.1007/978-1-4939-7598-3_32
- Wang, Z., Gui, C., Zhao, E., Wang, J., Li, X., Qin, A., Zhao, Z., Yu, Z., & Tang, B. Z. (2016). Specific fluorescence probes for lipid droplets based on simple AIEgens. *ACS Applied Materials & Interfaces*, 8(16), 10193-10200. <https://doi.org/10.1021/acsami.6b01282>
- Wang, E., Zhao, E., , Hong, Y., , Lam, J., , & Tang, B. Z., (2014). A highly selective AIE fluorogen for lipid droplet imaging in live cells and green algae. *Journal of Materials Chemistry. B*, 2(14), 2013-2019. <https://doi.org/10.1039/c3tb21675f>
- Wang, H., & Joseph, J. A. (1999). Quantifying cellular oxidative stress by dichlorofluorescein assay using microplate reader. *Free Radical Biology & Medicine*, 27(5-6), 612-616. [https://doi.org/10.1016/s0891-5849\(99\)00107-0](https://doi.org/10.1016/s0891-5849(99)00107-0)
- Xin, L., Hu, H. Y., Ke, G., & Sun, Y. X. (2010). Effects of different nitrogen and phosphorus concentrations on the growth, nutrient uptake, and lipid accumulation of a freshwater microalga *Scenedesmus* sp. *Bioresource Technology*, 101(14), 5494-5500. <https://doi.org/10.1016/j.biortech.2010.02.016>
- Yu, S. J., Kang, M. W., Chang, H. C., Chen, K. M., & Yu, Y. C. (2005). Bright fluorescent nanodiamonds: no photobleaching and low cytotoxicity. *Journal of the American Chemical Society*, 127(50), 17604-17605. <https://doi.org/10.1021/ja0567081>

Zhang, X., Tang, X., Wang, M., Zhang, W., Zhou, B., & Wang, Y. (2017). ROS and calcium signaling mediated pathways involved in stress responses of the marine microalgae *Dunaliella salina* to enhanced UV-B radiation. *Journal of Photochemistry and Photobiology. B, Biology*, *173*, 360-367. <https://doi.org/10.1016/j.jphotobiol.2017.05.038>

Zhang, W., Liu, W., Li, P., Huang, F., Wang, H., & Tang, B. (2015). Rapid-response fluorescent probe for hydrogen peroxide in living cells based on increased polarity of C-B bonds. *Analytical Chemistry*, *87*(19), 9825-9828. <https://doi.org/10.1021/acs.analchem.5b02194>

Zhao, G., Etherton, T. D., Martin, K. R., West, S. G., Gillies, P. J., & Kris-Etherton, P. M. (2004). Dietary alpha-linolenic acid reduces inflammatory and lipid cardiovascular risk factors in hypercholesterolemic men and women. *The Journal of Nutrition*, *134*(11), 2991-2997. <https://doi.org/10.1093/jn/134.11.2991>

Chapter 5: General Discussion, Conclusions and Future Research

5.1 General discussion

Lipid droplets (LDs) are evolutionarily conserved organelles involved in energy homeostasis and versatile intracellular processes in different cell types, including microalgae (Beller et al., 2010). Microalgal lipids could be utilized for biodiesel and health supplements (Sun et al., 2018). Polyunsaturated fatty acids (PUFAs) with more than 18 carbons have many health benefits in humans (Kapoor et al., 2021). However, humans are not able to synthesize some of the essential PUFAs, such as linoleic acid (18:2(n-6), LA) and α -linolenic acid (C18:3(n-3), ALA), which are the precursors of eicosapentaenoic acid (20:5(n-3) and docosahexaenoic acid (22:6(n-3). Therefore, the PUFAs in humans must be supplied from external sources, such as fish, molluscs, crustaceans, meat, milk, eggs, and vegetable sources (Abedi and Sahari, 2014). Currently, 22% of the world population is predicted as vegetarians, and this proportion continues to rise. The alternative consumers are omnivores. Consequently, the global demands for plant-based diets are rapidly escalating. On the contrary, the limitations of the lands and their unrenowable nature have caused fierce competition between agricultural and non-agricultural sectors to significantly threaten the food supply (Rondhi et al., 2018). Unlike terrestrial plants, microalgae do not require arable lands and much freshwater for cultivation (Khan et al., 2018). These photosynthetic organisms can also grow in a wide range of aquatic habitats and play critical roles in environment preservation through utilizing wastewater and mitigating atmospheric CO₂. Additionally, the absence of lignocellulosic materials in the cell wall reduces the requirement for pretreatments, hence the processing costs. Microalgae can be produced in mass quantity and sold directly as food and nutrient supplements that can also ensure the availability of the dietary essential FAs requirement of vegetarians and vegans.

However, the lipid profile in microalgae greatly varies from species to species. The biosynthesis of lipids can be triggered by multiple factors related to the organismal

physiology and surrounding environment. Complex interactions between the lipid inducing factors also make lipid production unpredictable in microalgae. Additionally, FAs composition can be changed from saturation to more unsaturation in the later growth phases and could be reduced at post-maximal lipid accumulation stages (Morales et al., 2021). Therefore, selecting the appropriate species and developing microalgal stock with optimum lipid content are crucial for industrial success. The discovery of a rapid and easy *in vivo* lipid detection tool can provide the crucial link that helps accelerate the development of microalgal species into beneficial human health supplements. Appropriate LDs visualization tools can also give molecular insight into the regulatory mechanisms and the underlying connections with other cellular structures. Traditional bioprobes for LD detection often suffer from different dye-specific limitations, such as aggregation-caused quenching and self-decomposition phenomena to hinder research progress. The emergence of lipid-specific nanoprobe with aggregation-induced emission (AIE) attributes is promising in terms of remunerative characteristics with defined bioimaging properties. By utilizing an easy synthetic technique and exploiting the unique physical features of these molecules, highly selective and stable fluorescent probes with AIE attributes have been fabricated for lipid detection. However, to thrive against adverse environmental conditions, microalgae develop unique self-defence mechanisms and possess different biomolecules that cause autofluorescence and reduce the efficiency of lipid detection. Therefore, the selection of the appropriate probes is a prerequisite to successfully penetrating the cell wall without triggering autofluorescence properties.

The focus of this thesis was to use microalgae as the source of lipids to compensate and balance the ever-increasing demands for the production of health beneficiary food supplements. The lipid inducing conditions were determined in microalgae with two different cell structures, *Euglena gracilis*, without a cell wall, and *Chlamydomonas reinhardtii*, with a

carbohydrates-based cell wall. This thesis also aimed to develop novel AIE-based multicolor fluorescence imaging techniques to rapidly detect the lipid-inducing conditions in these microalgae. Additionally, the roles of hydrogen peroxide (H_2O_2) in *C. reinhardtii* have been determined as the natural by-products and a component of secondary messengers in lipid induction. Research of this thesis identifies the lipid induction conditions in algae with different cell wall structures, *Euglena gracilis* (without a cell wall) and *Chlamydomonas reinhardtii* (with a cell wall). Furthermore, the role of H_2O_2 in stimulating lipid accumulation in algae has been discovered in this thesis.

5.1.1 Identification of the lipid induction conditions in *Euglena gracilis*

Among microalgae, the *E. gracilis* has a unique structure outside the cell consisting of protein and glycan in the cell membrane to protect the cell from adverse environmental conditions (O'Neill et al., 2017). This organism is also one of the eukaryotic microalgae studied in cell biology and biochemistry for its capability to biosynthesize multiple beneficiary compounds for humans (Gissibl et al., 2019). In Chapter 2, different environmental conditions have been explored in *E. gracilis* by visualizing the lipid production *in vivo* with flow cytometry and confocal microscopy. In particular, five different treatments have been tested (1) modified Cramer-Myers medium (MCM) (24 h light), (2) MCM, nitrogen (-) (24 h light), (3) MCM, nitrogen (-), calcium (-) (24 h, light), (4) MCM, nitrogen (-), calcium (-), glucose (+) (24 h light), and (5) MCM, nitrogen (-), calcium (-), glucose (+) (Dark). The conditions that can produce more health beneficiary fatty acids have also been determined.

Linoleic acid and α -linolenic acid have been found in large amounts in all the treatments. Palmitoleic acid and palmitic acid are also found in profusion. Interestingly, the maximum amount of omega-3 fatty acids eicosapentaenoic acid (EPA) and docosahexaenoic acid (DHA) was obtained from nitrogen and calcium deprivation, but glucose supplemented dark

condition of Treatment 5. These FAs have several health implications for humans. Dietary supplementation of palmitoleic acid can reduce obesity, diabetes and hepatosteatorosis (Tricò et al., 2020; Frigolet & Gutiérrez-Aguilar, 2017). Linoleic acid can prevent hair loss and assist wound healing (Silva et al., 2018; Guo and Katta, 2017). The α -linolenic acid is also crucial since humans cannot synthesize α -linolenic acid, and this FA can improve the biosynthesis of beneficiary long-chain PUFAs. DHA can support the functions of the brain and retina by improving cell signalling, whereas improved cardiovascular functions have been observed due to the dietary incorporation of DHA and EPA. Since the results of this chapter suggest the biosynthesis of these essential FAs in large proportion, culturing *E. gracilis* in the applied condition is promising to utilize this microalga as a health supplement.

LDs in *E. gracilis* cells were also analyzed with DPAS ($C_{20}H_{16}N_2O$), a lipid-specific AIE fluorogen, and BODIPY, a well-known traditional staining probe to compare with the AIE fluorogenic results. The results demonstrate that DPAS is a highly effective biocompatible and photostable fluorophore for rapid and sensitive visualization of LDs. Luminogen DPAS is synthesized from very cheap materials and has surpassed the performances of the traditional fluorophore for lipid droplets staining in terms of photostability, rapidity and ease of sample preparation. The DPAS can significantly ease the lipid study in this algal cell type. This fluorescent probe has also been biocompatible and suitable for multicolour imaging. Therefore, this novel staining method could be used to screen lipid production mechanisms in other microalgae as potential alternatives to health supplementation for humans. A summary of the results of Chapter 3 is demonstrated in Fig. 5.1.

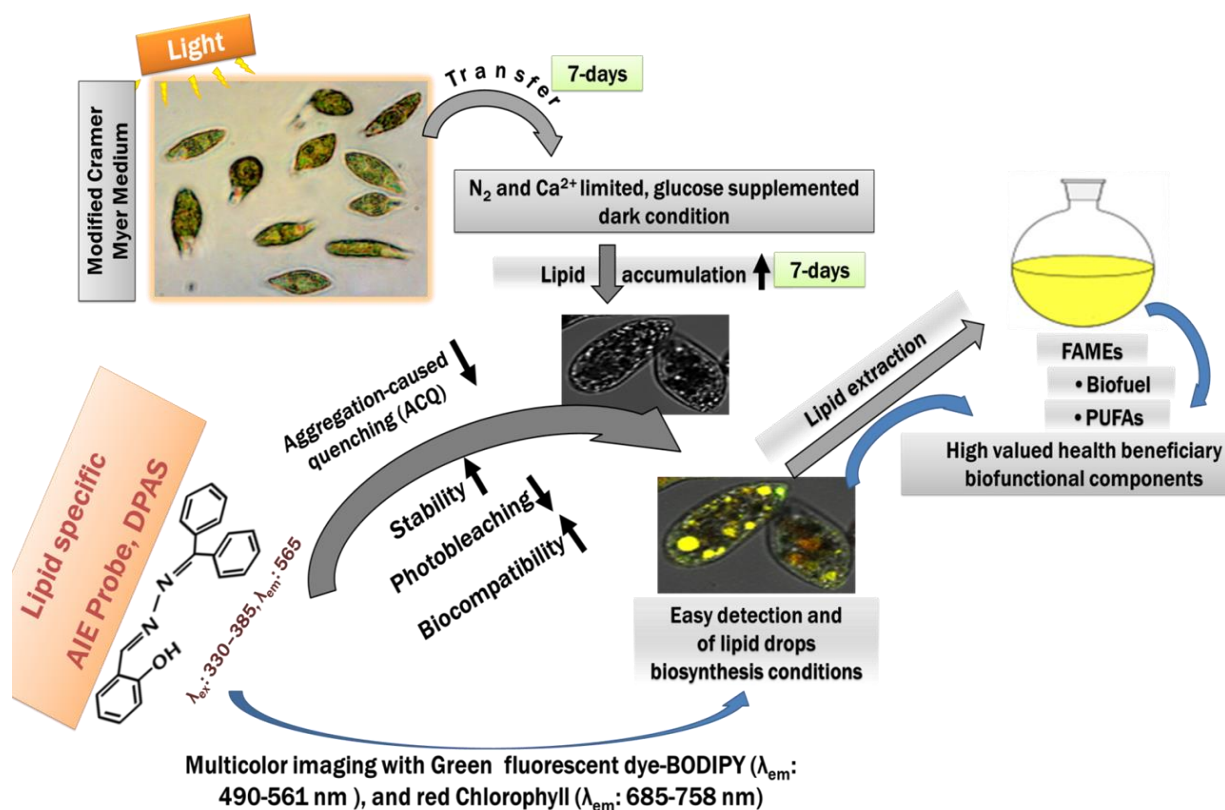


Fig. 5.1 Identification of lipid inducing conditions in *E. gracilis* with aggregation-induced emission probe, DPAS. Under nitrogen and calcium deprivation and glucose supplementation in dark *E. gracilis* cells can produce maximum lipid. The AIE-probe (DPAS) shows high lipid specificity and can rapidly detect lipid drops in *E. gracilis*. DPAS is also suitable for multicolor imaging. Due to the AIE properties, this lipid-specific AIE probe is more stable and free from aggregation caused quenching phenomena due to the AIE properties. This AIE probe demonstrates a straightforward sample preparation technique and better performance than the traditional BODIPY dye.

5.1.2 Identification of the lipid induction conditions in *Chlamydomonas reinhardtii*

In Chapter 3, a novel strategy has been adopted to detect LDs with a new lipid-specific AIE probe, 2-DPAN (C₂₄H₁₈N₂O), in the complex carbohydrates-based cell walls containing

green microalga, *C. reinhardtii*. The *C. reinhardtii* is an important model organism in biological science that has been widely investigated for biopharmaceuticals, protein and hydrogen production (Demurtas et al., 2013; Darwish et al., 2020; Melis and Happe, 2004). This study has investigated the impacts of nutrient starvation, carbon source and light on lipid bioaccumulation and fatty acid composition in this microalga. The cultural environment was enriched with (1) modified Woolds Hole (MBL) medium (24 h light), (2) nitrogen-deprived MBL medium (24 h light), (3) nitrogen and calcium-deprived MBL medium (24 h light), (4) nitrogen and calcium-deprived but sodium acetate (2.0 g/L) supplemented MBL medium (24 h light), (5) nitrogen and calcium-deprived but sodium acetate (2.0 g/L) supplemented MBL medium (24 h dark). The performances of 2-DPAN have been compared to the AIE probe, DPAS and the traditional dye BODIPY. Lipid composition and hydrogen peroxide (H₂O₂) content in the cells of different cultural conditions have also been analyzed. 2-DPAN has shown better fluorescence intensity for detecting LDs in *C. reinhardtii* than the DPAS and BODIPY. Compared to the traditional dye, BODIPY, AIEgens, 2-DPAN, and DPAS have demonstrated rapid, easy and efficient sample preparation techniques without washing steps. Therefore, both the AIE probes are considered more biocompatible, photostable and efficient multicolour fluorescence imaging tools than BODIPY for LD detection in microalgae.

The dark condition in this experiment could not induce lipid production in *C. reinhardtii*. The alga also could not utilize glucose as the carbon source. Instead, the optimum lipid and maximum health beneficiary PUFA (α -linolenic acid) were synthesized in the 24 h light condition with deprivation of nitrogen and calcium and supplementation of sodium acetate to the MBL medium. The presence of sodium acetate in the growth media may redirect the metabolic pathways towards lipid synthesis, leading to increased LD biosynthesis. However, a lower algal growth rate with a maximum reduction of chlorophyll and a surge of H₂O₂ has also been observed in the condition of the optimum lipid production. During lipid

biosynthesis, chlorophyll can be used as the internal nitrogen reserve and decrease the light uptake to reduce excessive ROS accumulation (Miller et al., 2010). The high H₂O₂ content in the lipid-induced *C. reinhardtii* cells also indicates a possible modulation of the signalling pathways towards lipid biosynthesis in the nutrient-starved cells. The result of Chapter 3 (Fig. 5.2) further inspired to test the effects of direct supplementation of H₂O₂ on lipid biosynthesis and FAs composition of this microalga in Chapter 4.

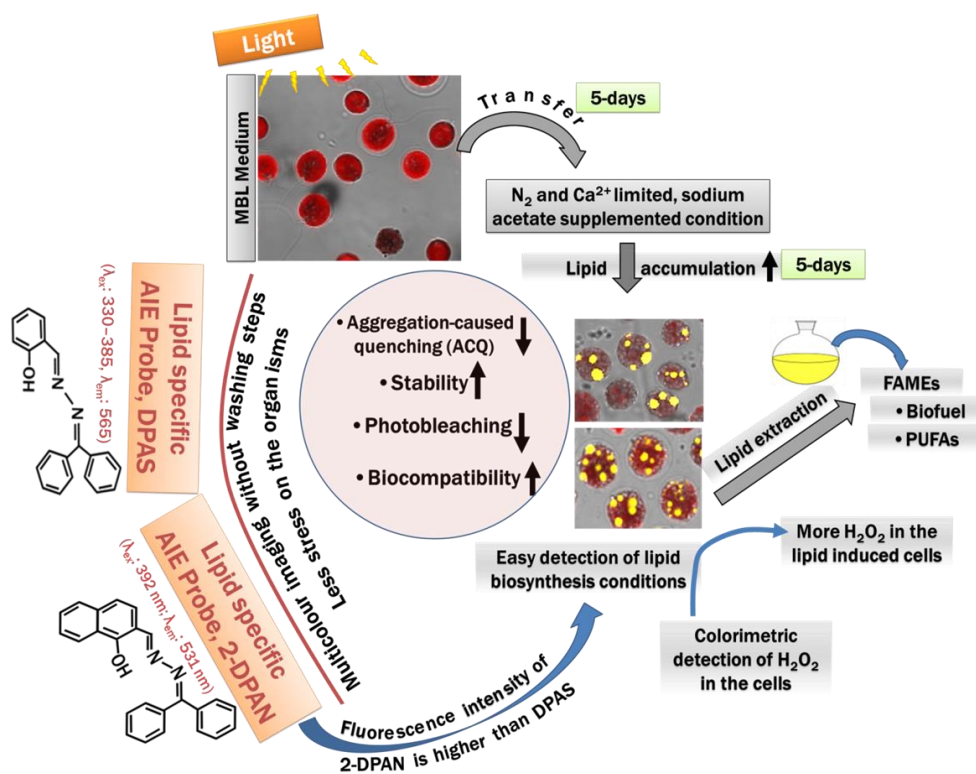


Fig. 5.2 Identification of the lipid inducing conditions in *Chlamydomonas reinhardtii* with aggregation-induced emission probe, DPAS and 2-DPAN. Under nitrogen and calcium deprivation, sodium acetate supplemented light condition, *C. reinhardtii* cells can produce maximum lipid. AIE probes, DPAS and 2-DPAN can rapidly detect lipid drops in algae with the complex carbohydrate-based cell walls. 2-DPAN shows better fluorescence intensity than DPAS and traditional BODIPY dye, whereas both the AIEgens can be utilized without the

tedious washing steps. More H₂O₂ content in the lipid-induced *C. reinhardtii* cells indicates the involvement of ROS molecules in lipid biosynthesis.

5.1.3 Effects of H₂O₂ on the lipid accumulation and fatty acid composition in *Chlamydomonas reinhardtii*

During stress, reactive oxygen species (ROS) serve a crucial role in preserving cellular integrity, development, defence processes, and controlled cell death in organisms. Among the ROS molecules, H₂O₂ is relatively more stable, quickly passes across the phospholipid bilayer, and interferes with many complex biological systems (Reczek and Chandel, 2015; Niethammer et al., 2009). While a high level of ROS is detrimental to cells, increasing evidence suggests that a certain amount of ROS can act as the secondary messenger and is associated with normal cell functions (Shi et al., 2017).

In Chapter 3, a surge in H₂O₂ activity has been observed. To demonstrate further the roles of this ROS molecule as the messenger molecule and stress marker in the lipid induced *C. reinhardtii* cells, in Chapter 5, a novel AIE-based technique has been adopted. A new H₂O₂-specific AIEgen, TPE-BO (C₃₈H₄₂B₂O₄), has been utilized for rapid, wash free and multicolour imaging *in vivo* to visualize the H₂O₂ activity in the lipid-induced cells during stress exposure. Effects of different concentrations of H₂O₂ supplementation on lipid accumulation and FAs composition in *C. reinhardtii* cells have also been analyzed with lipid specific AIE probe 2-DPAN. Interestingly, compared to the control group, almost no change in the growth of *C. reinhardtii* cells has been observed in 0.4 mM and 0.6 mM H₂O₂ supplementation, whereas the biosynthesis of lipid and health beneficiary α -linolenic acid has been significantly increased. More H₂O₂ activities have been observed in lipid-induced cells, during cell division, in autophagic cells and during cell death. The supplementation of H₂O₂

at a certain level (0.4 and 0.6 mM) can modulate the cell signalling by inducing glutathione (GSH) activity, altering the calmodulin and *MAPK* expression levels, resulting in increased lipid production without affecting the algal growth (Shi et al., 2017; Ikner & Shiozaki, 2005; Zhang et al., 2017). However, this chapter suggests that H_2O_2 concentration is critical because a slight increase in H_2O_2 concentration by 0.2 mM (from 0.4 mM to 0.6 mM) has caused 60% of cell growth inhibition. This suggests that H_2O_2 can increase oxidative stress, cell damage, and cell death (Fig. 5.3).

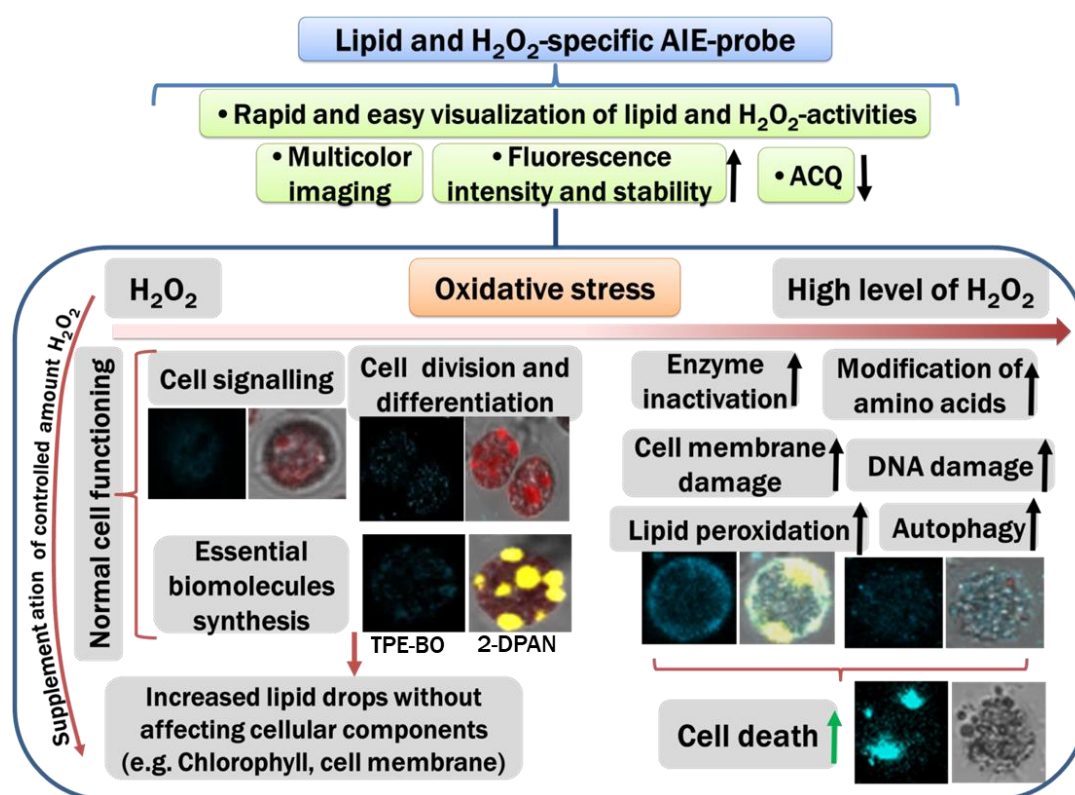


Fig. 5.3 Summary of the H_2O_2 activity during lipid biogenesis in *Chlamydomonas reinhardtii* with AIE-based techniques. H_2O_2 activity in the lipid-induced cells can be detected with H_2O_2 -specific AIE probe, TPEBO and lipid-specific AIE-probe, 2-DPAN, respectively. A higher amount of H_2O_2 can increase the oxidative stress that might increase cell damage and lead to cell death, while up to a certain level, ROS can act as messenger molecules for normal cell functions and biosynthesis of essential molecules.

5.2 Conclusion

This thesis provides insights into the lipid inducing conditions in two different types of microalgae, *E. gracilis* and *C. reinhardtii*. The presence of organic carbon in the form of glucose and deprivation of nitrogen and calcium in the algal culture can enhance lipid and produce more PUFAs as a health supplement in *E. gracilis* in a dark condition. However, *C. reinhardtii* can biosynthesize more lipid and health beneficiary α -linolenic acid in the 24 h light condition with nitrogen and calcium deprivation, and sodium acetate supplementation in the MBL medium and the MBL medium supplemented with 0.4 mM and 0.6 mM H_2O_2 . Unlike the nutrient-starved conditions, the results demonstrate that 0.4 mM and 0.6 mM H_2O_2 supplementation in the MBL medium can induce lipid and α -linolenic acid production without affecting the algal growth, which can compromise the industrial limitation of reduced algal biomass during microalgal lipid production. Details of the lipid-inducing conditions have also been analyzed with AIE-based techniques. The novel strategies of LDs visualization with AIEgens, DPAS and 2-DPAN have provided new opportunities to study LDs in microalgae with less effort. The AIE-based techniques enable us to visualize the distribution and quantity of LDs in live *E. gracilis* and *C. reinhardtii* cells on a confocal microscope. These lipid-specific AIE fluorogens are synthesized from cheap materials. They can improve traditional fluorescent probes currently used for lipid imaging, which often suffer from reduced photostability and difficulties in dye acquisition techniques that limit their microscopic imaging usage. These new AIE bioprobes could surpass the performances of the traditional fluorophore for lipid droplets staining in terms of photostability and rapid and easy sample preparation techniques. Thus this new technique significantly eases the lipid study in this algal cell type. A rapid, wash-free, multicolor AIE-base study opportunity has also been developed through *in vivo* visualization of H_2O_2 and LDs under the same assay condition using H_2O_2 -specific AIEgen, TPE-BO and lipid-specific AIEgen, 2-DPAN that

broadens the horizon of these dyes for biological studies. These fluorescent probes are biocompatible, therefore would help to screen the capacity of lipid droplet production in other algal species that have the potential as a source to produce healthy food for humans.

5.3 Implications

Conditions for the lipid bioaccumulation in microalgae could be rapidly and easily detected with biocompatible lipid-specific AIE probes. AIE-based early and semi-quantitative lipid prediction in microalgae can provide information to take necessary steps in advance for lipid induction. This would be more time-saving and labour-efficient, therefore economically viable for the commercial production of lipids from microalgae. Bioaccumulation of lipid molecules in microalgae can be increased by altering the biosynthesis pathways involved. Therefore, the conditions need to be optimized for each microalgal species. Targeting the ROS as the chemical signals, different chemical-based strategies have been reported that shifted environment-induced physiological responses towards synthesizing valuable microalgal biomolecules (Montero-Lobato et al., 2018). Direct employment of H_2O_2 in the culture has been observed to enhance the yield of lipid productivity in *Chlorella zofingiensis* (Ip and Chen, 2005) and *Chlorella vulgaris* (Battah et al., 2015), respectively. Alongside early detection of lipid accumulation, lipid production could also be improved in microalgae through AIE-based techniques. Recently, two AIEgens, 3-diphenylamino-6-(2-pyridinyl)phenyldiphenylboron (TPBA) and 4-((2,2-difluoro-5-phenyl-2,3-dihydro-1,3,4,2-oxadiazaborol-3-ylidene)methyl)-N,N-dimethylaniline (APO) have been deployed to increase the production of lipid and the biomass by fivefold in cyanobacteria (Liu et al., 2020). Both the AIEgens have exhibited strong absorptivity in the UV and blue regions with peaks of around 420 nm and 380 nm for TPBA and APO, respectively. TPBA and APO emitted intense fluorescence at 450-550 nm and 500-650 nm, respectively. It has been predicted that the absorbed UV and blue light by the AIE aggregates from the light source have prevented

harmful effects, and the cyanobacteria have reabsorbed the efficient fluorescence in the range of 450-600 nm for enhancing photosynthesis. Thus with AIE probes, the light could be utilized in a promising way to enhance the bioaccumulation of the lipid components in microalgae (Fig. 5.4).

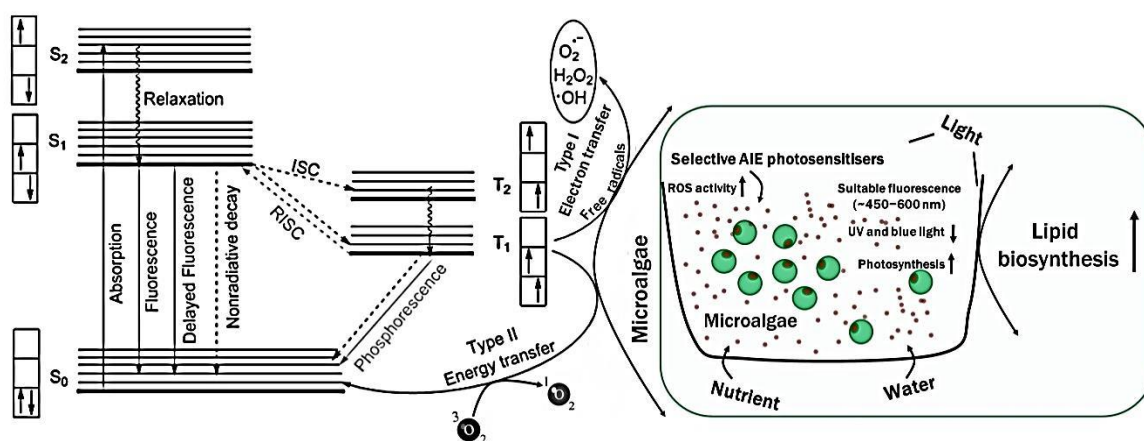


Fig. 5.4 Proposed pathway for the bioactivities of the aggregation-induced emission photosensitizers (AIE-PSs) in algal cells for lipid production. Due to the absorption of a photon, excited photosensitizing agents (PSs) encounter three electronic states: singlet ground state (S_0), singlet excited states (S_1 , S_2), and longer-lived triplet excited state (T_1). Absorption of the electron happens somewhere in between the vibrational and rotational energy levels of the excited singlet states. Among different photophysical and photochemical courses, the first process is most likely the relaxation of the first excited state to the lowest vibrational energy level. Upon restriction of the intramolecular rotation (RIR) and intramolecular vibration (RIV) in the aggregated excited state, AIE-based PSs might relax from singlet excited states by emitting a photon as fluorescence. One of the most important nonradiative photonic processes to the T_1 is intersystem crossing, which emits a photon from T_1 through spin-forbidden phosphorescence or other photochemical reactions. Molecules in the excited states are generally stronger oxidizing and reducing species. Apart from the radiative decay processes of fluorescence and phosphorescence, the excitation may generate heat and ROS by

the electron transfer (Type I)/ energy transfer (Type II) of triplet oxygen. In algal cells, selective AIE-PSs might absorb UV and blue light, thus preventing the harmful effects, and the efficient fluorescence range might enhance photosynthesis. Additionally, increased ROS activity might increase the accumulation of the lipid. Upward and downward arrows, respectively, indicate the increase and decrease of the associated processes. Part of the image is adapted from Ni et al. (2021).

5.4 Future Research

Current research outcomes have provided a solid foundation to improve health beneficiary lipid biosynthesis in *E. gracilis* and *C. reinhardtii*. It also has suggested conditions to maximize the lipid production in *C. reinhardtii* without compromising the growth. It has contributed new knowledge to our understanding of algal lipid in H₂O₂ supplementation. However, some questions are still remarkable and need to be focused on advancing further in microalgal lipid research:

1. Lipid biosynthesis in microalgae and nutrient requirements are highly species-specific and immensely vary from species to species. Therefore, systematic identification of the lipid-producing microalgae and lipid-inducing conditions are required.
2. FAs profile largely varies from species to species and changes during different growth phases. Therefore, it is essential to analyze the FAs composition at different growth phases of an algal species to get the optimum amount of health beneficiary PUFAs.
3. The amount of H₂O₂ to promote the secondary messenger system for lipid bioaccumulation in microalgae is critical. Therefore, species-specific studies are required for H₂O₂ treatments prior to recommendation.

4. The in-depth structure-property relationships of other ROS molecules and synthesized essential biomolecules in microalgae are required to advance further in lipid research.

5. This thesis has established a rapid and easy detection technique of LDs in two types of microalgae, *E. gracilis* without a cell wall and *C. reinhardtii* with a carbohydrates-based cell wall. However, lipid detection techniques with AIE probes need to be established in other cell types, such as silica-based cell walls.

6. Photosynthetic organisms contain different biomolecules that have their autofluorescence. Therefore, a study of species-specific autofluorescence properties and synthesis of more probes are in demand to detect the target molecules for lipid research.

5.5 References

- Abedi, E., & Sahari, M. A. (2014). Long-chain polyunsaturated fatty acid sources and evaluation of their nutritional and functional properties. *Food Science & Nutrition*, 2(5), 443-463. <https://doi.org/10.1002/fsn3.121>
- Battah, M., El-Ayoty, Y., Abomohra, A.EF. El-Ghany, S. A. & Esmael, A. (2015). Effect of Mn^{2+} , Co^{2+} and H_2O_2 on biomass and lipids of the green microalga *Chlorella vulgaris* as a potential candidate for biodiesel production. *Annals of Microbiology*, 65, 155-162. <https://doi.org/10.1007/s13213-014-0846-7>
- Beller, M., Thiel, K., Thul, P. J., & Jäckle, H. (2010). Lipid droplets: a dynamic organelle moves into focus. *FEBS Letters*, 584(11), 2176-2182. <https://doi.org/10.1016/j.febslet.2010.03.022>
- Darwish, R., Gedi, M.A., Akepach, P., Assaye, H., Zaky, A. S., Gray, D. A. (2020). *Chlamydomonas reinhardtii* is a potential food supplement with the capacity to outperform *Chlorella* and *Spirulina*. *Applied Sciences*, 10(19), 6736. <https://doi.org/10.3390/app10196736>
- Demurtas, O. C., Massa, S., Ferrante, P., Venuti, A., Franconi, R., & Giuliano, G. (2013). A *Chlamydomonas*-derived human papillomavirus 16 E7 vaccine induces specific tumor protection. *PloS One*, 8(4), e61473. <https://doi.org/10.1371/journal.pone.0061473>
- Friгоlet, M. E., & Gutiérrez-Aguilar, R. (2017). The role of the novel lipokine palmitoleic acid in health and disease. *Advances in Nutrition (Bethesda, Md.)*, 8(1), 173S-181S. <https://doi.org/10.3945/an.115.011130>

- Gissibl, A., Sun, A., Care, A., Nevalainen, H., & Sunna, A. (2019). Bioproducts From *Euglena gracilis*: Synthesis and Applications. *Frontiers in Bioengineering and Biotechnology*, 7, 108. <https://doi.org/10.3389/fbioe.2019.00108>
- Guo, E. L., & Katta, R. (2017). Diet and hair loss: effects of nutrient deficiency and supplement use. *Dermatology Practical & Conceptual*, 7(1), 1-10. <https://doi.org/10.5826/dpc.0701a01>
- Ikner, A., & Shiozaki, K. (2005). Yeast signaling pathways in the oxidative stress response. *Mutation Research*, 569(1-2), 13-27. <https://doi.org/10.1016/j.mrfmmm.2004.09.006>
- Ip, P. F., & Chen, F. (2005). Employment of reactive oxygen species to enhance astaxanthin formation in *Chlorella zofingiensis* in heterotrophic culture. *Process Biochemistry*, 40(11), 3491-3496. <https://doi.org/10.1016/j.procbio.2005.02.014>
- Kapoor, B., Kapoor, D., Gautam, S., Singh, R., & Bhardwaj, S. (2021). Dietary polyunsaturated fatty acids (PUFAs): uses and potential health benefits. *Current Nutrition Reports*, 10(3), 232-242. <https://doi.org/10.1007/s13668-021-00363-3>
- Khan, M. I., Shin, J. H., & Kim, J. D. (2018). The promising future of microalgae: current status, challenges, and optimization of a sustainable and renewable industry for biofuels, feed, and other products. *Microbial Cell Factories*, 17(1), 36. <https://doi.org/10.1186/s12934-018-0879-x>
- Leahy, E., Lyons, S., & Tol, R. S. J. 2010. An estimate of the number of vegetarians in the world. Dublin. <https://www.researchgate.net/publication/254412281>

Liu, H., Bai, H., Yan, N., Wong, T. Y., Dang, D., Ni, J. S., Kwok, R. T. K., Wang, W. X., Tang, B. Z. (2020). Boosting algal bloom by five-fold with AIEgens: Towards the development of biofactory. *ChemRxiv*, <https://doi.org/10.26434/chemrxiv.12739241>

Melis, A., & Happe, T. (2004). Trails of green alga hydrogen research - from hans gaffron to new frontiers. *Photosynthesis Research*, 80(1-3), 401-409. <https://doi.org/10.1023/B:PRES.0000030421.31730.cb>

Miller, R., Wu, G., Deshpande, R. R., Vieler, A., Gärtner, K., Li, X., Moellering, E. R., Zäuner, S., Cornish, A. J., Liu, B., Bullard, B., Sears, B. B., Kuo, M. H., Hegg, E. L., Shachar-Hill, Y., Shiu, S. H., & Benning, C. (2010). Changes in transcript abundance in *Chlamydomonas reinhardtii* following nitrogen deprivation predict diversion of metabolism. *Plant Physiology*, 154(4), 1737-1752. <https://doi.org/10.1104/pp.110.165159>

Montero-Lobato, Z., Vázquez, M., Navarro, F., Fuentes, J. L., Bermejo, E., Garbayo, I., Vílchez, C., & Cuaresma, M. (2018). Chemically-induced production of anti-inflammatory molecules in microalgae. *Marine Drugs*, 16(12), 478. <https://doi.org/10.3390/md16120478>

Morales, M., Aflalo, C., & Bernard, O. (2021). Microalgal lipids: A review of lipids potential and quantification for 95 phytoplankton species. *Biomass and Bioenergy*, 150, 106108. <https://doi.org/10.1016/j.biombioe.2021.106108>

Ni, J., Wang, Y., Zhang, H., Sun, J. Z., & Tang, B. Z. (2021). Aggregation-Induced Generation of Reactive Oxygen Species: Mechanism and Photosensitizer Construction. *Molecules (Basel, Switzerland)*, 26(2), 268. <https://doi.org/10.3390/molecules26020268>

Niethammer, P., Grabher, C., Look, A. T., & Mitchison, T. J. (2009). A tissue-scale gradient of hydrogen peroxide mediates rapid wound detection in zebrafish. *Nature*, *459*(7249), 996-999. <https://doi.org/10.1038/nature08119>

O'Neill, E. C., Kuhaudomlarp, S., Rejzek, M., Fangel, J. U., Alagesan, K., Kolarich, D., Willats, W., & Field, R. A. (2017). Exploring the glycans of *Euglena gracilis*. *Biology*, *6*(4), 45. <https://doi.org/10.3390/biology6040045>

Reczek, C. R., & Chandel, N. S. (2015). ROS-dependent signal transduction. *Current Opinion in Cell Biology*, *33*, 8-13. <https://doi.org/10.1016/j.ceb.2014.09.010>

Rondhi, M., Pratiwi, P. A., Handini, V. T., Sunartomo, A. F., Budiman, S. A. (2018). Agricultural land conversion, land economic value, and sustainable agriculture: A case study in East Java, Indonesia. *Land*, *7*, 148, <https://doi:10.3390/land7040148>

Shi, K., Gao, Z., Shi, T.Q., Song, P., Ren, L.J., Huang, H., & Ji, X.J. (2017). Reactive oxygen species-mediated cellular stress response and lipid accumulation in oleaginous microorganisms: The state of the art and future perspectives. *Frontiers in Microbiology*, *8*, 793. <https://doi.org/10.3389/fmicb.2017.00793>

Silva, J. R., Burger, B., Kühn, C., Candreva, T., Dos Anjos, M., & Rodrigues, H. G. (2018). Wound Healing and Omega-6 Fatty Acids: From Inflammation to Repair. *Mediators of Inflammation*, *2018*, 2503950. <https://doi.org/10.1155/2018/2503950>

Sun, X. M., Ren, L. J., Zhao, Q. Y., Ji, X. J., & Huang, H. (2018). Microalgae for the production of lipid and carotenoids: a review with focus on stress regulation and adaptation. *Biotechnology for Biofuels*, *11*, 272. <https://doi.org/10.1186/s13068-018-1275-9>

Tricò, D., Mengozzi, A., Nesti, L., Hatunic, M., Gabriel Sanchez, R., Konrad, T., Lalić, K., Lalić, N. M., Mari, A., Natali, A., & EGIR-RISC Study Group (2020). Circulating

palmitoleic acid is an independent determinant of insulin sensitivity, beta cell function and glucose tolerance in non-diabetic individuals: a longitudinal analysis. *Diabetologia*, 63(1), 206-218. <https://doi.org/10.1007/s00125-019-05013-6>

Zhang, X., Tang, X., Wang, M., Zhang, W., Zhou, B., & Wang, Y. (2017). ROS and calcium signaling mediated pathways involved in stress responses of the marine microalgae *Dunaliella salina* to enhanced UV-B radiation. *Journal of Photochemistry and Photobiology. B, Biology*, 173, 360-367. <https://doi.org/10.1016/j.jphotobiol.2017.05.038>